Satellite altimeter calibration and validation using GPS buoy technology

By

Christopher S. Watson, B. Surv (Hons) UTAS

Submitted in fulfilment of the requirements for the
Degree of Doctor of Philosophy

Centre for Spatial Information Science
University of Tasmania

July 2005

Declaration

This Thesis contains no material which has been accepted for a degree or diploma by the University or any other institution, except by way of background information and duly acknowledged in the Thesis, and to the best of the candidate's knowledge and belief no material previously published or written by another person except where due acknowledgement is made in the text of the Thesis.

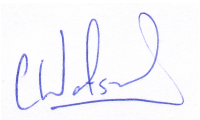

Digitally signed by Christopher Watson
Reason: I am the author of this document
Location: Hobart, Australia
Date: 2005.10.26 16:35:56 +11'00'

.....

Christopher S. Watson

Authority of Access

.....

Christopher S. Watson

Supporting Publications

A number of publications have been produced while undertaking this Thesis. Where parts of these publications have been reproduced in this Thesis, the work is my original contribution to the publication. Dr Neil White is acknowledged with undertaking the initial data processing of the oceanographic moorings, and extracting the altimeter GDR data. The publications include:

Watson, C., Coleman, R., White, N., Church, J., and Govind, R. (2003). "Absolute Calibration of TOPEX/Poseidon and Jason-1 Using GPS Buoys in Bass Strait, Australia." *Marine Geodesy*, 26(3-4), pp285-304.

Watson, C., White, N., Coleman, R., Church, J., Morgan, P., and Govind, R. (2004). "TOPEX/Poseidon and Jason-1: Absolute Calibration in Bass Strait, Australia." *Marine Geodesy*, 27(1-2), pp107-132.

Watson, C., Coleman, R., White, N., Church, J., and Govind, R. (2002). "In situ Calibration Activities in Bass Strait, Australia." *Poster at the NASA/CNES Jason-1 Science Working Team (SWT) meeting,* Biarritz, France, June 10-12, 2002.

Watson, C., Coleman, R., White, N., Church, J., and Govind, R. (2002). "In situ Calibration Activities in Bass Strait, Australia." *Poster at the NASA/CNES Jason-1 Science Working Team (SWT) meeting,* New Orleans, USA, October 21-23, 2002.

Watson, C., White, N., Coleman, R., Church, J., and Govind, R. (2003). "TOPEX/Poseidon and Jason-1: Absolute Calibration in Bass Strait, Australia." *Poster at the NASA/CNES Jason-1 Science Working Team (SWT) meeting,* Arles, France, November 18-22, 2003.

Watson, C., White, N., Coleman, R., and Church, J. (2004). "Updated Results from Bass Strait and Other Sites in the Australasian Region." *Poster at the NASA/CNES Ocean Surface Topography Science Team Meeting,* St Petersburg, Florida, USA, November 4-6, 2004.

To A.R. Gear

Abstract

Satellite altimeters have become an important tool for the study of global and regional mean sea level change, offering near global coverage and unprecedented accuracy. Issues of calibration and validation remain central to their ability to determine estimates of change at accuracies of better than 0.5 mm/yr. This Thesis provides an absolute calibration of the TOPEX/Poseidon (T/P) and Jason-1 satellite altimeters, undertaken in Bass Strait, Australia. The research provides a contribution to the international calibration effort, with the Bass Strait site situated as the only one of its kind in the Southern Hemisphere.

A unique in situ absolute calibration methodology is presented, reliant on the episodic deployment of GPS equipped buoys at an offshore comparison point. In contrast to other calibration studies, data from the GPS buoys are used to solve for the absolute datum of an offshore oceanographic array (incorporating a pressure sensor, temperature and salinity recorders and a current meter array). Combined with data from a coastal tide gauge and a regional GPS network, the methodology enables the cycle-by-cycle computation of absolute bias, without the necessity of estimating a marine geoid. Emphasis within this Thesis is given to the design and development of the GPS equipped buoys, in addition to the standardisation requirements of the geodetic analysis. The GPS buoy design is applied to both the altimeter calibration problem, in addition to a near shore application involving the calibration of tide gauges in the Antarctic and Sub-Antarctic. The attention to standardisation ensures comparable estimates of in situ and altimeter sea surface height. Differences at the 9 mm level for the pole tide displacement and $\pm$15 mm for the solid Earth tide displacement are revealed when using the GAMIT GPS analysis suite. The implications of non-standardisation are further illustrated with the presentation of time series analysis from various continuous GPS datasets.

Absolute bias and 1-sigma uncertainties from a formal error budget are 0 $\pm$ 14 mm for T/P and +152 $\pm$ 13 mm for Jason-1 (for the GDR POE orbits, computed over the calibration phase, 18 Jan 2002 – 14 Aug 2002). Results over the duration of the T/P mission confirm a dependence on the choice of Sea State Bias (SSB), with the overall mean absolute bias not statistically different from zero. Extending the comparison period between Jason-1 cycles 1 to 101 (18 Jan 2002 – 06 Oct 2004) reduces the Jason-1 mean absolute bias by approximately 10 mm and reveals a significant slope of -7.6 $\pm$ 5.6 mm/yr. Whilst the cause for the significant absolute bias remains unexplained, the source of the drift appears attributable to the microwave radiometer, observed to be measuring drier over time (-5.9 $\pm$ 2.1 mm/yr). Drift of the POE orbit relative to the JPL GPS orbit is shown to account for the remaining trend observed at the Bass Strait site. After considering geographically correlated errors, absolute bias results show excellent agreement with other international calibration studies. These results aid in understanding the performance of both the T/P and Jason-1 altimeters, further underscoring calibration and cross calibration of altimeters as essential for the study of low frequency oceanographic processes, including regional and global mean sea level change. The inference of geographically correlated orbit errors, and the significant unexplained Jason-1 absolute bias emphasises the need for maintaining globally distributed verification sites and makes it clear that further work is required to improve our understanding of the Jason-1 instrument and its algorithm behaviour.

Table of Contents

Chapter 3

Chapter 4

Chapter 5

Acknowledgements

I can not escape a feeling of selfishness by writing just one name on the cover of this Thesis. Many people are to be thanked for their contribution, both professionally and personally.

Firstly, I sincerely thank Richard Coleman for his supervision, guidance and friendship so generously given both before and throughout my candidature. I can't imagine a better mentor, and I have no doubt this Thesis would not be what it is without Richard's untiring involvement. John Church and Neil White also deserve special thanks for their significant contribution to the fieldwork, analysis, and persistence in answering so many questions. It has been a delight to work as part of a team and be considered an equal with these people.

Peter Morgan and Tony Sprent have also provided significant assistance throughout this project. I thank Peter for sharing his knowledge of satellite geodesy, particularly the intricacies of the GAMIT/GLOBK software suite. Peter also generously provided his time series for analysis in this Thesis. Tony came up with the GPS buoy design and provided numerous answers to practical questions along the way.

Roger Handsworth and the Australian Antarctic Data Centre team are thanked for their assistance in the field work undertaken at Macquarie Island and in Antarctica. Thanks to John Hunter for providing his tidal analysis software and answering questions in relation to the tide gauge work. The CSIRO Marine Research mooring group are thanked for undertaking the setup, deployment and retrieval of the mooring array.

Numerous individuals and groups must be thanked for providing funding and data for this study. The CSIRO Earth Observation Centre (EOC) provided funding for main component of this study. I was supported by an Australian Postgraduate Award and CSIRO scholarship for which I was very grateful. Bob Twilley and the Geoscience Australia team maintain the data from the BUR1 GPS installation and also operate the Australian Regional GPS Network (ARGN). The National Tidal Facility (NTF) operates and maintains the Burnie tide gauge with the assistance from the Burnie Ports Corporation. Neil Adams from the Australian Bureau of Meteorology provided atmospheric pressure information. Veronique Dehant and Leonid Petrov generously provided their solid Earth tide routines. Bob King and Tom Herring answered many questions in relation to the GAMIT/GLOBK and Track software suites. Altimetry products were obtained from the Jet Propulsion Laboratory (JPL) PO.DAAC and Centre National d'Études Spatiales (CNES) AVISO archives. Bruce Haines, Pascal Bonnefond, Phil Callahan and other members of the TOPEX/Poseidon and Jason-1 SWT/OSTST provided valuable responses to numerous technical questions. Bruce Haines was particularly patient in answering my many questions and also providing the GPS reduced dynamic orbits. Michael and Bradley Hardy operated the boat in Bass Strait and provided assistance during the buoy deployment campaign. Thanks to all these people for their valuable contributions.

I would like to thank my colleagues within CenSIS and my wider group of friends for making the last three and a bit years an enjoyable time. The regular coffee group has done a fine job in keeping my caffeine levels at their optimum best.

Before I make my final acknowledgement, I would like to thank my parents, Janne and Stephen. It is a great privilege to be in the position to undertake academic research, and I thank my parents for providing the opportunities to learn and explore, enabling me to do now what I so much enjoy.

I reserve my final thankyou to Rachael for sharing in the successes and struggles that this work represents. Rachael has comforted and motivated during the difficult times and celebrated and congratulated during the good times. I look forward to the next phase in our lives together.

List of Figures

List of Tables

Chapter 1

Introduction

1.1 Overview

The Earth's climate is a complex and dynamic system which undergoes variation due to local, regional and global processes operating on very different temporal and spatial scales. Sea level is just one component of this system and a central indicator of climatic change on this planet.

The scientific consensus presented by the Intergovernmental Panel for Climate Change (IPCC) suggests the global trend in mean sea level over the 20th century is close to 2 mm/yr (Church et al., 2001). Based on historical evidence, this rate is significantly higher than that estimated for several millennia prior to the industrial revolution (Fleming et al., 1998). The IPCC concluded the changes currently being observed in mean sea level are most probably occurring as a result of 20th century warming and the corresponding thermal expansion of sea water and the loss of glacial ice (Church et al., 2001). These results provided the most compelling evidence to date that climatic change is occurring as a result of anthropogenic influence.

The findings presented in the 2001 IPCC report have focussed attention on issues surrounding climate change, resulting in climate change becoming a mainstream issue within the broader community. With estimates of 100 million people living within a 1 m height range of the current mean sea level, the social, economic and environmental consequences of sea level rise are very real and tangible to the general community (Leatherman, 2001). Most at risk are low-lying island nations (Kirabati and Tuvalu for example) and expansive deltaic regions such as those found in Bangladesh, Egypt, Vietnam and China. The potential human impact alone in these areas, which also correspond to some of the world's poorest and less developed countries, is overwhelming.

It is therefore not surprising that considerable scientific effort has been placed on monitoring sea level to increase our capacity to monitor, understand and manage climate change. An integrated measurement approach is required, incorporating data from historic geological evidence, well distributed tide gauge instruments, and modern satellite techniques.

The emergence of satellite altimetry has provided the scientific community with a unique and extremely powerful tool to study global ocean circulation and its change over time. Modern altimeters, such as TOPEX/Poseidon (Fu et al., 1994) and Jason-1 (Menard et al., 2003), have revolutionised the measurement of global sea level change, largely by achieving unprecedented accuracy and mostly uninterrupted global repeat coverage. In the process, altimeters have refined and advanced our understanding of numerous oceanographic processes such as ocean tides, Rossby waves, boundary currents, eddy formation and small scale periodic oscillation to name a few. For a detailed review of the applications of satellite altimetry across a wide variety of Earth sciences, readers are referred to Fu and Cazenave (2001).

TOPEX/Poseidon and Jason-1 have set the standard in relation to the accuracy and performance of modern altimeters. Their accuracy and precision, global coverage and repeat sampling make them the tool of choice for many scientific and commercial applications, the most demanding of which is the measurement of global and regional mean sea level change (Nerem and Mitchum (2001a) and Leuliette et al. (2004) for example). Two main problems exist with using altimeters for the determination of mean sea level change:

1) The sea surface height time series generated from satellite altimeters is short in comparison to the time scale of the climatological and oceanographic processes under observation.

2) The altimeter time series also incorporates data from different satellite missions, each utilising different instrument platforms and observational strategies, hence obtaining different observational accuracies.

Given these reasons combined with the comparatively short life span of a satellite mission, issues of calibration and cross calibration between satellite missions are fundamental to the measurement of sea level change. Calibration and validation of altimeter missions is therefore a pressing and significant issue facing both the scientific community and government bodies (Fu and Cazenave, 2001).

The motivation for this Thesis is drawn from the calibration requirements of the Jason-1 altimeter launched in December 2001 (Menard and Haines, 2001). The primary aim of this Thesis is to develop an improved in situ calibration methodology for use at the Bass Strait calibration site, first used for the calibration of T/P in 1992 (White et al., 1994). The methodology will be centred on the use of an integrated measurement approach capable of achieving absolute calibration over the dedicated calibration phase of the Jason-1 mission. The calibration site will allow continued cycle-by-cycle calibration throughout the life of the Jason-1 mission, and then beyond for future missions such as Jason-2 (Fu, 2003). As the sole calibration site of its kind in the Southern Hemisphere, the work presented in this Thesis makes an important contribution to the global calibration effort.

To introduce many of the multidisciplinary challenges that face the calibration and validation process, a brief review of the development of satellite altimeters, together with a review of the various independent measurement systems on board an altimeter is required. This review material is presented in the following sections as a means of defining the primary research questions, the aims of the research, and the subsequent structure of this Thesis.

1.2 Satellite Altimetry

1.2.1 Review

A brief review of the history of satellite altimetry (see for example Fu and Cheney 1995; Wunsch and Stammer, 1998) highlights the progress made since the first observation of the Earth by an altimeter from the manned SkyLab mission launched in May 1973 (see Table 1-1). The Geodynamics Explorer Ocean Satellite 3 (GEOS-3) mission was launched in April 1975, and provided the proof of concept for satellite based oceanographic studies. With improved range precision and radial orbit accuracy (at the ~25 cm and ~500 cm level respectively), the GEOS-3 mission provided useful information on short wavelength features, such as eddy variability within the Gulf Stream (Douglas et al., 1983). The analysis of medium to long wavelength features (100's to 1000's of kilometres) remained limited due to uncertainty in the radial orbit positioning of the satellite.

Table 1-1 Evolution of satellite altimeter missions showing approximate range precision and radial orbit accuracy. (Adapted from Chelton et al., 2001).

Satellite / Mission	Mission Period	Range Precision (cm)	Radial Orbit Accuracy (cm)
SkyLab	May 1973 – Feb 1974	~100	~1000
GEOS-3	Apr 1975 – Dec 1978	25	~500
SeaSat	Jul 1978 – Oct 1978	5	~100
GeoSat	Mar 1985 – Dec 1989	4	30-50
ERS-1	Jul 1991 – May 1996	3	8-15
TOPEX/Poseidon	Aug 1992 – Present	2	2-3
ERS-2	Aug 1995 – Present	3-4	7-8
GFO	Feb 1998 – Present	2	4-5
Jason-1	Dec 2001 – Present	1-2	1-2
EnviSat	Mar 2002 – Present	2	2

SeaSat was launched in July 1978 and was the first altimeter to carry a microwave radiometer allowing the determination of the range delay caused by water vapour in the atmosphere. The range precision improved to the ~5 cm level with orbits at the ~100 cm level (Table 1-1). While the mission was only operational for 3 months, the SeaSat mission provided the first altimeter data suitable for global oceanographic studies (Giberson, 1991). Subsequent missions including GeoSat (March 1985) and the European Remote-Sensing Satellite (ERS-1, July 1991) represented further improvement in range precision and orbit accuracy. Radial

orbit errors at the ~8-15 cm level for ERS-1 still precluded studies involving global and regional absolute sea level change.

The joint U.S. National Aeronautics and Space Administration (NASA) and French Space Agency, Centre National d'Etudes Spatiales (CNES) established the TOPEX/Poseidon (T/P) mission, launched in August 1992. T/P was the first altimetry mission designed specifically for studying the variation in the circulation of the world's oceans (Fu et al., 1994). With advances in both range precision and radial orbit accuracy, together with improvements in algorithms and correction products, Sea Surface Height (SSH) from T/P can now be determined to an unprecedented accuracy of ~3-4 cm. This unprecedented accuracy was achieved through improvements across three areas (Nerem and Mitchum, 2001b):

1. Eliminating the effect of the ionosphere on the range by observing the range using two different frequencies (the K_u and C microwave bands);
2. Improvements using an onboard microwave radiometer to determine the path delay induced by the water vapour content of the atmosphere; and
3. Improvements in orbit determination using updated tracking techniques (DORIS, GPS and Laser) and geopotential models (JGM-3 for example).

The success of the T/P mission has revolutionised the way the ocean is observed and advanced a wide range of Earth sciences in the process. T/P has been central in improving our understanding of ocean circulation and its impact on the Earth's climate. Studies involving mesoscale ocean variability (see Pedlosky, 1996 and Wunsch and Stammer, 1998 for example), boundary current determination (Kelly et al., 1996), seasonal and inter-annual ocean variability (Stammer, 1997), El-Niño / La Niña southern oscillation (Chambers et al., 1999), global tidal modelling (Le Provost et al., 1995), marine meteorology and fields, such as marine geodesy and gravimetry (Tapley and Kim, 2001), have all benefited from, and in some cases been made possible by the T/P mission. For further reading relating to the T/P mission, see the Journal of Geophysical Research special issues on geophysical evaluation (JGR, 1994) and scientific results (JGR, 1995). The T/P mission is made all the more remarkable by the fact that it remains operating at the time of writing, almost 9 years after the completion of its primary mission of 3 years.

Since the launch of T/P, additional missions including the second European Remote-Sensing Satellite (ERS-2, August 1995) and the GeoSat Follow-On (GFO, February, 1998) were launched. The GFO mission has had difficulties with instrument problems; hence has been of limited use for studies of mean sea level

change. Data from the GFO mission was beginning to be disseminated on a regular basis at the time of writing. The follow-on mission for T/P, designated Jason-1, was developed by NASA/CNES and launched in December 2001. The Jason-1 mission was built upon the success of the T/P mission, with the aim of providing a comparable or improved accuracy to that demonstrated by its predecessor (Menard et al., 2003). Jason-1, in conjunction with the ERS-2 follow-on, EnviSat (March 2002), represents the beginning of a new era of operational altimetry with the emergence of a range of applications routinely utilising altimetry data (see for example the GODAE and MERCATOR projects, Bahurel et al., 2002). Jason-1 is the first of a series of planned follow-on missions ensuring the continuation of the global ocean observation time series. The planned Jason-2 Ocean Sea-Surface Topography Mission (OSTM) is due for launch in 2007, incorporating the first wide-swath altimetric measurement of ocean topography (Fu, 2003). Assuming the proposal for the wide swath instrument is successful, Jason-2 OSTM will significantly improve the spatial resolution of altimeter products while maintaining the continuous global SSH time series critical to studies of regional and global mean sea level change.

There is no doubt satellite altimetry has revolutionised the understanding of the dynamic ocean environment, providing a powerful tool for the study of the ocean-climate interaction. As stated in the overview to this Chapter, the altimetric time series is however very short in comparison with many of the oceanographic processes under investigation (for example mesoscale ocean variability, thermal expansion of the oceans, changes in the freshwater exchange, inter-annual, and decadal variability) . As underscored in Table 1-1, the time series is also subject to frequent changes in the satellite platform. The risks and challenges associated with satellite technology do not guarantee continuous observations with success comparable to T/P, for each and every mission. This point is clearly demonstrated early in the development of altimetry with the SeaSat mission lasting just 3 months. The instrument difficulties associated with the GFO mission and the delayed launch of the Jason-1 mission further emphasize this point. The benefit of the altimetric SSH time series may only be maximised through individual calibration and cross calibration of successive missions. Linking each mission in an absolute terrestrial reference frame allows the continuation of the altimetric time series which is particularly important for investigations into low frequency oceanographic processes. These include inter-annual and decadal oceanographic variability (El Niño, the North Atlantic Oscillation and the Pacific Decadal Oscillation for example) and importantly, studies involving global and regional

mean sea level change. Accurate calibration and cross calibration is therefore fundamental for these studies.

To gain a further appreciation of the demands placed on both the altimeter measurement system and the calibration process, it is important to review the components that combine to form the altimeter measurement system. The following sections provide a basic review of the measurement system with an emphasis on associated error budgets. The review does not attempt to provide a comprehensive description at a technical level, for this readers are referred to the relevant literature (for example Chelton et al., 2001, JGR, 1994 and Marine Geodesy, 2003). What is more important in the context of this Thesis is the identification of measurement components that are subject to systematic offset, geographically correlated error, or time dependent drift, and hence require the focus of the calibration effort at the 1 cm level or better.

1.2.2 The Altimeter Measurement System

The altimeter measurement system is made up of a number of independent instruments and measurement processes, which combine to allow the determination of SSH in an absolute coordinate reference frame. The measurement process can be divided into three basic components (shown schematically in Figure 1-1):

1. Range determination from the satellite to the sea surface.
2. Orbit determination of the satellite with respect to a mathematical representation of the Earth, the reference ellipsoid.
3. Corrections to the range due to observed atmospheric refraction (troposphere and ionosphere), instrumental corrections and sea surface corrections.

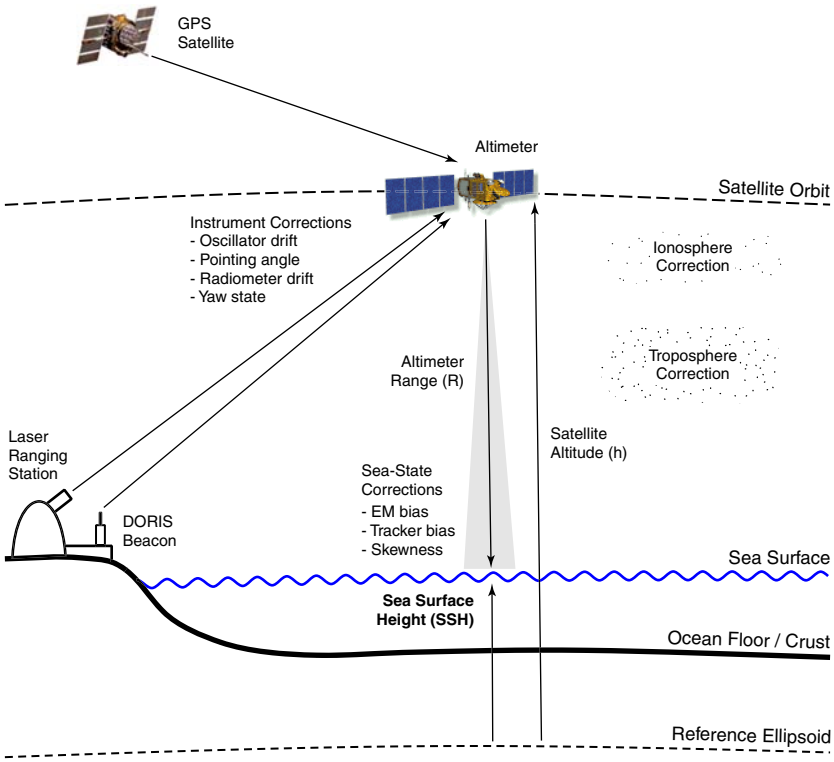

Figure 1-1 Schematic view of the altimeter measurement system.

With reference to Figure 1-1 and using the terminology adopted for the Jason-1 mission calibration/validation (CALVAL) standards (Menard and Haines, 2001), the SSH derived from the altimeter (SSH_{Alt}) is defined as:

$$SSH_{Alt} = h - \left(R + \Delta R_{DRY} + \Delta R_{WET} + \Delta R_{ION} + \Delta R_{SSB} \right) \qquad \text{Eqn 1-1}$$

where:

h is the height of the centre of mass of the satellite above the reference ellipsoid, determined from the Precise Orbit Determination (POD) analysis;

R is the nadir range from the centre of mass of the satellite to the sea surface, corrected for instrument effects;

ΔR_{DRY} is the atmospheric refraction range delay caused by the dry gas component of the troposphere;

ΔR_{WET} is the atmospheric refraction range delay caused by the water vapour and cloud liquid water content of the troposphere;

ΔR_{ION} is the atmospheric refraction range delay caused by the free electron content of the ionosphere; and

ΔR_{SSB} is the range correction caused by the interaction of the large radar footprint and the sea surface. The 'Sea State Bias' (SSB) is a combined correction referring collectively to the electromagnetic (EM), skewness and tracker biases (see further details in §1.2.2.3).

The following sections review each of the primary measurement system components.

1.2.2.1 Range Determination

The determination of the range to the sea surface from a satellite altimeter is conceptually straightforward. A pulse or waveform of microwave radiation is transmitted (at time t_T) from the spacecraft, reflected from the sea surface and received back at the spacecraft (at time t_R). Neglecting the influence of the atmosphere and the interaction with the sea surface, the range (R) from the satellite to the sea surface can be defined using the basic relationship:

$$R = \frac{(t_R - t_T) \cdot c}{2} \qquad \text{Eqn 1-2}$$

where:

t_T is the time of transmission of the microwave waveform from the spacecraft;

t_R is the time of reception of the waveform at the spacecraft; and

c is the speed of light.

In practice the range measurement is significantly more complicated. The 1-Hz data provided in the Geophysical Data Records (GDRs) are in fact averages of several thousand return waveforms. Due to the ground speed of the altimeter, this averaging procedure results in a SSH estimate every 1 second that is an average along a 6-7 km ground track profile (for T/P for example).

The averaged return waveform is further processed to derive secondary quantities of interest relating to the sea state. The Significant Wave Height (SWH or $H_{1/3}$) is derived from the slope of the waveform leading edge while an estimate of wind speed is derived from the radar backscatter coefficient. For a detailed discussion

relating to the range measurement, readers are referred to Stewart (1985) and Chelton et al. (2001).

The accuracy of the range estimate (neglecting the effect of the atmosphere and other corrections) is primarily a function of the stability and accuracy of the timing oscillator on board the spacecraft. From a calibration perspective, oscillator drift was identified as a potential source of low frequency error early in the development of altimetry. An internal calibration procedure was developed for the T/P mission, with the design requirement to maintain calibration for drift to within ±1.5 cm (Hayne et al., 1994). Results from Hayne (2004) show the success of the technique in successfully identifying the degradation and increased drift associated with the TOPEX side A altimeter electronics (Figure 1-2). As a result, the T/P mission switched to the backup side B electronics in February 1999 (T/P cycle 236).

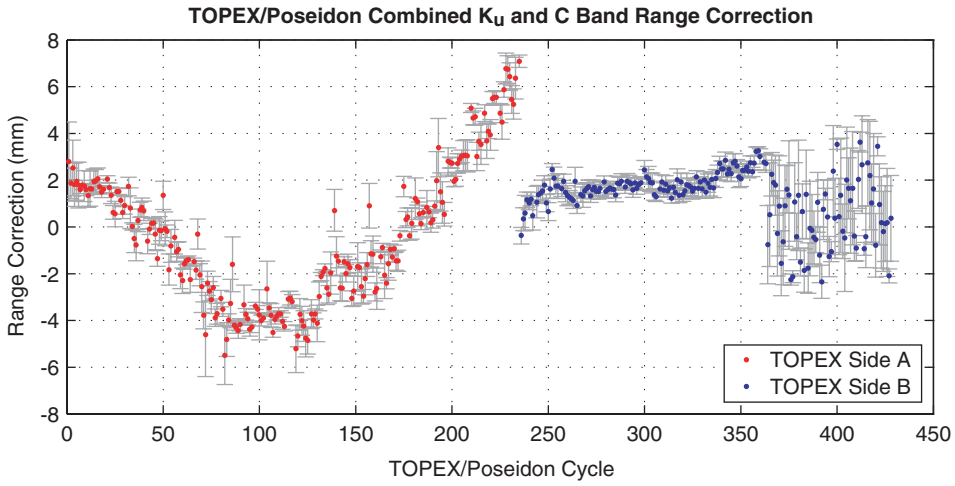

Figure 1-2 TOPEX range correction determined from the combined dual frequency range calibration. Note the increased noise on side B from cycle 364, this is from an unknown source at the time of writing (data and description from Hayne, 2004).

Before switching to the side B system, the side A drift of ~3.5 mm/yr was significantly larger than the emerging mean sea level change signal (~2 mm/yr). This emphasises the importance of monitoring and quality control of the range correction and provides further indication of the demands placed on the altimetry system to measure low frequency signals such as decadal variability and global mean sea level change.

1.2.2.2 Orbit Determination

To accurately determine SSH from the range measurements, the position of the centre of mass of the satellite must be known with respect to a Terrestrial Reference Frame (TRF) and expressed relative to a mathematical figure, the reference ellipsoid. The determination of the position of the spacecraft at the 1-2 cm level requires a comprehensive tracking system incorporating a range of different technologies. The orbit of satellites such as T/P and Jason-1 is determined using ground based Satellite Laser Ranging (SLR) techniques in conjunction with observations taken from onboard GPS and DORIS systems (see for example Tapley and et, 1994 and Luthcke et al., 2003). Information from these predominantly independent techniques is combined with models describing the dynamic behaviour of the spacecraft in response to various external forces (the Earth's gravity field, atmospheric drag and solar radiation pressure for example).

Historically, the accuracy of the orbit is governed predominantly by the knowledge of the Earth's gravity field, and to a lesser extent by effects such as radiation pressure and atmospheric drag. Improvements in geopotential models have driven the increased radial orbit accuracy between the satellite missions as shown in Table 1-1. Developments in technologies such as the onboard GPS tracking system now allow 'reduced-dynamic' orbit solutions which are less reliant on models defining the dynamic behaviour of the spacecraft, and more reliant on actual observations (see for example Haines et al., 2004).

Inter-comparison of different orbit computation strategies plays an important role in the calibration and verification of altimeter SSH measurements. It is important to note that the orbit accuracy relates directly to the accuracy of the Earth based tracking stations that form part of the SLR, DORIS and GPS tracking network. The definition of the TRF and the monitoring of the Earth's centre of mass (about which the satellite orbits) is therefore of fundamental importance. With reference to low frequency oceanographic processes, the stability of this reference frame and hence the long-term gradual variability of the orbit position is an important consideration (see for example Nerem et al., 2000). The coordination of ground based calibration sites in an identical TRF to the altimeter represents a complex problem. Chapter 3 of this Thesis is devoted to this process.

1.2.2.3 Path Length and Other Corrections

A range of environmental path length and other instrument-based corrections are required to complete the measurement system. During the range determination process, the waveform must travel through both the ionosphere and troposphere before being reflected from the ocean surface and returning back to the spacecraft (travelling through the atmosphere a second time). Both levels of atmosphere introduce a range delay caused by the refractive characteristics of the medium.

At radial orbit heights of altimeter satellites of between 800 to 1400 km, the microwave pulse first encounters the ionosphere. The transmitted pulse interacts with the free electron content and typically undergoes a range delay in the order of 10-30 mm and up to 100 mm over equatorial regions during particularly active periods (Chelton et al., 2001). Modern altimeters use a dual frequency ranging system to take advantage of the known relationship between the ionospheric delay and the frequency of the travelling electromagnetic waveform. T/P, for example, uses K_u and C band microwave frequencies at 13.6 and 5.3 GHz respectively. This allows the determination of the range correction to a precision of 11 mm for the 1-Hz data (Chelton et al., 2001). The ionospheric correction for Jason-1 appears to be marginally more accurate at the 5 mm level following smoothing over horizontal length scales of 100 km (Menard et al., 2003). There appears little likelihood that the ionosphere correction is subject to low frequency drift or scale error, hence it is not a prime candidate for investigation in the calibration process (Nerem and Mitchum, 2001a).

The correction due to the refractive nature of the troposphere is divided into the dry and wet components. The dry component is proportional to the density of the atmosphere along the path length and is computed from surface pressure models, such as the European Centre for Medium Range Weather Forecasting (ECMWF) model. The dry correction is quite large (~2.3 m) and highly spatially correlated due to the scale of the underlying atmospheric pressure systems. The accuracy of the dry correction is a function of the accuracy of the underlying pressure model, with a 1 mbar error translating to a 2.3 mm error in the dry correction (Picot et al., 2001). The average RMS accuracy of the dry correction for the Jason-1 mission has been estimated to be 7 mm (Menard and Haines, 2001). The dry correction is unlikely to drift over time due to the assimilation of extensive in situ pressure data into the meteorological model. For the same reason the dry correction is unlikely to introduce any systematic scale error.

The wet component provides a correction to the delay introduced by the water vapour content of the atmosphere. The correction is much smaller than the dry component (between 40 to 900 mm, Keihm et al., 2000), yet is considerably more variable in time and space. The SeaSat mission was the first to carry a microwave radiometer to measure the columnar water vapour along the path length. The improved accuracy of the corrected range is clearly evident in Table 1-1. A radiometer measures the water content by observing the brightness temperature near the water vapour absorption line centred at 22.2356 GHz. The radiometer on board Jason-1 (JMR), measures three brightness temperatures at 18.7, 23.8 and 34.0 GHz. This allows the sampling of the water vapour on the 23.8 GHz channel and removal of the surface influence and atmospheric contributions from the 18.7 and 34.0 GHz channels respectively. The estimated precision of the JMR wet troposphere correction is at the 12 mm level (Menard et al., 2003).

The measurement of the water vapour content of the atmosphere represents an independent and vital supporting component to the observational system. Experience with the T/P radiometer (TMR) has shown the system is subject to both mean offset biases and time dependent drifts with magnitudes comparable or exceeding the current global trend in mean sea level change. Validation of the wet correction is therefore of fundamental importance to the calibration process. Keihm et al. (2000) present the results from the TMR investigation which revealed a hardware drift in the TMR 18-GHz channel equivalent to 0.27 °K/yr in measured brightness temperature. This translates into an artificial reduction in T/P global sea level of 1.3–1.4 mm/yr underscoring the importance of accurate calibration. The calibration of the JMR and cross calibration with the TMR instrument is revisited in Chapter 4 of this Thesis.

The final correction refers collectively to three individual corrections, all arising due to intrinsic properties of the large footprint radar range determination system. Each of the corrections contributing to the 'Sea State Bias' (SSB) are a function of the sea state as described by the significant wave height (SWH or $H_{1/3}$) and the surface wind speed. The main effect is the electromagnetic (EM) bias which arises due to differences in surface reflection properties of the sea surface. Greater reflection is received from the wave troughs in comparison to the peaked wave crests. The mean reflection surface is therefore shifted below the actual mean sea surface. Without the correction, the altimeter overestimates the range measurement (see for example Millet et al., 2003a and Millet et al., 2003b). The second component of the SSB correction is the skewness bias, arising due to the

skewed distribution of the sea surface height within the radar footprint. The skewness correction is required as the tracker measures the median height rather than the mean height of the reflecting surface (see Chelton et al., 2001 for further information). The final effect is an instrumental correction termed the tracker bias which relates purely to the performance of the waveform tracking algorithm. Typical magnitudes of the SSB correction, for 2 m SWH conditions, are at the 100 mm level. The complexity of the combined SSB correction makes it difficult to verify each component using in situ data (Menard and Haines, 2001). The group of corrections are also under continuous development (see Chambers et al., 2003 for an illustration). Despite these issues, the SSB correction is unlikely to contribute to long term drift error provided a uniform algorithm is applied to the entire time series. The correction must however be considered as a source of error when comparing calibration results from different areas or cross-calibrating separate altimeter missions.

1.2.2.4 Error Budget

To provide an indication of the performance of modern altimetry, the error budget for the Jason-1 measurement system is presented in Table 1-2 (adapted from Menard et al., 2003). The final precision for the corrected SSH (for an individual 1 Hz, GDR, SSH estimate) is at the 33 mm level.

Table 1-2 Jason-1 error budget (both mission specifications and actual performance) for 1 Hz GDR data (from Menard et al., 2003).

	GDR Error Budget	
Component	**Specification**	**Performance**
Altimeter Noise (mm) ($H_{1/3}$ = 2 m, σ = 11 dB, 1 Hz)	17	16
Sea State Bias (% SWH)	1.2 %	1 %
Ionosphere (mm)	5	5
Dry Troposphere (mm)	7	7
Wet Troposphere (mm)	12	12
Corrected Range (mm) (RSS, $H_{1/3}$ = 2 m, σ = 11 dB, 1 Hz)	**33**	**30**
Orbit (mm) (Radial component)	25	15
Corrected SSH (mm) (RSS, $H_{1/3}$ = 2 m, σ = 11 dB, 1 Hz)	**41**	**33**
SWH ($H_{1/3}$) (m or % of $H_{1/3}$, whichever is greater)	0.5 / 10 %	0.4 / 10 %
Wind Speed (m/s)	1.7	1.5

The altimeter error budget has direct influence on the obtainable precision of absolute bias and bias drift estimates during the calibration and cross calibration process. Studies such as Cheney et al. (1994) indicate errors from the T/P system (and similarly Jason-1) are largely uncorrelated in the temporal domain, hence filtering both through the spatial and temporal domains has the effect of averaging the error terms similar to random noise. This is an important concept when determining the final error contribution to calibration parameters of interest (absolute bias and bias drift) or estimates of low frequency oceanographic variability.

1.3 The Problem – Altimeter Calibration

The T/P mission underscores the essential role of the calibration and validation process using ground based in situ data. Shortly after the launch of T/P, Christensen et al. (1994) reported an absolute SSH bias of 145 ± 29 mm, indicating that the altimeter SSH estimates were erroneously high. At the end of the primary 3 year mission, Haines et al. (1996) reported a refined value of 125 ± 20 mm. Subsequent investigations revealed a software error related to adjustments of the spacecraft oscillator as the cause of the bias[1], introducing a mean error of 133 mm. The software error was also found to introduce a spurious drift of approximately 7 mm/yr (Nerem et al., 1997), clearly above the anticipated mean sea level trend at the ~2 mm/yr level.

The outcome of the exhaustive T/P calibration process, combined with the exceptional precision of the T/P measurement system, yielded the realisation that the measurement of global mean sea level change was at least achievable using satellite altimetry (Haines et al., 2003). Subsequently, the monitoring of mean sea level to an accuracy of 1 mm/yr was defined as a major research objective for the Jason-1 mission (Menard et al., 2003). Central to this research objective was the calibration of Jason-1 and cross calibration with T/P. Subsequently, ground based absolute calibration using in situ data has become an integral part of the mission design (see for example the Jason-1 and EnviSat calibration and validation plans, Menard and Haines, 2001 and Roca et al., 2002 respectively). The primary motivation for this Thesis is therefore drawn from the demanding calibration requirements of the Jason-1 mission.

The aim of the calibration process is to characterise the performance of the altimeter measurement system, with the specific goal of identifying absolute SSH bias and any drift of that bias over time. The basic concept consists of the measurement of SSH at a specific location coincident with altimeter-derived estimates of SSH. Assuming both estimates of SSH are made in an equivalent absolute reference frame, the difference in SSH represents the SSH bias. Changes in this estimate over time represent the bias drift.

Considering the accuracy tolerances, altimeter calibration represents an extremely challenging geodetic and geophysical problem. Two main techniques have emerged

[1] O. Zanifé, P. Escudier and P. Vincent are credited with the discovery of the software error in June 1996. See Nerem et al. (1997) for further information.

in the global calibration effort, namely the development of dedicated absolute calibration sites (primarily for the estimation of *absolute* SSH bias, as in the case of this Thesis, Bonnefond et al. (2003a) and Haines et al. (2003) for example), and calibration based on the utilisation of the global tide gauge network (primarily for the estimation of SSH bias *drift*, as in the case of Mitchum (2000) and Leuliette et al. (2004) for example).

For the purposes of review, the two complementary calibration techniques are introduced in the following sections.

1.3.1 Dedicated Absolute Calibration Sites

A dedicated calibration site, as investigated in this Thesis, monitors successive passes of the altimeter at an individual location using an extensive array of space geodetic and sea level observing systems. The in situ 'comparison point' is located along one of the satellite altimeter ground tracks, enabling the comparison of altimeter SSH with in situ SSH for each overflight. In the case of the T/P and Jason-1 missions, this translates to one comparison every 9.9 days along a particular ascending or descending ground track. The overflight frequency is higher if the comparison point is situated at an altimeter crossover location, in which case both the ascending and descending altimeter passes will be observed within the 9.9 day period.

In its most basic form, the altimeter absolute SSH bias ($Bias_{Alt}$) is defined as:

$$Bias_{Alt} = SSH_{Alt} - SSH_{InSitu} \qquad \text{Eqn 1-3}$$

where:

SSH_{Alt} is the sea surface height derived from the altimeter; and

$SSH_{In\ Situ}$ is the sea surface height derived from the in situ instrumentation.

A negative (-)ve bias is indicative of SSH being measured too low by the altimeter (i.e., the altimeter range is too long or the orbit position is too low).

This seemingly straightforward problem has three main difficulties:

1) The comparison point must be located sufficiently out in the open sea to avoid land contamination to any of the altimeter instruments (constrained primarily by the large footprint size of the water vapour radiometer). This introduces considerable logistical and operational difficulties.

2) The SSH estimates from the in situ instrumentation must be computed in a reference frame consistent to the altimeter-derived estimates to allow direct comparison.

3) The accuracy required at the in situ comparison point (a dynamic open sea environment) represents a demanding geodetic problem at the very limit of currently known techniques.

For the calibration of T/P, the NASA and CNES agencies operated dedicated absolute calibration sites at Harvest platform offshore from California (Christensen et al., 1994) and offshore from Lampedusa Island in the Mediterranean Sea (Menard et al., 1994). The Harvest platform site (Figure 1-3) illustrates the concept of the in situ calibration site. The platform is located on an ascending altimeter ground track approaching the coast of California. Sea level at the platform is observed using a series of sea level measurement systems mounted to the platform structure. Filtering techniques are used to remove the effect of wind waves and swell on the in situ estimate of SSH. The position of the platform (and hence the tide gauge) is fixed in an absolute reference frame using Global Positioning System (GPS) data from a receiver mounted to the top surface of the platform (readers not familiar with geodetic applications of GPS are referred to Herring (1999) for an in depth review of contemporary techniques). The in situ SSH estimate at the time of overflight is used to directly estimate the altimeter absolute bias (see Christensen et al., 1994 for site details). The measurement of additional variables, such as meteorological, atmospheric and sea state parameters, allows further investigation into the various error sources of the altimetric measurement system.

Figure 1-3 The Harvest platform dedicated calibration site (NASA) for T/P and Jason-1. (image courtesy B. Haines).

A number of techniques are available to measure in situ SSH at a chosen comparison point. GPS equipped buoys have been used by both the NASA and CNES sites for the direct measurement of SSH around a specific comparison point (see Born et al., 1994 and Bonnefond et al., 2003b for example). The concept, which consists of a GPS antenna and receiver mounted on a floating platform, ideally suits altimeter calibration experiments. Data from the GPS buoy allow the estimation of sea level on an epoch-by-epoch basis in an absolute reference frame, directly comparable to the altimeter. GPS buoy technology forms the focus of the improved calibration methodology presented in this Thesis, and is the subject of the following Chapter.

The buoy technique also allows the estimation of a local precise geoid at the altimeter comparison point (Key et al., 1998 and Bonnefond et al., 2003a for example). Precise knowledge of the geoid allows the extrapolation of coastal tide gauge SSH to an offshore comparison point. The extrapolated SSH estimates remain in the same reference frame as the altimeter enabling direct comparison against the altimeter SSH, and computation of the absolute SSH bias. A similar technique may be utilised in areas covered by precise regional geoid models. Studies such as Dong et al. (2002b) and Woodworth et al. (2004) have successfully integrated geoid models, such as the European Gravimetric Geoid (EGG97), with GPS equipped tide gauge data, and tidal difference modelling to estimate absolute bias in areas surrounding the United Kingdom.

In relation to individual calibration sites, the direct estimation of SSH at the comparison point using an in situ platform or a GPS buoy is accepted as the most accurate technique, as it is not limited by extrapolation methods and the use of

geoid models. A further review of results from different in situ calibration techniques in relation to the Jason-1 mission is presented in Chapter 4.

Whilst a dedicated calibration site offers the ability to solve for the absolute SSH bias, the limited number of observations (one bias estimate every 9.9 days in the case of T/P and Jason-1) precludes any statistically significant estimation of bias drift over a short period. Over the 6-month calibration phase of the Jason-1 mission for example, an individual calibration site will derive a maximum of 18 absolute SSH bias estimates. The precision (σ, at 1 standard deviation) of a single absolute bias estimate is determined by assimilating error terms from both the in situ ground system and the altimeter measurement system (see Table 1-2). Assuming independent observations, the precision of the mean absolute bias estimate will be $\sigma/\sqrt{18}$. This small sample size prevents any statistically significant estimate of bias drift from an individual calibration site over such a short period (especially at the 1 mm/yr level). To achieve statistically significant estimates of bias drift, either the measurement precision must be significantly reduced, or the number of observations needs to be significantly increased. Given σ is dominated by the error terms from the altimeter, the only possible option over such a short period is to significantly increase the number of observations, in effect creating many 'calibration sites'.

This introduces the concept of the second well established calibration technique which effectively increases the number of observations to allow the determination of statistically significant estimates of bias drift. The technique known as the "tide gauge network calibration" achieves this by sacrificing the ability to determine *absolute* bias, as per the previously discussed methodology. The two very different techniques complement each other in the overall calibration process.

1.3.2 Tide Gauge Network Calibration

The tide gauge network technique relies on monitoring the altimeter SSH bias drift using the global tide gauge network. Mitchum (1994) first reported a 300 day comparison of T/P data with data from 71 tide gauges. The Mitchum (1998) study further refined the technique highlighting the sensitivity of the methodology to determining low frequency drift in the altimeter. Chambers et al. (1998) and subsequently Mitchum (2000) have further developed this technique.

In its most basic form, the technique relies on a relative comparison of coastal tide gauge data with nearby altimeter SSH estimates. A time series of altimeter SSH is compiled at a point relatively close to a tide gauge location (typically within ~50 km). The altimeter time series is differenced from the tide gauge sea level time series to generate a differential SSH series in which ocean signals common to both sites are predominantly cancelled. The signal remaining in the differenced series is dominated by the drift of the altimeter and the land motion at the tide gauge. Relying on statistical independence of the differenced time series computed at different tide gauge sites (Mitchum, 1998), the variance of the combined drift series is significantly reduced in comparison to the individual differenced series used in the computation (Leuliette et al., 2004).

The dominant error term and primary difficulty of the tide gauge technique relates to the estimation of the land motion at the tide gauge. As for sea level, the Earth's crust responds to a range of processes acting over very different spatial and temporal scales. Over geological timescales, the dominant global process is glacial isostatic adjustment (Peltier, 2001). Other contributing factors include regional tectonic uplift or subsidence (Yokoyama et al., 2001 and Cazenave et al., 1999 for example), volcanic effects, surface mass loadings (van Dam et al., 1994 and van Dam et al., 2001 for example), subsurface water extraction and seasonal effects (Blewitt et al., 2001) for example. Space geodetic techniques such as GPS and DORIS are used to determine estimates of vertical crustal velocity with varying degrees of success. The determination of these velocity rates and their uncertainties is a complex problem that represents the crux of current research within the geodetic positioning literature (see for example Blewitt, 2003 and Dong et al., 2002a). The use of GPS for precise vertical positioning, a vital component for both calibration techniques, is further reviewed in Chapter 3 of this Thesis.

Whilst the tide gauge calibration technique has proved sensitive to bias drift and distinct jumps in the drift series, the technique is however purely relative and hence is unable to detect time independent offsets. Issues of geographically correlated error (Haines et al., 2004 for example) are also indistinguishable using the tide gauge technique, highlighting the need for a multi faceted calibration approach incorporating both calibration approaches.

1.3.3 The Jason-1 Calibration Plan

The continued operation of TOPEX/Poseidon after the launch of Jason-1 in December 2001 provided the ideal opportunity for the cross calibration of the two missions. To support the cross calibration, Jason-1 was placed in an orbit achieving identical ground tracks to T/P, ensuring the two altimeters sampled the same spatial location (within ~1 km) separated by ~70 seconds (Menard et al., 2003).

This formation flight phase provided unprecedented ability to compare the measurement systems and ensure the consistency of the long-term sea-level record. The configuration was central to the Jason-1 calibration plan (Menard and Haines, 2001), as defined by the T/P and Jason-1 Science Working Team (SWT). The tandem phase ran for approximately seven months from Jason-1 cycle 1 (18^{th} January, 2002), up to and including cycle 22 (14^{th} August, 2002).

The Jason-1 calibration plan presents proposed calibration experiments to verify the altimetric range and associated corrections, orbit, wind speed and SWH observables (Menard and Haines, 2001). Both the absolute bias and bias drift of specific instruments were required as outputs of the calibration process. The plan also sets out requirements for ongoing strategies to monitor the performance of the spacecraft throughout the life of the mission.

1.4 Thesis Aims and Outline

The primary aim of this Thesis is to develop and implement an improved in situ altimeter calibration methodology for the Bass Strait calibration site, first utilised in 1992 for the calibration of the T/P mission (White et al., 1994). As the sole in situ calibration site in the Southern Hemisphere, and the only one of its kind on a descending T/P – Jason-1 altimeter track, the Bass Strait site has an important contribution to make to the global calibration and validation effort. The motivation to revisit and improve the White et al. (1994) study for this research has been the launch and calibration requirements of the Jason-1 altimeter. Unprecedented in the history of satellite altimetry, the T/P and Jason-1 altimeters flew in formation flight during the seven-month calibration phase of the new mission. This calibration phase between January-August 2002 represents the primary data acquisition period for this research.

This introductory Chapter has outlined the importance of satellite altimeter calibration and cross calibration to the measurement of oceanographic processes which reflect, and in many cases influence, the climate of this planet. Calibration is vital to the improved measurement and understanding of low frequency oceanographic signals, such as the El Niño Southern Oscillation (ENSO), decadal variability and regional and global mean sea level change. A brief history of satellite altimetry has been presented highlighting the progressively improving quality of altimeter missions. The basic altimeter measurement system has also been reviewed with an emphasis on identifying components that may contribute to systematic offsets or long-term erroneous drifts. Each of these components are revisited in the later analysis of data observed at the Bass Strait calibration site.

Calibration of the satellite altimeter 'system' is clearly a multi-faceted, complex problem which requires a multi-disciplinary approach from many different research groups, using many different techniques. The two main calibration techniques for the determination of absolute bias and bias drift have been briefly reviewed in this Chapter, highlighting the challenges that confront them. The continuous improvement in altimeter accuracy and precision dictates a parallel improvement is required from both the calibration methodologies and associated instrumentation.

The framework of the methodology developed throughout this Thesis was proposed and included in the SWT calibration plan (Menard and Haines, 2001), and subsequently refined throughout the calibration process. The methodology focuses on the development of an innovative geometric technique which is based on the

integration of unique GPS-equipped buoys, with a continuously operating oceanographic mooring array and a coastal tide gauge. The multi-faceted nature of the calibration problem and integrated approach to the methodology is reflected in the structure of the Thesis.

Chapter 2 introduces the concept of water level measurement using the Global Positioning System. The development and utilisation of GPS buoys is central to the methodology developed in this Thesis, providing an elegant geometrical solution to the absolute calibration problem. The GPS buoy concept has been frequently applied to in situ altimeter calibration with mixed results presented in the recent scientific literature. A contemporary review of GPS buoy research is presented, with a focus on design considerations and the relevant research application. Various designs within the literature are contrasted before presenting the development of the University of Tasmania (UTAS) Mk I and Mk II designs. Operational considerations for the highest accuracy applications are investigated, with particular reference to testing the Mk II design in preparation for integration into the Bass Strait calibration methodology.

Chapter 3 discusses the geodetic framework required to achieve absolute calibration of the altimeter at the 1 cm level or better. The Chapter provides an initial review of reference frames, discussing some of the issues which are especially important in the context of this study. The GPS analyses undertaken at the Bass Strait site are then presented. The analysis aims to determine in situ estimates of sea surface height (determined using the GPS buoy deployments in conjunction with an oceanographic mooring and coastal tide gauge) in the same coordinate reference frame as the altimeter. This investigation incorporates a review of the geodetic computational standards, which are required to ensure a homogeneous set of comparative time series data. As part of this investigation, improvements made to a number of routines in the GPS analysis suite 'GAMIT' (King and Bock, 2003) are reviewed. As part of an accuracy assessment of the land based GPS reference processing, this Chapter progresses to explore GPS time series analysis, particularly in the vertical component. Using sites in the region surrounding the Bass Strait calibration site, solutions from various analysis centres are compared to assist in the preparation of a formal error budget for the Bass Strait calibration results.

Chapter 4 forms the main body of the Thesis, presenting the methodology, experiment design, processing strategy and results from the Bass Strait calibration site. The methodology is first introduced with a review of concurrent calibration experiments, developed for the launch of the Jason-1 mission. The experiment

design is then given, with an initial emphasis on instrumentation and calibration geometry. Data processing strategies adopted for each instrumentation component are presented followed by a rigorous error budget. Absolute bias results from the Bass Strait site for both T/P and Jason-1 are presented with comparison to the dedicated NASA and CNES calibration sites offshore from California and Corsica respectively. Finally, investigations surrounding the suspected drift of the JMR instrument are presented.

Chapter 5 revisits the tide gauge, as the final component of the altimeter calibration instrument ensemble. As discussed previously, the tide gauge network remains fundamentally important for monitoring altimeter bias drift. The GPS buoy instrumentation developed and presented in Chapter 2 is utilised in a second series of experiments focussing on tide gauge accuracy in the Australian and Antarctic regions. Results and analysis from deployments at the Bass Strait calibration site, the unique tide gauge installation at Macquarie Island and at the tide gauge site at Davis Station, Antarctica, are presented as part of the calibration study.

The concluding Chapter summarises the developments made during this Thesis. Conclusions and recommendations are presented in relation to future calibration and validation requirements for sea level studies. The importance of continued calibration and cross calibration is reiterated, demonstrating the fundamental requirement of the calibration process to proposed follow-on missions, such as Jason-2.

Readers are referred to the relevant appendices (both hard copy and CD-ROM) for supplementary material referenced throughout the Thesis.

Chapter 2

GPS Buoy Development

2.1 Introduction

A central component to the altimeter calibration methodology presented in this Thesis is the development of a robust and readily portable GPS buoy system capable of determining accurate sea surface height at the comparison point in Bass Strait.

GPS buoys enable the measurement of sea level in an absolute reference frame on an epoch-by-epoch basis. The concept consists quite simply of a floating platform equipped with GPS instrumentation. Provided the position of the antenna is known with respect to the water surface, the instantaneous position of the buoy and the height of the water surface may be determined at sampling rates of up to 10-20 Hz (0.1-0.05 sec).

The GPS approach to sea level measurement offers many advantages over other traditional techniques, primarily due to the flexible sampling strategy and the ability to determine sea surface height in an absolute reference frame. Whilst the technique has progressed since early designs in the late 1980s, many of the design criteria remain the same. Application areas are now as diverse as buoy designs, ranging from satellite altimeter calibration to tsunami research and river level monitoring. The breadth of applications is demonstrated in the literature and within the International Association of Geodesy (IAG) Special Study Group 2.194 (SSG 2.194: GPS Water Level Measurements) and Working Group 4.5.3 (WG 4.5.3: High Precision Positioning on Buoys and Moving Platforms).

This Chapter commences with a review of literature associated with GPS based water level measurement. The development of GPS buoys at the University of Tasmania (UTAS) is detailed with specific emphasis on the Mk II design utilised for the Bass Strait calibration of T/P and Jason-1 (Chapter 4) and tide gauge

verification experiments in Tasmania, the Sub-Antarctic and Antarctic (Chapter 5). The Chapter concludes with an analysis of various operational considerations that relate specifically to the UTAS Mk II buoy, yet apply to any GPS buoy application requiring the highest levels of absolute accuracy.

2.2 Water Level Measurement using GPS

The following sections provide a review of contemporary literature, with an emphasis on the research application and buoy design considerations. Little emphasis has been given to GPS processing techniques, as these are discussed in Chapters 3 and 4. The review begins chronologically, with subsequent division according to design philosophy and application focus.

2.2.1 Initial Research

Early development of the GPS buoy technique was driven largely by the realisation that kinematic GPS estimates of sea surface height could be used as an independent calibration or verification to space based oceanographic missions such as ERS-1 and TOPEX/Poseidon. Early research, such as Hein et al. (1990) and Kelecy et al. (1992), were primarily proof of concept studies, utilising a range of different design configurations.

The work conducted by the Institute of Astronomical and Physical Geodesy at the University FAF Munich (Hein et al., 1990, Hein et al., 1992) utilised a large ruggedised navigation buoy deployed in the Medem-Reede region of the North Sea. The antenna was positioned approximately 5.7 m above the mean water level, necessitating the measurement of the inclination of the buoy structure to correctly resolve the antenna height to the vertical component. Hein et al. (1990) reported observed tilts at the 5-7° level which translated to corrections at the 0.5 to 5 cm level at the water surface. Measurement of the antenna height during calm conditions was only achieved to an accuracy of $\pm$ 7 mm. The buoy was designed with the intention of running autonomously; hence issues such as power supply and data telemetry were first raised. Further operational issues discussed were potential buoyancy changes due to gas discharge used for power consumption. Other important issues included the floatation position when the buoy is tight on

the tether and potential techniques that would enable the measurement of 'dip-in' depth of the buoy.

Research at the Colorado Center for Astrodynamics Research (CCAR) at the University of Colorado began in 1989, with an emphasis on sea level measurement at the centimetre level. Papers by Rocken et al. (1990) and Kelecy et al. (1992) present results from buoy deployments offshore from La Jolla and Point Conception in California. These experiments tested the suitability of GPS water level measurement as a means of providing an in situ calibration to satellite altimeter missions. Specifically, Kelecy et al. (1992) presented a proof of concept experiment based at the Texaco owned Harvest platform, designated as the NASA/JPL verification site for the TOPEX radar altimeter (to be launched later in the year of publication). The experiment utilised a spar type buoy, deployed within 400 m of Harvest platform. The design differed considerably to Hein et al. (1990), attaching only the antenna on the buoy structure, with the buoy tethered to a nearby boat from where the receiver was operated. The spar buoy consisted of a 40 ft length of 6" PVC pipe with approximately 170 kg of ballast. The design aimed to minimise vertical and rotational motion resulting from wave action. Vertical oscillations and tilting were still evident, underscoring the need to monitor the antenna position and orientation with respect to the instantaneous water surface.

Kelecy et al. (1992) made the following statement in relation to buoy design which remains central to present day GPS buoy development: "Dynamically, a design that minimizes motion in all directions is desirable. The GPS antenna should be mounted in such a way as to make calibration of the antenna phase centre to the mean sea surface both easy and accurate. The buoy should be large enough to contain the instrumentation and be dynamically stable, yet small enough to be manageable when deploying and retrieving".

Kelecy et al. (1994) revisited the spar buoy with further trials approximately 15 km offshore from La Jolla, California. The spar buoy was augmented with two pressure transducers enabling the measurement of tilt and dip-in depth of the buoy. A second buoy design was also deployed, this time utilising a life preserver as the floating platform. This wave rider concept consisted quite simply of an antenna fixed to a life preserver, protected with a clear dome and tethered to a boat where the receiver and power system were operated. The wave rider design positioned the antenna approximately 120 mm above the mean water level, determined in calm conditions to an accuracy of $\pm$ 4 mm. As opposed to the spar design, the

wave rider was designed to follow the exact water surface; hence the dynamic accelerations experienced by the antenna were expected to be greater than from the spar design. To the wave rider's advantage, the low profile design precluded the requirement to monitor the buoy's tilt and vertical motion with respect to the water surface. The design was also symmetrical about the central vertical axis (a toroid) which assists the understanding of the buoy dynamics. Results from the trial indicated that comparable results could be obtained from the two very different designs.

This early research into GPS based water level measurement set the foundation for future design and application development. The basic concepts behind the wave rider style and the more sophisticated offshore platforms remain largely unchanged. Application areas identified by the early publications include:

- Satellite altimeter calibration
- Sea level monitoring to supplement tide gauge networks
- Estimation of a precise relative geoid
- Determination of wave spectra and direction
- Current / eddy tracking

Several advantages and disadvantages of different buoy designs and limitations to the methodology were also identified:

- Each buoy design will have its own dynamic response to the ocean, which must be understood for the highest accuracy applications.
- The position of the antenna with respect to the water surface must be known at all times. This is particularly critical for large offshore buoys subject to significant dynamic motion, and high platform tilting.
- Lightweight buoys operated from a boat are restricted logistically due to the boat and crew requirements.
- An important consideration is the effect of the tether on the buoy dynamics and floatation level.
- Instrumentation complexity increases significantly for offshore, continuously operating systems. Issues of power management and data telemetry become significant.
- Finally, the highest accuracy applications are restricted to short baseline differential GPS processing, with a static reference station located within 15 km (or less) of the buoy site.

2.2.2 Lightweight Buoy Development

Following the initial research, Born et al. (1994) present the first T/P calibration results using a GPS buoy at the Harvest platform. The CCAR spar buoy used in Kelecy et al. (1994) was modified with the addition of a Magnerule™ sensor to provide an additional independent measurement of the distance between the waterline and the GPS antenna. The buoy was deployed for a 1 hr period (centred on the T/P overflight time) acquiring data at 1 Hz. Bias estimates for T/P determined from the GPS buoy were comparable to those computed from the in situ instrumentation at Harvest platform (Christensen et al., 1994). The study represented a successful conclusion to the development of the CCAR spar buoy.

The second dedicated calibration site for the T/P mission was located at Lampedusa in the Mediterranean (Menard et al., 1994), and operated by the Centre National d'Etudes Spatiales (CNES). The CNES calibration methodology utilised the large ruggedised buoys developed by Hein et al. (1990). The Lampedusa experiments were compromised due to damage of in situ equipment in rough weather, hence the CNES calibration site was moved to the island of Corsica.

Further research conducted by the CCAR group focused on the development of GPS processing algorithms for medium accuracy (~1 m RMS) positioning of ocean buoys as part of the Fast Pegasus experiments (Key et al., 1996 and Key et al., 1999). In comparison with the centimetre level differential kinematic processing of previous experiments, Key et al. (1999) presented a precise point positioning (PPP) algorithm for single receivers. With a reduced accuracy in comparison to short to medium baseline differential processing, the PPP technique eliminated the need for land based reference receivers allowing significantly greater range for the Fast Pegasus application.

By the mid 1990s many groups were investigating GPS buoys for a range of applications. Schutz et al. (1995) developed a wave rider buoy similar to Kelecy et al. (1994) as part of a T/P calibration study in the Galveston Bay region of the Gulf of Mexico. Key et al. (1998) also revisited the wave rider buoy at Harvest platform, with a series of deployments undertaken in 1995. Sixteen deployment locations were chosen with the primary aim of mapping the sea surface over a 10 km diameter circular area surrounding the Harvest platform. The new wave rider buoy was again based on a life preserver as the floatation platform (Figure 2-1), with the receiver operated from a boat within ~6 m (20 ft). The choke ring

Antenna Reference Point (ARP) was positioned approximately 87 mm above the mean water level. The project demonstrated the ability to map the sea surface for regional oceanographic experiments. The Key et al. (1998) experiment also suggested a preference for the simple wave rider style in comparison to more complex designs.

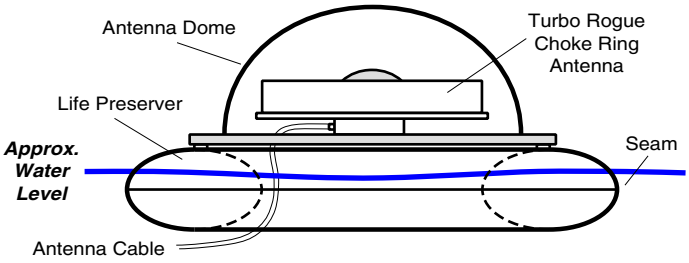

Figure 2-1 Schematic view of the CCAR wave rider GPS buoy (adapted from Key et al., 1998).

Parke et al. (1997) provided a review of GPS based water level measurement, with an emphasis on existing and potential applications. In particular, the authors drew attention to the potential value of GPS buoys for regional oceanographic experiments, including investigations into tides, currents, jets, fronts and eddies. Parke et al. (1997) stress that for routine applications, the GPS buoy technique requires demonstration of high accuracy at significant distances from shore. This is a reoccurring statement throughout the relevant literature.

The first in situ measurement campaign at the relocated CNES calibration site in the Corsica area was undertaken in 1996/97. Large geoid gradients in the area lead to a series of experiments using the CCAR wave rider buoy design to map the geoid slope using similar methodology to the Key et al. (1998) study. The first experiment was carried out in May 1998 using two buoys (Figure 2-2a), with different antenna and receiver combinations (Exertier et al., 1998). Continuous deployment and retrieval from a small boat at different locations made the wave rider technique time consuming and logistically difficult. Subsequent investigations included the development of a catamaran style floating platform (Figure 2-2b), equipped with two GPS antennas. The design was first deployed in 1999 (Bonnefond et al., 2003b), towed at a constant speed covering an area approximately 20 km x 5.4 km centred on the ground track of the altimeter. The catamaran represented an innovative approach to mapping the sea surface, using two receivers on the catamaran to provide a redundant check. The differences in the height component between the two GPS antennae throughout the experiment had a standard deviation of 12 mm. Comparisons with a nearby tide gauge showed

a mean bias of 19 mm which (partly) reflects uncertainty in the floatation position of the catamaran when under tow. This bias was not considered to affect the geoid slope estimation due to the assumption of a constant towing speed through the water. This point does however underscore the importance of understanding the dynamics of the floating platform for absolute applications. The geoid gradients derived from the GPS catamaran have been integrated into the determination of the CNES and Observatoire de la Côte d'Azur (CERGA) altimeter calibration values, reducing the variability of T/P bias estimates from 49 mm to 33 mm (Bonnefond et al., 2003b). The episodic deployment (dependent on sea state conditions) of individual life preserver style GPS buoys (Figure 2-2c), remains central to the CNES/CERGA calibration methodology (Bonnefond et al., 2003a). The CNES/CERGA calibration strategy is discussed in further detail in Chapter 4.

Figure 2-2 CNES/CERGA buoy designs. (a) CCAR buoy design used in the Exertier et al. (1998) study. (b) GPS catamaran used for the Bonnefond et al. (2003b) sea surface mapping experiment. (c) Individual buoy used at the CNES/CERGA calibration site Bonnefond et al. (2003a). Images courtesy P. Bonnefond.

With increased significance placed on in situ verification of satellite altimeters in the lead up to the launch of the Jason-1 mission (December 2001), various groups developed GPS buoy based calibration experiments. Following an evaluation of the performance of T/P over the Great Lakes of the USA (Morris and Gill, 1994), researchers at Ohio State University (OSU) developed a series of calibration experiments undertaken in 1999-2001 utilising CCAR life preserver style buoys in Lake Michigan and Lake Erie (see Shum et al., 2003 and summaries in Cheng, 2004a and Cheng, 2004b).

Cardellach et al. (1999) and Cardellach et al. (2000) from the Institut d'Estudis Espacials de Catalunya (IEEC, Barcelona, Spain) presented results from a range of experiments for the calibration of ERS-1, ERS-2 and T/P off the Catalonian Coast and around the Balearic Islands. The IEEC work differs to previous studies due to

the extended baseline length (~80 km) and the development of a tri-buoy system (Figure 2-3a). The design was based on the connection of three life preserver style GPS buoys, each separated by a flexible ~2.8 m connection. Two of the buoys housed a choke ring antenna, connected to a separate receiver operated in a boat approximately 50 m away. The third buoy was simply a dummy of the same design and weight, included to ensure the entire system was symmetrical about the central axis. This innovative set-up was designed to enable a check between two solutions and provide a redundant data set to fill possible gaps. The second phase of the research was directed towards absolute calibration of the EnviSat altimeter (Torrobella and the GRAC-II team, 2003). The research refined the design, developing the 'bi-buoy' system (Figure 2-3b). The bi-buoy incorporates two wave rider buoys which are fixed 1.6 m apart using a rigid connection. Despite altered dynamics, the bi-buoy system allows additional quality control through comparison of observed versus known separation distance between the two buoys. Constraining this known distance in a combined multi-rover, single reference station GPS solution also has the potential to assist long baseline kinematic solutions.

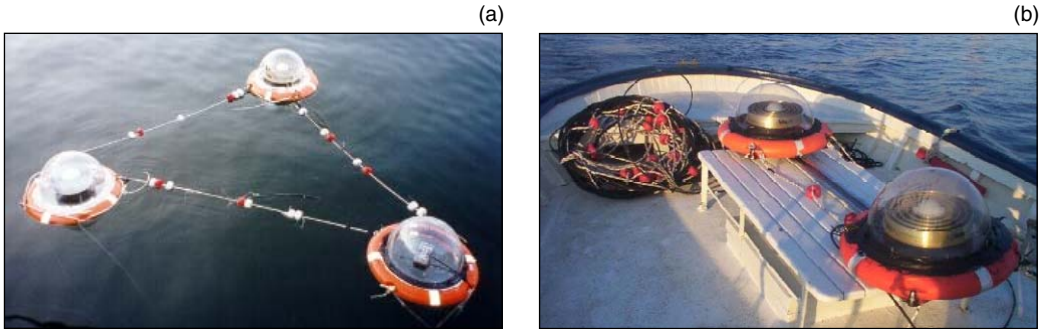

Figure 2-3 Multiple wave rider designs from the Institut d'Estudis Espacials de Catalunya (IEEC), CSIC Research Unit, Barcelona, Spain. (a) Tri-buoy design (Cardellach et al., 2000), Image courtesy J. Font. (b) 'Bi-buoy' design (Torrobella and the GRAC-II team, 2003), Image courtesy J. Torobella.

A second Spanish team (Universitat Politecnica de Catalunya (UPC) in Barcelona, Spain) have undertaken a range of GPS buoy experiments, primarily for Jason-1 calibration in the area surrounding Ibiza Island in the NW Mediterranean Sea. The buoy design is once again based on the CCAR life preserver, however the antenna is situated within the life preserver ring, reducing the antenna height with respect to the mean water level by ~100 mm (Figure 2-4a). The lower position of the antenna was found to be an improvement to the initial design (Figure 2-1),

lowering the centre of mass and hence stabilising the buoy and reducing buoy tilt (Martinez-Garcia et al., 2004).

Calibration activities in the eastern Mediterranean Sea are undertaken in the area surrounding the Greek island of Gavdos (Mertikas and the Gavdos team, 2002). The Gavdos collaborative project has incorporated GPS buoys developed at the Geodesy and Geodynamics Laboratory (GGL), at ETH Zürich. The buoys have aided in the calibration of airborne altimetry in the region of the calibration site (Geiger et al., 2003). The ETH design has moved away from the life preserver style, adopting a 0.4 m diameter spherical design (Figure 2-4b). The buoy is capable of autonomous operation as it houses the antenna, receiver and battery. Using a Novatel antenna and receiver the buoy is able to operate for approximately 20 hours.

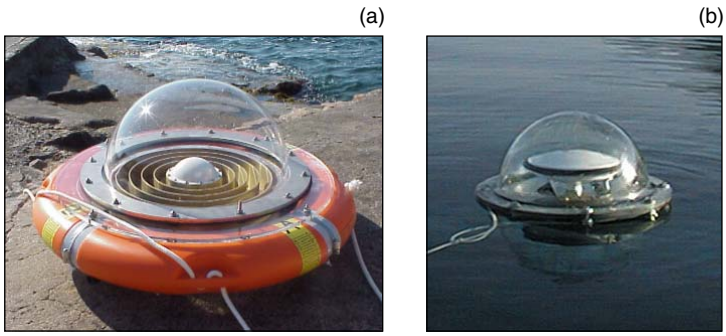

Figure 2-4 Wave rider 'life preserver' buoy designs. (a) Universitat Politecnica de Catalunya (UPC) design with choke ring antenna. Image courtesy M. Martinez-Garcia. (b) Geodesy and Geodynamics Laboratory (GGL), ETH Zürich design with a Novatel antenna. Image courtesy H-G. Kahle.

The move towards light weight, wave rider style buoys capable of autonomous operation over short periods, was also adopted for the UTAS Mk II buoy presented in §2.3 of this Chapter.

2.2.3 Autonomous 'Oceanic' Buoy Development

Lightweight buoys have the obvious advantages of portability, simplicity of design, low cost and ease of deployment. The lightweight designs are not however suitable for continuous deployment, where issues such as power generation and physical strength to survive the hostile oceanic environment is required. Since the initial development of the autonomous ruggedised GPS buoy by Hein et al. (1990), many groups have continued to use and develop large navigation beacon style buoys as GPS floating platforms. Regardless of the floating platform used, the development has focused on the accurate determination of the antenna height and orientation of the antenna with respect to the water surface. This measurement is crucial to the accuracy of the autonomous buoy design, and represents the main limitation to the absolute accuracy of the technique. Considerations such as power consumption, data telemetry, tethering techniques and project cost remain significant hurdles from an operational perspective. Deployment locations are also presently limited by minimising baseline lengths from land-based reference receivers for accurate differential GPS processing.

The development of offshore buoys has continued at the Institute of Geodesy and Navigation, University FAF in Munich, Germany, focussing on the in situ calibration of the EnviSat mission (Schueler et al., 2003). The buoy platform is cylindrical in shape, floating horizontally in the water, moored in ~120-140 m of water. To provide an indication of size, the buoy weighs approximately 2400 kg and has a volume of 9.4 m^3. Orientation of the antenna is achieved using a dual axis inclinometer and 'dip-in' depth of the buoy is measured using a pressure sensor attached to the base of the buoy. The pressure method proved partly problematic for the Schueler et al. (2003) study, recommending a replacement to alternative devices (for example, magnetic/resistive or capacitive devices, or infrared or sonar sensors).

Two further groups within Germany have progressed with developing ruggedised GPS buoy systems in support of altimetry calibration projects. Schone et al. (2003) and Forberg et al. (2003) present the design from GeoForschungsZentrum (GFZ) in Potsdam (Figure 2-5a). The GFZ buoy is completely autonomous, relying on solar energy to charge a large bank of batteries, which also act as ballast for the 6.4 m high buoy. The buoy system has been designed to withstand the rigours of deployment in the North Sea, subject to frequent storms and high sea states. Sensors, in addition to the GPS onboard the buoy, include a full meteorological sensor array, an accelerometer and gyro for tilt determination, a

pressure sensor for the measurement of 'dip-in' distance, water temperature and salinity and a visible spectrum camera (see the SEAL project page, Schone, 2003).

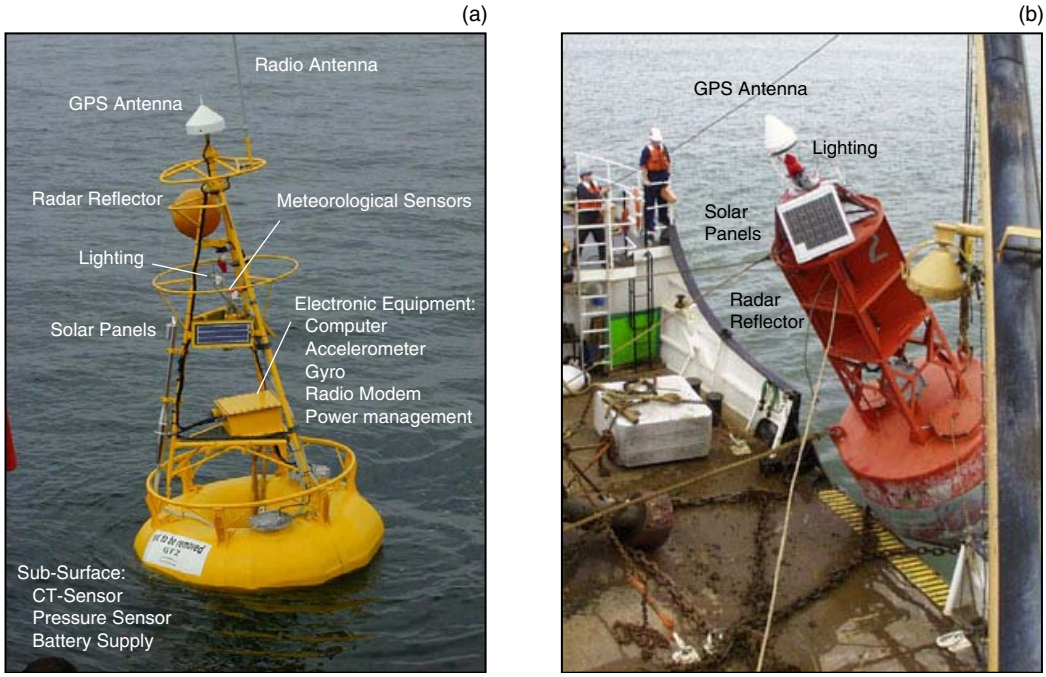

Figure 2-5 Offshore buoys developed for continuous operation. (a) SEAL/GFZ buoy deployed in the North Sea (image courtesy T. Schone). (b) NOS/NGS buoy being deployed in the San Francisco Bay (image courtesy G. Mader).

An alternative approach presented by the Technical University (TU) in Dresden has been to retrofit existing Marine Environmental Monitoring Network (MARNET) buoys, deployed at areas of interest in the Southern Baltic Sea (Liebsch et al., 2003). The system uses pressure sensors and dual axis inclinometers to monitor the orientation and position of the antenna and water surface respectively. Complete results for both the GFZ and TU projects were not published at the time of writing.

National Ocean Service (NOS) and the National Geodetic Survey (NGS) in the USA have developed a series of large buoys equipped with GPS for real-time monitoring applications in US harbours (Figure 2-5b). Similar real time buoys have been deployed in the Mississippi coastal waters for tidal datum determination (Bisnath et al., 2004), and in also in Japan as part of a tsunami monitoring system (Kato et al., 2001). The Japanese system is large (Figure 2-6), with the GPS antenna 6.4 m above the mean water level, with a further 7 m of buoy structure below the water surface. Orientation and position of the draught line of the buoy is measured with an array of three sensors onboard the buoy. A dual axis

inclinometer and vertical accelerometer monitors the tilt of the buoy while an ultrasonic distance measurement system monitors the draught line (Kato et al., 2001). Other studies, such as Colombo (2000), have also investigated the application of GPS to tsunami warning systems.

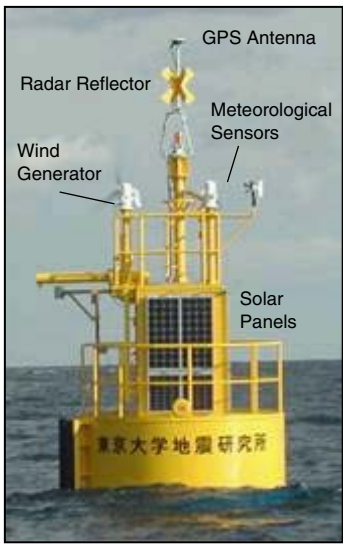

Figure 2-6 Tsunami monitoring buoy deployed offshore from the Sanriku coast in Japan (Kato et al., 2001). The distance from water level to GPS antenna is ~6.4 m. (Image courtesy T. Kato).

Oceanic GPS buoys capable of measuring to high accuracies remain under continuous development. The examples taken from the literature demonstrate the concept is well established. Durability and reliability remain to be demonstrated over significant deployment durations. Parallel developments in GPS processing techniques will extend the application of these large autonomous buoys, allowing deployment at greater distances from land and static reference stations.

2.2.4 Miscellaneous Water Level Applications

GPS water level measurement has been applied to a number of applications outside the previously mentioned coastal and offshore oceanographic and geodetic applications. Moore et al. (2000) and Moore et al. (2002) present a review of the RiGHt project, monitoring river levels using GPS heighting. The project developed a small autonomous buoy to monitor river levels in the UK. The project proposed near real-time monitoring at comparable accuracy (1-2 cm) to traditional river monitoring equipment using a modified RTK GPS technique.

Winkler and Wooley (2002) present a spar buoy application designed to measure currents in rivers and dams. The study involved the use of medium accuracy (decimetre level), single frequency DGPS to monitor current direction and velocity.

Doppler-based measurements from GPS are being applied to wave buoys for coastal weather forecasting. de Vries et al. (2003) present a review of the spherical Datawell Dwr-G GPS wave buoy designed to provide relative estimates of wave magnitude and direction.

This brief range of miscellaneous applications provides an indication of the breadth of GPS-based water level measurement, extending across all levels of the accuracy spectrum from sub-centimetre to decimetre level positioning.

2.2.5 Summary

The literature reveals three common buoy design styles:

1. Light weight wave riders, tethered and operated from a boat.
2. Light weight wave riders capable of short periods of autonomous operation.
3. Ruggedised oceanic buoys capable of autonomous operation for extended periods in any sea conditions.

Each design has individual advantages and disadvantages in addition to suitability to specific applications, as summarised in Table 2-1.

Regardless of buoy design, the measurement and monitoring of the antenna height with respect to the water surface remains central to high accuracy applications. The wave rider style removes the need to monitor buoy tilt and 'dip-in' depth, however the mean height of the antenna above the water surface must still be accurately determined.

The effect of the tether on the buoyancy and dynamics of the buoy must also be considered; an issue that was found regularly overlooked within the literature. Almost universally ignored in the GPS buoy literature is the effect of the antenna dome on the position and variability of the antenna phase centre. The range of antenna domes is significant, as shown in Figures 2-2, 2-3, 2-4 and 2-5 respectively. The suitability of standard 'static' antenna phase centre variation patterns for buoy applications where the antenna is continuously changing orientation (both in elevation and azimuth) is also not discussed.

The highest accuracy GPS buoy applications remain constrained to differential processing over short to medium baseline lengths. This constraint prevents high accuracy water level measurements at significant distances ($>$ 30 km) from land based reference receivers. Colombo et al. (2000) and Colombo et al. (2001) provide interesting discussion on the distance and accuracy limitations for long baseline kinematic solutions (including the use of a novel mean height constraint to speed the algorithm convergence over long baseline distances). The baseline constraints at the Bass Strait calibration site are discussed in Chapter 4.

Table 2-1 Advantages, disadvantages and applications of current GPS buoy designs.

Buoy Design	*Description*	*Advantages*	*Disadvantages*	*Applications*
Light weight, toroid wave rider design (Antenna only) 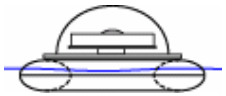 e.g. Key et al. (1998)	• A light weight buoy, commonly constructed using a life preserver as the floating platform. • The buoy houses the GPS antenna only, and is operated from a boat. • The antenna ARP is positioned 50 to 200 mm above the mean water level.	• Low cost, readily available construction materials • Readily portable • Follows the instantaneous sea surface • No requirement to monitor 'dip-in' depth or platform tilt	• Deployment requires logistical support (personnel and boat) during the entire deployment • Must be tethered during operation • Restricted deployment due to sea state and waves breaking over the buoy structure. • Short duration deployment only	• In situ absolute calibration of altimeters (both aircraft and spacecraft based) • Sea surface mapping • High frequency wave spectra and direction • Precise orthometric height transfer over water • Current tracking (limited by boat tether) • River / lake height monitoring
Light weight, toroid wave rider design (Autonomous)  e.g. Watson et al. (2003)	• A light weight buoy, housing the GPS receiver, antenna and battery power. • Autonomous operation possible either tethered or free to drift. • The antenna ARP is positioned 50 to 200 mm above the mean water level.	• See directly above • Can be tethered or free to drift • Low centre of mass helps reduce platform tilts • Dynamics not affected by the antenna cable • Autonomous operation for periods up to ~5 days	• Deployment requires logistical support • Restricted deployment due to sea state and waves breaking over the buoy structure. • Short to medium duration deployment only	• See directly above • This design is suited to applications requiring autonomous operation for short periods • Current / eddy tracking • River / lake height monitoring • Tide gauge verification
Ruggedised, oceanic, autonomous design  e.g. Schone et al. (2003)	• A large, ruggedised buoy housing GPS system, power storage and generation and data telemetry. • Autonomous operation over significant durations. • The antenna ARP is generally positioned 5 to 7 m above the mean water level.	• Ruggedised design allows continuous deployment regardless of sea conditions • Buoy can house additional sensors such as meteorological sensors, sea temperature, salinity, air quality etc. • Does not require personnel at sea to operate	• High cost, not readily portable • Antenna does not follow the instantaneous water surface • Difficult to accurately monitor the position of the antenna with respect to the water surface • Reliability issues with power and telemetry systems	• In situ absolute calibration of altimeters • Continuous sea level / tidal monitoring • Continuous tsunami monitoring • Real time applications

2.3 UTAS GPS Buoy Development

GPS buoy research at UTAS was initiated during a study involving a historic tidal benchmark at Port Arthur on Tasmania's south east coast (Watson, 1999 and Pugh et al. 2002). The project required an accurate height transfer between two locations separated by approximately 1.2 km of water. The UTAS Mk I buoy design was used at the Port Arthur site, subsequently leading to the development of an improved and more robust Mk II design, suitable for both coastal and offshore deployments.

2.3.1 Mk I Design

The very simple 'Mk I' prototype design followed the wave rider style developed by Kelecy et al. (1994) and later by Key et al. (1998). The buoy design supported solely the GPS antenna, restricting operation to within approximately 5-10 m of the shoreline or tethered to a boat where the GPS receiver is stored and operated (i.e., within antenna cable length). The floating platform consisted of a section cut from a heavy-duty plastic drum, braced and partially filled with polystyrene foam for buoyancy. Leica AT202+GP antennas and custom made Perspex antenna domes were fitted to the buoys. The buoy design is shown in Figure 2-7.

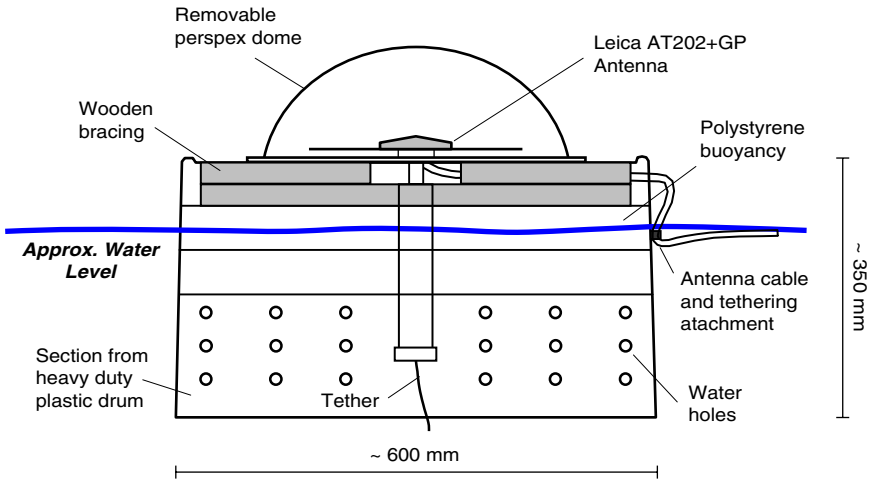

Figure 2-7 The UTAS Mk I buoy design. Shown in section.

The buoys were successful in aiding the determination of a precise water level slope and hence a relative geoid. This enabled the precise height transfer over a 1.2 km stretch of water. The buoys were also instrumental in quantifying local oceanographic behaviour, specifically the measurement of a seiche oscillation with a

period and amplitude of approximately 50 minutes and 30 mm respectively (Watson, 1999).

The main design limitation was found to be the restriction of operating the GPS receiver from the shore or a boat. This was considered a logistical restriction, especially for inshore applications requiring relatively long measurement campaigns. The design also has a relatively high centre of mass and was found susceptible to tilt from small surface waves. For studies requiring absolute sea level, a choke ring antenna and improved antenna dome were also required, leading to the development of the Mk II design.

2.3.2 Mk II Design

The Mk II buoy design is a ruggedised wave rider style of buoy overcoming the limitations of the 'life preserver' approach as mentioned above. The buoy was designed in conjunction with Dr Tony Sprent (UTAS), for both inshore and offshore applications requiring absolute SSH estimates for periods up to 5 days. The most significant difference in the design is the ability to operate the buoy autonomously, with the antenna, receiver and associated battery power housed within the central buoy capsule. The buoy can therefore operate tethered to a mooring or boat or be free to drift. When tethered from a boat, the tether can be sufficiently long to prevent any influence from the boat, both with respect to wave conditions and GPS multipath. The battery and receiver are positioned low within the capsule, lowering the centre of mass and stabilising the buoy in the water. The primary floatation system consists of a triangular stainless steel tubular frame (25 mm in diameter) which supports three compressed cell polystyrene floats, each 300 mm in diameter. The buoy design is shown in section in Figure 2-8.

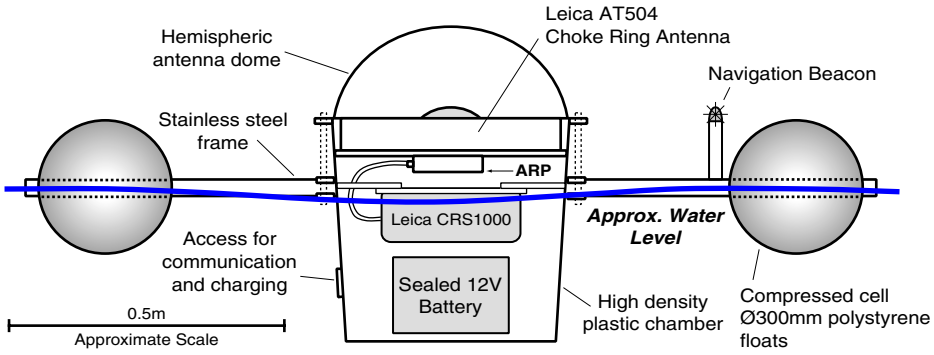

Figure 2-8 Schematic view of the UTAS Mk II buoy design.

The central capsule is designed around the strength of a GPS choke ring antenna. A hemispheric antenna dome covers the antenna and is custom made out of an acrylic polyvinyl chloride plastic alloy, generically called 'Sunloid-KD'. The material is uniformly 3 mm thick and is held in place using two 10 mm high-density plastic rings. The rings clamp the dome to the buoy capsule using a 6 mm O-ring and 12 stainless steel fasteners, achieving a waterproof seal (Figure 2-9).

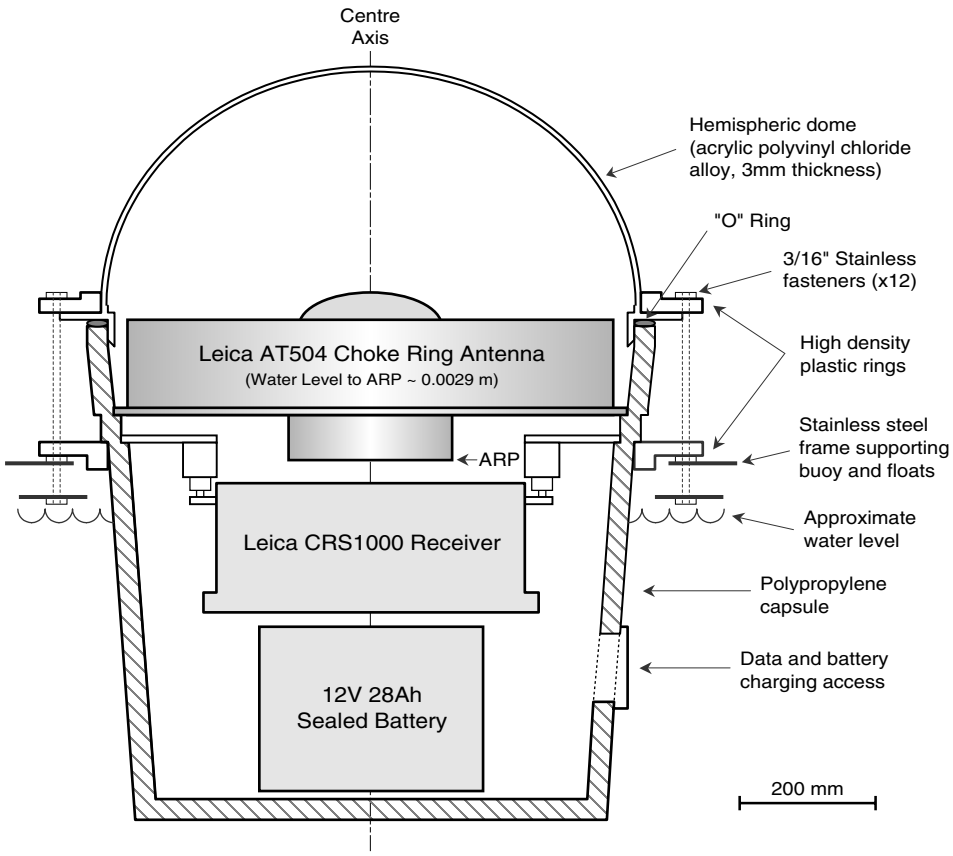

Figure 2-9 Schematic view of the internal layout of the Mk II capsule.

The Mk II design is large enough to incorporate most geodetic GPS receivers, with enough space for a sealed 12V battery of approximately 28 Ah capacity. The UTAS buoys utilised Leica CRS1000 receivers and Leica AT504 choke ring antennae. The high power consumption of the CRS1000 units enable only ~20 hours of continuous operation with the 28 Ah battery capacity. Recent low power receivers (for example the Trimble 5700 unit) would allow approximately 5 days continuous operation without battery charging. Typically observation rates are 1 Hz, with the option of 10 to 20 Hz measurements for improved determination of the wave characteristics.

The antenna, receiver and battery are constrained about the central axis of the capsule and floatation frame, making the buoy symmetrical about this axis. The Antenna Reference Point (ARP) sits approximately 29 mm above the mean water surface (see §2.4.1). The only feature that is positioned above the plane of the top surface of the antenna (apart from the antenna dome) is a small battery-operated navigation light for night deployment (see Figure 2-8).

The Mk II buoy maintains the advantage of portability, with an operational weight of approximately 31 kg (battery alone is 11 kg) and diameter of 1.6 m. The buoy can be placed in the water by hand or in rougher conditions lowered using a rope attached to each apex of the floatation frame. The completed buoy is shown deployed in Figure 2-10(a) and in plan view in Figure 2-10(b).

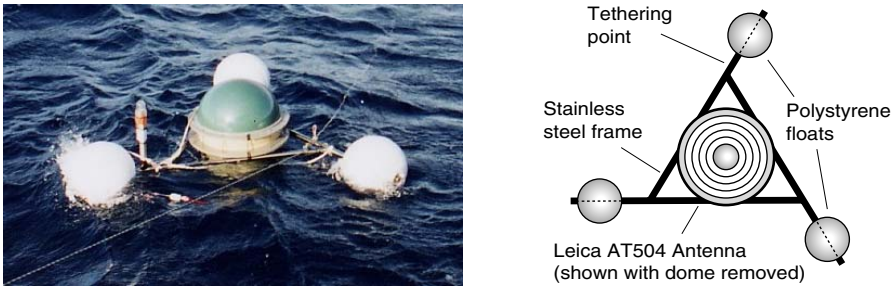

Figure 2-10 Photograph of the completed buoy in operation. (a) Deployed in Bass Strait, note the tether. (b) Plan view of the Mk II design (shown with the antenna dome removed).

Results from the first deployment of the Mk II design at the Port Arthur site are presented in Pugh et al. (2002).

One perceived limitation of the Mk II design is a restriction to deployment in low sea states (less than 3 to 4 on the Beaufort scale). During higher sea states the low position of the antenna with respect to the water surface makes it susceptible to waves breaking over the antenna dome. Structurally, this is not a problem, however, acquisition of the GPS signals is often interrupted, leading to complex processing for the kinematic GPS solution. Depending on the sea state and tethering configuration, this effect may prevent an adequate solution for the highest accuracy applications. An example of this rough weather issue is given in §2.4.3.

2.4 Mk II Operational Considerations

In order to determine accurate absolute sea level height from a GPS buoy, several operational issues must be considered. The most basic of these is the determination of the antenna height above the mean water level. The influence of the antenna dome on the phase centre position and the effect of the tether on the buoy dynamics must also be considered.

2.4.1 Antenna Height Determination

The determination of the position of the GPS antenna with respect to the mean water surface is fundamental to any GPS buoy design, and must be determined at the 1 mm level for the highest accuracy applications. The height of the antenna within the UTAS Mk II buoy was determined with the buoy placed in a ~6000 litre tank, filled with seawater of known salinity (33.2 ppt). The buoy was placed in the tank in complete deployment configuration and left to settle.

The measurement technique involved the attachment of three lightweight scales to three sides of the buoy capsule rings (Figure 2-11). The scales were attached vertically to the capsule rings, each extending into the water.

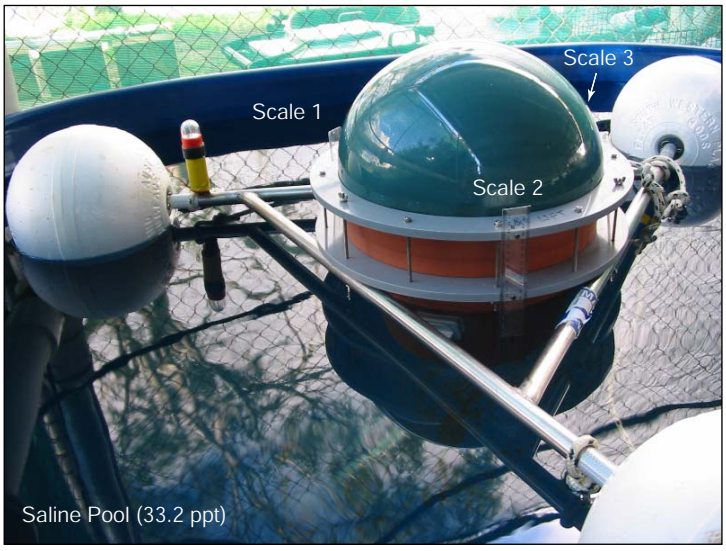

Figure 2-11 GPS Buoy in deployment configuration in a saline pool. Note the position of the three scales.

Given there was no wind or other external forces disturbing the water level within the tank, the water level meniscus on the three scales could be clearly observed

with the naked eye to the 1 mm level. A series of four observations to each scale were made, disturbing the buoy and allowing it to settle between each observation.

The observations taken in the tank defined the water level relative to each scale (i.e., scales 1, 2 and 3). With the buoy out of the water, the positions of each scale with respect to the buoy capsule were required. These height differences were observed using a Zeiss Ni 2 precise level with parallel plate micrometer, with the buoy resting on a solid horizontal surface. These measurements were combined with the measurements taken in the tank to derive the height difference A to B, as shown in Figure 2-12.

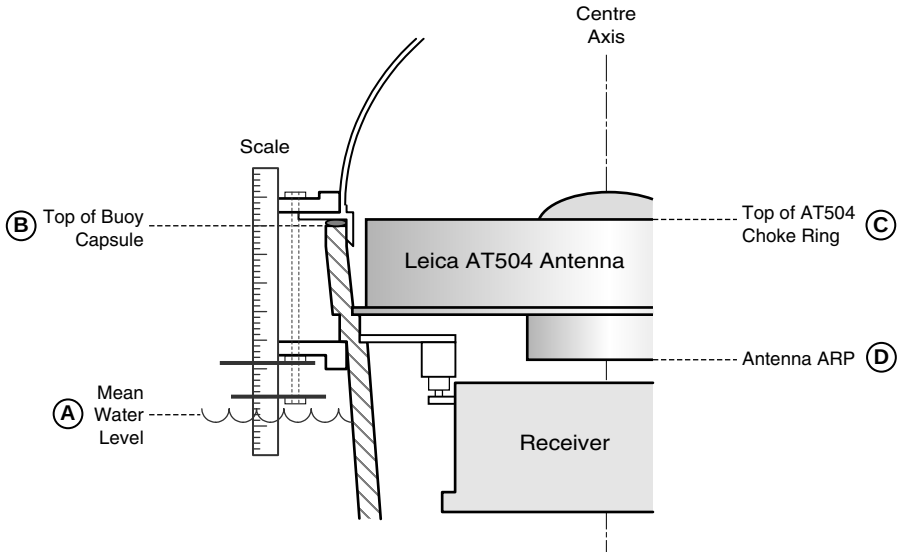

Figure 2-12 Schematic view of the surfaces involved in the determination of the antenna ARP height above the mean water level.

The next height difference required was that between the top of the buoy capsule and the top of the GPS antenna (height difference B to C, Figure 2-12). With the dome removed, this level difference could be observed using the same levelling instrument. Dimensions of the antenna (height difference C to D, Figure 2-12) were adopted from the NGS antenna calibration facility (NGS, 2004). These dimensions allowed the reduction of the height difference from the water level to the antenna ARP (i.e. final height difference A to D, Figure 2-12). The final reduced height of the antenna ARP above the water surface for the UTAS Mk II buoys is 0.029 ± 0.0015 m. The uncertainty is considered conservative and is dominated by observation of the water level against each of the scales.

Final reductions show negligible difference between the antenna heights determined from each individual scale. This result confirms the buoy is well balanced about

the central vertical axis. The weight distribution within the buoy is maintained by rigid foam supports within the buoy capsule that constrain the battery position about the vertical axis. The receiver is also fixed in place as indicated in Figure 2-9.

The antenna height for the Mk II design is assumed invariant to the degree of tilt expected under normal operating conditions. This is an advantage common to most wave rider styles of GPS buoy as discussed in §2.2.2.

2.4.2 Phase Centre Variation

GPS derived co-ordinate components are determined relative to the electrical centre, or phase centre of the antenna. The position of the phase centre varies as a function of the frequency and direction of the incoming GPS signal. The modelling of the phase centre variations is of particular importance and has been the focus of considerable research effort (see Mader and MacKay, 1996 and Schupler, 2001 for example). For introductory materials relating to GPS antennas and phase centre variation, readers are referred to Schupler and Clark (1991) and Langley (1998).

The phase centre of an antenna is generally defined for both GPS carrier frequencies by an offset parameter, and secondly, a series of elevation and azimuth dependent variations. The phase centre offset defines the position of mean phase centre (for each frequency) with respect to a physical surface on the antenna, referred to as the Antenna Reference Point (ARP). The phase centre variation as a function of signal elevation and azimuth can be determined using a range of methodologies. Results from these techniques may then be applied in the form of corrections to the GPS range observables during the pre processing stages of any GPS analysis.

Absolute methodologies involve the use of anechoic chamber calibrations (Schupler and Clark, 1991; Rocken et al., 1995; and Akrour et al., 2003 for example) or in situ measurements using a robotic arm or customised antenna mount to position the antenna at known orientations (Wubbena et al., 1997 and Wubbena et al., 2000). Relative phase centre variations are also commonly used (Mader, 1999 and NGS, 2004) whereby zero phase centre variation is assumed for a reference antenna (usually the Dorne-Margolin choke ring). Relative variations as a function of both elevation and azimuth are then determined for the second antenna of interest.

The problematic issue of antenna phase centre variation is compounded with the use of protective antenna domes. The use of a dome over an antenna is often dictated by the installation site, and requirements to shield the antenna from environmental effects such as water, snow and unwanted fauna. Various studies have shown the dome has the potential to introduce a delay in signal reception, affecting the estimates of site position (King et al., 1996; Braun et al., 1997; and Andreatta et al., 2001 for example). The Braun et al. (1997) study concluded that the effect of the dome is dependent on several factors including the size, shape and composition of the dome. In the worst case, variations at the 40 mm level were observed following the addition of an antenna dome.

The design of the antenna dome used on the UTAS Mk II buoy design was undertaken following many of the recommendations developed as part of the Southern Californian Integration GPS Network (SCIGN) radome project (Hudnut, 1999). Important characteristics identified in the study which were attributed to minimising the potential effect from a dome include:

- hemispherical shape, i.e., symmetrical about the central vertical axis;
- uniform wall thickness which is as thin as possible; and
- centre of curvature of the dome as close as possible to the mean phase centre of the antenna.

Within the relevant community, the short SCIGN dome (Figure 2-13) is unofficially considered the preferred antenna dome of choice for permanent GPS installations. The Andreatta et al. (2001) study on the effect of the SCIGN domes on positional accuracy reported a maximum difference in the vertical component of 5.65 mm $\pm$ 1.21 mm when using a pair of Trimble 4000 SSI receivers and a 15 degree elevation mask.

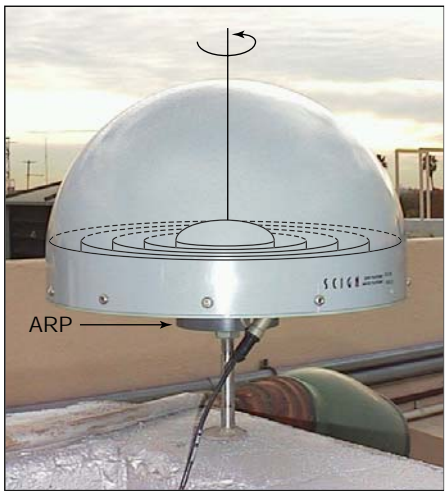

Figure 2-13 SCIGN short dome shown with the choke ring antenna surface superimposed over the dome. The section below the top of the choke ring is cylindrical, the section above is hemispherical. (Photograph from Hudnut, 1999).

The Mk II buoy dome design was complicated with the mandatory requirement that it generate a watertight seal between the dome and the buoy capsule (see Figure 2-9). The final design enabled a strong, watertight seal whilst maintaining many of the SCIGN dome characteristics.

The influence of the dome on both signal acquisition and the estimation of baseline components was investigated during a 6-day GPS measurement campaign. Two precise antenna mounts were used at the facility on top of the Physics building at the University of Tasmania (Figure 2-14). The antenna mounts have been precisely surveyed, such that their relative three-dimensional positions are known to within 0.1 mm. The two mounts used were separated horizontally by approximately 2.75 m. The observed height difference between the mounts was 6.2 mm.

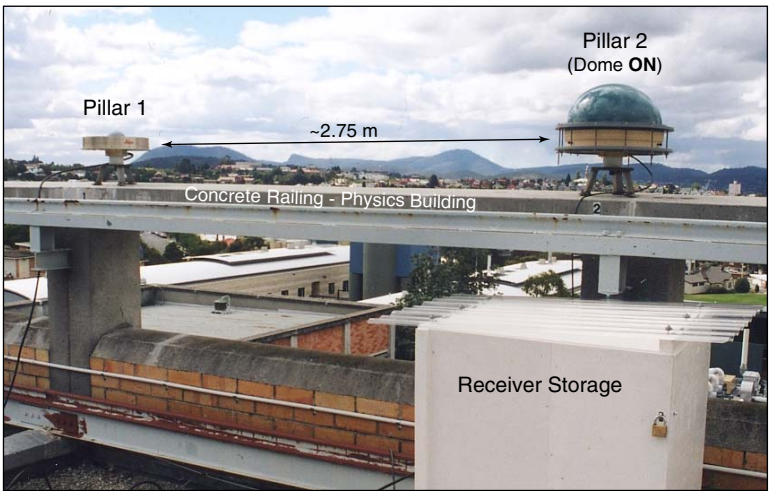

Figure 2-14 Antenna mounts on the UTAS physics building.

Three days of GPS data (recorded at 30-second intervals) were observed using two Leica CRS1000 receivers and Leica AT504 antennae. A GPS buoy dome was then attached to one antenna and a further 3 days of data acquired. To precisely replicate the GPS buoy configuration, an exact replica of the upper section of the buoy capsule (including dome, polypropylene capsule, clamping rings and stainless steel fasteners) was fastened to the antenna. The apparatus is shown attached to the antenna on Pillar 2 in Figure 2-15.

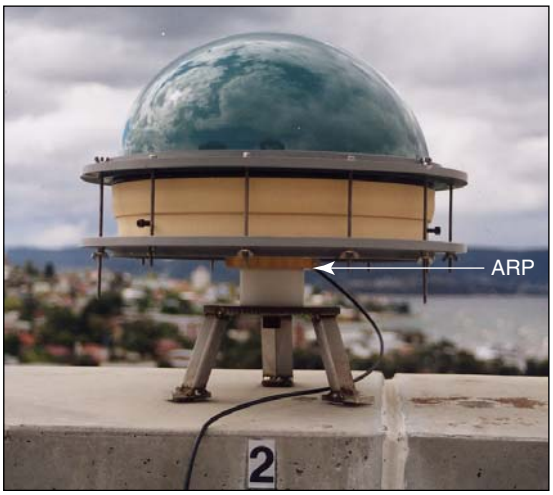

Figure 2-15 The GPS dome apparatus attached to the Leica AT504 antenna on Pillar 2. Note the position of the antenna ARP which normally sits 0.029 m above the mean water level when the buoy is deployed.

2.4.2.1 TEQC Analysis

TEQC software allows translation, editing and quality checking of both raw and Rinex format GPS data (Estey and Meertens, 1999). The quality check component of the software has been used in a first pass analysis of the data collected during the Mk II dome trial. Three quality indicators have been used in this analysis; multipath on L1 and L2 and the total number of cycle slips (using standard TEQC tolerance configuration). Readers are referred to Estey and Meertens (1999) for the derivation of MP1 and MP2 multipath estimates. Daily GPS data files were used in the TEQC analysis (Figure 2-16).

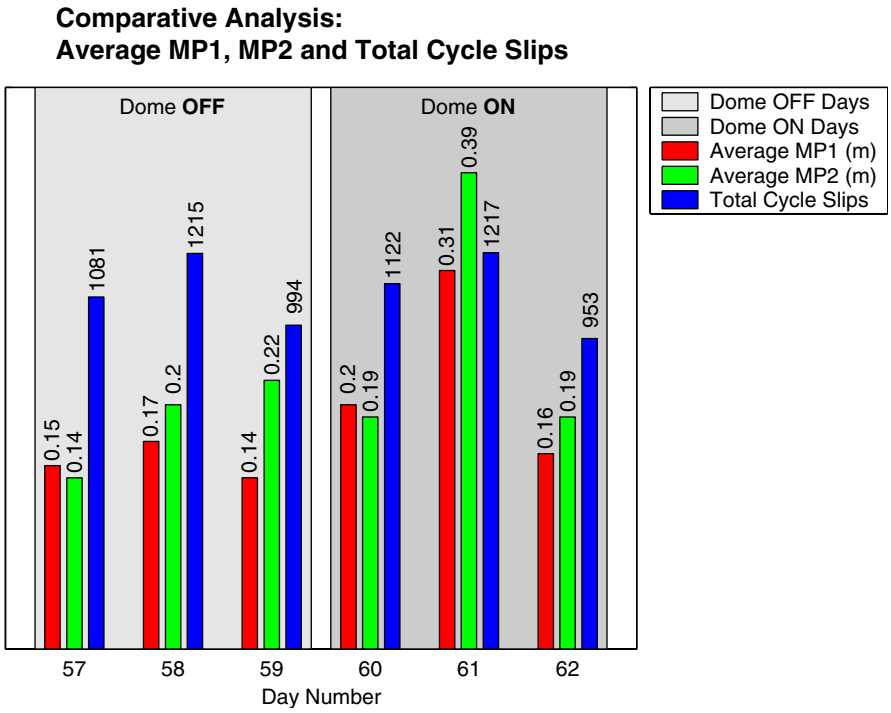

Figure 2-16 Daily comparison of multipath (MP1 and MP2) and total cycle slips for the dome OFF and dome ON cases.

Figure 2-16 reveals no significant changes in receiver performance between the dome OFF and ON tracking sessions. Day 61 (dome ON) appears to be an outlier with MP1, MP2 and number of cycle slips all elevated over the mean dome OFF levels. All quality indicators on day 62 (dome ON) return to approximately equivalent dome OFF levels. This increased variability on day 61 with the dome ON is most likely attributed to environmental/atmospheric effects, and not the introduction of the dome.

The TEQC MP1 and MP2 variables provide an indication of the root mean square variation of the MP1 and MP2 linear combinations (Estey and Meertens, 1999).

The estimates are determined for each observation allowing the analysis of multipath variability versus signal elevation (Figure 2-17).

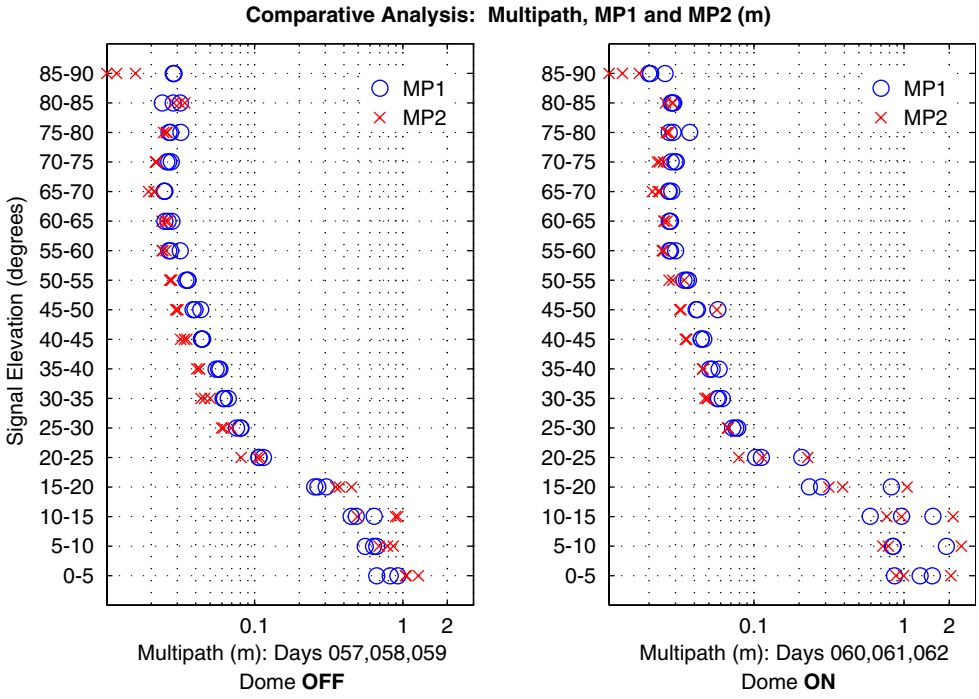

Figure 2-17 TEQC multipath analysis. MP1 and MP2 multipath in 5 degree signal elevation bins

Figure 2-17 shows MP1 and MP2 multipath for the dome OFF and ON cases, grouped into 5-degree signal elevation bins. Data for each individual day are plotted (but not individually differentiated) in each panel. As expected the MP1 and MP2 values are much higher for low elevation data, hence a logarithmic scale has been used. The multipath estimates reduce to a minimum between 65 to 90 degrees elevation. The influence of the outlier day (61) for the dome ON case is clear between elevations 0 to 25 and 45-50 degrees. There is very little significant difference between remaining elevation bins for the dome OFF and ON cases. This adds weight to the hypothesis that the outlier day is in fact a consequence of temporary variation in the surrounding environment or satellite performance and not due to the addition of the antenna dome.

2.4.2.2 SNR Analysis

The translation component of the TEQC software allows the extraction of the L1 and L2 signal to noise ratio (SNR) observable (S1 and S2 respectively) from the binary GPS data. The SNR data have been analysed using the SVSNR and SPCSNR analysis software (Herring, 2001). The dimensionless signal to noise ratio, or carrier-to-noise power density ratio (C/No) has been used by a number of authors as a quality indicator of GPS observations. For example, Comp and Axelrad (1996) investigated the use of the SNR observable in an attempt to reduce the effect of carrier phase multipath. Brunner et al. (1999) uses the C/No ratio to derive an improved stochastic model for GPS data observed in noisy environments where signal obstruction, diffraction and multipath are likely to cause difficulty. The observed SNR from a specific antenna, antenna cable and receiver combination will vary firstly as a function of incoming signal elevation. The previous papers take advantage of epoch-by-epoch variation occurring due to site-specific effects, which include multipath. In this analysis, the underlying SNR gain curve, as a function of elevation, is investigated over the 6 days of observation. The SVSNR and SPCSNR packages firstly extract the S1 and S2 observables from the RINEX data before fitting a fourth order polynomial in sin(elevation) as shown in Eqn 2-1.

$$SNR_{Gain} = A \cdot \sin^1(el) + B \cdot \sin^2(el) + C \cdot \sin^3(el) + D \cdot \sin^4(el) + E \quad \text{Eqn 2-1}$$

where SNR_{Gain} is the best fit antenna gain response (for L1 or L2), el is the signal elevation angle and A, B, C, D and E are dimensionless model coefficients solved for using a least squares methodology. Antenna gain curves were computed for each 24-hour observation session for both the S1 and S2 observables. The mean gain curve was computed for both carrier frequencies over the three dome OFF sessions (see Figure 2-18(a) and Figure 2-19(a) respectively). The gain curves from each observation session were then compared to determine the influence of the Mk II dome in the final three sessions. Note the antennae, antenna cables and receivers remained the same between the dome ON and OFF scenarios. The differences with respect to the mean gain curves are presented in Figure 2-18(b) and Figure 2-19(b) respectively.

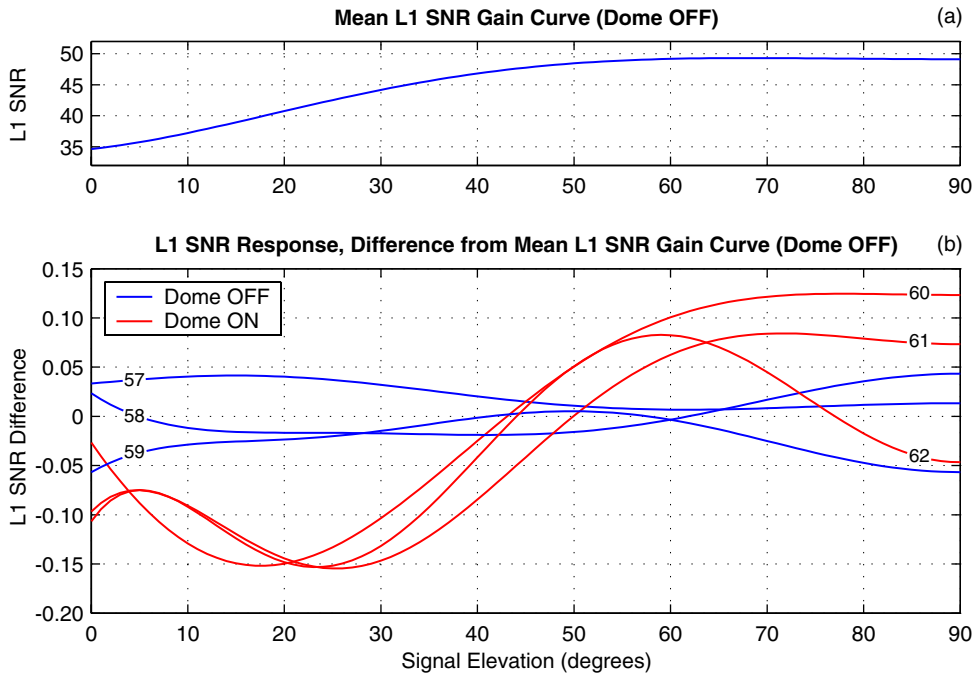

Figure 2-18 L1 SNR Analysis. (a) Mean L1 SNR gain curve computed from the three dome OFF days. (b) L1 SNR response of each day differenced from the mean L1 SNR gain curve (blue = dome OFF, red = dome ON). Note the day numbers are indicated on each response line.

The SNR response of the antenna on the L1 frequency, following the addition of the dome is of particular interest. Figure 2-18(b) reveals consistent differences between the dome OFF and ON cases. The difference is greatest between the elevation range of ~15-30 degrees. Within this elevation range, the difference is negative indicating an observed increase in SNR with the dome ON. At higher elevations the difference reverses sign and the variability increases.

The L2 response (Figure 2-19b) shows significant difference between 10-40 degrees elevation, with negligible differences at higher elevations. The difference within the 10-40 degree elevation band indicates an observed decrease in SNR with the dome ON, which is the reverse of the L1 response. The L2 response below 10 degrees elevation is particularly variable, which is consistent with the multipath analysis (Figure 2-17).

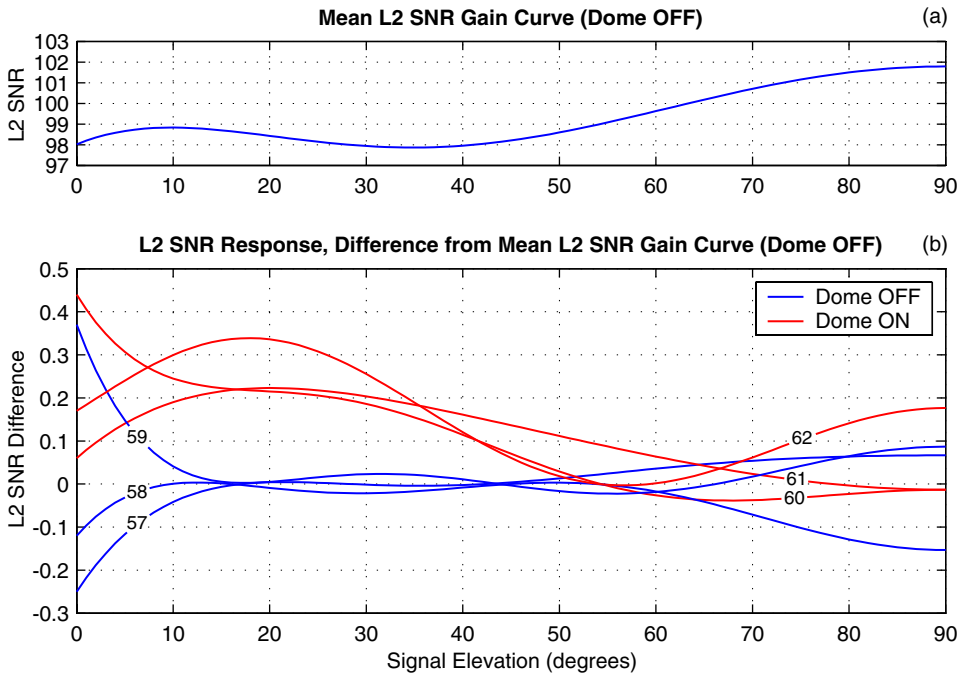

Figure 2-19 L2 SNR Analysis. (a) Mean L2 SNR gain curve computed from the three dome OFF days. (b) L2 SNR response of each day differenced from the mean L2 SNR gain curve. Note the day numbers are indicated on each response line.

The SNR analysis has shown clear and consistent change on both carrier frequencies in response to the addition of the antenna dome. It is difficult to make quantitative conclusions as to the influence of these changes. The effect on baseline component estimation is discussed in the following section.

2.4.2.3 Short Baseline Analysis

The short baseline analysis has involved the processing of six 24-hr observation sessions between pillars 1 and 2. Pillar 1 was held fixed as the reference station, solving for North, East and Up baseline components to pillar 2. L1, L2 and LC solutions were computed for each session using an elevation mask of 10°. The data rate for processing remained at 30-second intervals. Given the short baseline, standard commercial GPS processing software (GeoGenius©) was utilised. NGS phase centre tables were adopted for both AT504 antennae (NGS, 2004).

Differences with respect to the terrestrially observed ground truth estimates for each L1, L2 and LC solutions in the North, East and Up components are presented in Figure 2-20.

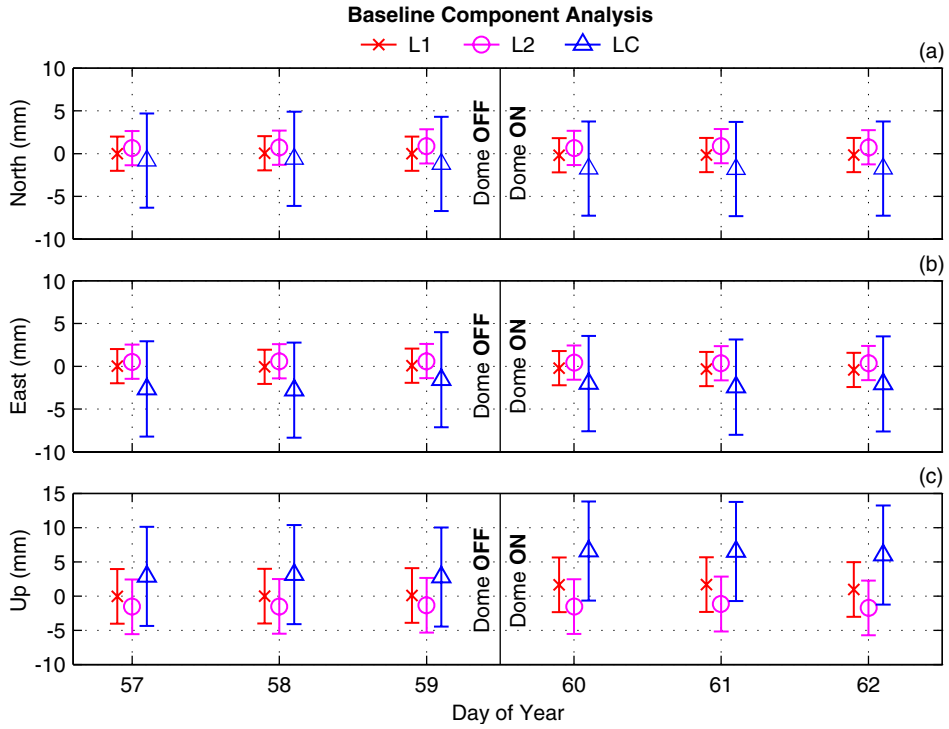

Figure 2-20 Dome ON and OFF short baseline component analysis (note the slightly difference y-scales). (a) North, (b) East, and (c) Up components. All quantities refer to differences from the ground truth estimates.

Results shown in Figure 2-20 highlight some interesting antenna behaviour both before and after the addition of the dome. L1 and L2 solutions are consistently different (1~2 mm) for all baseline components, before the addition of the dome. While the differences are well within the uncertainties, the consistent difference suggests the two antennas are not operating identically, despite being identical models (with identical NGS models used in the processing software). The L1 and L2 solutions show no discernable change following the addition of the dome in the North and East components. For the Up component (Figure 2-20c), the L1 solution increases marginally (1~2 mm) while the L2 solution decreases marginally ($<$ 1 mm), following the addition of the dome. The effect of the dome on the L1 and L2 solution is therefore to exacerbate the relative difference between the L1 and L2 solution as observed in the three solutions preceding the addition of the dome.

The differences observed between the L1 and L2 solutions before adding the dome are amplified when the LC combination is formed. Seeber et al. (1997) underscores the fact that any error in the determination of the L1 and L2 phase offset will propagate into the LC offset by a factor of approximately 3.1. The dome OFF LC solutions are therefore biased by -1 to -2 mm in the North component, -2 to -3 mm

in the East component and +3 to +4 mm in the Up component. Once again, there is no discernable difference in the North and East components for the dome ON scenario, with the LC solution. In the Up component, the LC solution increases a further ~3 mm with the dome ON. The increased variability in the LC solution is consistent with other studies such as King et al. (1996) and Andreatta et al. (2001). To gauge the significance of the LC solutions, differences observed in the Up component, over a longer baseline were analysed. The HOB2 ARGN site, located approximately 14.2 km from Pillar 2 was used as the reference station (approaching the baseline lengths required at the Bass Strait calibration site). The results for the LC solution (Up component only) are shown in Figure 2-21.

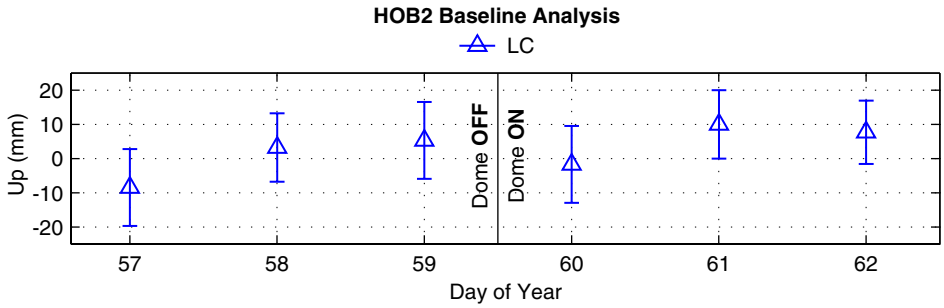

Figure 2-21 LC Up component of the HOB2 Baseline analysis (~14.2 km).

As expected, the LC solution shows greater variability over the longer baseline. Given the increased variability *before* the addition of the dome, it is difficult to draw any significant conclusions related to the effect of the dome over the longer baseline.

2.4.2.4 Summary

The investigation into the effect of the Mk II antenna dome has revealed the dome introduces a measurable change in the SNR gain pattern of an antenna. During a short baseline analysis, negligible differences were found in the North and East baseline components, for the dome ON and OFF scenarios. In the vertical component, differences were at the -1 mm to +1 mm level, for the L1 and L2 solutions. Comparing the L1 and L2 results in the vertical component for the three dome OFF solutions indicates the two identical model antennas (both Leica AT504) are in fact different in terms of phase centre position at the 1~2 mm level (Figure 2-20c). These differences in the L1 and L2 phase centre position are amplified when forming the LC combination (Figure 2-20c). This variability

between antennas makes it difficult to determine the effect of adding the dome, as results are only applicable to this particular antenna combination. In terms of this specific combination, variability appears to increase with the addition of the dome, however it is not possible to conclusively determine if there is any constant offset following the addition of the dome. The effect of the dome is therefore ambiguous depending on the antenna combination, with the worst-case difference at the 4 mm level.

2.4.3 Tethering Techniques

Buoy deployment for many applications, including altimeter calibration, typically requires SSH estimates at a defined position. In this case, the intended application necessitated tethering the buoy to an anchored boat. For other applications a ocean mooring could be used, or for current studies, a sea anchor. A fixed tether must constrain the buoy position to within a given area whilst allowing sufficient free movement for tidal, swell and wave displacement. The tethering system must not bias the average vertical position of the antenna with respect to the water surface. Two preferred tethering configurations have been developed for near shore and offshore wave rider buoy deployments. Both tethers ensure only a horizontal constraint, allowing the buoy to move freely in the vertical direction.

The near shore tether (Figure 2-22) is based on a running float mooring system. A large (0.7 m diameter) surface float is attached via a running linkage to a mooring anchor and suspended counter weight. The counter weight must be heavy enough to keep the float approximately above the mooring, yet light enough to allow the float to move with the tide and any large swell. The tether to the buoy (typically 10 m in length) is connected above the running linkage on the surface float ensuring the constraint is solely in the horizontal direction. The horizontal position of the buoy will vary with tidal currents and wind over a range of approximately 25 m (surface tether diameter plus tilt of the running float/mooring system). For applications requiring less horizontal variability, a shorter surface tether and heavier counter weight on the mooring system can be utilised.

The near shore tether has been successfully deployed with the Mk II buoy at Macquarie Island (see Chapter 5). The tidal range was approximately 0.8 m, with swell and wave range at the 1 m level. The system provided the necessary horizontal constraint whilst maintaining flexibility during large swell events.

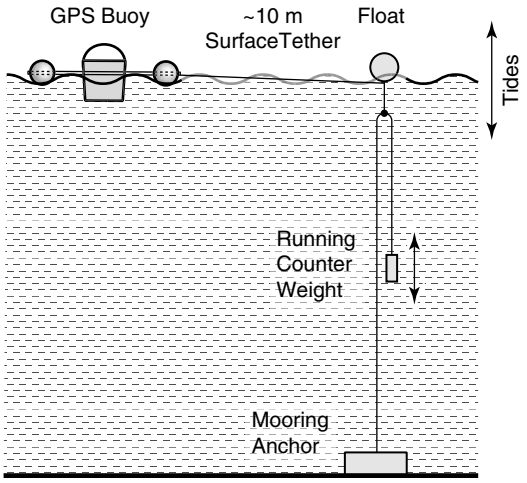

Figure 2-22 Buoy deployment configuration for coastal applications.

Episodic offshore deployments that require horizontal constraint of the buoy (altimeter calibration for example) are best achieved using an anchored boat as the mooring. Oceanic moorings are generally reserved for continuous applications and larger buoy platforms. To ensure the buoy follows the instantaneous sea surface, the tethering system must be sufficiently flexible to prevent the tether from "pulling" the buoy through the wave crest. This is particularly a problem during rougher sea conditions in areas subject to significant tidal currents (i.e., the current causes a higher tension on the tether). The tethering system used for altimeter calibration deployment in Bass Strait used a long floating line (approximately 50 m) from the anchored boat to the first buoy. The response of the tether was dampened slightly using a small weight on the line approximately 10 m from the boat. A second buoy was tethered to the first with an additional 15~20 m line. An example taken from rougher conditions using this tethering system is shown in Figure 2-23. Time stamped video footage was correlated with signal acquisition determined from the GPS RINEX file during the passage of a large swell front, shown plotted in Figure 2-23. The breaking swell and tension on the tether does not allow the buoy to rise over the swell, rather the buoy breaks through the wash on the crest of the wavefront (Figure 2-23c). This causes complete loss of GPS tracking, with full reacquisition taking approximately 21 seconds. Interestingly, in this example, the dampening effect of the closer buoy ('B1') prevents the same occurring to the distant buoy ('B2').

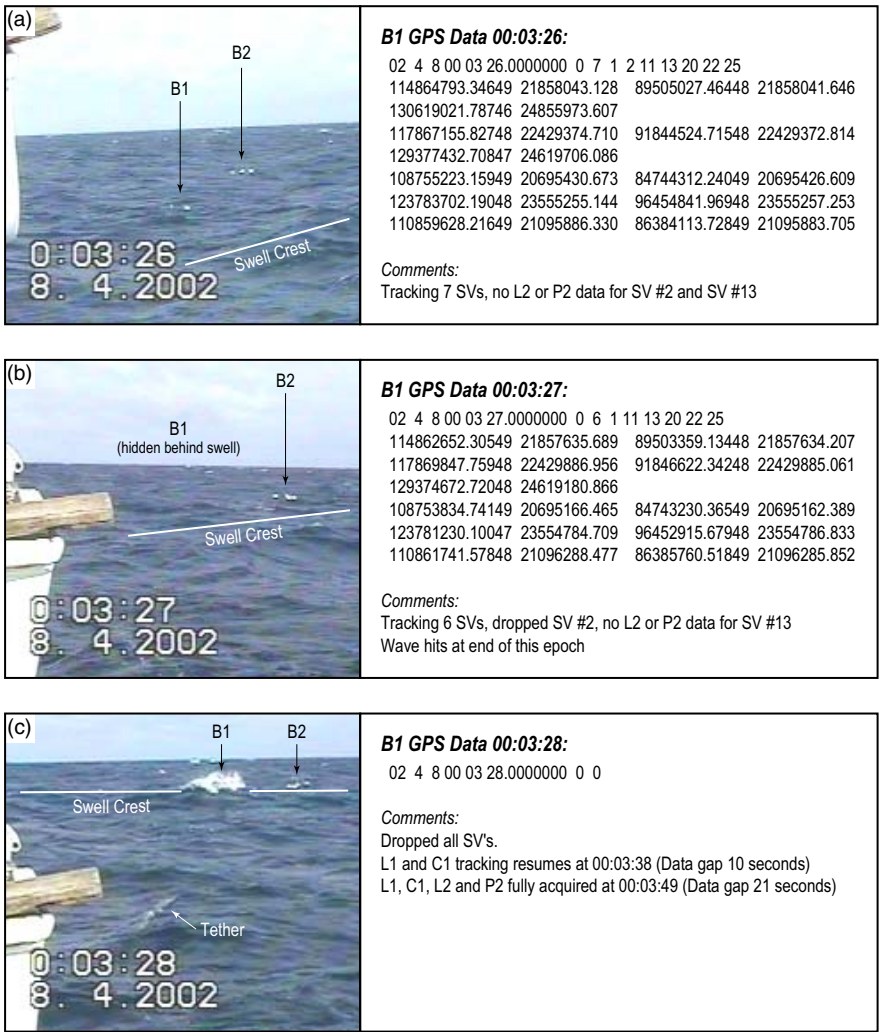

Figure 2-23 Video footage and corresponding GPS RINEX data from buoy 'B1' deployed in Bass Strait during the passage of a large (~2 m) steep swell front. (a) Swell approaching, GPS tracking 7 L1 / 5 L2. (b) Swell just about to hit 'B1', GPS tracking 6 L1 / 5 L2. (c) Swell breaks and hits 'B1' causing complete loss of GPS tracking (0 L1 / 0 L2). Note the sudden tension on the tether and the whitecaps as the buoy is pulled through the crest.

An improved concept is shown in Figure 2-24 whereby the tether response is dampened by the inclusion of elastic cord. The elastic must be sufficiently taut to only extend during large swell events, preventing the buoy from dipping through the wave crest.

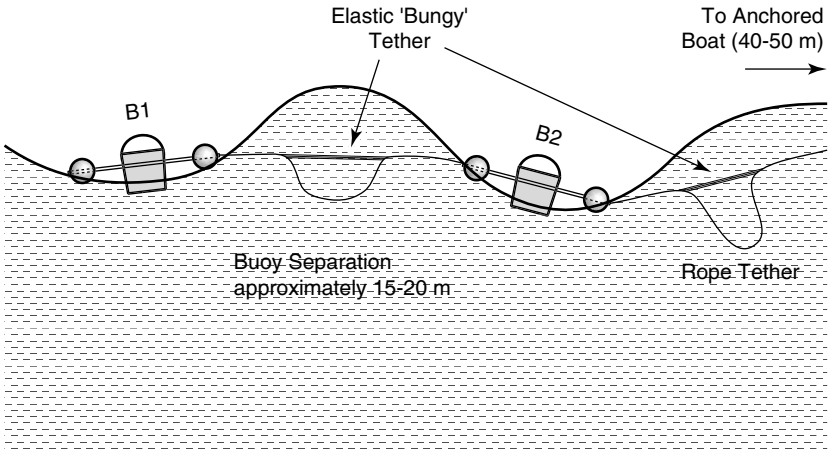

Figure 2-24 Exaggerated schematic view of an improved tethering system. Note the elastic shock cord tethering system.

2.4.4 Influence of the Tether on Buoy Dynamics

The addition of a tether to any floating platform has the potential to vary the dynamics of that platform. The shape of the platform itself also influences the buoyancy dynamics. A concern for any GPS buoy application requiring absolute water level determination is the potential change in the mean vertical position of the buoy with respect to the water level. The influence of both the shape of the buoy and the horizontal tethering system described in §2.4.3 has been investigated with the deployment of a 1:2 scale model of the Mk II buoy in a series of wave tank experiments. The aim of the experiments was to determine if the shape of the buoy combined with tether rope biases the mean vertical position of the buoy whilst undergoing dynamic motion as the buoy follows the wave profile or sea surface.

The model buoy was tethered horizontally to one end of the wave tank and subjected to two different wave regimes (Case 1, ~1 Hz, and Case 2, ~0.6 Hz). The choice of the wave regimes reflects an attempt to exacerbate any potential effect of the tether. For this reason, the wave frequency is much higher than expected during a full-scale deployment, hence any effect of the tether was expected to be clearly apparent. Two points of interest on the buoy were tracked using high-speed digital video and image tracking software (Mikromak, 1998). The digital video recorded at 60 frames per second, with approximately nine seconds of video acquired for each experiment. Video capture for each trial was initiated only after the waves stabilised at the specific frequency configured on the wave generator.

The video equipment was set up level with the mean height of the buoy and orthogonal to the direction of the wave front. Image tracking above and below the water surface was possible due to the clear glass sides of the tank. The component of interest in the image tracking was the vertical position of each target point, recorded in units of pixels.

The subsequent analysis is centred on the comparison of the position of the buoy when at rest to the mean position of the buoy computed from image tracking whilst waves were being generated. The two tracking targets (upper and lower) were fixed to the scale buoy in the positions as shown in Figure 2-25(a). The positions of the two targets during the Case 1 trial are shown superimposed over a single frame in Figure 2-25(b).

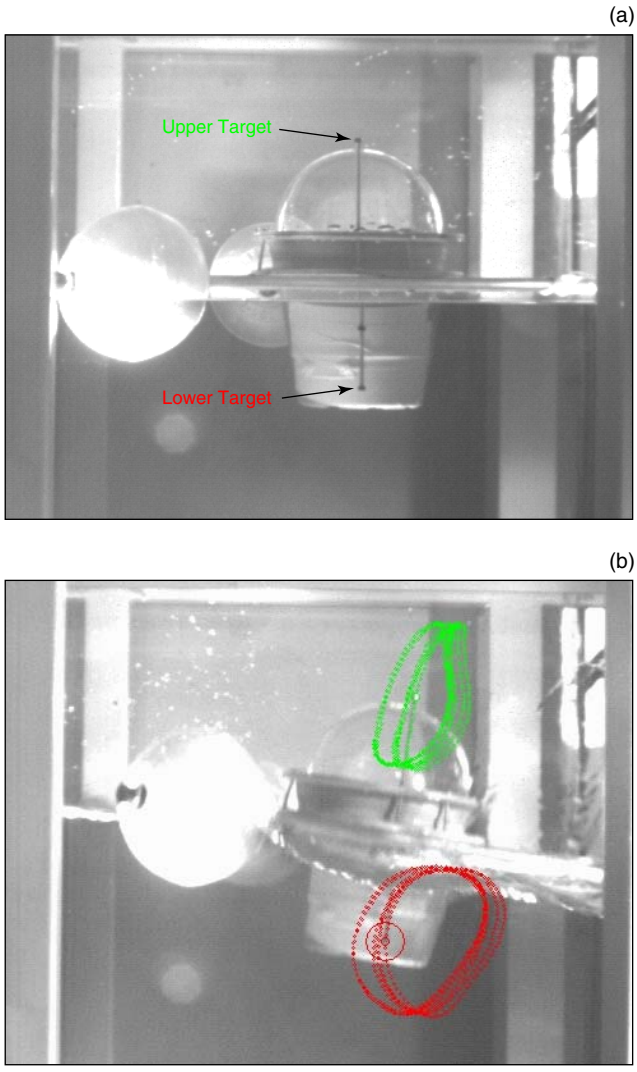

Figure 2-25 Wave tank tether analysis. (a) Upper and lower tracking targets used by the motion analysis software (shown with the buoy at rest). (b) Positions of the upper and lower targets tracked over approximately 9 seconds (frame rate: 60 Hz).

Results from the image tracking were converted from units of pixels to millimetres using a conversion factor defined from the apriori measurement of the distance between the upper and lower targets (265 mm). The mean positions of each target were computed using image tracking data from an even number of wave cycles. The positions of each target whilst at rest were determined from a range of images taken before and after each trial, when the wave tank had completely settled and the water surface was horizontal. The positions at rest are estimated to have an uncertainty of ± 1.5 mm, largely dominated by limited resolution of the video capture and errors of perspective geometry caused by movements of the buoy away from, or closer to, the camera. Results from the image tracking for both cases are shown in Figure 2-26.

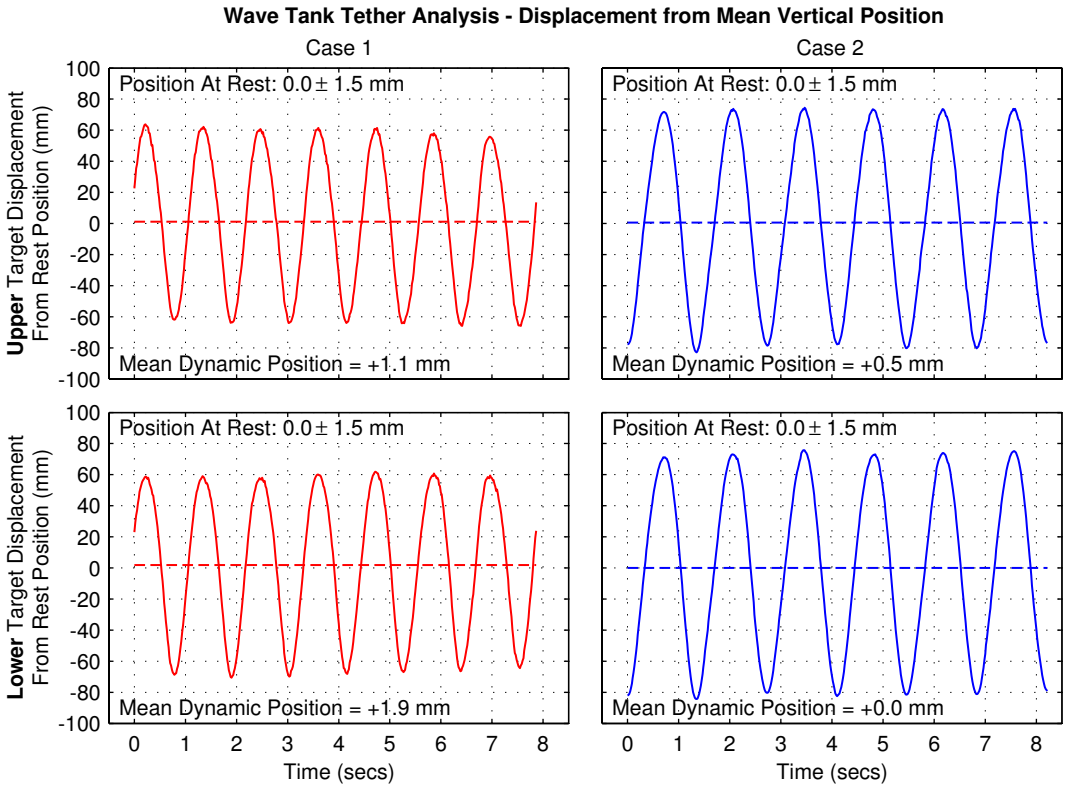

Figure 2-26 Positions of the upper (top panels) and lower targets (bottom panels) relative to their positions at rest for both Case 1 and Case 2 trials. Note the 'at rest' position and the mean position of each target is displayed in the upper and lower left hand corner (respectively) of each panel.

Results from the target tracking (Figure 2-26) highlight negligible difference between the computed mean position of the target and the position of the target at rest. The lower target in case 1 has the largest difference at +1.9 mm. This is not significantly different to the anticipated uncertainty of ±1.5 mm. The remaining differences are all appreciably lower than the uncertainty, adding confidence to the

conclusion that the horizontal tether (or buoy design) is not biasing the mean position of the buoy when deployed in a dynamic environment.

2.5 Summary

The measurement of water level using GPS, situated on or inside floating platforms, remains a powerful and valuable technique to the geodetic and oceanographic community. The development of the technique has been driven largely by the evolution of satellite altimetry, and the requirement for in situ verification and calibration of these satellite missions. This has been particularly evident in the lead up to the launch of the Jason-1 altimeter mission.

For high accuracy, absolute applications, the fundamental requirement is the measurement and monitoring of the position of the antenna with respect to the sea surface. Variations in the weight of the floating platform (for example, due to rope strops, or marine growth), the tethering system, and the antenna dome all affect this measurement. The highest accuracy applications remain limited to deployments within short (0-10 km) to medium (10-100 km) distances from land based GPS reference stations. Colombo (2000) and Colombo et al. (2001) investigate extending these baselines lengths to 100-1000 km. Improvements in processing techniques and GPS satellite modernisation (for example, the introduction of a third frequency) will reduce this baseline distance constraint and allow buoy deployments in offshore oceanic areas. These developments will therefore aid applications such as continuous in situ altimeter calibration, tsunami early warning systems and remote area tidal studies.

The UTAS Mk II GPS buoy design represents a progression from traditional wave rider buoy designs by allowing autonomous operation yet maintaining compact size and low operational weight. More importantly, the low centre of mass and low position of the antenna removes the requirement to continuously measure the position and orientation of the antenna with respect to the water surface, as in the case of spar type buoy systems. The buoy is suited to both inshore and offshore applications, limited for high accuracy applications only by calm to moderate sea conditions (maximum sea states of 3 to 4 on the Beaufort scale). Improved tethering systems, or allowing the buoys to drift extends the sea state restriction by reducing the likelihood of waves breaking over the antenna dome.

Investigations into the measurement of antenna height, phase centre variability, and the effect of the tethering system on the mean position of the buoy show that the buoy is suitable for use in the highest accuracy (sub-centimetre in the vertical component) absolute measurement applications. The strength of the Mk II design is illustrated with two markedly different applications as presented in this Thesis. The primary application of the design is the measurement of absolute SSH for the calibration of T/P and Jason-1 at the Bass Strait calibration site (see Chapter 4). Secondly, the Mk II design is applied to a localised application requiring precise relative SSH estimates for the in situ verification of tide gauges. The tide gauge verification methodology has been trialled successfully in Tasmania, the Sub-Antarctic and Antarctic (see Chapter 5). These tide gauge experiments provide estimates of tide gauge accuracy, improving the potential contribution of the specific gauges to global studies requiring tide gauge data, particularly the tide gauge based calibration of satellite altimeters as discussed in the introductory Chapter.

Chapter 3

Working at the 1 cm Level

3.1 Introduction

The development of the GPS buoys in the previous Chapter provides the first component required for the Bass Strait calibration methodology. Before the complete methodology can be presented, the geodetic framework at the Bass Strait site must first be defined and discussed. Successful absolute calibration is dependent upon the comparison of both in situ and altimeter estimates of sea surface height, observed in an equivalent terrestrial reference system. For this reason, the geodetic reference points at the Bass Strait site must be positioned in the same reference system as used for the satellite altimeter orbit. All coordinates must also be derived using comparable computational standards.

Issues surrounding the reference frame realisation process, and the computational standards adopted for both the calibration site and the satellite altimeter are therefore of fundamental importance for this study. The comparison of absolute bias estimates between different calibration studies is only possible following a rigorous assessment of the geodetic procedures adopted. This concept can be extended for the comparison and geophysical interpretation of any geodetic time series. A rigorous treatment of issues, such as computational standards (in particular model homogeneity), aids in the development of a more realistic error budget for the absolute bias estimates presented in the following Chapter.

The determination of vertical position and velocity at the mm and mm/yr level respectively remains a challenge within the geodetic community, and hence is the focus of considerable research effort (see for example Sanli and Blewitt, 2001, Johansson et al., 2002, Elosegui et al., 2003 and Williams et al., 2004). Analysis of Global Positioning System (GPS) data has taken a leading role in these investigations, with continuous improvements in accuracy in recent years (see van Dam and Francis, 2003 for example). Allied space geodetic techniques, such as

Very Long Baseline Interferometry (VLBI), Satellite and Lunar Laser Ranging (SLR, LLR), and Doppler Orbitography Radiopositioning Integrated by Satellite (DORIS), all contribute relative strengths to the reference frame realisation process and the problem at hand. GPS is the primary technique adopted for datum determination at the Bass Strait calibration site, and is the focus of this Chapter.

This Chapter has three primary aims. Firstly, geodetic positioning is reviewed with an emphasis on many of the current issues surrounding the reference frame and its realisation. Computational standards are discussed, with an emphasis on the treatment of known site deformations which affect the GPS solution and its interpretation. This section includes details on modifications made to the GAMIT GPS analysis software (King and Bock, 2003), undertaken to ensure standardisation to the satellite altimeter reference frame and current international standards (McCarthy and Petit, 2004). This leads to the second aim of the Chapter, the geodetic positioning of the reference stations at the Bass Strait calibration site. The positioning requirements for a calibration site are first reviewed. The GPS processing methodology, results and associated uncertainties are discussed. To further assess the uncertainty of the datum at the Bass Strait site, coordinates derived from episodic campaigns are compared with long term continuous time series. An exploration of some of the issues surrounding the time series analysis of continuous GPS positions, particularly in the vertical component, is the final part of this Chapter. In conjunction with examples from the literature, this section utilises a small sub-set of available sites and solutions from IGS analysis centres as case study presentations.

3.2 Reference Frames for Geodetic Positioning

Geodetic positioning defines the position and velocity of a site in three dimensional space, relative to some defined reference system. The point of interest may be a crustal reference point on the surface of the Earth, or also perhaps, as in the case of this Thesis, the centre of mass of a satellite altimeter spacecraft. Clearly, to compare geodetic measurements made from different platforms, locations, or techniques, a common reference system is required. To extend this concept to comparisons of geodetic measurements observed over time (for example, the determination of vertical velocity), the reference system and its realisation must also be sufficiently stable over time.

A Terrestrial Reference System (TRS) defines a three dimensional 'ideal' mathematical reference system which is described by an origin, scale and orientations at a given epoch and their corresponding time evolution (Boucher, 2001). As any number of TRSs may be defined (each with a different origin, scale etc), the adopted TRS for Earth science applications is called the International Terrestrial Reference System (ITRS), as discussed in McCarthy and Petit (2004) and Anderson (2004). The ITRS is somewhat intangible, requiring the system to be 'realised' by a set of coordinates and velocities for a selected global set of stations. The realisation of the ITRS is called the International Terrestrial Reference Frame (ITRF), and forms the basis for most geodetic positioning, including that undertaken in this Thesis.

As the stations contributing to the ITRF are attached to the deformable Earth, the International Earth Rotation and Reference Systems Service (IERS), undertakes regular revisions of the ITRF. Each revision shows continued improvement, taking advantage of advances in analysis strategies to achieve the optimum combination of the space geodetic data available at the time. Recent realisations include ITRF96 (Sillard et al., 1998), ITRF97 (Boucher et al., 1999) and the latest solution, ITRF2000 (Altamimi et al., 2002 and Boucher et al., 2004). As each realisation is subtlety different, transformation between ITRFs is required by utilising a 14-parameter similarity transformation (with parameters typically derived using a least squares methodology between each TRF).

The ITRF2000 combines unconstrained space geodetic solutions from VLBI, SLR, LLR, GPS and DORIS from contributing analysis centres. As the most extensive frame yet developed, ITRF2000 contains approximately 800 stations which are located at around 500 different sites (Altamimi et al., 2002). The orbit of both the

T/P and Jason-1 satellites is aligned with ITRF2000 by adopting ITRF2000 coordinates for SLR, DORIS and GPS sites used in the orbit computation procedure (see for example Luthcke et al., 2003 and Haines et al., 2004).

A typical technique used by the GPS community to compute site coordinates and velocities relative to the ITRF can be described most simply as a two step process. Firstly, station coordinates, satellite orbits, Earth orientation and atmospheric delay parameters are estimated with loose constraints applied to the parameters of interest. The constraints serve to prevent the normal matrix becoming singular and to prevent rounding error in the adjustment. The parameter constraints must be sufficiently loose to prevent bias to the parameter estimation (Dong et al., 1998). The results of this first step of the analysis is a polyhedron of site coordinates which are internally well determined, yet are not "fixed" in absolute space relative to a defined TRF. The second part of the analysis maps this loosely constrained solution (with complete variance-covariance matrix) onto the ITRF. This step involves the estimation of scale, translation and rotation parameters using a sub-set of stations which have well determined position and velocity on the ITRF. This analysis strategy is often termed the 'fiducial-free' or 'free-network' approach (Henriksen, 1977, Heflin et al., 1992, Zumberge et al., 1997 and Dong et al., 1998 for example). This analysis strategy is adopted for the geodetic analysis presented in this Chapter. The ITRF2000 coordinate and velocity set is adopted ensuring a homogeneous dataset for use in the calibration study.

3.2.1 Limitations

There is no doubt the demands placed on the ITRF have steadily increased with the gradual improvement in space geodetic techniques. Many application areas within the Earth sciences work at the limits of current signal to noise ratios within a specific geodetic time series (post glacial rebound, mass transfer, absolute sea level and subsidence monitoring for example). At this level, issues of reference frame definition and stability become particularly important (especially for the sea level change / altimeter bias drift problem at hand). Considering the accuracy required for the calibration problem (amongst others), it is important to briefly review the possible limitations of the TRF and discuss proposed future enhancements.

The linear velocity model adopted in the realisation of the ITRF (and other reference frames, such as IGS00), is defined to accommodate un-modelled geophysical motion which is primarily of tectonic origin (Ray et al., 2004a). Non-linear variation in the temporal evolution of site position further complicates the realisation of the ITRF. Prior to more recent improvements in geodetic techniques, the interpretation of non-linear motion as a systematic error or a signal of interest was especially difficult (Ray et al., 2004a). Within a given geodetic analysis, the modelled instantaneous position of a site can be defined as a function of time t, according to the relation given by McCarthy and Petit (2004):

$$\vec{X}(t) = \vec{X}_0 + \vec{V}_0(t - t_0) + \sum_i \Delta\vec{X}_i(t) \qquad \text{Eqn 3-1}$$

where X_0 and V_0 are cartesian coordinates and velocities defined at a reference epoch t_0, with the summation referring to modelled time dependent motions which are considered at the model stage of a given analysis. These may include phenomena such as the solid Earth tide, the pole tide, ocean tide loading and atmospheric loading as discussed later in this Chapter. Modelling these displacement signals raises two points of concern in relation to the realisation of the ITRF. Firstly, standardisation (outlined in McCarthy and Petit, 2004, for example) is required by all analysis centres to ensure the most accurate and up-to-date models are utilised when modelling each of these time dependent effects. Secondly, inaccuracies in the adopted models will contaminate the resultant geodetic time series, leaving a residual non-linear signal which is most likely to be site specific. Penna and Stewart (2003) show the potential impact of aliased tidal signals which can arise as a consequence of mis-modelling of periodic site displacement signals, such as those mentioned above. Issues surrounding the standardisation of model corrections, particularly in relation to the geodetic analysis undertaken for this study is investigated throughout §3.3.

Whilst many periodic site displacement effects may be removed at the model stage, many other non periodic geophysical phenomena will manifest with a non-linear signature in the geodetic time series. Seismic displacement, un-modelled continental water loading and local subsidence caused by fluid removal are just three effects which can never be adequately defined by a linear model. Again, until recently however, the interpretation of non-linear residuals computed from a sufficiently long time series have been at a similar magnitude to errors in the definition of the reference frame itself (Ray et al., 2004a). The geophysical interpretation of these residuals has therefore been difficult. Low frequency

seasonal signals (water and mass transfer for example, Blewitt et al., 2001) also affect the estimation of site velocity, as investigated by Blewitt and Lavallee (2002). Blewitt and Lavallee (2002) showed a minimum period of 2.5 years is required to minimise the effect of the low frequency signal on geodetic velocity.

Also contributing to difficulties in the interpretation of "signal" versus "noise" are site specific and environmental effects (Park et al., 2004), antenna model limitations (Zhu et al., 2003), and the influence of aliased periodic signals (Penna and Stewart, 2003). Other influences, such as receiver firmware and antenna changes, have also been shown to introduce offsets in site position (Tregoning et al., 2004), and are not considered in the modelled time evolution of a site position. Likewise, high frequency seismic displacements occurring during tectonic activity bias the estimation of "linear" velocity. With improvements in the understanding of non-linear site motion, and the ability to model discontinuity, co-seismic and post-seismic displacements, an improved description of site velocity is readily possible (for example Nikolaidis, 2002). These effects must be fully considered in order to improve the definition and accuracy of future realisations of the TRF.

In addition to the adequate treatment of periodic effects at the observation level, issues relating to the origin of the TRF are particularly important when investigating higher frequency, non secular, geophysical motion (Chen et al., 1999 and Dong et al., 2003 for example). Blewitt (2003) emphasises that the reference frame must be defined in a manner consistent with the dynamics of the surface loading. Only if this can be achieved will the crustal deformation be accurately related to its effect on the processes under investigation (sea level change, for example).

To expand on these issues, the origin of the ITRF is defined as the Earth's centre of mass (CM), which includes the atmosphere, oceans and surface groundwater (Altamimi et al., 2002). Dong et al. (2003) showed that the centre of the ITRF figure (CF) is no longer indistinguishable from the CM, with seasonal variation at the 1 to 10 mm level (termed 'geocentre' motion[1]). SLR observations have provided the main technique to determine the CM, taking advantage of the sensitivity of a satellite's orbit to the Earth's centre of mass (see for example Pavlis, 2003, Ray, 1999, and Cretaux et al., 2002). An important consideration here is the continuous deformation of the sparse SLR tracking network on the

[1] The definition of the term "geocenter" is not universally accepted. Dong et al. (2003) defines the term as the translation between the CF with respect to the CM. Chen et al. (1999) however uses the translation of the CM with respect to the CE. Blewitt (2003) provides further discussion.

Earth's surface. The reference frame realisation process is clearly highly coupled with the separation of surface processes (Blewitt, 2003 and van Dam and Francis, 2003, for example). To complicate the problem, the invariance of the location of centre of mass of the solid Earth (CE) to surface deformation makes the CE frame the logical choice to determine surface deformation (Blewitt, 2003), using relevant models such as those developed by Farrell (1972) for example. The positional accuracy of crustal reference points is therefore dependent on how well the analysis technique can separate the surface deformations from the relative motion of the centre of mass of the total Earth system (CM) from the solid Earth (CE), in which the surface deformations are modelled (Tregoning and van Dam, 2005). The geometrically defined centre of the ITRF figure (CF) closely approximates the CE. As Blewitt (2003) states, the load Love numbers from Farrell (1972) used in the CE frame are not however identical to those required in the CF frame which are used in geodetic practice. Whilst the differences reach just 2% of their magnitudes (Blewitt, 2003), they represent an important issue which requires consideration in future geodetic analyses and reference frame revisions (such as those discussed by Ray et al., 2004a). These differences have not been considered any further in this analysis as the theory remains an area of active research and debate within the geodetic community. Given identical methodologies have been adopted by the altimetry community (in terms of Love number application in the CF frame), minimal effect is expected in terms of the altimeter absolute bias.

All of these above issues are of importance from the altimeter calibration perspective. Systematic differences in the centre or origin of different orbit solutions (caused by different reference frame realisation processes, or a poorly distributed set of tracking stations for example) will generate geographically correlated 'hemispheric' patterns in the SSH estimates (Haines et al., 2004). Such differences must be considered in the error budget of absolute calibration studies. Issues surrounding the ambiguous definition and treatment of 'geocentre motion' will directly affect results from absolute calibration sites, and again need to be considered in the error budget. The long term temporal stability of the reference frame is also of critical importance to studies of long-term altimeter bias drift.

Many of the issues discussed throughout this section are set to be addressed to some extent in the next release of the ITRF (ITRF2004), due for release in 2005 (Ferland, 2004). Potential improvements and strategies which may be adopted to overcome some of the limitations mentioned are also set for discussion at the upcoming EGU meeting in April 2005 (Ray et al., 2004b). Outcomes from these

future revisions will have a direct impact on altimeter calibration and validation. In the context of this Thesis, computational considerations at the model stage of an analysis will now be investigated.

3.3 Computational Considerations

The position of a site on the Earth's crust varies over a range of temporal scales due to the effects of different geophysical processes. These processes can be categorised as follows:

1. Tectonic motions (both secular and non secular);
2. Tidal displacement (solid Earth tide, the pole tide and ocean tide loading);
3. Mass loadings from the atmosphere, ocean (non steric sea level change for example) and continental water (soil moisture, groundwater, snow, ice etc);
4. Localised effects (fluid extraction and local subsidence for example).

In any geodetic analysis, it is important to consider how each of these processes may affect the site position and hence alter any interpretation of the final time series. Typical sampling strategies for GPS analyses involve 24 hours of sampling at 30 second epochs (Herring, 1999). Tectonic motions (excluding high frequency seismic events) typically operate at very low frequencies in comparison to the sampling strategy. Over the duration of a typical 24 hour observation session, these effects can be considered negligible, with only many successive 24 hour sessions yielding the underlying motion signature.

Tidal displacement and mass loadings on the other hand operate at much higher frequencies and hence must be considered during the processing of each 24 hour session. Tidal displacements may range through ~0.4 m at semi-diurnal and diurnal frequencies, yet average to nearly zero over a 24 hour period. Ocean tide loading is a much smaller effect, still however operating at similar frequencies. Atmospheric pressure loading is typically smaller again, with maximum displacements at the 20-30 mm level (often with high frequency variability). Despite the fact many of these signals average to zero over a 24 hour period, each effect must be considered at the observation level in order to derive a representative estimate of site position for a specific processing session. This therefore implies the use of models to correct for these high frequency displacements, effectively removing their effect from the solution. This approach is particularly important for GPS analysis given the reliance on ambiguity resolution and tropospheric delay estimation over the duration of the 24 hour observation session.

Issues of model selection, accuracy and standardisation therefore become critical when dealing with these high frequency phenomena. The International Earth

Rotation and Reference Systems Service (IERS) have published a series of computation conventions which aid in the treatment of these effects. Published editions include the IERS 1992 (McCarthy, 1992), IERS 1996 (McCarthy, 1996) and most recently the IERS 2003[2] conventions (McCarthy and Petit, 2004). Each addition incorporates changes introduced as a result of developments in theory and/or improvements to relevant models. Indeed, the continued improvements in space geodetic accuracy and precision has forced a parallel development in many of the models such as those presented in McCarthy and Petit (2004). For example, errors introduced in the approximation of the solid Earth tide (at the level of 2% of its magnitude) were initially well within the noise level of geodetic techniques available at the time of release of the IERS 1992 standards. Clearly this is not the case over a decade since the IERS 1992 conventions were published. McCarthy and Petit (2002) provides an additional perspective on the role of adopted conventions on the accuracy and precision of geodetic analyses.

Any investigation into the homogeneity of models adopted by the various geodetic analysis centres (each utilising different software suites) reveals quite dramatic inconsistencies. Weber et al. (2002) for example presents a report from the solid Earth tides subgroup of the IAG/ETC Working Group 6. The study shows an overview of eight IGS analysis centres taken in July 2000, underscoring the considerable variation between models and indeed the actual application of a specific model (ocean tide loading for example). Clearly this situation is changing (Ray et al., 2004a for example), however the burdensome task of recomputation dictates many geodetic time series analysed in the literature contain data computed using significantly different modelling strategies (see Williams et al., 2004 for example). This point, together with its implications for absolute positioning are further emphasised in the analysis presented in §3.5 of this Chapter.

Processing standards and model selection are especially relevant in the context of this Thesis. A rigorous comparison of in situ versus altimeter-derived estimates of SSH can only be achieved following an assessment of the processing algorithms and modelling standards adopted for both measurement systems. These issues are investigated in detail throughout the following sections with a detailed investigation of significant geophysical effects including the solid Earth tide, the permanent tide, the pole tide and ocean tide loading. The much smaller effects of atmospheric and hydrological loading conclude the section.

[2] Note the IERS 2003 publication was initially referred to as the 'draft IERS 2000 conventions', hence the both terms 'IERS 2000' and 'IERS 2003' may be found interchangeably in the literature.

3.3.1 Solid Earth Tide

The solid Earth tide (otherwise termed the Earth body tide) is caused by the elastic response of the crust to the external tide generating potential (TGP). Tidal displacements arise almost entirely from the degree 2 spherical harmonic components of the TGP, with the degree 3 harmonic component contributing a small effect (Mathews et al., 1997). Higher degree harmonics can be considered insignificant to well within the sub-mm accuracy level (Mathews et al., 1997). Estimation of the tidal displacement is typically based on the Love number formalism, described in Munk and MacDonald (1975). This technique expresses the radial and transverse displacement of a point on the Earth's crust in terms of Love and Shida numbers (h and l respectively) in addition to the perturbation in the geopotential field using the Love number k (Mathews et al., 1997).

Initial formulations of the solid Earth tide used in geodetic analyses, such as those presented in the IERS 1992 conventions (McCarthy, 1992), adopted frequency independent Love and Shida numbers which were selected to correspond to the semi-diurnal tides (see also Poutanen et al., 1996). An additional correction is applied in this early formulation to account for the deviation of the Love numbers for the dominant diurnal K_1 tide. This correction is applied solely to the vertical component.

More recently, Mathews et al. (1997) discussed the effect of Love number dependence on station latitude, which arises due to the ellipticity of the Earth and the Coriolis force. Mathews et al. (1997) also discusses the strong frequency dependence of the Love number parameters associated with the diurnal tidal band (an extension of the existing K_1 correction in the IERS 1992 formulation). This frequency dependence arises due to the resonance of the nearly diurnal free wobble (NDFW), associated with the free core nutation (FCN) of the Earth (as discussed in Mathews et al. (1995)). Importantly for geodetic applications, the effect of the resonance is at the centimetre level and hence must be considered. An additional consideration (at the few mm level) is the effect of taking mantle anelasticity into account. Anelasticity introduces a small imaginary component to the Love numbers which reflect a phase lag in the response of the Earth's crust to the TGP. Variations with frequency within the long period tidal frequency band also arise as a result of mantle anelasticity (see Mathews et al., 1997).

The computations described in Mathews et al. (1997) have been incorporated in the recently published IERS 2003 conventions (McCarthy and Petit, 2004). An

even more recent model defining an alternate treatment of the Love numbers is given by Mathews (2001) (the MAT01 model), implemented using a frequency domain approach described in Petrov and Ma (2003). The '*sotid*' software by Petrov, available from http://gemini.gsfc.nasa.gov/sotid, has been utilised to generate an independent verification dataset for IERS 2003 solid Earth tides in the following section.

The solid Earth tide displacements provided with the T/P and Jason-1 altimeter GDR data currently reflect the IERS 2003 conventions (personal communication, B. Haines, 2002). To ensure standardisation with the geodetic analysis presented in this Chapter, the solid Earth tide formulation within the GAMIT GPS analysis suite was investigated. GAMIT was found to utilise IERS 1992 conventions (or more correctly, a truncated version of the Wahr (1981) model), implementing the K_1 frequency dependence as a user selectable option within the sestbl configuration file (King and Bock, 2003). To investigate the differences between the IERS 1992 and 2003 models, the formulation presented in Mathews et al. (1997) (with code available from ftp://omaftp.oma.be/dist/astro/dehant/IERS/) was re-coded within GAMIT. Given that the MAT01 model has been independently verified to within the mm level of the IERS 2003 formulation (personal communication, L. Petrov, 2005), the MAT01 model (accessed through the *sotid* software, independent to GAMIT) was used as an independent verification data set to test the GAMIT implementation. The IERS 2003 compliant GAMIT code has since been supplied to the developers of GAMIT at the Massachusetts Institute of Technology (MIT) and will be made available in the general release of V10.2.

Over a 24 hour observing session, the average difference between the IERS 1992 and IERS 2003 solid Earth tide modelling was found to be negligible (sub mm level) in all components (north, east and up). The difference does however become significant in the height component if the session time is appreciably less than 24 hours. A typical example taken on DOY 110, 2003, at the continuous GPS site at Burnie (used for the Bass Strait calibration study) is shown in Figure 3-1. Figure 3-1(a) shows the solid Earth tide displacement for each topocentric component using the IERS 2003 model, with Figure 3-1(b) showing the difference between the IERS 2003 and 1992 models. Over the duration of this sample, the difference ranges through ~11 mm with a dominant diurnal frequency.

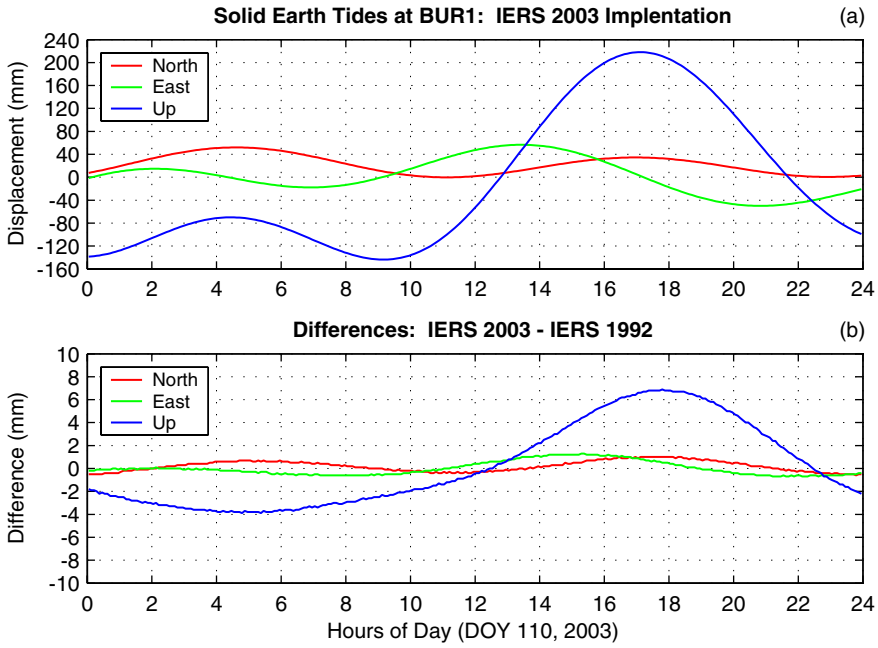

Figure 3-1 Solid Earth tide at the BUR1 GPS site. (a) North, east and up displacement using IERS 2003 standards and (b) North, east and up differences between IERS 2003 and IERS 1992 (up to GAMIT V10.2) standards.

Given the accuracy required in this study, and the potential for observation sessions less than 24 hours (in which case the difference shown in Figure 3-1(b) will not average to zero), the IERS 2003 model was adopted for the GPS analysis presented in this Chapter. To assess the latitudinal dependence of the model differences (and hence gauge its potential effect on long term time series), solid Earth tide displacements for a range of sites in the Australian region (Table 3-1) were computed over an arbitrary 20 day period.

Table 3-1 Sites in the Australian region used to test the latitudinal dependence of the IERS 2003 – IERS 1992 solid Earth tide displacement differences.

Site	Latitude
DARW	-12.84
ALIC	-23.67
CEDU	-31.87
HOB2	-42.80
MAC1	-54.50
CAS1	-66.28

Differences for each site in the vertical component between the IERS 2003 and IERS 1992 formulations are presented in Figure 3-2.

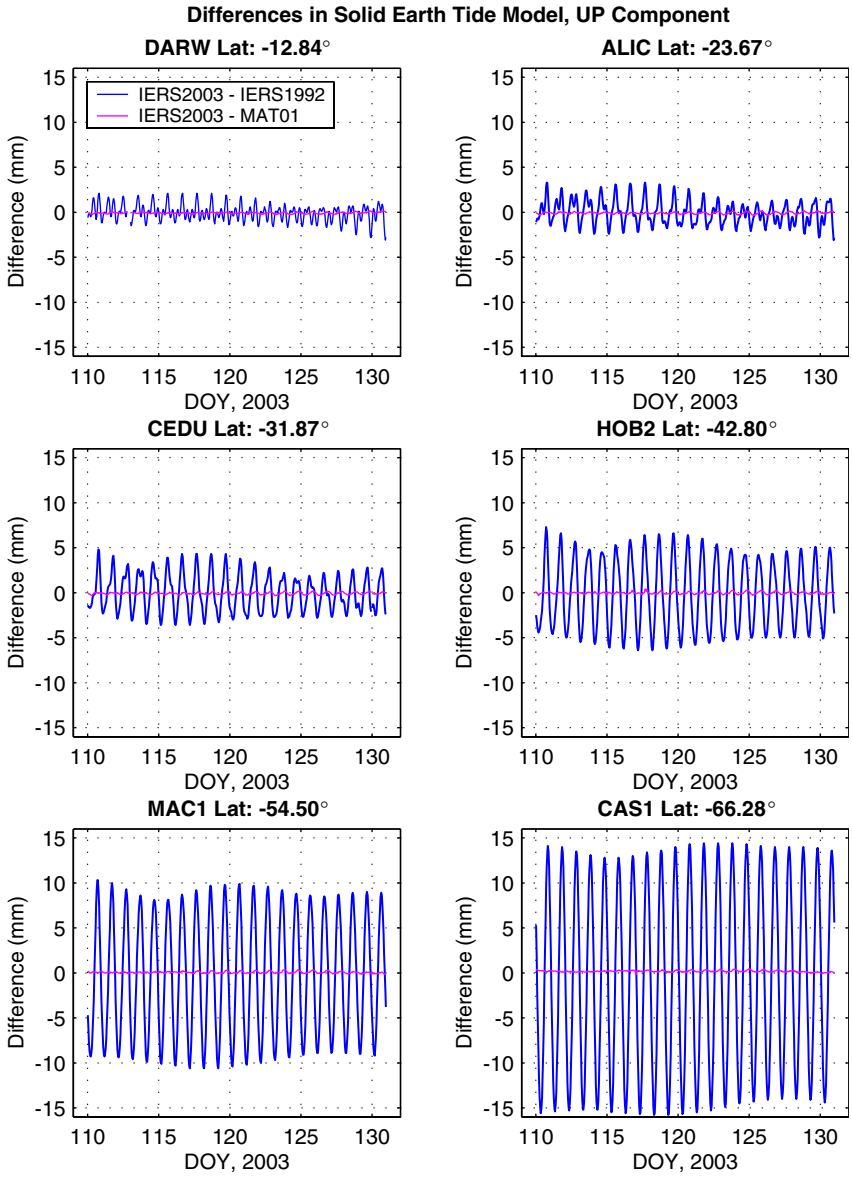

Figure 3-2 Differences in modelled solid Earth tide displacement in the UP component at sites DARW, ALIC, CEDU, HOB2, MAC1 and CAS1 (DOY 110-130, 2003). Note the difference between the GAMIT implementation of IERS 2003 and the validation dataset (MAT01) is also shown.

The latitudinal dependence of the Love numbers is clearly evident in the differences shown in Figure 3-2. Instantaneous differences range through ~30 mm as far south as CAS1 (-66.28°), with the dominant frequency of the difference in the diurnal band. At the most northern site, DARW (-12.84°), the difference ranges through ~5 mm with comparable contributions from both the semi-diurnal and diurnal terms. Figures showing the absolute magnitude of the solid Earth tide

displacements, in addition to the differences between models in the north and east components are provided in Appendix B.

Differences between the GAMIT implementation of IERS 2003 and the MAT01 model are at the sub-mm level (Figure 3-2), providing confidence that the implementation was coded correctly within GAMIT. The same IERS 2003 routine was incorrectly implemented in the Bernese GPS analysis suite (see Hugentobler, 2004 for details). The effect of the coding error was to introduce a diurnal error with a ~10 mm amplitude, in addition to an annual term of similar magnitude. In a similar manner, the inaccuracy of the IERS 1992 model relative to the IERS 2003 implementation (as demonstrated in Figure 3-2) raises interesting implications for the analysis of GAMIT derived time series (Williams et al., 2004 for example). Both of these issues are investigated in the concluding section of this Chapter.

The observed solid Earth tide at a specific point on the Earth's crust includes a time independent (permanent) component which is of particular importance for this study. The so called 'permanent tide' is a source of confusion within the literature (see Poutanen et al., 1996, Sun and Sjoberg, 2001 and Weber et al., 2002 for example). The model formulations presented in the previous paragraphs include the time independent component of the solid Earth tide. Site coordinates derived using these formulations (the ITRF2000 for example) are described as "conventional tide free" values (McCarthy and Petit, 2004). Despite the term "tide free", it is important to note that these values do not truly correspond to what would be observed in an environment devoid of a TGP. The permanent component enters the model formulation due to a degree 2 zonal tide which has a component of zero frequency. The permanent tide is latitude dependent, amounting to approximately -12 cm at the poles and +6 cm at the equator (McCarthy and Petit, 2004).

As discussed in McCarthy and Petit (2004), resolution 16 of the 18th General Assembly of the IAG (1983) stated the need for the uniform treatment of tidal corrections to various geodetic quantities including gravity and station positions. In relation to the permanent tide, the recommendation was "the indirect effect due to the permanent yielding of the Earth be not removed". This implies the use of "mean-tide" values relating to station displacement. Despite the IAG recommendation, the practice adopted within the geodetic community is to compute "conventional tide free" coordinates, i.e., the effect of the permanent deformation is not restored. The GAMIT GPS analysis package is aligned to this practice, and the permanent tide is not restored following the correction for the

Earth body tide. An in-depth discussion in relation to the permanent tide and GPS positioning is provided in Poutanen et al. (1996). It is important to note the terms "zero-tide" and "mean-tide" have the same meaning in relation to the solid Earth tide displacement (McCarthy and Petit, 2004).

A truly "tide free" surface is fundamentally unobservable given the fact the tide generating potential is always present. The solid Earth tide displacements are derived using nominal or "conventional" values for the Love numbers. Restoring the permanent component of the Earth tide using these conventional formulations would yield "mean tide" coordinates as shown in Figure 3-3. It is important to note that the response of the Earth to the permanent component of the TGP is not actually defined by the conventional Love numbers, but the "fluid limit" or "secular" Love numbers (McCarthy and Petit, 2004). The fluid limit values for the Love numbers must therefore be used to remove the permanent tide and define a truly "tide free" surface (Figure 3-3).

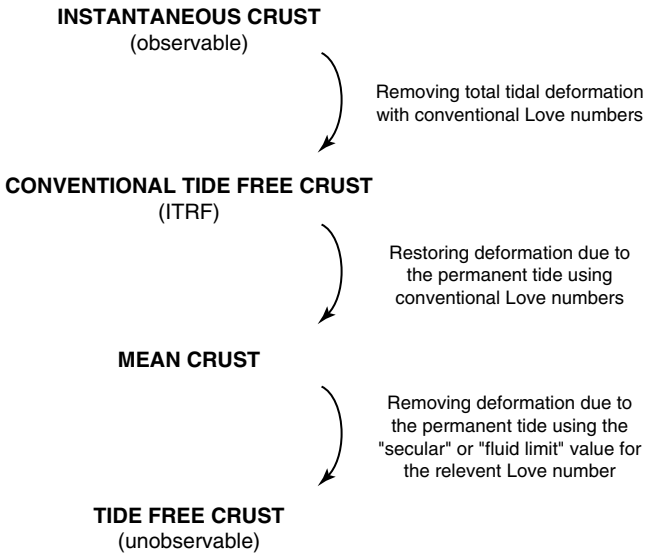

Figure 3-3 Tidal surfaces used in geodetic analyses. (Adapted from McCarthy and Petit, 2004)

In the context of this study, the altimeter measurement is made in a system which includes the permanent attraction of the sun and moon. The altimetry community choose to adhere to the IAG resolution, hence the altimeter GDR solid Earth tide correction has had the permanent component of the Earth tide restored (to yield the "mean tide" position). A correction for the in situ GPS derived coordinates is therefore required to achieve comparable estimates. This correction is applied to in situ estimates of SSH just prior to comparison with the altimeter measurements. Using the IERS 2003 formulation (with "conventional" Love numbers), the

permanent tide at the offshore comparison point at the Bass Strait calibration site has a magnitude of 16.8 mm in the vertical component (see Eqn 3-2 and Eqn 3-3, from McCarthy and Petit, 2004).

$$\Delta h = \left[-0.1206 + 0.0001 P_2\left(\sin\varphi\right) \right] P_2\left(\sin\varphi\right) \qquad \text{Eqn 3-2}$$

where:

$$P_2\left(\sin\varphi\right) = \left(3\sin^2\varphi - 1\right)/2 \qquad \text{Eqn 3-3}$$

where Δh is the permanent tide vertical displacement and φ is the geocentric latitude of the station.

3.3.2 Pole Tide

The pole tide displacement arises due to changes in the pole of rotation of the Earth, which causes changes in the centrifugal potential at a given location. The instantaneous pole position varies over time with two dominant frequencies. The first has an annual period and the second has a period of approximately 14 months (430 days), corresponding to the Chandler wobble period of the Earth (Munk and MacDonald, 1975).

The pole tide has a maximum displacement in the vertical component of approximately 25 mm and 7 mm in the horizontal component (McCarthy and Petit, 2004). Using a conventional Love number approach, McCarthy and Petit (2004) defines the pole tide displacement at a given geocentric latitude (φ) and longitude (λ) according to the relations given in Eqn 3-4.

$$\begin{aligned} S_r &= -32\sin 2\varphi\left(m_1\cos\lambda + m_2\sin\lambda\right) \quad mm, \\ S_\varphi &= -9\cos 2\varphi\left(m_1\cos\lambda + m_2\sin\lambda\right) \quad mm, \\ S_\lambda &= +9\cos\varphi\left(m_1\sin\lambda - m_2\cos\lambda\right) \quad mm. \end{aligned} \qquad \text{Eqn 3-4}$$

where S_r is the radial displacement (positive upwards), S_φ and S_λ are the horizontal displacements (positive south and east respectively) and m_1 and m_2 define the time dependent offset of the instantaneous rotation pole from a defined mean position (in seconds of arc). More explicitly, the pole positions (m_1 and m_2) can be defined according to McCarthy and Petit (2004), in Eqn 3-5.

$$m_1 = x_p - \bar{x}_p, \qquad m_2 = -\left(y_p - \bar{y}_p\right) \qquad \text{Eqn 3-5}$$

where x_p and y_p refer to the instantaneous pole position, and $\bar{x}_p$ and $\bar{y}_p$ refer to the mean position of the pole.

The requirement of a "mean pole" position introduces an ambiguity into the computation of a standardised pole tide displacement. Once again, to ensure comparable estimates with the altimeter, the pole tide applied with the GAMIT GPS analysis suite was investigated. GAMIT derived estimates of the pole tide were compared with those supplied with the altimeter (corrected to remove the ocean pole tide as discussed in Desai, 2002). Comparisons made in the vertical component for each episodic GPS campaign (discussed in §3.4) reveal a constant difference between the modelled pole tide displacement at the 7 to 8 mm level (Figure 3-4).

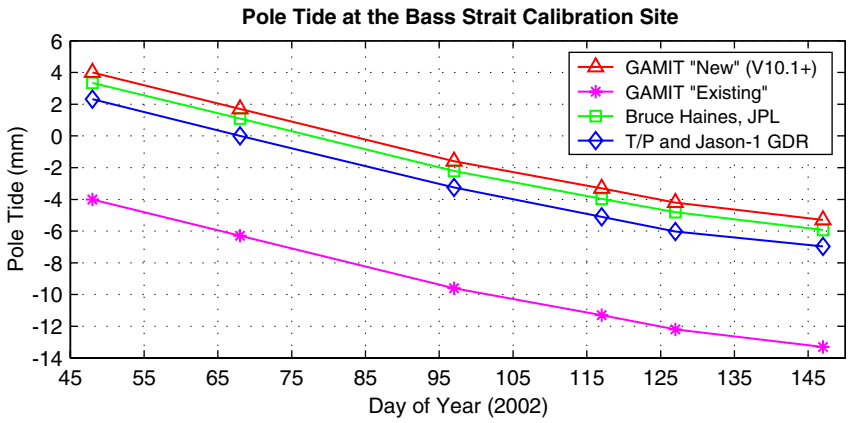

Figure 3-4 Pole tide displacement in the vertical component at the Bass Strait comparison point. Models shown include the "existing" GAMIT model, the "new" GAMIT model (V10.1 and above), B Haines IERS 2003 implementation and the T/P~Jason-1 GDR implementation.

Investigations into the GAMIT/GLOBK code showed that the adopted position of the mean pole (defined by $\bar{x}_p$ and $\bar{y}_p$) was set to the Celestial Intermediate Origin (the CIO, i.e., $\bar{x}_p = 0$ and $\bar{y}_p = 0$). The IERS 2003 standard adopts a mean pole position which varies linearly over time according to Eqn 3-6 (McCarthy and Petit, 2004):

$$\begin{aligned} \bar{x}_p(t) &= \bar{x}_p(t_0) + (t - t_0)\dot{\bar{x}}_p(t_0) \\ \bar{y}_p(t) &= \bar{y}_p(t_0) + (t - t_0)\dot{\bar{y}}_p(t_0) \end{aligned} \qquad \text{Eqn 3-6}$$

$$\bar{x}_p(t_0) = 0.054,\ \dot{\bar{x}}_p(t_0) = 0.00083,\ \bar{y}_p(t_0) = 0.357,\ \dot{\bar{y}}_p(t_0) = 0.00395$$

where $\overline{x}_p$ and $\overline{y}_p$ are in arcseconds, rates in arcseconds per year and t_0 is epoch 2000.0. The IERS 2003 standard was again coded into the GAMIT/GLOBK suite (this particular code change was undertaken by Professor Tom Herring, MIT in 2003), with the results comparable to the estimates from Dr Bruce Haines (JPL, IERS 2003 implementation) and the T/P and Jason-1 estimates. The slight discrepancy between the altimeter and GAMIT IERS 2003 estimates is most likely related to the technique used to remove the ocean contribution from the altimeter pole tide (see Desai, 2002). The effect of the pole tide change on GAMIT based GPS analyses is largely dependent on the network size and reference frame realisation process. For global solutions, this represents a significant change which demonstrates the meticulous (and continuous) approach required to standardise solutions, and compute accurate heights in an absolute reference frame.

3.3.3 Mass Loading Deformations

In addition to the solid Earth tide and pole tide, various mass loadings introduce site displacements which are both periodic and non-periodic in nature. van Dam and Wahr (1998) provides an overview of these 'environmental' loading effects, with a more contemporary review given by van Dam et al. (2002). The later is a report from the Special Bureau of Loading (SBL), which reports directly to the IERS.

3.3.3.1 Ocean Tide Loading

Ocean tide loading (OTL) introduces both radial and tangential displacement of the Earth's crust due to the temporal variation of the ocean mass distribution which accompanies ocean tides. The effect of OTL on site position is typically an order of magnitude higher than the current precision of space geodetic techniques, and hence has received considerable attention in the literature (Lambert et al., 1998, Scherneck and Haas, 1999, Dach and Dietrich, 2000 and Allinson et al., 2004 for example). Penna and Baker (2002) provide an Australian context, emphasising OTL displacements can (in extreme cases), vary over 100 mm in a period as short as 6 hours. OTL is therefore an important consideration in the analysis of space geodetic data, with correction for site displacement required at the observation level. As described in McCarthy and Petit (2004), OTL displacement (Δc) can be

described as a summation of significant tidal species (amplitude and phase), with corrections for the modulating effect of the lunar node (Eqn 3-7).

$$\Delta c = \sum_j f_j A_{cj} \cos\left(\omega_j t + \chi_j + u_j - \Phi_{cj}\right) \qquad \text{Eqn 3-7}$$

where A_{cj} and Φ_{cj} are the tidal amplitudes and phases of the displacement (for site c and constituent j), ω_j is the tidal angular velocity, χ_j is the astronomical argument and f_j and u_j depend on the longitude of the lunar node (Doodson and Warburg, 1941). The accepted standard for the computation of the displacement constituents uses a parameterised model of the solid Earth, as described in Scherneck (1991). Amplitudes and phases for 11 primary constituents are computed, namely the semi-diurnal tides (M_2, S_2, N_2 and K_2), the diurnal tides (O_1, K_1, P_1 and Q_1) and the long period tides (M_f, M_m and S_{sa}). An example for the Hobart VLBI and GPS site is provided in Table 3-2.

Table 3-2 OTL Amplitudes and phases for the Hobart VLBI and GPS site from GAMIT GPS analysis suite, stations.oct (V10.1).

```
  HOBART    7242
$$ CSR4_CC_PP_PTM ID: Jun  16, 1999 19:44
$$ Computed by H.G.Scherneck on gere.oso.chalmers.se, 1999
$$ HOBART          50116S002, VLBI      RADI TANG lon/lat:  147.4405  -42.8036
$$ M2       S2       N2       K2       K1       O1       P1       Q1       Mf       Mm       Ssa
  .01032 .00152 .00255 .00039 .00737 .00673 .00244 .00161 .00026 .00021 .00017
  .00456 .00190 .00084 .00052 .00110 .00059 .00035 .00011 .00002 .00011 .00000
  .00104 .00064 .00019 .00018 .00147 .00132 .00049 .00032 .00003 .00003 .00003
   155.4 -120.4  130.7 -101.6   88.8   56.5   86.8   46.0    9.5  -62.7 -180.0
   102.0  134.5  101.0  138.8 -162.0 -165.7 -161.8 -171.6  -50.3   70.8     .0
   119.3  104.5  122.5  103.3 -142.8 -162.3 -143.0 -175.3 -152.6  100.9     .0
```

The largest uncertainty associated with OTL displacements arises from inaccuracies in the global ocean tide models as opposed to the solid Earth model (Penna and Baker, 2002). The example shown in Table 3-2 uses a combined model with semi-diurnal and diurnal terms from the CSR4.0 model (Eanes and Bettadpur, 1995) and long period tides from the Schwiderski model (Schwiderski, 1980).

Within the GAMIT analysis suite, ocean loading is modelled according to Scherneck (1991), with transverse and radial amplitudes and phases for the 11 tidal components read directly (c.f Table 3-2) or interpolated from a global grid. The GAMIT implementation uses station and grid tables derived from tables created by Hans-Georg Scherneck from the Onsala Space Observatory. An automated loading service is available at http://www.oso.chalmers.se/~loading which allows the

computation of OTL parameters (amplitudes and phases) for 12 different tidal models.

Existing constituents from Scherneck, distributed with the GAMIT suite, were adopted for the geodetic analysis presented in this Chapter. Instantaneous OTL estimates from both altimeters were compared to the GAMIT estimates with differences within the ± 2 mm level ($< 10\%$ of the absolute magnitude of the correction). This was deemed sufficiently accurate given the averaging effect over the duration of the measurement session. The effect of modelling OTL and its impact on long term time series is revisited in the concluding section of this Chapter.

3.3.3.2 Atmospheric Loading

Changes in atmospheric mass load the Earth's crust and cause measurable, quasi-periodic displacement. Atmospheric pressure variations show typical periods of ~2 weeks with amplitudes at the 20 HPa level (McCarthy and Petit, 2004). Pressure systems are highly spatially correlated (1000-2000 km) which influences the response of the Earth's surface at coastal areas (assuming an inverse barometer response from the ocean). Seasonal and inter-annual signals also contribute to the loading signal. At the upper limit, displacements in the vertical component of 20-30 mm can be observed with the passage of a 50 HPa change in atmospheric pressure (Sun et al., 1995). Values in the horizontal component are typically one third to one tenth of this magnitude. The loading effect is greatest at the poles due to the intensity of the synoptic systems and the high spatial coherence of those systems (McCarthy and Petit, 2004)

The influence of atmospheric pressure loading has been the focus of attention in the literature since relatively early works by Rabbel and Schuh (1986) and van Dam and Wahr (1987). Corrections for the loading signal have been applied to both VLBI (van Dam and Herring, 1994, Petrov and Boy, 2004) and GPS (van Dam et al., 1994, Tregoning and van Dam, 2005). Results show significant improvements in the scatter of geodetic time series when adopting atmospheric loading models at the observation level within the analysis.

The standard approach used to model atmospheric loading involves the convolution of Green's functions (Farrell, 1972) with a surface pressure field such as the

National Centre for Environmental Prediction (NCEP) assimilation. Given sub-daily variations as high as 15 HPa, displacements must be considered at the observational level in a geodetic (GPS) analysis (as investigated in van Dam and Tregoning, 2005, for example). At the time of writing, the IERS Special Bureau on loading was preparing to distribute near real time loading corrections to the geodetic community (see http://www.sbl.statkart.no/), enabling the integration of the correction within existing software.

Within the GAMIT analysis adopted for this study, the effect of atmospheric loading was not considered. At the time of writing, the ability to correct for atmospheric loading had just been integrated into the software, and was in preparation for standard release in V10.2 (personal communication, P. Tregoning, 2005).

The impact of neglecting to consider the modelling of atmospheric loading is not considered significant in terms of biasing the datum for this calibration study. There is no doubt however that the correction remains a source of further investigation in relation to the analysis of long term geodetic time series used in the computation of site velocity (particularly in the vertical component), as required to compute estimates of altimeter bias drift.

3.3.3.3 Hydrological Loading

The final remaining loading signal of interest relates to the influence of the variation in water mass accumulating on, or distributed around, the Earth's crust (see van Dam and Wahr, 1998, for a review). Changes in soil moisture and groundwater volume, in addition to snow and ice cover introduce variations in mass load leading to site displacement. Non steric changes in sea level also introduce a variable mass loading which requires consideration. Of the mass loadings discussed, hydrological loading is particularly problematic, primarily due to the inherent difficulty in quantifying and modelling the load signal. Recent results from the twin Gravity Recovery and Climate Experiment (GRACE) satellites confirm seasonal cycles in geoid variation attributed to surface and groundwater variations (Tapley et al., 2004a). Blewitt et al. (2001) showed seasonal displacements observed from GPS analyses which are again attributed to hydrological loading (exceeding seasonal atmospheric loading displacements). Munekane and Matsuzaka (2004) review the influence of non tidal ocean mass

loading on site displacement. By estimating the non tidal ocean mass change (determined by subtracting the steric change from the net sea level change observed from satellite altimetry), Munekane and Matsuzaka (2004) show positive correlation with observed GPS vertical movements in their study area in the tropical Pacific. Other studies investigating continental water loading, such as van Dam et al. (2001), showed displacements as high as 15-30 mm in equatorial areas, such as the Amazon Basin and throughout parts of northern India. Of particular interest in the van Dam et al. (2001) study is the low frequency power of the hydrological signal, which can introduce long term variability appearing as a secular signal over periods of a few years. These rates were typically less than 0.5 mm/yr over a three year period, however as high as 2.5 mm/yr in some areas (south from the Amazon Basin for example). These results have considerable influence on estimates of altimeter bias drift in the context of this study.

As for atmospheric loading, hydrological modelling has not been considered for this analysis. Results presented in both Tapley et al. (2004a) and van Dam et al. (2001) show minimal displacement in the region surrounding the Bass Strait study site. There is no doubt however that hydrological loading has an influence over other sites used in the GPS regional analysis (DARW in northern tropical Australia for example), and hence the loading term must be considered in the overall error budget. As for atmospheric loading, the hydrological loading of the crust would require increased attention when estimating vertical site velocity from long term geodetic time series.

3.3.4 Summary

At this intermediate stage of Chapter 3, it is important to summarise the discussion in the context of this study:

- Absolute altimeter calibration requires comparison across different space geodetic platforms. Issues of reference frame realisation are therefore fundamentally important to ensure comparable estimates of SSH, and a reliable estimate of absolute bias.

- Issues of reference frame stability become important in the computation of vertical site velocity, as required for studies involving altimeter bias drift.

- The continued improvement in space geodetic accuracy has placed a renewed emphasis on various loading signals which were previously well within the noise level present in geodetic time series. The treatment of these loading signals in the definition of the reference frame is playing an increasingly important role.

- Typical analyses of GPS data (as utilised in this study) require the assimilation of observed data over a 24 hour period. Various tidal and non-tidal phenomena displace the Earth's crust at various frequencies (including many at sub-daily frequencies). These displacements must therefore be treated at the observation level which raises issues of model accuracy and standardisation.

- Discrepancies were found in the modelling of the solid Earth tide and the pole tide in the GAMIT GPS analysis suite. Changes were made to conform to both the IERS conventions and the corrections supplied with the satellite altimeter GDR product. This raises interesting implications for many analyses presented in the literature (see §3.5)

- Reliable estimates of vertical velocity and their associated uncertainty may only be determined following a holistic approach, taking each of these separate issues into consideration. Remaining secular, geophysical signals of interest (such as glacial isostatic adjustment, Scherneck et al., 2003 and Scherneck et al., 2001) and tectonic motion can only then be meaningfully interpreted.

3.4 Geodetic Analysis at the Bass Strait Calibration Site

3.4.1 Overview

The primary aim of the geodetic analysis at the Bass Strait calibration site is the computation of reference station coordinates relative to ITRF2000. These coordinates are then adopted in the kinematic analysis of the episodic GPS buoy deployments, as presented in Chapter 4. The output of the GPS buoy analysis is therefore sea level relative to ITRF2000, directly comparable with T/P and Jason-1 products. A secondary aim is the estimation of the vertical velocity of the local tide gauge site. This long term velocity (and uncertainty) is required for the future estimation of bias drift at the calibration site. The vertical velocity at the Bass Strait calibration site is investigated in §3.5 as part of an inter-comparison of various long term geodetic time series. For this analysis, the time series from the continuously operating GPS located at the Burnie tide gauge site is investigated. These data are processed by Assoc. Professor Peter Morgan (University of Canberra), as part of a regional GPS solution.

The methodology adopted for the GPS analysis presented in this section involves the integration of local reference stations at the Bass Strait calibration site with a larger regional network. The regional network is processed using a fiducial free strategy (as discussed in §3.2) using the GAMIT suite (King and Bock, 2003). Results from the regional analysis are combined with global solutions computed by the Scripps Orbital and Permanent Array Centre (SOPAC) using the GLOBK package (Herring, 2002). The output is subsequently transformed onto the latest realisation of the ITRF using the ITRF2000 coordinate and velocity set (Altamimi et al., 2002).

This section of the Chapter begins with a review of the reference station selection, then progresses to detail both the GAMIT and GLOBK analysis and results.

3.4.2 GPS Reference Stations

When selecting GPS reference sites for the Bass Strait calibration study, three main factors influenced the number and location of sites:

1) Co-location with the Burnie tide gauge to allow the estimation of vertical velocity of the tide gauge over the long term.

2) Redundancy to support the GPS buoy processing (i.e., multiple base station sites to allow for solution inter-comparison and physical redundancy in case of instrument failure); and

3) Minimum baseline lengths to the GPS buoy deployment site to improve the accuracy of the kinematic processing.

The long term monitoring of site position requires a continuously operating GPS installation. The first criterion was therefore achieved with the installation of a receiver co-located with the Burnie tide gauge. To satisfy the final two criteria, two additional sites were installed. Due to logistical and operational considerations, these additional sites are operated on a purely episodic basis in support of the GPS buoy deployments (Table 3-3). Each additional site is located on a prominent headland, minimising the baseline lengths to the buoy deployment locations.

Table 3-3 Episodic GPS sessions at the Bass Strait calibration site.

Session	Date	Day of Year
1	21/09/2001	264
2	17/02/2002	048
3	09/03/2002	068
4	07/04/2002	097
5	27/04/2002	117
6	07/05/2002	127
7	27/05/2002	147

3.4.2.1 Local Area GPS Reference Stations

The primary GPS station is a continuously operating receiver, co-located with the Burnie tide gauge (site name: BUR1). The receiver has been in operation since installation in April 1999. The Burnie GPS antenna is mounted on a stainless steel pillar which is directly attached to the tide gauge support structure (Figure 3-5). Both the antenna reference point (ARP) and the tide gauge zero are connected to a network of tide gauge benchmarks (TGBM's) by traditional survey techniques. The GPS hardware includes an Ashtech Z-Fx receiver, Ashtech choke ring antenna and SCIGN antenna dome (Hudnut, 1999). Data are logged on-site at 30-second intervals. On a daily basis, these data are uploaded and archived by Geoscience Australia.

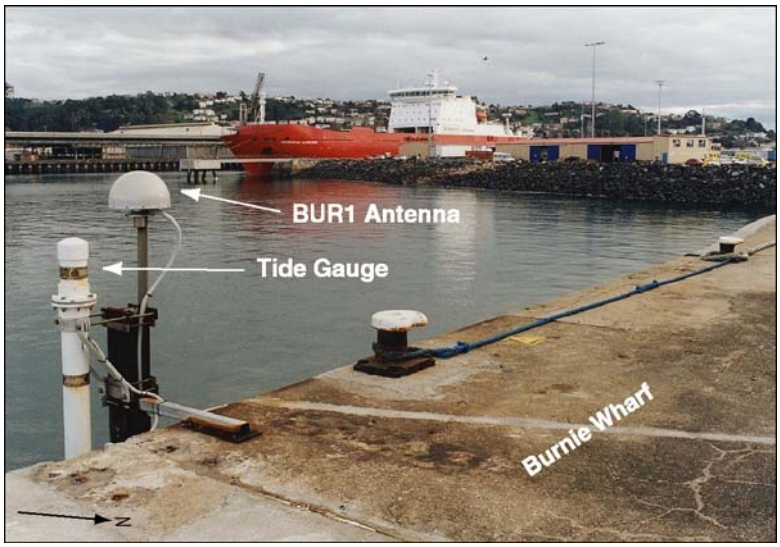

Figure 3-5 Continuously operating GPS station (BUR1), collocated with the Burnie tide gauge.

The tide gauge and GPS antenna are located on a concrete wharf which acts as a breakwater for the nearby Burnie port. The breakwater wall extends approximately 3 m above the concrete level shown in Figure 3-5. Potential signal obstructions, in addition to the breakwater wall, include a meteorological sensor mast and a steel handrail positioned on top of the breakwater. These site conditions combined with a cyclone and razor wire security fence located on the seaward extremity of the breakwater (approximately 6 to 8 m away) make the BUR1 GPS site less than ideal from a GPS signal reception and multipath perspective (see Park et al., 2004 for example). Given the tide gauge is located on a structure built on reclaimed land, the emphasis must however be monitoring the vertical position and velocity of the tide gauge, which may or may not be aligned

with the underlying crustal position and velocity. Figure 3-6 shows a sky-plot highlighting the azimuth and elevation of the various obstructions at the BUR1 GPS site. Scale diagrams in plan and elevation for the BUR1 site are provided for further inspection in Appendix B.

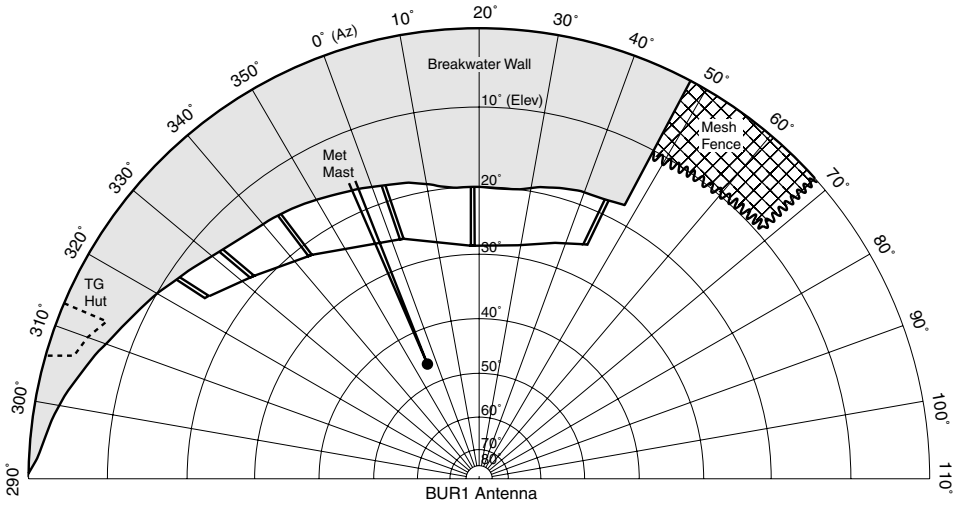

Figure 3-6 *Sky-plot from the BUR1 Antenna showing the azimuth and elevation of the breakwater wall, hand rail, met sensor mast and mesh security fence. There are no obstructions between 110° and 290°.*

Various outages to the BUR1 data supply have occurred since its installation in 1999. The percentage of daily data obtained at the BUR1 site is shown in Figure 3-7, extracted using TEQC software (Estey and Meertens, 1999). Two significant periods are clearly noticeable where data availability drops to less than 50%. These periods correspond to failures within the receiver, caused as a result of a storm which also damaged the tide gauge hut. Since January 2003, the BUR1 site has been performing to its maximum potential with the exception of some short power outages.

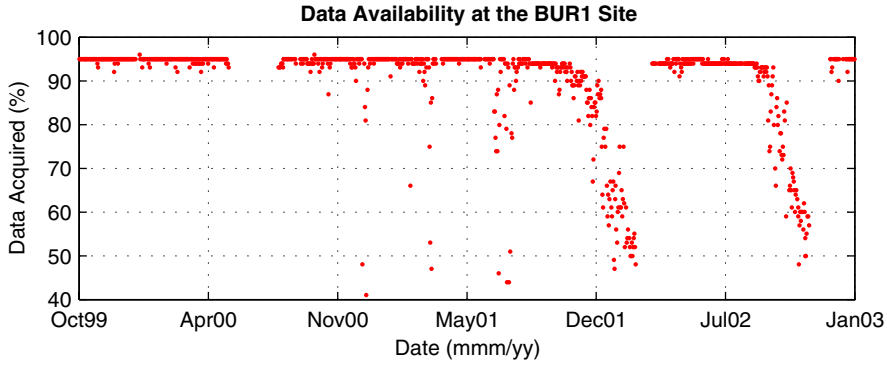

Figure 3-7 *Data availability at the BUR1 GPS site. Note the two periods of significant degradation and subsequent failure of the receiver.*

The performance of the BUR1 site is revisited in §3.5 when the coordinate time series from the site is investigated.

The two supplementary GPS stations (operated on an episodic basis during each buoy deployment campaign) were installed at Table Cape (site name: TBCP) and Rocky Cape (site name: RKCP). TBCP and RKCP consist of stainless bolts drilled and set into bedrock on the two prominent headlands (Figure 3-8). Leica AT504 choke ring antennas are fixed to the permanent bolts when required. Leica CRS1000 receivers are used at both sites to match the receivers used in the GPS buoys. This was an important design consideration to ensure identical performance (both in terms of the stochastic behaviour of code and carrier measurements and signal tracking ability) for the kinematic analysis of the GPS buoys.

Figure 3-8 *Table Cape (TBCP) and Rocky Cape (RKCP) GPS reference stations.*

During the buoy deployment window (typically 4 hours), all reference stations log at 1 second intervals to support kinematic GPS processing. In addition, receivers at TBCP and RKCP log data at 30-second intervals for approximately 12 hours either side of the altimeter overflight. These data are used during the reference station analysis presented in this Chapter. The use of TBCP and RKCP as reference stations simplifies the differential kinematic processing of the GPS buoy data by minimising baseline lengths to the offshore comparison point (see discussion in Chapter 4).

3.4.2.2 Regional GPS Reference Stations

During the processing of the reference stations, data from local sites BUR1, TBCP and RKCP are augmented with data from the Australian Regional GPS Network (ARGN) forming a 17 site regional network (Twilley and Digney, 2001). The network incorporates stations from the Australian and Antarctic regions (Figure 3-9).

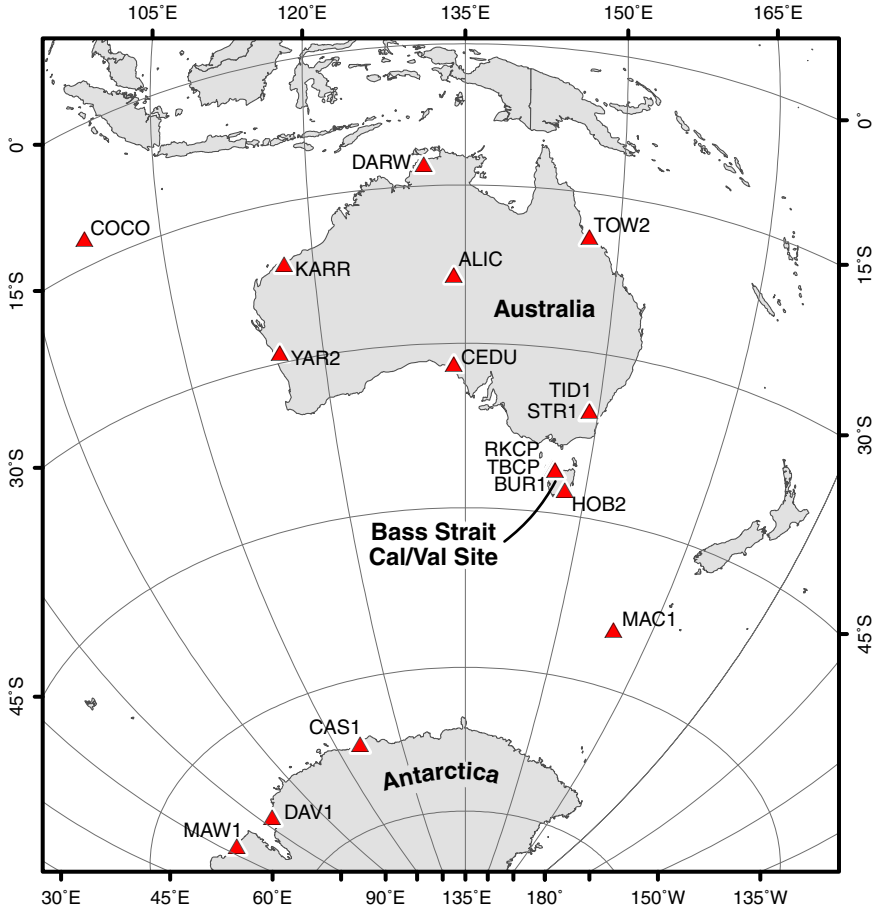

Figure 3-9 The Australian Regional GPS Network (ARGN) and the Bass Strait calibration site reference stations. The ARGN also contributes to the International GPS Service (IGS) global network, which is used in the definition of the International Terrestrial Reference Frame (ITRF).

The majority of the ARGN sites processed in the regional network (Figure 3-9) are also processed as part of the "IGS" global network. This therefore provides the necessary link to combining daily solutions from the regional network with global data to define a global reference frame aligned to the ITRF2000 coordinate and velocity set.

3.4.3 GPS Analysis Methodology and Computational Standards

The GAMIT (King and Bock, 2003) and GLOBK (Herring, 2002) analysis procedures have been well documented in the literature, with notable examples which track the development of GAMIT presented by Dong and Bock (1989), Feigl et al. (1993), Bock et al. (1997) and Tregoning et al. (1998). More recent studies utilising the software include Beavan et al. (2002) and Steblov et al. (2003), with Zhang et al. (1997), Dong et al. (2002) and Williams et al. (2004) analysing time series of geodetic sites (computed using GAMIT software). Other notable publications include McClusky et al. (2000) who provide an excellent discussion surrounding the regional analysis strategy, with Dong et al. (1998) providing the best discussion surrounding the development and operation of the GLOBK software.

In an Australian context, Morgan et al. (1996) utilised a regional analysis approach using the GAMIT suite. Pas (2004) tests the equivalence of regional and global GPS solutions, using a recent Australian regional network time series computed by Assoc. Professor Peter Morgan (University of Canberra).

The GPS analysis methodology adopted here largely follows these studies and can be briefly described as a three step process:

1) Double differenced GPS observations (using the 'LC' ionosphere-free linear combination) from each site within the regional network (Figure 3-9) are processed within GAMIT using a least squares methodology to derive estimates of station coordinates, tropospheric zenith delay parameters (computed at each station at given time intervals), orbital parameters and Earth orientation parameters (EOPs). The parameters are held loosely fixed achieving a free network solution as discussed in §3.2. A solution for each episodic observing session is determined (seven sessions in total).

2) The second stage of the analysis involves combining the regional solutions from the previous step with global solutions computed by SOPAC, also derived using the GAMIT suite. In this step, estimates of the parameters (station coordinates, orbits and EOPs) and their associated variance / covariance matrices are combined as quasi-observations in a Kalman filter implemented using the GLOBK suite (see Dong et al., 1998). The link between the regional and global networks is achieved using common sites existing between the various networks (the ARGN used in the regional

network contributes to the IGS global network, hence the ARGN sites are included in the SOPAC global solutions).

3) The final stage defines the reference frame by transforming the combined global polyhedra determined in the previous step onto the ITRF2000 coordinate and velocity set (Altamimi et al., 2002). The GLORG utility within the GLOBK suite is used for this reference frame realisation and stabilisation process.

Specific issues relating to the GAMIT and GLOBK analysis for this study are discussed throughout the following sections.

3.4.3.1 The GAMIT Analysis

The GAMIT processing configuration selected for the regional network solution remains relatively standard for this analysis, largely adopting the SOPAC regional analysis strategy (Jamason et al., 2004). As discussed in §3.3, updated versions of the solid Earth tide and the pole tide aligned to IERS 2003 standards were coded into GAMIT and adopted for this analysis. The GAMIT "Relax" mode of processing was adopted, solving for both station position and constrained orbital parameters using the IGS final orbits as the apriori orbit. The double differenced ionosphere-free combination 'LC' was used as the basic observable, with ambiguity fixing attempted using both an ionospheric constraint and pseudo range data (the GAMIT "LC_Help" strategy). One zenith delay parameter was solved for every one hour. A piecewise linear model is used with variation between steps constrained with a Gauss-Markov process defined by 0.02 $m/\sqrt{hr}$ and a correlation time of 100 hours. An elevation cut-off of 10° was adopted (see discussion in Tregoning et al., 1998). Elevation dependent re-weighting of observations was performed using the AUTCLN utility (King and Bock, 2003) using a weighting function of the form $a^2 + b^2/\sin(elevation)^2$. Elevation dependent phase centre modelling was adopted, based on the NGS models (Mader, 1999). .

Following each daily solution in GAMIT (see Table 3-3 for the dates of each individual observation session), the normalised root mean square (nrms) statistic provides the first quality indictor for the solution. The nrms is a scalar statistic

which is defined as the square root of chi-square (χ^2) per degree of freedom (Eqn 3-8):

$$nrms = \sqrt{\chi^2 / f} \qquad \text{Eqn 3-8}$$

where f is the degrees of freedom. Early experience with regional networks by Morgan et al. (1996) suggests a normal range for this statistic is between 0.2 and 0.4, assuming a nominal apriori measurement error at the 10 mm level. Improvements in the nrms are to be expected since the Morgan et al. (1996) study due to improvements in orbit modelling, receiver tracking ability, antenna modelling and loading models to name a few. The nrms for the seven solutions undertaken in this analysis remained between 0.17 and 0.18 (Figure 3-10), suggesting a satisfactory fit between the observations and the model adopted within the GAMIT parameter estimation process.

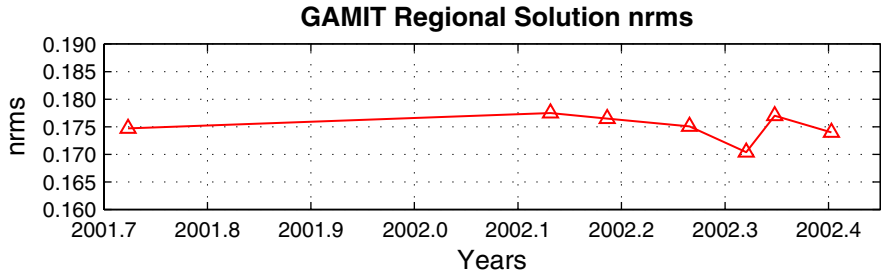

Figure 3-10 GAMIT nrms from the seven episodic solutions of the regional network.

The formal uncertainties computed in each GAMIT solution are a second indicator of solution quality. The uncertainty derived within GAMIT relates directly to the strength of the network in addition to the levels of constraint placed on the parameters in the solution (Morgan et al., 1996). Station constraints for sites in the regional solution were typically at the 1 m level in each of the three coordinate components, with the exception of four well known sites in the ARGN (Hobart, Karratha, Townsville and Yarragadee), which were constrained at the 0.05 m and 0.1 m level in the horizontal and vertical components respectively. Orbital constraints were relatively tight given IGS final orbits were utilised (0.1 ppm or 20 cm for the Keplerian elements and a 0.01% value for the non-gravitational force parameters). The computed uncertainties (in the radial or up component) for the Bass Strait reference sites are at the 30-32 mm level (Figure 3-11).

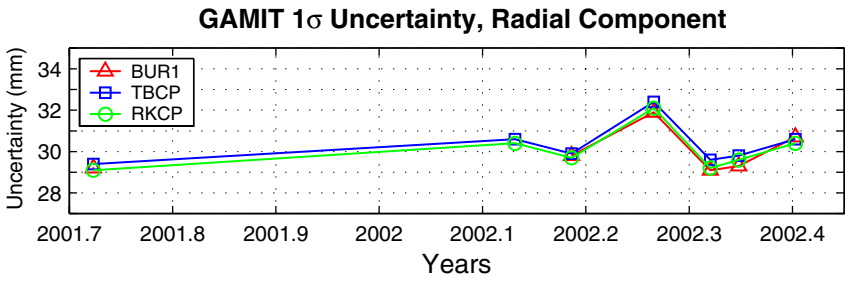

Figure 3-11 GAMIT 1-sigma uncertainties in the radial component at the BUR1, TBCP and RKCP sites.

The uncertainties from the GAMIT analysis (Figure 3-11) are considered well within acceptable limits, underscoring a successful series of analyses for the episodic measurement sessions.

3.4.3.2 The GLOBK Analysis

Two separate analyses were undertaken in the GLOBK suite using the loosely constrained GAMIT solutions described in the previous section.

1) Firstly, the GLOBK/GLORG utilities were used to combine three SOPAC global network solutions (the IGS1, IGS2 and IGS3 networks respectively, see Jamason et al., 2004 for information on the division of the networks) with the ARGN / Bass Strait regional solutions for each observation session. This analysis aims to determine the best estimate of site position and uncertainty over the complete duration of the campaign. As only seven episodic sessions were observed, velocities were not estimated. This analysis produced the definitive ITRF2000 positions for BUR1, TBCP and RKCP used for the Bass Strait Calibration study.

2) Secondly, the GLRED/GLORG utilities were used to investigate the repeatability in each coordinate component between the seven episodic solutions. This analysis is undertaken purely to further investigate the uncertainty of the final coordinates as discussed in §3.4.4.

The ARGN, IGS1, IGS2 and IGS3 networks used in the GLOBK analysis are shown in Figure 3-12.

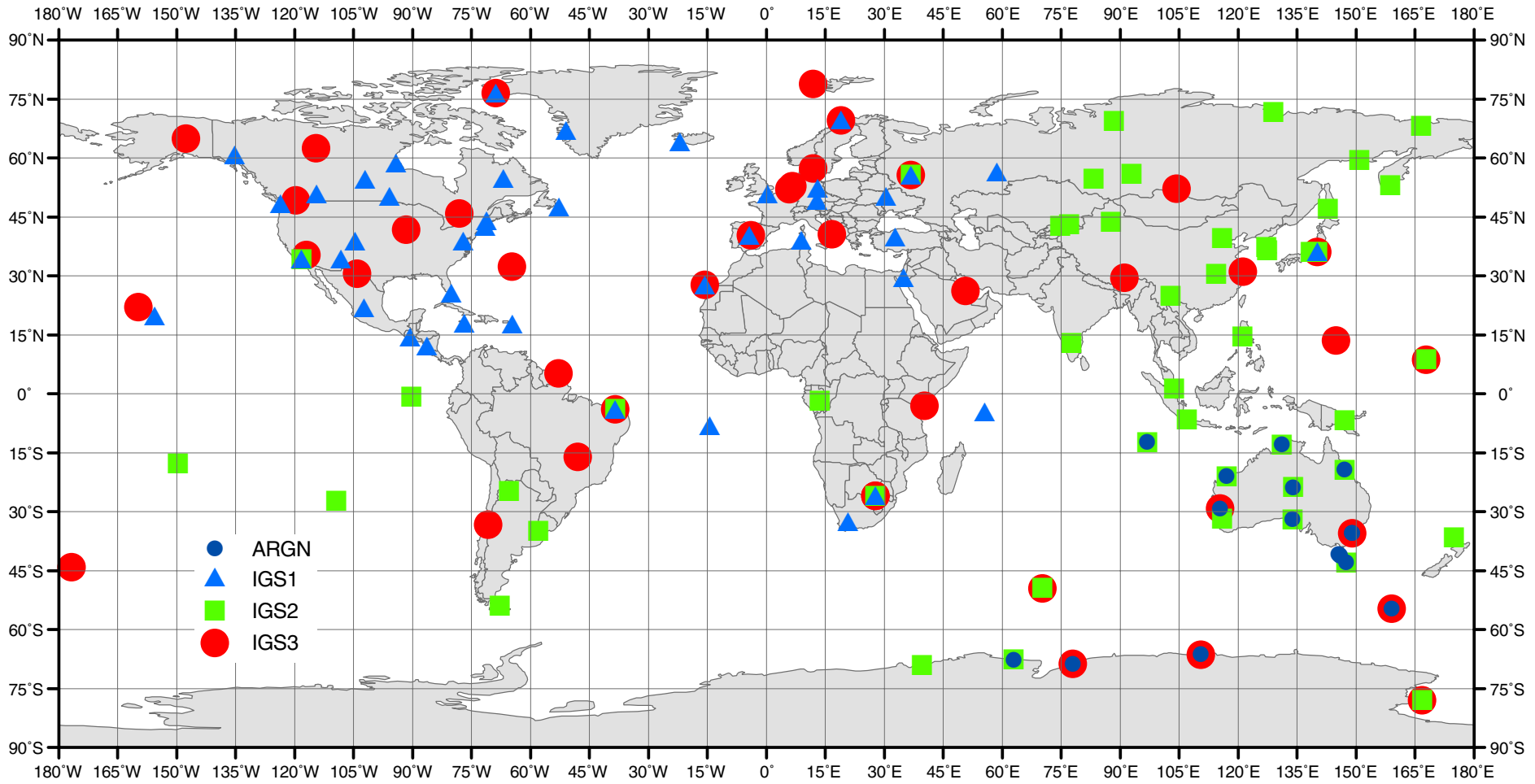

Figure 3-12 ARGN, IGS1, IGS2 and IGS3 networks used in the GLOBK analysis.

When combining networks in GLOBK, unit weighting of the daily GAMIT variance/covariance matrices was applied. The χ^2/f statistic (c.f. Eqn 3-8) is important to assess the consistency of each new loosely constrained GAMIT solution to GLOBK's existing knowledge of the parameters (Dong et al., 1998 and Herring, 2002). The χ^2/f statistic typically increases as additional networks are added to the analysis. Ideally, the statistic should be close to unity, with higher values indicating distortions or strain exists between networks (indicative of differences in modelling or gross errors in antenna height reductions for example). Figure 3-13 shows the GLOBK χ^2/f statistic computed after the addition of each network (the order of combining the networks for each session was IGS1-IGS2-IGS3-ARGN, which remained the same throughout the GLOBK analysis).

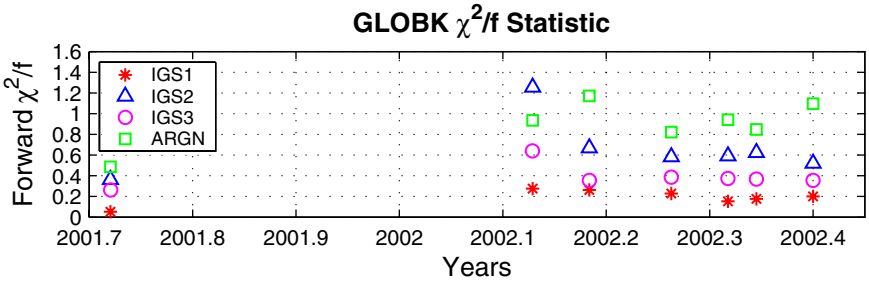

Figure 3-13 Forward χ^2/f statistic for the GLOBK combination of the various networks.

The results shown in Figure 3-13 show no evidence of distortion between the respective networks. The IGS2 network behaves marginally different during the second observation session, with the statistic elevated to ~1.2 in comparison to typical values at the 0.6 level. This is not a significant misfit hence the network was left within the solution. More importantly, the final estimate of the χ^2/f statistic following the addition of the regional ARGN network remains close to 1 throughout the entire campaign (average value 0.92). This provides confidence in the network consistency in addition to the validity of both the assumption of unit weight of the GAMIT variance/covariance matrices and the decision not to add process noise to the GLOBK analysis (see Herring, 2002 for discussion).

Following the combination of the loosely constrained GAMIT solutions as quasi observations in GLOBK, the reference frame is realised using the GLORG utility. A combination of well determined global and ARGN sites were selected for the stabilisation process. GLORG iteratively weights the contribution from each site using a 40% constant and 60% site dependent weighting scheme. Sites were deleted from the stabilisation if their residual was more than 3.5 times the RMS of the fit, provided its residual was not less than 10.5 mm in position. A ratio of

computed uncertainties in the height component was also used to flag sites for removal from the frame stabilisation process. A 'height ratio' of 2 was set, effectively preventing sites with large height uncertainties biasing the reference frame (see Herring, 2002, for further details). Heights were also down weighted by a factor of 100 in comparison to position in the realisation process. The final sites and relative weights used in the stabilisation are shown in Table 3-4.

Table 3-4 Final sites and relative sigmas used in the frame stabilisation process.

MAS1 0.99	**STJO** 0.98	**BRMU** 1.05	**WES2** 1.01	**ALGO** 0.98	**PIE1** 1.04
YELL 1.03	**DRAO** 1.02	**ALBH** 1.00	**KOKB** 1.17	**CHAT** 1.25	**AUCK** 1.10
TIDB 0.91	**HOB2** 0.90	**TOW2** 0.95	**ALIC** 0.90	**CEDU** 0.89	**DARW** 1.00
KARR 0.96	**PERT** 1.02	**YAR1** 0.93	**CAS1** 0.90	**DAV1** 0.92	**KERG** 1.01
MAW1 0.94	**BAHR** 1.14	**ONSA** 0.96	**KOSG** 0.96		

The final postfit RMS for this realisation consisting of 28 sites (Table 3-4) was 2.0 mm indicating an acceptable fit to the ITRF2000 coordinate and velocity set. The postfit RMS increases to 3.6 mm when down weighting heights by a factor of 10, with coordinates at the Bass Strait calibration site changing at the 1 mm level. Final ITRF2000 coordinates for the Bass Strait reference sites are shown in Table 3-5.

Table 3-5 ITRF2000 coordinates for BUR1, TBCP and RKCP (at epoch 2002.401)

Site	X (m)	Y (m)	Z (m)
BUR1	-3989419.829	2699532.928	-4166619.715
TBCP	-3986972.533	2716688.497	-4158076.084
RKCP	-3981934.611	2735833.078	-4150248.381

The formal 1-sigma uncertainties from the GLOBK/GLORG analysis are of particular interest for this study. Unscaled uncertainties for the BUR1, TBCP and RKCP sites are at the 1.8 mm to 2.3 mm level (for each global Cartesian coordinate component). Given the reliance on such a small sample of episodic observation sessions, these uncertainties are without doubt considered overly optimistic for a range of reasons. The methodology adopted to assess the true uncertainty uses output from the GLRED/GLORG repeatability analysis, in addition to a long term time series of the BUR1 site computed in a separate analysis. These investigations are presented as part of the error analysis in §3.4.4.

3.4.3.3 Limitations Caused by the Tide Model

As discussed throughout §3.3, some level of inconsistency in the combination of space geodetic data is difficult to avoid. In this study, emphasis has been placed on the standardisation of the pole tide and solid Earth tide at the model stage of the analysis. Changes to the GLOBK software enabled the correction of the pole tide to any given set of quasi-observations. This therefore ensures that a standardised estimate of the pole tide is added to the ARGN, IGS1, IGS2 and IGS3 networks used in this analysis.

The use of the SOPAC solutions does however dictate the use of the IERS 1992 solid Earth tide model (see description in Nikolaidis, 2002), which is in conflict with the updated IERS 2003 model used in the regional solution. As discussed in §3.3.1, the primary reason the tide model was updated for this study was to maximise the accuracy at the TBCP and RKCP sites (unique to the regional solution). The effect of mis-modelling the solid Earth tide will be greatest for observation spans less than the complete 24 hour session (differences between the two tide models averaged to sub-mm over a daily period). As observation sessions at the TBCP and RKCP sites ranged between 16 and 22 hours (due to logistical constraints), the IERS 2003 model was adopted. Given the sub-mm average difference over 24 hours, the apparent conflict with using IERS 1992 based global solutions with IERS 2003 regional solutions is not expected to be significant.

The effect of changing to the IERS 2003 model for TBCP and RKCP sites was tested by incorporating the IERS 1992 regional GAMIT solution in GLOBK. Differences in the final GLOBK coordinate estimates were at the 1 mm level. Such small differences may imply no significant benefit was gained from updating the solid Earth tide routine to IERS 2003 standards. First results from the processing of global networks (undertaken at the time of writing) do however show significant changes in site velocity, at the 2 mm/yr level, when adopting the new model (personal communication, P. Tregoning, 2005). These studies have been undertaken at the Australian National University, using the IERS 2003 code implemented in this Thesis, together with the existing IERS 1992 code. These preliminary results without doubt highlight the significance of the model change, despite its relatively small effect for the overall campaign coordinates determined for the TBCP and RKCP sites.

3.4.4 Error Analysis

The estimation of robust formal error estimates for geodetic site position is problematic and even more difficult for site velocity. In the context of this study, the primary requirement is to correctly estimate the uncertainty of the vertical position of the BUR1, TBCP and RKCP sites. The difficulty in estimating a realistic uncertainty is three fold:

1) Firstly and most importantly, the uncertainty estimate from GLOBK is biased due to the small sample size of episodic based GPS deployments. Without a significantly larger time series it is difficult to assess the variability of the time series.

2) The short-term estimate of site position may also be contaminated by residual seasonal signals, measurement noise and model uncertainty (amongst others). These effects potentially offset the observed site position from the long-term mean position. The magnitude of this effect is dependent on the exact time of observation and the periodicity and magnitude of the residual geophysical signals (and other components) involved. Studies such as Mao et al. (1999), Dong et al. (2002) investigate these issues, underscoring the frequent underestimation of uncertainty by factors of typically between 2 and 5 for example.

3) The uncertainty in site position (and velocity) is also dependent on the noise model assumed in the time series. Assuming a white noise process in the presence of time-correlated noise processes will result in an underestimation of the uncertainty (see Zhang et al., 1997 and Williams, 2002 for example).

To gain an improved estimate of the uncertainty expected at the BUR1, TBCP and RKCP sites, a significantly long time series is required. For this analysis, the full time series in the vertical component at BUR1 and HOB2 (using 4 years of common data) have been utilised. HOB2 is located near Hobart on the southern Tasmanian coast, with a baseline separation from BUR1 of 232 km. Analysis of the common mode displacement between these two sites provides an indication of the common mode behaviour to be expected between the much closer TBCP and RKCP sites, for which no long term time series solutions are available. The long-term time series for BUR1 and HOB2 were computed as part of an analysis for the TIGA tide gauge monitoring project (Schone, 2005). The analysis represents the

"CTA" analysis centre solution by Assoc. Professor Peter Morgan (see Schone, 2005 for details). The solution was computed using the GAMIT/GLOBK software suite, also adopting a regional analysis approach.

Analysis of the full BUR1 and HOB2 time series (Figure 3-14a) shows significant correlation between their vertical components (correlation coefficient of 0.82 using unsmoothed data and 0.85 using smoothed data, smoothed with a monthly moving average). The weighted RMS variability (assuming a white noise process) of the unsmoothed BUR1 and HOB2 vertical time series is 9.9 mm and 10.9 mm respectively. This variability reduces significantly to 7.2 mm for the residual (the smoothed residual has a standard deviation of just 4.1 mm, Figure 3-14b). Common mode seasonal effects which may be contributing to this signal structure include contributions from un-modelled loading signals (groundwater and atmospheric loading for example) and aliased mis-modelled geophysical signals (solid Earth tide and ocean tide loading for example), as discussed in Penna and Stewart (2003).

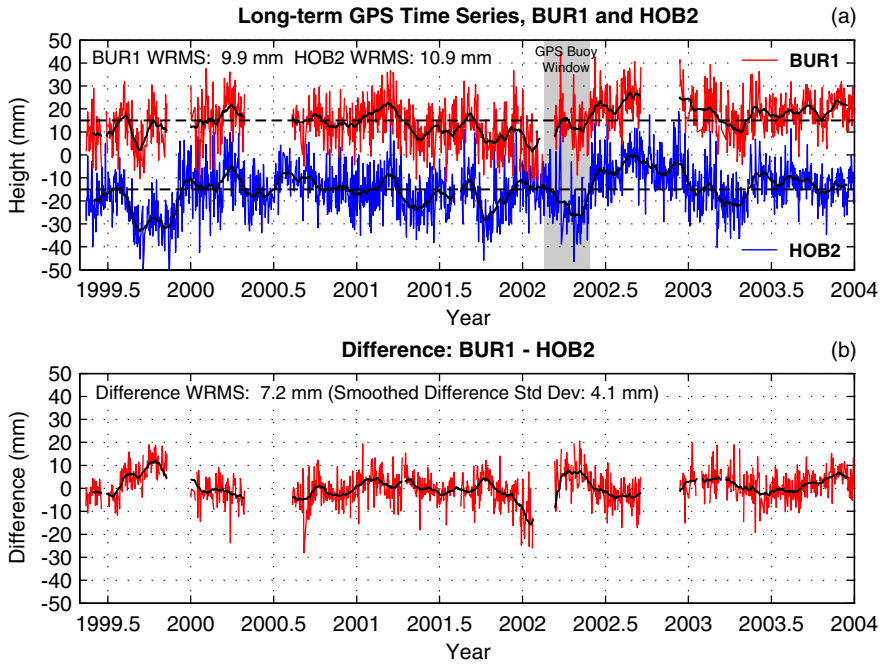

Figure 3-14 Burnie (BUR1) and Hobart (HOB2) GPS time series. (a) BUR1 and HOB2 vertical GPS time series, (without error bars and arbitrary offset applied). Note the shaded section which encompasses the GPS buoy deployment window. The bold smoothed line on both time series shows a 31-day mean. (b) Difference: BUR1-HOB2.

Given the high correlation of BUR1 and HOB2 over ~200 km, we assume the underlying signal at BUR1 (Figure 3-14a) would be largely reflected at the TBCP and RKCP sites. The BUR1 site therefore forms a proxy for our analysis of the

TBCP and RKCP sites. Estimating the components of the noise structure present with the BUR1 and HOB2 time series provides interesting results. Using the methodology described in Williams (2003), white noise estimates are 15.3 mm and 9.4 mm for BUR1 and HOB2 respectively. Power law noise estimates are significantly higher at 19.3 mm/yr$^{1/4}$ and 22.9 mm/yr$^{1/4}$ respectively. A further discussion surrounding the interpretation of this power law noise structure is provided in §3.5. In the context of this study, these results serve to highlight the need to scale uncertainties determined from the GLOBK analysis.

In addition to considering the seasonal (and possibly systematic) structure of the time series, and the influence of the frequency dependent noise structure, the short, episodic deployment of the TBCP and RKCP receivers must be considered. To assess this effect, the episodic determinations of the BUR1 site position are compared against the long term mean estimate, as computed from the long term series (Figure 3-14). The episodic determinations are derived from the GLRED/GLORG repeatability analysis (§3.4.3.2).

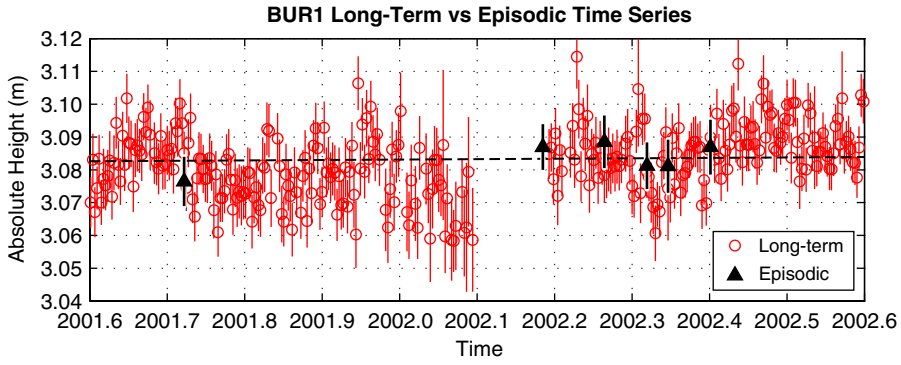

Figure 3-15 Long-term and episodic BUR1 absolute height time series. Values are shown with 1-sigma error bars.

Figure 3-15 shows six determinations of BUR1 position between 2001.7 and 2002.4 (seven determinations were available at both TBCP and RKCP due to equipment failure at the BUR1 site during the second experiment). Output from the GLRED analysis for the BUR1, TBCP, RKCP and HOB2 sites is provided for further inspection in Appendix B. The important observation to be made from Figure 3-15 is that the episodic data does not lie at seasonal or daily extremes, and are well distributed around the trend computed from the long-term time series. The long-term trend passes well within the 1-sigma error estimates for each episodic position determination. Quantitatively, the short-term BUR1 position from our GLOBK analysis falls within 2 mm of the long-term estimate indicating the episodic deployments have satisfactorily sampled the underlying signal. Combining

these analyses with recommendations presented in Mao et al. (1999), Williams (2002) and Williams et al. (2004), we choose a subjective (yet conservative) scaling constant of 5 for our GLOBK positional uncertainties. This results in an uncertainty at the 10 mm level. An additional 'fixed' or 'systematic' error term of 10 mm is added to the error budget to be carried forward into the following Chapter which focuses on the altimeter calibration. The systematic term is included to recognise many of the systematic components of the GPS analysis strategy discussed throughout this Chapter (for example, variability associated with observation weighting and model selection, methods used to stabilise the reference frame, frequency dependent noise structure and uncertainties associated with handling the scale of the reference frame and the influence of geocentre motion).

3.5 GPS Time Series Analysis

The primary objective of this Chapter has been the definition of the coordinate datum for the Bass Strait calibration study. Associated with this work has been the investigation of some of the issues surrounding the estimation of site velocity in the vertical component. This investigation is undertaken using data from a number of the permanent GPS sites in the Australian region, where the time series are longer and site conditions are likely to vary. The analysis provides a brief introduction to the difficulties involved with the accurate estimation of vertical velocity of geodetic reference sites, as required for the estimation of absolute sea level change and altimeter bias drift.

The objective of this section is not to provide a definitive set of time series analyses, complete with velocities, uncertainties and estimates of noise structure. For this, readers are referred to recent studies such as Dong et al. (2002), Nikolaidis (2002), Heflin (2001) and Williams et al. (2004). Instead, the objective here is to provide a comparative investigation of a subset of contemporary time series, which have been computed using various analysis strategies and software suites. Through the presentation of these comparative analyses, various points of interest can be made to demonstrate many of the complexities surrounding the estimation of vertical velocity at reference sites. The section begins with a brief review of the current understanding of the noise structure present within geodetic GPS time series. The different time series utilised are introduced, followed by a summary of the analysis techniques adopted. Readers are referred to Appendix B for additional results from the time series analysis undertaken in this section.

3.5.1 Noise Structure in Geodetic Time Series

Improving our understanding of the noise structure present in space geodetic time series has become an increasingly important issue. The distinction between signal and noise in many cases remains unclear, especially at the low frequency end of the spectrum. Many geophysical signals of interest (un-modelled), as discussed throughout this Chapter, exist at low frequency. The interpretation of these signals in the presence of time correlated and/or coloured noise is a non trivial problem.

It has long been understood that the noise structure of GPS time series (and many other natural phenomena) is not purely white and has increased power at the lower frequencies (Langbein and Johnson, 1997, Mao et al., 1999 and Williams, 2002 for example). The noise within a GPS time series can be described as a power law process, such that its power spectrum ($P_x(f)$) in the time domain ($x(t)$) has the form (Eqn 3-9):

$$P_x(f) = P_0(f/f_0)^k \qquad \text{Eqn 3-9}$$

where f is the temporal frequency, P_0 and f_0 are the normalising constants and k is the spectral index (also the slope of the power spectra in log-log space). Agnew (1992) discusses the time domain behaviour of power law noises, showing spectral indices (k) of between -3 to -1 commonly occur throughout the natural sciences. This translates to an increased noise power in the low frequency spectrum, hence why the noise is often described as shifted to the 'red' end of the spectrum. Special cases of spectral indices include -2 (classical Brownian motion or "random walk" noise), -1 ("flicker" noise) and 0 (pure white noise).

In the estimation of site velocity (in any component), the uncertainty in the rate (σ_r^2) will be proportional to some function of the number of data points used in the estimation (n). Zhang et al. (1997) show how this proportionality varies with the assumption of white noise ($\sigma_r^2 \propto 1/n^3$), flicker noise ($\sigma_r^2 \propto 1/n^2$) and random walk noise ($\sigma_r^2 \propto 1/n$), clearly underscoring the requirement for significantly more data when estimating velocity in the presence of flicker or random walk noise (to achieve a comparable uncertainty compared with the white noise case). Williams (2002) continues this discussion showing relationships between the variance of the velocity and the number of data points, for noise models with spectral indices between 0 and -3.

Mao et al. (1999) investigated three years of continuous GPS data and found a combination of white and flicker noise best approximates the noise structure in the time series. The white noise component in the vertical direction was at a maximum at the equator leading to speculation of the effect of the troposphere in the GPS solution. Mao et al. (1999) concluded that coordinate velocities can be underestimated by factors of between 5-11 if a white noise only model is assumed.

Nikolaidis (2002) gives results from a 11 year time series, adopting the techniques developed in Williams (2002) to estimate white and flicker noise components to each topocentric coordinate component. Using simple slope estimation of the

power spectra, Nikolaidis (2002) determined spectral indices for all coordinate components between -0.74 and -0.84, for frequencies between 1/(7.4 years) and 1/(15 days), and assumed white noise dominated in the high frequency ($>$ 1/(15 days)) end of the spectrum.

A recent study by Williams et al. (2004) looked at a range of regional and global geodetic GPS time series computed using various analysis strategies. Williams et al. (2004) confirmed a latitudinal dependence in the magnitude of the white noise component (higher in equatorial regions) in addition to a bias to higher values in the Southern Hemisphere. Once again, the study concluded that a combination of white and flicker noise is the most appropriate noise model for geodetic time series.

The source of the noise at low frequencies remains an open question. Williams et al. (2004) make an important point underscoring that comparable flicker noise amplitudes between different solution methodologies most likely reflects a common physical basis. The Williams et al. (2004) study referred specifically to mass distributions, such as those described in Blewitt et al. (2001) and Dong et al. (2002), for example, atmospheric noise (Williams et al., 1998) and second order ionospheric effects (Kedar et al., 2003) as key physical influences in the introduction of flicker noise. Software specific issues and the influence that aliased or mis-modelled periodic signals play are also of considerable importance, as shown throughout the following section.

The geophysical interpretation of many low frequency signals present in geodetic time series must therefore be undertaken with considerable caution. Whilst many real signals (as described above) will contribute to the coloured noise in the time series, much of the noise may also be introduced as a result of the interaction of software specific issues and any mis-modelling of "known" periodic signals (OTL or the solid Earth tide, for example). An example illustrated later in this section underscores the effect of aliased tidal signals (as discussed from a theoretical standpoint in Penna and Stewart, 2003). Penna and Stewart (2003) show that un-modelled (or mis-modelled) periodic geophysical signals are generally under sampled by the standard GPS analysis strategy involving discrete 24 hour solutions. The sidereal day repeat orbit of the GPS satellites is also shown to generate aliased signals which have typically been ignored in most standard GPS analyses. Both of these effects are demonstrated in §3.5.4.4.

3.5.2 Time Series Selection

Time series data have been extracted for sites in the Australian region from four separate geodetic analyses including:

1) *"CTA" TIGA solution.* This solution was processed by Assoc. Professor Peter Morgan, as described in §3.4.4. The analysis is a regional solution using the GAMIT/GLOBK suite, and includes sites in the Australian region. The solution is given the analyst's initials as a prefix: "PJM".

2) *SOPAC global solution.* The SOPAC analysis is a GAMIT/GLOBK global solution as described by Nikolaidis (2002). The solution is given the prefix: "SOP".

3) *JPL global solution.* The Jet Propulsion Laboratory (JPL) global solution (Heflin, 2001) was processed using a precise point positioning strategy implemented using the GIPSY-OASIS II suite (Zumberge et al., 1997). The solution is given the prefix: "JPL".

4) *GA regional solution.* The Geoscience Australia (GA) solution was processed for the South Pacific Sea Level and Climate Monitoring Project (SPSLCMP) using the Bernese software (Hugentobler et al., 2001). Information on the project can be found at http://www.pacificsealevel.org/. The solution has been given the prefix: "GA".

3.5.3 Analysis Strategy

A simple analysis strategy has been adopted for the investigations presented in this section. Data between 1998-2004 were utilised (where available), to standardise the available data across the four solutions. Daily topocentric (north, east and up) coordinates for each time series solution formed the fundamental dataset for analyses. Outlier detection was done using a simple sliding window with a length of 1 year run over de-trended data. Within the 1 year period, data were eliminated if its absolute value was greater than 2.5 times the inter-quartile range of the windowed data. This technique allows for improvements in the variability of GPS time series over time (see Herring, 1999, for a historic perspective).

Following the outlier detection, standard weighted least squares techniques were used to fit a simple model defining the offset, linear trend, and annual and semi-annual terms according to Eqn 3-10:

$$y(t) = x_1 + x_2(t) + x_3 \sin(2\pi t) + x_4 \cos(2\pi t) + \ldots \\ \ldots x_5 \sin(4\pi t) + x_6 \cos(4\pi t) \qquad \text{Eqn 3-10}$$

where *y(t)* defines the modelled site coordinate at time, *t,* (in decimal years), and x_1-x_6 are model parameters. No attempt was made to model discontinuities or seismic deformation for this analysis, as it was not required for the sites of interest.

3.5.3.1 Spectral Analysis

Spectral analysis was undertaken using the Welch method of spectral estimation (Welch, 1967), as implemented in Matlab®. Any gaps within the time series (arising from outages or outlier removal), were filled with white noise (5 mm for north and east components and 8 mm for the vertical components) prior to estimating the spectral density estimates. A standard Hanning window was used (with the length defined as the maximum power of two less than the length of the input time series).

Two separate spectral analyses were undertaken on each coordinate component:

1) Raw data with just the offset and linear trend removed; and
2) Raw data with offset, linear trend and periodic components removed.

The approximate spectral index (k) was estimated using a linear regression computed in log-log space, according to Eqn 3-11:

$$k = \frac{P_x(f)}{10\log_{10}(f)} \qquad \text{Eqn 3-11}$$

where P_x is the power spectrum of the input signal, x, estimated over the set of frequencies f. To avoid biasing the regression from spectral peaks present at the 13-14 day period in both the SOP and JPL solutions, the spectral index was computed over frequencies lower than 1/(15 days). See §3.5.4.4 for further discussion.

3.5.3.2 Wavelet Analysis

Wavelet analysis represents a powerful technique for the analysis of non stationary periodic signals. For the discrete analysis, coefficients were computed using a discrete approximation of the Meyer wavelet, "dmey", in the Matlab® Wavelet Toolbox. The "dmey" wavelet was well suited to this particular analysis due to its properties of symmetry, infinite regularity and suitability for single level decomposition. For the continuous analysis, the Morlet wavelet (Figure 3-16), was used due to its suitability for time series applications (see Daubechies, 1992 and Percival and Walden, 2000 for further discussion).

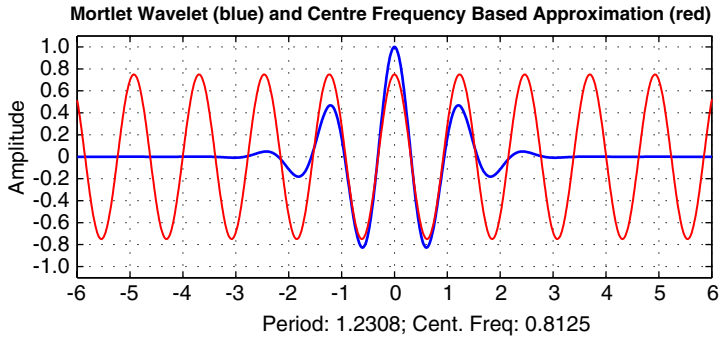

Figure 3-16 Mortlet wavelet and the centre frequency based approximation.

For the continuous analysis, the wavelet scale coefficients were converted to estimates of power and displayed on a two dimensional grid with colour scaled across blue, cyan, green, yellow and red according to wavelet power (with time on the x-axis and pseudo-frequency derived from wavelet scale, converted to period plotted on the y-axis). An analysis of a test dataset is shown in Figure 3-17. The synthetic signal consists of random white noise (standard deviation of 10 mm), an annual signal for the first half of the signal (amplitude 20 mm), a semi-annual signal for the last half of the signal (amplitude 20 mm) and a fortnightly signal throughout the entire signal (amplitude 10 mm). Each signal component is clearly visible in the continuous wavelet analysis, highlighting its usefulness for the analysis of non-stationary periodic time series.

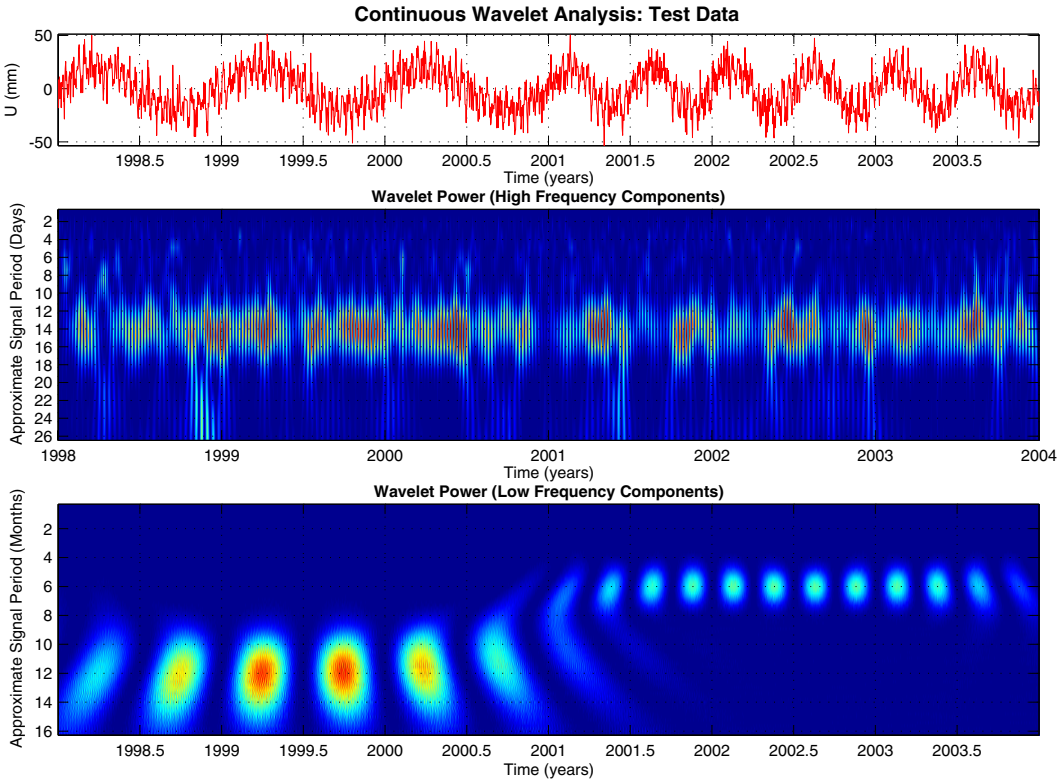

Figure 3-17 Continuous wavelet analysis of the test dataset.

3.5.3.3 Maximum Likelihood Estimation of Noise Structure

Maximum Likelihood Estimation (MLE) of both white noise and power law noise is described by Langbein and Johnson (1997) and Zhang et al. (1997), and most recently and comprehensively by Williams (2002). The technique is able to determine a best fit noise model made up of both white noise and power law noise based on the maximisation of a probability function. The probability function incorporates the data covariance terms, which include parameters defining the magnitude of the specific noise components. Results from the MLE allow the computation of regression or model parameters using a full variance covariance matrix which fully describes the time correlation of the noise structure, hence enabling the realistic determination of parameter uncertainty. The MLE technique has been applied by Assoc. Professor Peter Morgan to the PJM time series using the software developed by Williams (2002). The velocity uncertainties, spectral indices and noise magnitudes for this solution have been included in the following sections. As a complete treatment of the MLE technique is beyond the scope of this section, readers are referred to Williams (2002) for further detail.

3.5.4 Results

The results presented in the following sections have been limited to sites in the Australian region (see Figure 3-9). Five cases have been selected to highlight some of the issues surrounding the estimation of velocity in the vertical component.

1) a - Vertical velocity at the Bass Strait (BUR1) calibration site.
   b - The influence at BUR1 of mis-modelling the solid Earth tide in the Bernese suite.
2) The effect of noise structure on estimates of velocity uncertainty.
3) The influence of OTL on vertical time series.
4) Velocity differences between solutions.

3.5.4.1 Bass Strait (BUR1) Site Velocity

The estimation of vertical velocity at the Bass Strait (BUR1) GPS site is problematic due to a range of factors. Firstly, the length of the time series is still relatively short (1245 daily solutions, equating to just 3.4 years of coordinate data). The time series also exhibits a series of outages (as discussed in §3.4.2.1) which also influence the estimation of velocity and noise structure (Figure 3-18). Both the JPL and SOP solutions do not include the BUR1 site as the site is not one of the global IGS stations. The analysis is therefore limited to the PJM and GA solutions.

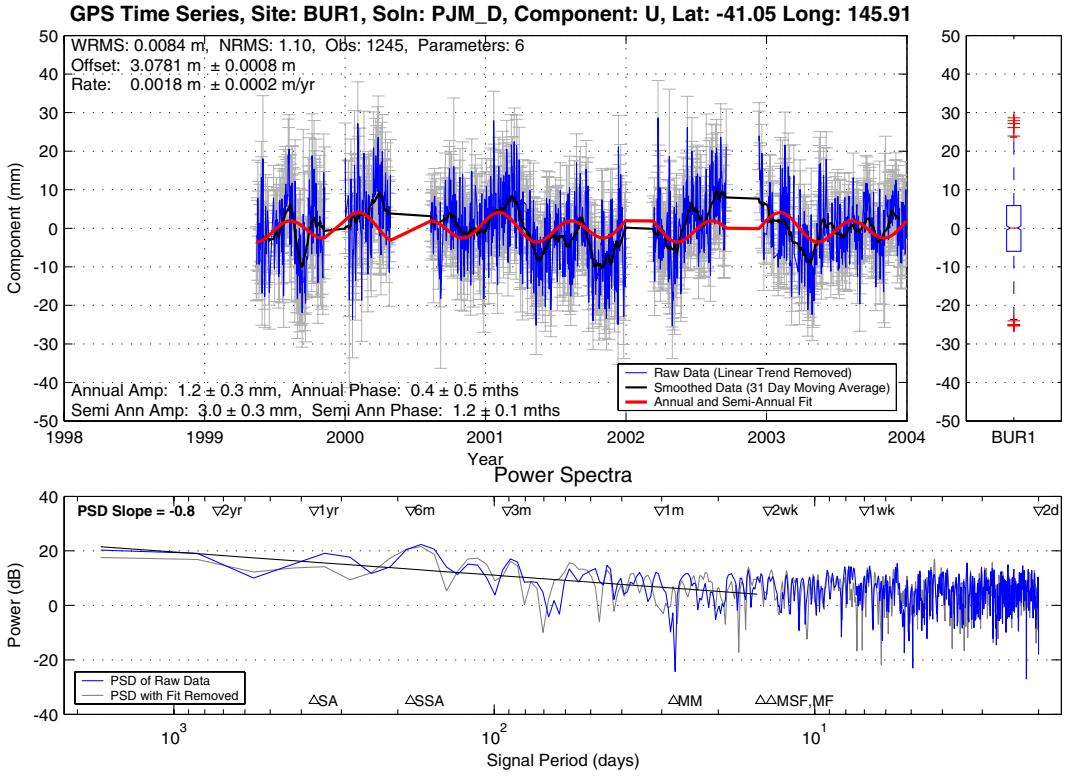

Figure 3-18 Vertical time series at the BUR1 site (PJM solution). For a complete description of each panel, refer to Appendix B.

The BUR1 time series for the vertical component (Figure 3-18) shows significant variability at low frequencies. The variability has no clear dominant frequency (note the quite broad peaks at annual and semi-annual periods). The spectral index, k, determined from the power spectra is -0.8, slightly lower than that determined using the MLE technique (-0.94, or very close to pure flicker noise). The magnitude of the power law noise from the Williams (2002) software is unusually high (in comparison to other sites in the region) at 17.5 mm/yr$^{1/4}$. The dominance of the noise at low frequencies will clearly affect the estimation of velocity and its uncertainty, further emphasising that the current time series is too short for the meaningful estimation of vertical velocity.

Historical levelling connections undertaken at the site shows no significant local deformation (Geoscience Australia, 2003a). This suggests that the reclaimed concrete wharf is not continuing to settle with respect to local benchmarks which are fixed to bedrock. The rate of relative sea level change, determined from the tide gauge measurements at the Burnie site is currently +2.8 mm/yr (National Tidal Centre, 2005). This estimate is computed from approximately 12.5 years of data (the tide gauge commenced operation in September 1992). The best estimate of long term absolute sea level change in the Tasmanian region is +0.8 ± 0.2

mm/yr (from data spanning a 160 year period), increasing to approximately +1.0 mm/yr when adopting the best available models for land motion (Pugh et al., 2002).

While the rate of relative sea level change at Burnie is broadly consistent with the long term absolute trend, the data duration at the Burnie tide gauge is still considered insufficient to derive a meaningful estimate of long term change (Church et al., 2001). The results from both the local benchmark surveys and the sea level change estimates do however provide a general indication that there is no *significant* land uplift, or subsidence, at the Burnie tide gauge site.

The vertical velocity of the BUR1 site, together with uncertainty estimates from both the weighted least squares (assuming white noise) and the maximum likelihood estimation are shown in Table 3-6.

Table 3-6 BUR1 Site Velocity and Uncertainty (1-sigma).

Velocity	Uncertainty	Methodology
+ 1.8 mm/yr	± 0.2 mm/yr	PJM Solution, Weighted Least Squares, Scaling VCV by NRMS
	± 1.23 mm/yr	PJM Solution, MLE Estimation

The influence of power law noise on the velocity uncertainty is clearly evident in Table 3-6, with the uncertainty from the weighted least squares methodology approximately a factor of 6 lower than the MLE (power law) equivalent. The BUR1 velocity (+1.8 mm/yr) is indicative of marginal uplift, however at 95% confidence levels (using the MLE uncertainty), the velocity is clearly not significant. The time series is simply too short for a reliable estimate of vertical velocity. Also, any systematic effect of the regional reference frame stabilisation undertaken in the PJM solution is yet to be considered.

The source of the increased power law noise at BUR1 is of particular interest. As discussed in §3.4.2.1, the BUR1 site is not ideal due to signal obstructions north of the antenna. Site specific effects, such as multipath and signal diffraction, are therefore expected to be higher than average, contributing to the noise at the site. The monument used for the site is also unique, with the antenna mounted on a steel I-beam (rolled steel joint, or 'RSJ' section), which is fixed to the side of the concrete wharf structure (Figure 3-19).

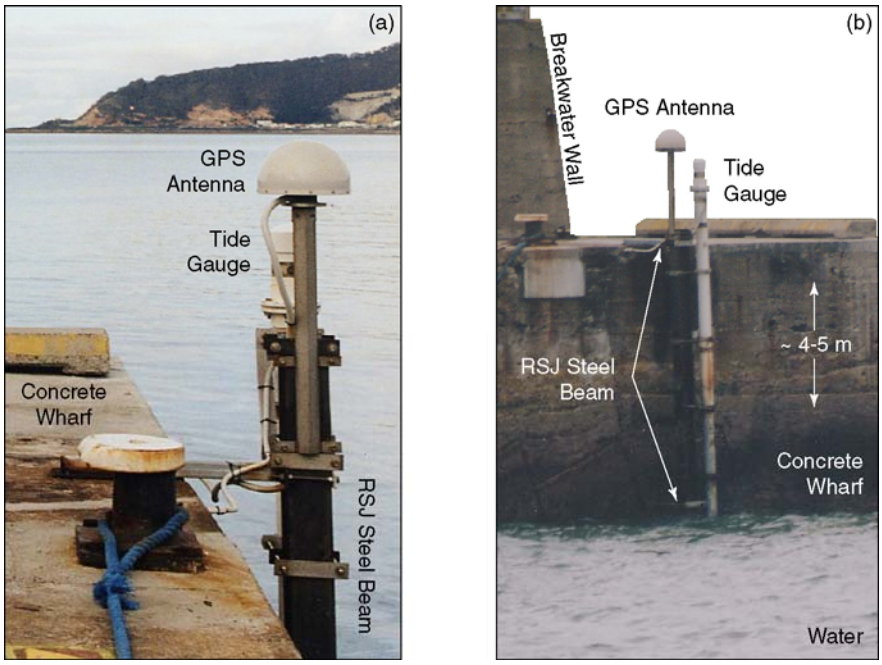

Figure 3-19 Burnie GPS and tide gauge installation showing the steel beam used to support both instruments. (a) Looking east. (b) Looking northeast. Note the breakwater wall in the distance (~300 m) has been digitally removed from this figure for clarity.

Within the geodetic literature, the noise introduced into a solution from a geodetic monument is typically regarded as a random walk process with magnitudes at the 0.4 mm/yr$^{1/2}$ level (Langbein and Johnson, 1997 for example). The noise from the monument at BUR1 is highly likely to be significantly greater due to the thermal response of the steel beam to the ambient air and water temperatures. Approximate calculations using the coefficient of expansion for mild steel and temperatures from the air and water temperature sensors installed with the tide gauge (see Hunter, 2003) show displacements (expansion/contraction of the beam) at the 3 mm level (with an annual signal in addition to high frequency variability related to diurnal heating and cooling). There is little doubt that monument noise is a contributing factor to the power law noise at the BUR1 site. It is anticipated however that this component is small in relation to the prevalence of (and potential aliasing of) site specific effects, such as multipath and signal diffraction. The second solution for BUR1 (GA) is now investigated revealing the effect of the erroneous solid Earth tide correction in the Bernese software suite.

3.5.4.2 Mis-modelling the Solid Earth Tide in Bernese

The second solution to include data from BUR1 was computed by Geoscience Australia (GA). The GA solutions used the Bernese analysis suite which was affected by the erroneous solid Earth code as previously described in §3.3.1. Hugentobler (2004) details the influence of the software error. One of the main effects discussed is the introduction of a spurious annual signal. The annual signal is clearly apparent in the GA BUR1 vertical time series (Figure 3-20) with an annual amplitude of approximately 16 mm.

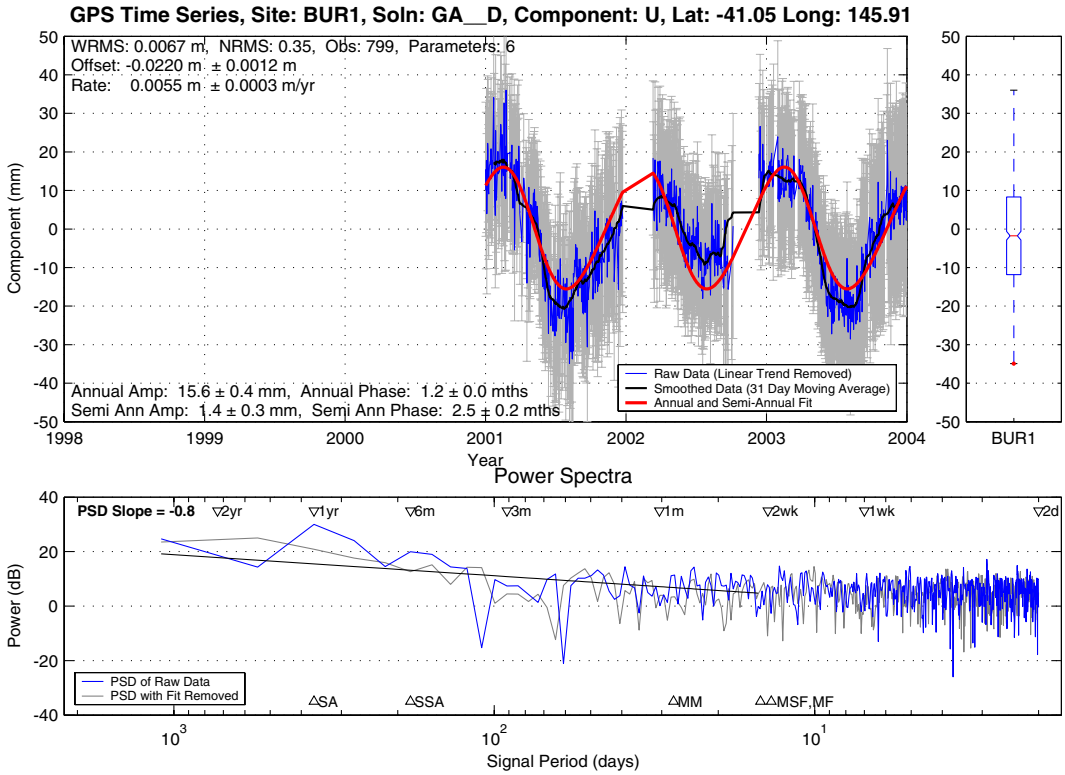

Figure 3-20 Vertical time series at the BUR1 site (GA solution). Note the GA solution only includes data post 2001. Refer to Appendix B for a full description of each panel within the Figure.

Given the apriori knowledge we have of the BUR1 site, there is no plausible geophysical explanation for the magnitude of the signal observed in Figure 3-20. The vertical velocity computed from the GA solution is at the +5.5 mm/yr level which is also not geophysically consistent (in this case the vertical velocity is affected by the large seasonal signal, as discussed in Blewitt and Lavallee, 2002, which is aliased from the error in the solid Earth tide correction).

Other sites in the GA solution, which have not been artificially constrained to apriori ITRF2000 positions, also exhibit this dramatic seasonal signal. Examples may be found in the time series viewer included in Appendix B.

3.5.4.3 The Effect of Noise Structure on Velocity Uncertainty

As discussed in §3.5.1, the assumption of a white noise process in geodetic time series leads to the underestimation of uncertainty in estimated geodetic velocities by factors of up to 11 (Mao et al., 1999). Using the PJM regional solution, comparison of velocity uncertainties derived from the Williams (2002) software using both the white noise and power law assumptions show underestimation by factors of between approximately 3 and 12, (consistent with the Mao et al., 1999 study). The ratio between uncertainties shows a dependence with site latitude (Figure 3-21a) with increased underestimation at polar latitudes (see Figure 3-9 for site locations). This intuitively indicates polar sites must have higher power law indices (higher in terms of absolute value), as determined using the Williams (2002) MLE approach. This is confirmed in Figure 3-21(b).

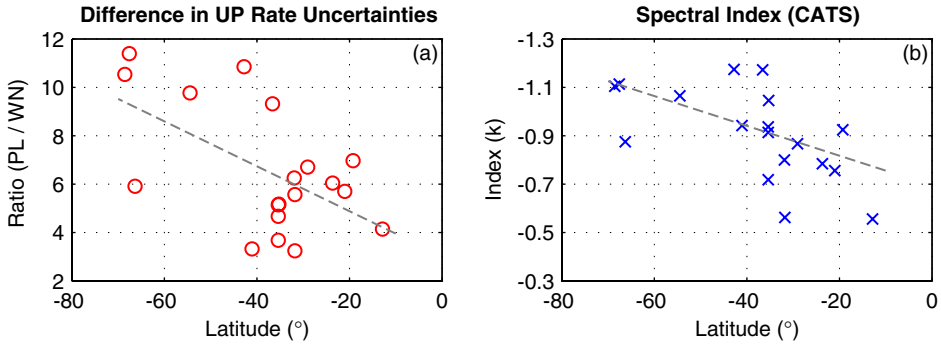

Figure 3-21 Latitudinal dependence of the vertical velocity uncertainty and the spectral index as determined using the Williams (2002) software. (a) Ratio of the uncertainty (assuming power law noise) to the uncertainty (assuming white noise only) against site latitude. (b) Spectral index (k) against site latitude.

The vertical component of the regional PJM solution proves to be particularly interesting. Both the white noise magnitude and power law noise magnitude show a dependence on latitude, with higher noise estimates at polar latitudes. This is in disagreement with the trends computed from global solutions, as presented in Williams et al. (2004). In the north and east component, the trend in the PJM solution reverses and is in agreement with Williams et al. (2004), i.e., higher noise exists at equatorial latitudes.

This interesting finding in the PJM solution is most likely a reflection on the regional reference frame stabilisation process undertaken in the PJM solution. An increased noise level in the vertical component, yet a corresponding reduction in noise in the horizontal components at Antarctic sites is suggestive that too much weight has been given to the horizontal components during the fit between the small number of sites in the regional solution and the ITRF2000 coordinate set. Adopting a high weight for the horizontal component with only a regional set of stabilisation sites is likely to force the solution noise into the vertical component. This provides one possible explanation for the behaviour of the Antarctic based sites in the PJM analysis.

Further comparison of the PJM, JPL and SOP solutions is made in the final section of this Chapter when vertical velocities are compared. The following section investigates the influence of modelling OTL within a solution.

3.5.4.4 The Influence of Ocean Tide Loading

Investigation of the analysis strategies adopted for each time series solution reveal both the JPL and SOPAC solutions have sections of the analysis where OTL was not modelled. The JPL solution began modelling OTL using the FES99 model on 03/03/2002 and then upgraded to the FES02 model on the 23/07/2002 (personal communication, M. Heflin, 2005). The SOPAC solution began modelling OTL (as per §3.3.3.1) on the 26/11/2000 (see Nikolaidis, 2002 for details). Both the PJM and GA solutions modelled OTL consistently throughout their respective analyses.

The influence of these periods of mixed OTL modelling is therefore expected to be clearly visible in the vertical time series. In an Australian context, Penna and Baker (2002) identify a maximum OTL displacement on the northwest Australian coast. The maximum displacement (with a dynamic range at the 10 cm level) occurs near the coastal city of Broome. The ARGN GPS site at Karratha (KARR) is close to this area of maximum loading and hence is ideally suited to the investigation of OTL on vertical position.

To begin this investigation, the power spectra at the KARR site for each time series is presented in Figure 3-22. Note the GA solution is not shown as insufficient data had been processed by GA at the time of writing.

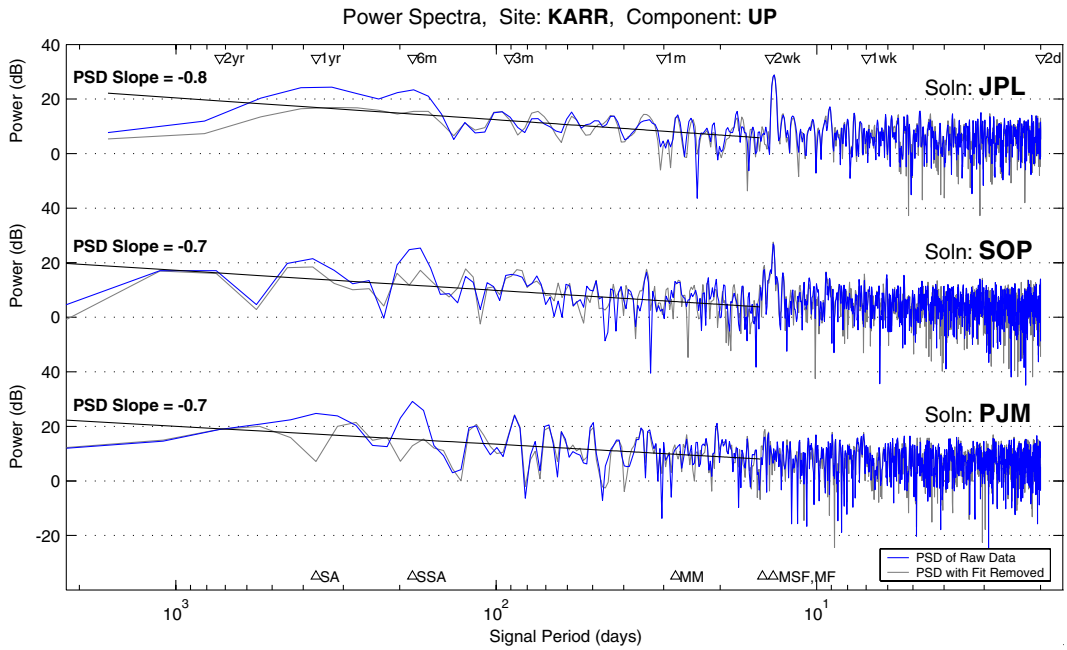

Figure 3-22 Power spectra for the vertical component at the KARR site, for the JPL, SOP and PJM solutions. Note the distinct peak at approximately 13.6 days, present in the JPL and SOP solutions, but not appearing in the PJM solution.

The power spectra for the three solutions shown in Figure 3-22 reveal several interesting features. Firstly, all three solutions show similar magnitudes of power at low frequencies, with the spectral indices determined at -0.8, -0.7 and -0.7 for the JPL, SOP and PJM solutions respectively. All three solutions show power at annual and semi-annual periods, with the JPL spectra showing less spectral resolution in the lower frequencies due to a shortened time series (the JPL series started in mid 1999). The most interesting observation is the significant peak at approximately 13.6 days (period) within the JPL and SOP solution (note the peak is also present in both the north and east coordinate components, see Appendix B). This peak is clearly not present in the PJM solution. The most probable source of this dominant frequency is the aliasing effect of not modelling OTL, as discussed in Penna and Stewart (2003). The Penna and Stewart (2003) study uses simulated data to determine the influence of aliased tidal signatures in a GPS time series, showing that both the dominant M2 and O1 tidal constituents (in OTL for example) are aliased to periods of 13.66 days due to the sidereal day repeat orbit of GPS satellites. The M2 and O1 constituents are also expected to alias to 14.76 and 14.19 days respectively, due to the effect of 24 hour batch processing. Low frequency aliased signals are also expected (K2 aliases to a semi-annual period, and K1 and P1 alias to an annual signal, due to the 24 hour batch processing effect). This effect could therefore be partially responsible for some of the low frequency

noise present in Figure 3-22. The 14.76 and 14.19 day period signals are investigated further below.

Comparison in the frequency domain gives no ability to assess if the dominant 13.6 day peak is eliminated when the modelling of OTL is commenced in both the SOP and JPL solutions. For this investigation the time series are analysed firstly in the spatial domain (Figure 3-23) and secondly using a continuous wavelet approach.

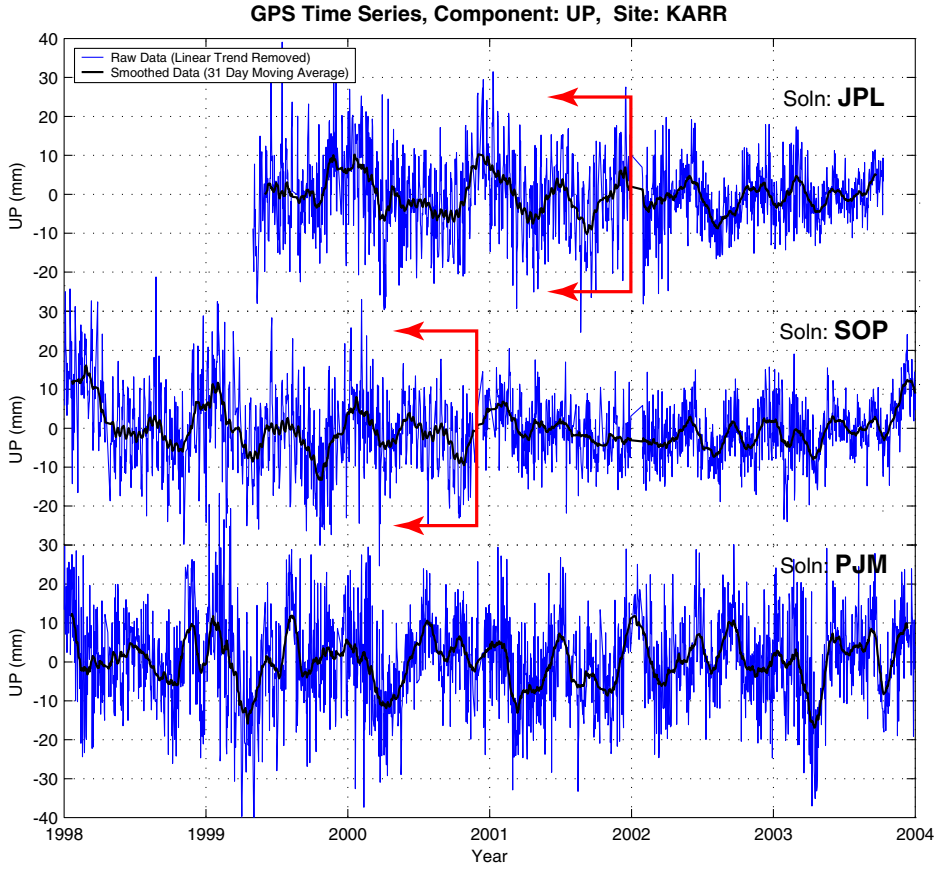

Figure 3-23 Vertical time series from the KARR site for each solution. Error bars have been removed for clarity. The red arrows indicate the period where OTL was not modelled in the respective solutions. The raw and smoothed time series are shown (a monthly moving average smoother was used).

Viewing the time series in the spatial domain (Figure 3-23) shows clear changes in the signal structure after OTL modelling was commenced in the JPL and SOP solutions. Visual inspection shows a reduction in scatter following the initiation of the OTL modelling. With careful inspection, the 13.6 day period signal can be readily identified, with an approximate amplitude at the 10 mm level. A more robust approach to investigating non stationary spectra involves both discrete and continuous wavelet analysis.

In the discrete analysis, the high frequency component, or "detail", from the level 3 decomposition (pseudo frequency of approximately 1/(14 days)) clearly shows the time OTL modelling commenced in both the JPL and SOP solutions (Figure 3-24).

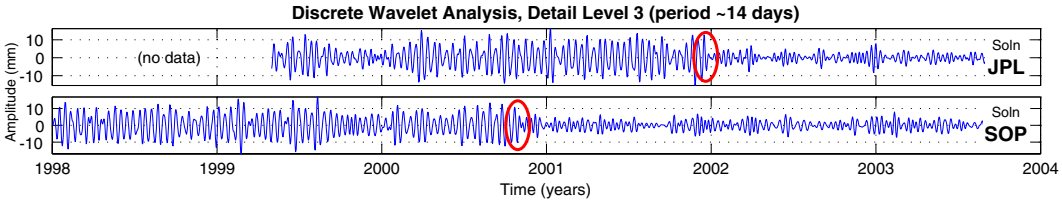

Figure 3-24 Level 3 wavelet decomposition (period ~14 days) for the JPL and SOP solutions at the KARR site (vertical component). The red circles indicate the commencement of OTL modelling in the JPL and SOP solutions.

Additional high frequency components are evident using continuous wavelet techniques providing further confirmation of modelling effects (Figure 3-25). Note there is no dominant periodic signal in the high frequency components in the PJM solution where OTL was modelled for the duration of the analysis.

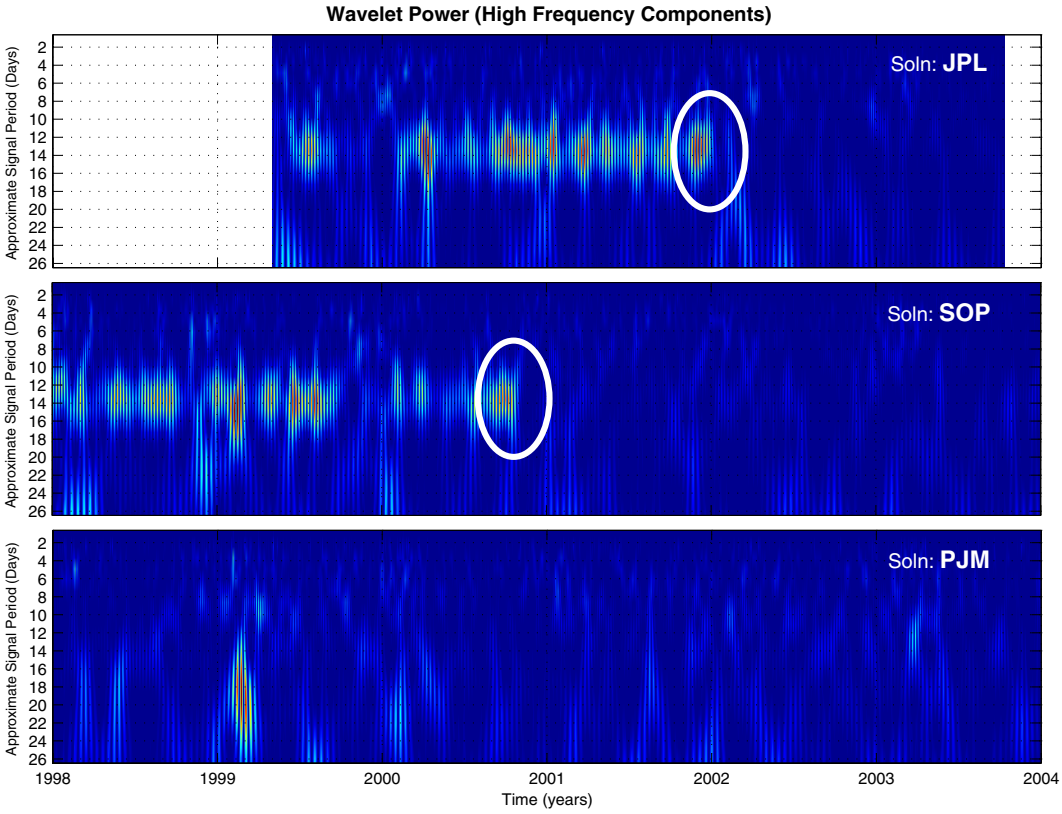

Figure 3-25 Wavelet power for the high frequency components of the KARR vertical time series. The white circles indicate the commencement of OTL modelling in the JPL and SOP solutions. Note the colours represent a relative scale, with blue indicating low power, and red showing high power.

Information from these plots is in contradiction to Nikolaidis (2002) who speculated the peak (determined to be at 13.6 ± 0.05 days) is not as a result of un-modelled OTL due to the prevalence of the spectral peak significant distances inland from the coast. Nikolaidis (2002) proposed the signal may be due to errors in the solid Earth tide or indirect tidal errors within the satellite orbits. Williams et al. (2004), also using the SOP solutions, cites tidal aliasing as the source of the 13.6 day peak, referring to Penna and Stewart (2003) for discussion.

Further investigation of power spectra in the vicinity of the 13.6 day period was undertaken using data from both the JPL and SOP solutions, using only the data from the period when OTL was not modelled.

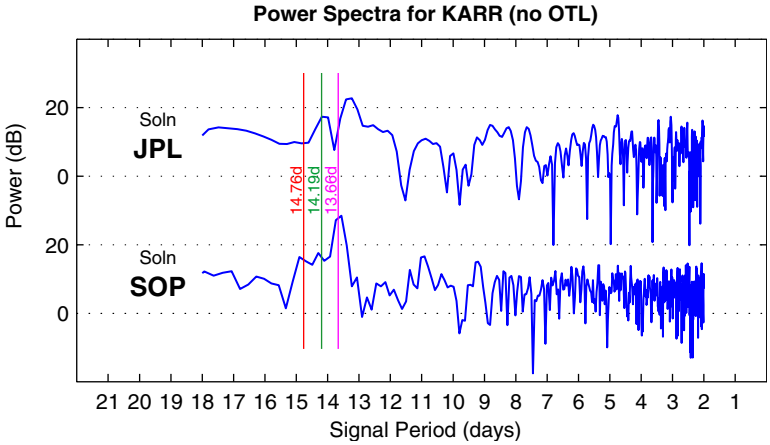

Figure 3-26 Power spectra at the KARR site for the period when no OTL was applied in the JPL and SOP solutions. Aliased periods for the M2 and O1 constituents from Penna and Stewart (2003) are shown as vertical lines.

Of particular interest in Figure 3-26 is the presence of power at 14.76 and 14.19 day periods, particularly in the SOP solution. This agrees with the theoretical aliased periods of the M2 and O1 constituents (due to the effect of 24 hour batch processing), as developed by Penna and Stewart (2003). The JPL solution shows peaks at 13.3 and 14.1 days, marginally higher (in terms of frequency) compared with the SOP solution. This is most likely caused by the fact that the duration and temporal extent of the period when OTL was not modelled in the SOP and JPL solutions is different (note the period when OTL was not modelled in the JPL solution begins 1.5 years, and finishes 1 year after the equivalent SOP solution). The difference in processing strategies between the two solutions is also expected to account for some of the difference observed. For example, differences in the ability of either technique (double differencing versus precise point positioning) to resolve correlated parameters such as the tropospheric delay may have an influence.

Components of the fortnightly signal in the vertical component may therefore map at different rates into these correlated parameters, such as the tropospheric delay.

The analysis presented here firmly indicates that the spectral power around the 13.6 day period is indeed caused by the failure to model OTL in the JPL and SOP solutions. Some of the power at lower frequencies (semi-annual and annual periods) can also be attributed to no or inadequate modelling of OTL, based on the findings in Penna and Stewart (2003). This is confirmed in the continuous wavelet analysis, with semi-annual and annual power significantly more dominant when OTL was not modelled (see Appendix B). As a consequence of this finding, it can be concluded that estimates of power law noise will be heavily influenced by failure to model, or mis-modelling, higher frequency geophysical signals, such as OTL or the solid Earth tide.

Analysis of the vertical signal in the spatial domain (from all three solutions), further underscores the difficulty in making a geophysical interpretation of the vertical component (Figure 3-23). Visual inspection shows minimal correlation between each of the solutions (with the exception of the JPL and SOP solutions, for the common period when OTL was not modelled). This lack of correlation occurs despite all solutions exhibiting power at annual and semi-annual periods. This gives weight to the hypothesis that the dominate signal structure, for this site at least, is solution specific. Determinant factors generating the non linear structure present in Figure 3-23 (besides tidal aliasing), are therefore likely to include the relative success of estimating other parameters correlated with the vertical component. For example, these parameters would include estimating tropospheric delay, atmospheric gradients and integer ambiguity parameters. These parameters will be solution specific, and each may amplify the effects of mis-modelling periodic signals (Penna and Stewart, 2003). In the case of the PJM solution, the non-linear structure seen in Figure 3-23 may be highly dependent on the regional reference frame stabilisation used in the analysis.

3.5.4.5 Velocity Differences between Solutions

Estimates of geodetic position and their rates over time are clearly dependent on the reference frame definition and its stability over time. Concentrating on the vertical component is crucial for altimeter calibration research. Systematic differences between vertical velocity estimates, therefore, not only reflect solution specific differences, but differences in the realisation of the reference frame. To assess these differences, weighted least squares velocity estimates from the JPL, PJM and SOP solutions were compared for sites in the Australian region (including Antarctic and offshore territories, as shown in Figure 3-9). The minimum data span used in the comparison was 3.3 years, helping to reduce bias from seasonal signals (Blewitt and Lavallee, 2002). When computing uncertainties of the velocity differences between solutions, uncertainties from each velocity estimate were scaled by a factor of 6 (median value from Figure 3-21a) to aid in the interpretation of the differences (Figure 3-27).

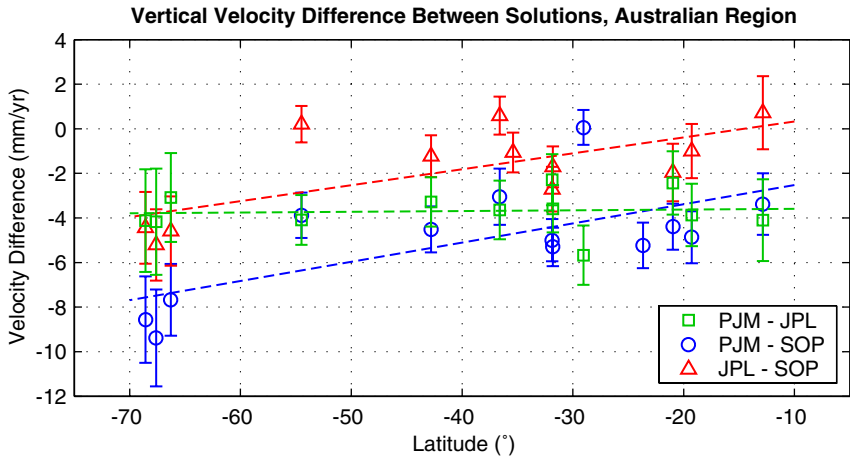

Figure 3-27 Differences in vertical velocity between solutions plotted against latitude. Note individual uncertainties have been scaled by a factor of 6 before generating the uncertainty of each difference.

Figure 3-27 shows negligible latitudinal dependence in the velocity differences between the PJM and JPL solutions (green line), yet the JPL velocities are biased higher than PJM by approximately 4 mm/yr. Both the PJM-SOP and JPL-SOP differences show latitudinal dependence, driven largely by significant differences in the velocities at the Antarctic sites. Differences at each of the three Antarctic sites (CAS1, DAV1 and MAW1) are tightly clustered for each solution difference. PJM-SOP shows the largest difference at around the -8 mm/yr level. Interestingly for these sites, the JPL-SOP difference is around the -5 mm/yr level. Neglecting these Antarctic sites, the JPL-SOP differences are not significantly different from zero.

On the other hand, the PJM regional solution underestimates velocity in relation to JPL and SOP.

This simple example underscores the difficulty encountered when attempting to use and interpret geodetic GPS estimates of vertical velocity. It is beyond the scope of this study to rigorously investigate the computational differences between the solutions investigated. A number of factors can however be identified which may influence the vertical velocity rates as presented:

- The data used in this example range from 3.3 to 6 years in duration; hence the effect of periodic signals may still have an influence.

- The regional reference frame defined in the PJM analysis appears to systematically affect velocity determination in relation to the global methodologies adopted in the JPL and SOP solutions.

- The failure to model OTL in sections of the JPL and SOP solutions will influence estimates of velocity through the introduction of low frequency aliased signals.

- The use of the IERS 1992 solid Earth tide in the PJM and SOP solutions, and the interaction of this outdated correction with the failure to model OTL in the early stages of the SOP solution, will undoubtedly affect vertical velocity estimates. This is especially relevant in Antarctic sites where the effect of the mis-modelling of the solid Earth tide is at its greatest (§3.3.1). This is therefore likely to account for some of the differences in vertical velocity observed at the Antarctic sites in this section.

3.6 Summary

The fundamental aim of this Chapter has been the definition of a coordinate datum at the Bass Strait calibration site, suitable for use in the absolute calibration of the T/P and Jason-1 altimeters. In achieving this aim, the reference frame realisation process and the computational standards adopted in a geodetic analysis have required review. Both the solid Earth tide and pole tide within the GAMIT/GLOBK suite were found to be inconsistent with accepted standards (as used in the processing of the satellite altimeter data). The effect of these differences were found to be minimal at the Bass Strait calibration site, yet significant at higher latitudes due to the influence of excluding the latitudinal dependence of the model Love numbers in the existing GAMIT formulation. Recent findings at the time of writing show that updating the Earth tide formulation significantly changes estimates of vertical velocity when comparing identical networks processed over a four year period (personal communication, P. Tregoning, 2005). This underscores the significance of this finding, especially given the reliance on velocity determination from the GAMIT/GLOBK suite in the literature (Williams et al., 2004 for example).

The coordinate datum at the Bass Strait site has been defined through the analysis of episodic GPS observations, made within a larger regional network. In assessing the effect of the small number of episodic observation sessions, results from the main reference station at the calibration site (BUR1) have been compared to results from its continuous time series computed in a separate solution. This analysis uses the BUR1 site as a proxy for the performance of the nearby TBCP and RKCP reference stations, both of which could not be operated as continuous installations due to logistical constraints. The BUR1 time series analysis has aided in the determination of an error budget for the final coordinate estimates. The coordinates can now be used to determine absolute sea surface height with the kinematic analysis of the GPS buoys in the following Chapter.

The Chapter has also investigated many of the difficulties surrounding the estimation of vertical velocity, required for the estimation of altimeter bias drift. Analysis of the continuous time series at the BUR1 site shows that the vertical velocity is indistinguishable from zero at the 95% confidence level due to its short duration, frequent outages and high power law noise content. Both monument noise and site specific issues relating to multipath and signal diffraction (and its potential aliasing due to the sidereal day repeat GPS orbit) are expected to

dominate the noise budget at the BUR1 site. Investigations into the influence of ocean tide loading has confirmed theoretical predictions presented in Penna and Stewart (2003), underscoring the prevalence of aliased periodic signals in both the early JPL and SOPAC geodetic time series. These aliased signals exist at both medium to low frequencies, contributing to the power law noise structure present in many long term geodetic time series. The presence of time correlated noise leads to the significant underestimation in velocity uncertainty when assuming only a white noise model. Clearly the various sources of the low frequency noise (both from a geophysical origin, in addition to software specific issues such as mis-modelling at the observation level) must be better understood in order to improve the quality of results in the vertical component.

Analysis of regional versus global solutions has shown systematic differences in velocity estimates, emphasising the importance of the reference frame definition and realisation process. The collection of case studies has shown that the standard linear model adopted in the definition of the International Terrestrial Reference Frame is insufficient to describe many of the non linear displacements present in each coordinate component. These case studies, although limited, are sufficient to point to past and present deficiencies in GPS processing methodologies that impact on high precision geodetic computations, especially in our case for the vertical component. Improvement therefore dictates a holistic approach, requiring improvement to the global reference frame, correct and up-to-date computational models, in addition to a greater understanding of both the geophysical and software specific causes of site "motion" and its time correlated behaviour.

Chapter 4

Absolute Calibration in Bass Strait

4.1 Introduction

The previous Chapters have provided the foundation required to undertake absolute satellite altimeter calibration at the Bass Strait calibration site. Chapter 2 presented the development and testing of the GPS buoy technology which is central to the overall methodology and results presented throughout this Chapter. Chapter 3 reviewed the geodetic framework required at the calibration site in order to determine in situ estimates of sea surface height in an absolute geodetic reference frame. Equally importantly, Chapter 3 discussed the uncertainty and current limitations of geodetic positioning in the vertical component, highlighting wide reaching implications to fields beyond altimeter calibration.

This Chapter, representing the core of this Thesis, presents both the methodology and results from the Bass Strait calibration study. The first results presented refer to the calibration and validation period of the Jason-1 mission. This period, also known as the 'formation flight' phase of the T/P and Jason-1 mission, lasted approximately seven months between Jason-1 cycle 1 (18^{th} January, 2002), up to and including cycle 22 (14^{th} August, 2002). This period corresponds with T/P cycles 344 to 365, at which stage T/P was shifted to an orbit achieving interleaving ground tracks between successive Jason-1 passes. Both the absolute bias results for T/P and Jason-1, in addition to the relative bias between the two missions are presented for this 'formation flight' period.

Additional analysis for the Jason-1 altimeter within this Chapter continues up to and including cycle 101 (06/10/2004), which was the most up-to-date Geophysical Data Record (GDR) release at the time of writing. Analysis for T/P is also presented extending back to the launch of the mission. Results are compared with those determined from other global and in situ calibration studies which contribute to the global altimeter calibration effort.

The calibration methodology presented in this Chapter builds extensively on the previous verification experiment conducted at the Bass Strait calibration site following the launch of the T/P altimeter in 1992 (White et al., 1994). Both the instrumentation and methodology adopted at the southern hemisphere site have been significantly augmented since the previous study. This Chapter begins by placing the Bass Strait study site in a wider global context. The methodology is presented followed by data processing, analysis, and finally results and comparative analysis with other calibration sites.

4.2 Absolute Calibration Methodologies

As reviewed in the introductory Chapter, the two primary in situ absolute calibration sites for T/P and Jason-1 are supported by the mission partners, the U.S. National Aeronautics and Space Administration (NASA) and the French Space Agency, Centre National d'Etudes Spatiales (CNES). The NASA site is located on the Harvest oil platform offshore from the Californian coast (34° 28' N, 239° 19' E) on T/P – Jason-1 ascending pass 043, (see Haines et al., 2003). The CNES site is located offshore from the island of Corsica (41° 33' N, 8° 48' E), in the Mediterranean Sea on ascending pass 085 (see Bonnefond et al., 2003a). These primary calibration sites are shown in Figure 4-1.

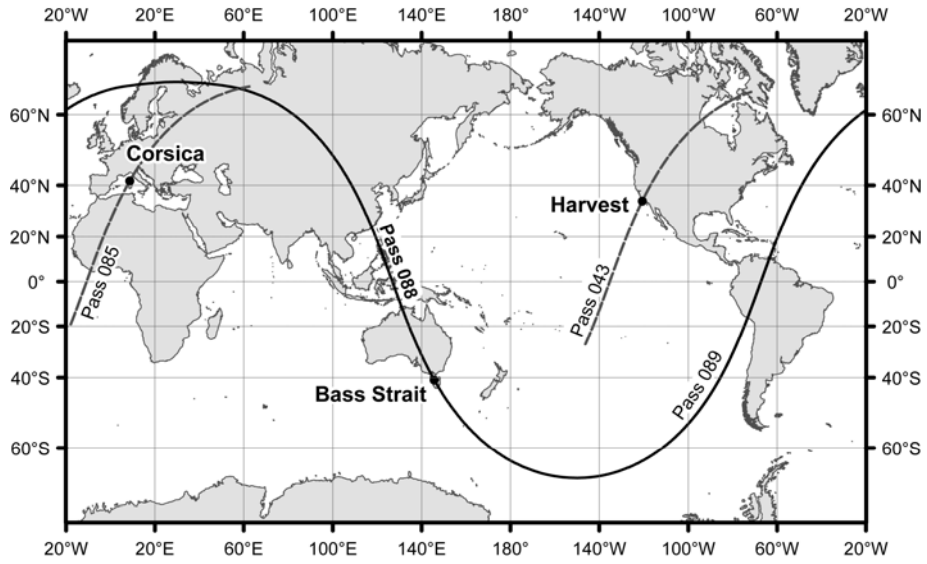

Figure 4-1 Location of the Bass Strait calibration site on descending T/P and Jason-1 pass 088. The NASA site at Harvest platform is shown on ascending pass 043 and the CNES site at Corsica is shown on ascending pass 085.

Additional absolute calibration activities planned for the Jason-1 mission (Menard and Haines, 2001) include various studies located around the European region (for example Woodworth et al. (2004) in the United Kingdom, Schone et al. (2004b) in the North Sea, Pavlis and Mertikas (2004) offshore from Crete in Greece and Martinez-Benjamin et al. (2004) offshore from Ibiza in Spain) in addition to over the Great Lakes in the United States (Shum et al., 2003). The development of a calibration site in Bass Strait provides a unique contribution to the international calibration effort. The Australian site is the sole location of its kind in the southern hemisphere, and unlike the NASA and CNES sites, is located on a descending altimeter pass. Bass Strait itself separates the state of Tasmania from

the Australian mainland, with the calibration site located on the south west side, near the coastal city of Burnie (Figure 4-2).

In review, the determination of absolute altimeter bias requires the in situ measurement of SSH in a comparable terrestrial reference frame at some chosen comparison point ($SSH_{ComparisonPoint}$). The absolute bias of the altimeter ($Bias_{Alt}$) may be determined using the simple relationship:

$$Bias_{Alt} = SSH_{Alt} - SSH_{Comparison\ Point} \qquad \text{Eqn 4-1}$$

where SSH_{Alt} is the altimeter derived SSH estimate. A negative (-)ve bias is therefore indicative of SSH being measured too low by the altimeter (i.e., the altimeter range is too long).

Two distinct methodologies exist for the measurement of in situ SSH at the comparison point (i.e., $SSH_{ComparisonPoint}$):

1) *Direct measurement.* In this case, SSH is physically observed at the comparison point. In the case of the NASA calibration site at Harvest (Haines et al., 2003), the platform itself (with associated geodetic and sea level instrumentation) is located at the comparison point, allowing the direct estimation of SSH for each overflight. Other studies utilising solely GPS equipped buoys are other examples of the direct calibration methodology.

2) *Indirect measurement.* In this case, the SSH measurement is not made directly at the comparison point, rather at a nearby (usually coastal) location. Examples such as the CNES calibration site (Bonnefond et al., 2003a), the United Kingdom project (Woodworth et al., 2004), and the Greek GAVDOS project (Pavlis and Mertikas, 2004) determine the SSH estimate at a coastal tide gauge site which is then 'transferred' or 'extrapolated' offshore through the use of precise regional geoid models, and in many cases, numerical tide models. The indirect technique provides logistical advantages whilst maintaining the ability to determine cycle-by-cycle estimates of absolute bias. The accuracy of the SSH transfer technique (i.e., the accuracy of the geoid and tidal models) is the limiting factor for this methodology.

The Bonnefond et al. (2003a) study provides an example of where both the direct and indirect methodology are combined. GPS equipped buoy deployments are made on an episodic basis allowing direct calibration. At the same time, the estimates of $SSH_{ComparisonPoint}$ are compared with SSH estimates taken at coastal tide gauge sites. Analysis of differences yields information on both the relative geoid and tidal phase and amplitude differences. This information can then be applied using the indirect methodology to transfer the tide gauge SSH estimates to the comparison point, without the need to deploy the GPS buoy. Bonnefond et al. (2003b) include an additional step to compute a 'map' of the sea surface topography between the coastal tide gauges and surrounding the offshore altimeter comparison point, which can then be used in the calibration process.

The initial study at the Bass Strait site is an early example of the indirect calibration methodology (White et al., 1994). The experiment combined data from a coastal tide gauge with episodic land based GPS measurements, a numerical tide model and a regional geoid model to extrapolate estimates of absolute SSH to the offshore comparison point. The offshore SSH estimates were then used to compute estimates of absolute bias during the calibration phase of the T/P mission. The limitations of this early study were twofold. Firstly, and most importantly, uncertainty associated with the regional geoid model significantly reduced the accuracy of the $SSH_{ComparisonPoint}$ estimates. Secondly, the use of the numerical tide model to determine tidal phase and amplitude differences between the tide gauge and offshore comparison point added uncertainty to that already accumulated due to the use of the regional geoid model.

Both of these limitations in the White et al. (1994) study (and in fact those associated with the indirect calibration technique in general), arise as a result of a lack of in situ data observed at or around the offshore comparison point. Combination techniques, as described in the Bonnefond et al. (2003b) study, improve the extrapolation technique and hence the accuracy of the $SSH_{ComparisonPoint}$ estimates. Techniques such as these are still however limited by the short time series of measurements used to determine the extrapolation parameters of interest (geoid slope, tidal differences, etc). Potential effects which can not be considered include aliasing from seasonal oceanographic signals and meteorological effects.

Calibration using a purely direct approach, as at the Harvest platform, was considered for the redevelopment of the Bass Strait calibration site. The use of an oil platform was not possible due to the proximity of platforms to the altimeter ground track, in addition to the significant capital and logistical investment

required to instrument the site and maintain it. Continuously operating GPS equipped buoys provide a solution to the direct approach, however, they suffer from the disadvantages discussed throughout Chapter 2.

To minimise logistical difficulties and limitations associated with the indirect calibration technique, a unique alternative methodology was developed. The methodology is outlined below:

1) Over the duration of the Jason-1 calibration phase, an oceanographic mooring array is deployed at the comparison point to allow the determination of a highly precise SSH time series (corrected for density changes in the water column). The datum of the mooring SSH time series at this point is purely arbitrary, defined by the depth of the pressure sensor on the mooring array.

2) During the deployment of the mooring array, episodic GPS buoy deployments are undertaken at the comparison point, directly above the mooring array. The GPS buoy derived estimates of SSH are then used to solve for the datum of the mooring SSH time series, allowing cycle-by-cycle absolute altimeter bias determination against the mooring time series, using a direct technique.

3) Over the duration of the calibration phase, a difference time series is computed between the offshore mooring (with the datum defined by the GPS buoys) and measurements from a coastal tide gauge. A tidal analysis of the difference time series is then used to compute tidal hindcast and forecast predictions of the tidal differences to effectively transform the coastal tide gauge observations (outside the mooring deployment time period) to the offshore comparison point. This therefore provides an improved indirect calibration technique for periods outside the primary calibration phase of the mission, without the need to estimate a precise relative geoid.

4) Finally, land based GPS stations utilised as reference stations for the GPS buoy analysis are also used to determine GPS based estimates of the tropospheric wet delay, suitable for use in calibrating the T/P and Jason microwave radiometers (TMR and JMR respectively).

More recently, other calibration teams have announced similar methodologies which utilise bottom mounted pressure sensors (for example Schone et al., 2004a in the North Sea and Calmant et al., 2004 in the southwest Pacific Ocean). An important distinction at the Bass Strait site is the ability to infer the density of the water column and solve for the absolute datum of the pressure gauge sensor. The Calmant et al. (2004) study uses two pressure gauges (corrected for density effects) however no attempt is made to solve for the absolute datum of the gauges. This restricts the study to relative bias drift with the associated disadvantages as discussed in the introductory Chapter. The refined Bass Strait methodology outlined above is discussed in detail throughout the following sections.

4.3 The Bass Strait Calibration Site

The calibration methodology developed for the Bass Strait site represents an innovative approach to both the direct and indirect calibration methodologies discussed in the previous section. A direct approach is used throughout the intensive calibration phase of the Jason-1 mission. Outside this dedicated period, a refined indirect process is used to allow the continuation of cycle-by-cycle estimates of absolute bias, without the disadvantage of estimating a precise relative geoid.

4.3.1 Site Details

Bass Strait is a relatively shallow body of water with typical depths between 60 and 80 m (approximately 51 m at the calibration site). The strongest currents throughout the region are of tidal origin (both diurnal and semidiurnal), with typical values at the calibration site of around 10-20 cms^{-1}. Low frequency wind driven currents are weak in the region surrounding the calibration site, typically less than 5-10 cms^{-1}). Mooring data collected at the calibration site also show the water column to be stratified during the austral summer, and well mixed from February onwards.

T/P and Jason-1 descending pass 088 crosses the south east coast of mainland Australia at the city of Lorne, Victoria. The pass follows a 325 km path over Bass Strait crossing the Tasmanian coast approximately 2 kilometres west of the city of Burnie. The absolute comparison point is located approximately 39.4 km north west of Burnie along the descending altimeter ground track (Figure 4-2). The Bass Strait site was initially selected due to the proximity of the ground track to the city of Burnie, and the ability to operate a tide gauge in the port complex (White et al., 1994). The selection of the offshore comparison point in this study (40° 45' S, 145° 40' E), has been made as a compromise between GPS network geometry (minimising baseline lengths for the GPS buoy processing) and maximising the distance from land to ensure integrity of the altimeter measurements (mainly due to contamination of radiometer and altimeter returns as the respective footprints pass on to land).

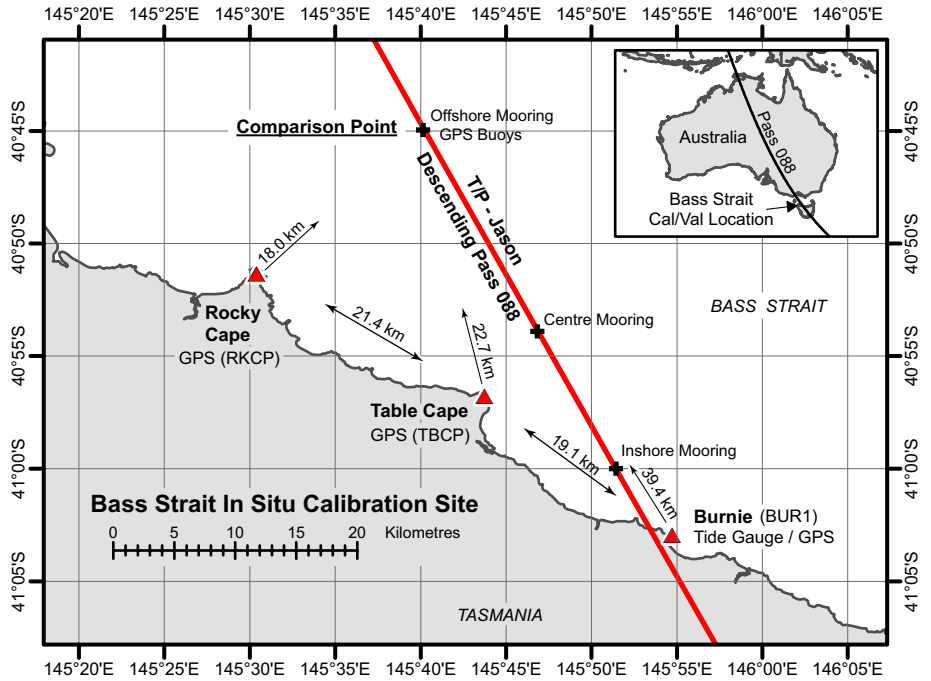

Figure 4-2 The Bass Strait Calibration Site. Note the position of the offshore comparison point, oceanographic mooring arrays, the coastal tide gauge and land based GPS reference sites (BUR1, TBCP and RKCP).

4.3.2 Calibration Methodology

The enhanced calibration methodology at the Bass Strait calibration site is focused on the determination of SSH at the chosen comparison point using data from three separate instrument ensembles:

1) episodic GPS buoy deployments;
2) oceanographic mooring array deployments; and
3) utilisation of a coastal tide gauge.

The methodology developed for the Bass Strait calibration site is shown in schematic form in Figure 4-3.

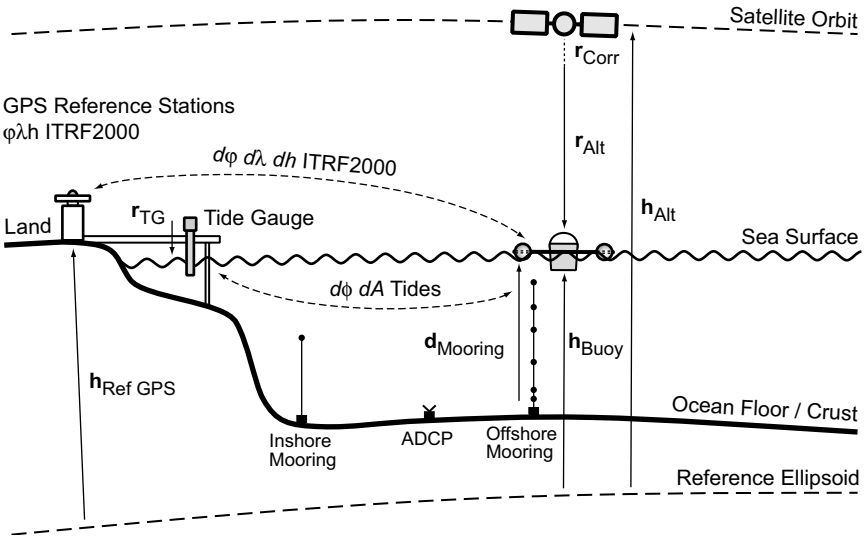

Figure 4-3 Calibration methodology and associated instrumentation at the Bass Strait calibration site.

To estimate the altimeter absolute bias (Eqn 4-1), estimates of $SSH_{ComparisonPoint}$ must be made in an equivalent terrestrial reference frame as that used by the altimeter. The reference system used by the altimeter is defined by the orbit computation technique. To ensure an equivalent reference frame for the terrestrial estimate at the Bass Strait site, $SSH_{ComparisonPoint}$ is determined relative to a regional GPS network, constrained to the ITRF2000 realisation of the International Terrestrial Reference Frame (Altamimi et al., 2002). As discussed in the previous Chapter, a typical regional GPS network solution involves the assimilation of 24 hours of observed data. During this time the Earth's crust behaves elastically in response to the lunisolar potential and various mass loadings (ocean and atmosphere for example). For this reason, corrections are made for each GPS observation in the GPS analysis, such that the final position and height estimates are derived relative to ITRF2000, expressed relative to an ellipsoid, but in relation to a non-tidal, rigid crust (i.e., the effect of the lunisolar attraction and loading signals are removed using available models). The datum used to define estimates of $SSH_{ComparisonPoint}$ therefore relates to a non-instantaneous, non-tidal crust, with co-ordinates referred to as conventional tide free coordinates (see discussion in Chapter 3). This is in contrast to altimeter SSH (SSH_{Alt}) measurements which relate to the instantaneous position of the crust and ocean (relative to the fixed surface of the ellipsoid). For comparison, SSH_{Alt} requires correction to refer the measurement to the non-tidal crustal position. With reference to Figure 4-3, the corrected sea surface height derived from the altimeter is defined in Eqn 4-2:

$$SSH_{Alt} = h_{Alt} - \left(r_{Alt} + r_{Corr}\right) + TL_{Corr} + ATGG_{Corr} \qquad \text{Eqn 4-2}$$

where h_{Alt} is the height of the altimeter above the reference ellipsoid, r_{Alt} is the observed altimeter range to the instantaneous sea surface, r_{Corr} is the sum of the associated path length and surface corrections, TL_{Corr} are corrections needed to reduce the SSH estimate to the non-tidal crust, making them consistent with $SSH_{ComparisonPoint}$, and $ATGG_{Corr}$ is a correction to account for the cross-track geoid gradient between the altimeter ground track and the position of the comparison point (see §4.4.4.5).

The critical in situ measurement at the comparison point is SSH determined on an episodic basis using the GPS buoys (SSH_{Buoy}) described in Chapter 2. With reference to Figure 4-3, SSH_{Buoy} is defined as:

$$SSH_{Buoy} = h_{Buoy} = h_{Ref\ GPS} + dh_{RefGPS\ to\ Buoy} \qquad \text{Eqn 4-3}$$

where h_{Buoy} is the height of the buoy (reduced to mean water level) above the reference ellipsoid. This measurement is derived relative to the three dimensional positions of the GPS reference stations (h_{RefGPS}) using the estimated change in ellipsoidal height to the buoy ($dh_{RefGPStoBuoy}$). $dh_{RefGPStoBuoy}$ includes a small contribution from differential tidal and mass loading signals. As discussed previously, the methodology and length of data required to compute h_{RefGPS} dictates that the final estimates of SSH_{Buoy} relate to a conventional tide free datum.

Also at the comparison point, the offshore mooring array is utilised to estimate water height ($d_{Mooring}$), relative to the pressure sensor anchored to the sea floor. The calculation of the $d_{Mooring}$ time series from the offshore mooring array is discussed in a later section of this Chapter (§4.4.1). The mooring data alone refer to an arbitrary datum and are hence not directly comparable to SSH_{Alt}. The absolute datum of the mooring data is defined using estimates of absolute SSH determined from the GPS buoys (SSH_{Buoy}). This technique involves direct comparison of the $d_{Mooring}$ series with data from the GPS buoys. This datum solution enables the calculation of the $SSH_{Mooring}$ time series, which is directly comparable with SSH estimates measured by the altimeters (Eqn 4-4).

$$SSH_{Mooring} = d_{Mooring} + mean\left(SSH_{Buoy} - d_{Mooring}\right) \qquad \text{Eqn 4-4}$$

Note that the mooring is considered fixed to the sea floor which is subject to the same elastic response to variations in gravitational potential and mass loading. No correction is however required to the mooring time series as the deformations are assumed identical at the ocean surface (i.e., the $d_{Mooring}$ time series does not include

a geophysical or mass loading component, hence the $SSH_{Mooring}$ and SSH_{Buoy} time series can be directly compared and are relative to the same non-instantaneous, non-tidal crustal position, expressed relative to the reference ellipsoid). The $SSH_{Mooring}$ time series is continuous over the deployment period, allowing comparison with the altimeter on a cycle-by-cycle basis. This represents the main advantage of this technique.

A third instrument operated at the Bass Strait calibration site is the acoustic tide gauge located at the Burnie port (Figure 4-2). The tide gauge measures ranges to the sea surface (r_{TG}) relative to the tide gauge zero. The tide gauge data are utilised to extend cycle-by-cycle comparison with the altimeter both before and after the mooring deployment (i.e., outside the primary calibration phase of the Jason-1 mission).

As stated previously, the use of a tide gauge located away from the altimeter comparison point complicates the determination of absolute bias. The sea surface height measured by the tide gauge will differ from sea level at the comparison point due to a range of influences including oceanographic conditions (tidal differences, along and cross-shore currents), meteorological differences (wind setup, atmospheric pressure differences), geophysical differences (differential tidal and non-tidal loading) and geometric differences (geoid slope). The improved indirect calibration methodology adopted to overcome these differences relies on both the $SSH_{Mooring}$ and the SSH_{Buoy} time series. In the most simplified form, the tide gauge data (r_{TG}) are transformed to absolute sea surface heights at the comparison point using the relation:

$$SSH_{TG} = r_{TG} + Tide_{Corr} \qquad \text{Eqn 4-5}$$

where $Tide_{Corr}$ is a tidal and datum correction computed using differences between r_{TG} and $SSH_{Mooring}$. The tidal correction comprises phase differences ($d\phi$) and amplitude differences (dA) for the major tidal constituents, as shown schematically in Figure 4-3. This correction is dominated by an approximate 4 degree phase offset in the M2 tidal constituent, with a corresponding amplitude difference of 0.089 m (see §4.4.3).

In summary, the calibration methodology presented in this Thesis is divided into two components. Firstly, during the calibration phase, or formation flight period of the T/P and Jason-1 missions, the altimeter absolute bias is determined using comparison against the mooring sea surface height time series ($SSH_{Mooring}$), i.e.,

using Eqn 4-1 and Eqn 4-4. This time series has an absolute datum defined using the SSH_{Buoy} data. Secondly, outside the formation flight period (i.e., both before and after the deployment of the mooring array), the cycle-by-cycle comparison with the altimeter is continued using the tide gauge time series (SSH_{TG}), which has been corrected for geometrical and tidal differences using both the mooring and GPS buoy datasets (i.e., Eqn 4-1 and Eqn 4-5).

4.3.3 Instrumentation

4.3.3.1 GPS Buoys and Reference Stations

As outlined in Chapter 2, two identical wave rider GPS buoys were developed and deployed on an episodic basis. Three land based GPS reference sites were used, including the continuously operating receiver which is collocated with the Burnie tide gauge (see Figure 4-2). Readers are referred back to Chapter 3 for further details relating to the GPS reference stations and analyses.

A total of seven buoy deployments were undertaken (Table 4-1). An 'ideal' deployment duration of 4 hours was set, centred on the time of overflight of the altimeter. This time period was chosen to be a compromise between a sufficient GPS measurement period to ensure high quality (~1-2 cm) height estimation and logistical constraints of buoy deployment and retrieval. The first deployment was undertaken as a trial prior to the launch of Jason-1, while the fourth deployment did not yield any useful data as ocean conditions were too rough (as discussed in Chapter 2), leaving 5 deployments available to compute the absolute datum of the $SSH_{Mooring}$ time series (Eqn 4-4).

Table 4-1 GPS buoy deployment at the Bass Strait calibration site.

Deployment	Date	T/P Cycle	Jason-1 Cycle
1	21/09/2001	332	-
2	17/02/2002	347	4
3	09/03/2002	349	6
4	07/04/2002	352	9
5	27/04/2002	354	11
6	07/05/2002	355	12
7	27/05/2002	357	14

4.3.3.2 Oceanographic Mooring Array

Three mooring arrays were deployed along the T/P and Jason-1 ground track between the altimeter comparison point and the Burnie tide gauge (Figure 4-2). The mooring array was deployed by CSIRO Marine Research technical staff shortly after the Jason-1 launch in December 2001 and retrieved after the completion of the T/P and Jason-1 formation flight phase in September 2002. The instrument arrays at the inshore, centre and offshore moorings were deployed at depths of 32 m, 47 m, and 51 m respectively (Figure 4-4).

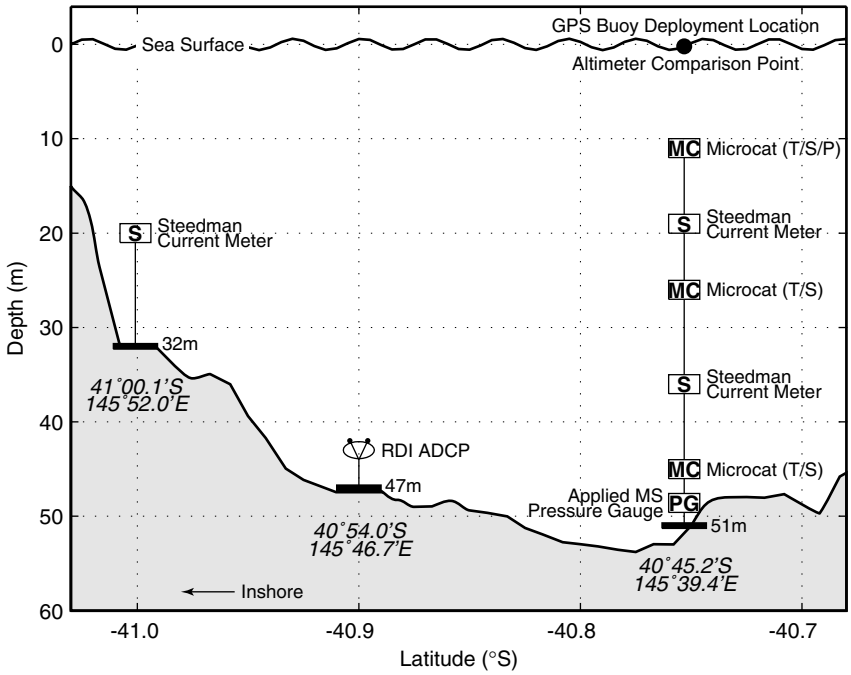

Figure 4-4 Mooring array placed along the altimeter ground track from Burnie to the comparison point location.

The offshore mooring (40° 45.2' S, 145° 39.4' E) was positioned close to the altimeter comparison point and GPS buoy deployment site (within 1 km). Working from the base of the mooring upward, the instruments included:

- Applied Microsystems™ pressure gauge (depth 49.5 m)
- Seabird Microcat™ temperature and salinity recorder (T/S, depth 45 m)
- Steedman™ acoustic current meter (depth 36 m)
- Seabird Microcat™ temperature and salinity recorder (T/S, depth 26 m)
- Steedman™ acoustic current meter (depth 19 m)
- Seabird Microcat™ temperature, salinity and pressure recorder (T/S/P, depth 11 m)

The centre mooring (40° 54.0' S, 145° 46.7' E) consisted of an RDI™ acoustic Doppler current profiler (ADCP) at a depth of 43 m. The inshore mooring (41° 00.1' S, 145° 52.0' E) consisted of a single Steedman™ acoustic current meter at a depth of 20 m.

The calculation of the $d_{Mooring}$ time series utilises data from the pressure gauge and the three Seabird Microcat™ instruments from the offshore mooring. Data from the other instruments is utilised for the determination of sea surface setup at the Burnie tide-gauge location.

4.3.3.3 Tide Gauge

The Burnie tide gauge is located on the northern extremity of the Burnie wharf complex, fixed to the inshore side of a large concrete headwall extending into the Bay (Figure 4-5). The Bay forms an elongated bight in the coastline leaving the gauge exposed to Bass Strait, without significant influence from local harbour effects. The gauge consists of an Aquatrak acoustic sensor and Sutron terminal unit. Data are logged every 6 minutes, with each data point an average of 180, 1-sec samples. The gauge is one of sixteen forming the Australian Baseline Sea Level Monitoring Project managed by the National Tidal Centre (NTC). Data are streamed from both the tide gauge and associated meteorological sensors to NTC and archived on a daily basis.

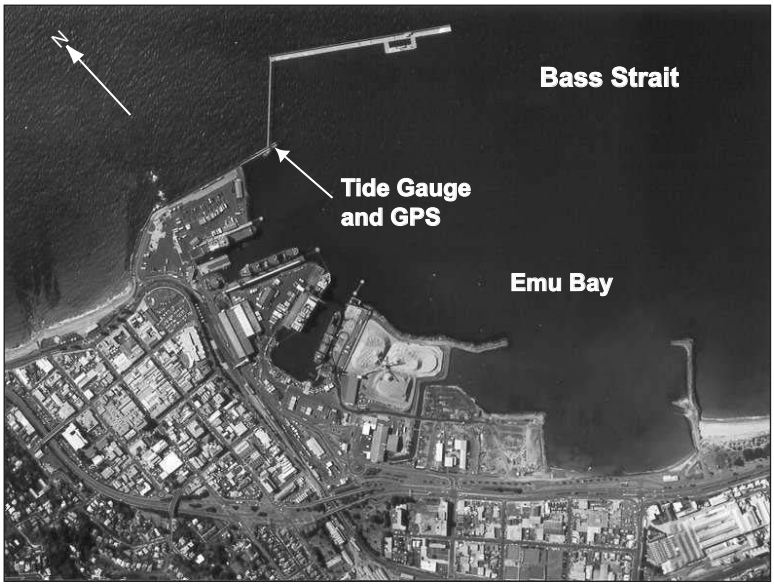

Figure 4-5 Burnie Tide Gauge and GPS location.

The Burnie tide gauge is revisited in the following Chapter which investigates tide gauge calibration using the GPS buoys developed in this Thesis.

4.4 Data Processing

4.4.1 Mooring Data Processing

Data from the Applied Microsystems pressure gauge (Paroscientific Digiquartz sensor) and three Seabird Microcat instruments at the offshore mooring were used to derive a sea surface height time series (with an arbitrary datum) for the duration of the mooring deployment ($d_{Mooring}$). The pressure gauge was calibrated early in 2001, and is quoted as having an absolute accuracy of 15 mm, with repeatability at the ~5-6 mm level. A small calibration correction to account for the temperature dependence of the pressure sensor (computed by CSIRO) was applied to this time series. This correction was small with an amplitude of ~5 mm.

The $d_{Mooring}$ time series was computed by first subtracting the local atmospheric pressure from the pressure gauge readings (half hourly samples) to give the pressure head of the water column. The atmospheric pressure time series (hourly samples) was obtained from the Burnie tide-gauge site, some 40 km along-track from the mooring location (Figure 4-2). To account for any potential differential atmospheric pressure between the two sites, model data from the Australian Bureau of Meteorology's Limited Area Prediction System (LAPS) was utilised (Puri et al., 1998). Atmospheric pressure data for this study were extracted using the model with 5 km resolution. The differential pressure obtained from the model was applied as a correction to the Burnie pressure time series. This correction ranged between ± 2 hPa and was indicative of the passage of pressure systems in the area in an eastward direction.

A time series of density profiles was calculated from the temperature and salinity data from the three Seabird Microcat instruments (5 minute sampling interval). The Seabird Microcat instruments were purchased new for this experiment, and the factory supplied calibrations were used. The temperature sensors are quoted as having an absolute accuracy of 0.002 °C, and a stability of 0.0002 °C per month or better. The salinity output is quoted as having an accuracy of 0.003 psu, and a stability of 0.003 psu per month. The two lower instruments showed clear evidence of fouling late in the deployment (31st March, 2002, following T/P cycle 351 and

Jason-1 cycle 8). Salinity data for these two instruments were therefore replaced for this period by the salinity time series from the top instrument. The temperature data showed that the water column was well mixed for this fouling period.

Finally, the computed density profiles were used to convert the water-column pressures to depths on a 5 minute time base. Variations in the observed density account for a range of approximately 5 cm in the sea level time series, underscoring the significance of the density measurements for this methodology. Plots of the dynamic ocean height component are provided in Appendix C. The uncertainty associated with the $d_{Mooring}$ time series is estimated to be at the 12 mm level. This includes contributions from the pressure sensor (4 mm), estimation of the dynamic height (5 mm) and estimation of the overhead atmospheric pressure (10 mm). The resultant $d_{Mooring}$ time series therefore provides a precise sea-surface height time series relative to an arbitrary datum defined by the depth of the pressure sensor on the sea floor.

4.4.2 GPS Data Processing

The GPS data processing involves two distinct stages in order to derive SSH estimates for each GPS buoy deployment, which are then used to define the absolute datum of the $SSH_{Mooring}$ time series. Firstly, as discussed in Chapter 3, the reference station analysis computes the absolute position of each reference station in a terrestrial reference frame, equivalent to the reference system used to define the orbits of both T/P and Jason-1. Secondly, the reference station positions are used to constrain the datum for the kinematic processing of each GPS buoy, producing raw 1 Hz SSH time series (SSH_{Buoy}). The following sections detail the kinematic analysis and the computation of the mooring SSH datum.

4.4.2.1 Kinematic GPS Analysis

The kinematic analysis involves the computation of the instantaneous ellipsoidal height of the GPS buoy relative to the accurate positions of the GPS reference stations determined in the previous Chapter. Coordinates from the GLOBK analysis are used together with GPS measurements from the BUR1, TBCP and

RKCP sites to process baselines between each site and the two GPS buoys (Buoy1 and Buoy2) using TRACK software developed at MIT (Herring, 2002). TRACK is a kinematic GPS positioning program, first developed by Chen (1998) for airborne laser altimetry applications. TRACK uses a differential or relative positioning methodology, implemented using a Kalman filter strategy (incorporating smoothing in the reverse time direction). For each observation epoch, parameters solved for in the observation models include the three-dimensional position of the GPS antenna, the receiver clock offset and a correction to the atmospheric model. The parameters are modelled as different stochastic processes (white noise, random walk and integrated random walk respectively), each with user defined initial conditions. The initial a priori standard deviation on the atmospheric delay parameter is set to 0.1 m, and the random walk process noise is constrained to 0.0001 $m/\sqrt{epoch}$. This process noise allows ± 3 cm variation over a 24 hour period corresponding to a relatively stable atmosphere. This is in agreement with other studies involving the estimation of tropospheric wet delay from a moving platform (Dodson et al., 2001 and Chadwell and Bock, 2001 for example). The position of the GPS antenna is modelled as a random walk with very loose constraints.

The primary observable used in the buoy analysis is the ionosphere-free linear combination, LC (otherwise referred to as the L3 combination). TRACK uses a station-to-station single difference algorithm for initial cycle slip detection. Initial bias estimates are computed using the Melbourne-Wubbena wide lane combination (Melbourne, 1985 and Wubbena, 1985). The bias fixing approach attempts to estimate ambiguity parameters from non-integer estimates, termed the 'float' analysis. The Kalman smoothing filter has been implemented in an attempt to achieve the optimum solution to the kinematic problem. The smoothing filter was found particularly useful when unresolved bias parameters existed in the solution, as also discussed by Herring (2002).

As highlighted in Chapter 2, breaking waves on the floating GPS buoy often caused loss of signal acquisition. This was the major difficulty encountered during the kinematic processing, as all bias parameters must be reset, disrupting the convergence of the filter operation. These events occurred on average one to two times over a typical deployment. No useful solution was obtained from the fourth buoy deployment (Table 4-1), due to frequent signal interruptions. Discontinuities arising due to these events often resulted in the incorrect resolution of bias parameters following re-acquisition of the signal. Biases were clearly evident in the resultant position time series, and / or in the adjustment to the tropospheric delay

parameter. In some cases, data from a specific solution were rejected due to bias fixing difficulties.

For this reason, measurements from the two GPS buoys were processed independently (as separate baselines) allowing some level of quality control on the resultant sea surface height time series. Kinematic solutions have been computed for each buoy (Buoy1 and Buoy2) from each reference station (TBCP and RKCP), resulting in four solutions for each of the five successful deployments coinciding with the mooring deployment period. Variability between solutions from different reference stations and between the two buoys provides an estimate of the precision obtained for a given deployment. A second indication of the variability in GPS buoy solutions is obtained by comparing SSH_{Buoy} with the mooring time series ($d_{Mooring}$), in a relative sense, before solving for the absolute datum of the mooring array.

The optimum processing parameters (for example, parameters controlling cycle slip detection and bias fixing) were defined in an iterative approach using differences between solutions and between the $d_{Mooring}$ time series as a proxy to the success of the solution. This technique helped identify areas of significant excursion caused by either data gaps or incorrectly solved bias parameters. Plots highlighting the resultant SSH_{Buoy} time series, position of data gaps / interruptions, and time series evolution of the tropospheric parameter and the number of fixed and unfixed bias parameters are included for each buoy solution in Appendix A.

4.4.2.2 Filtering and Transformation

The output of each TRACK analysis is a sea surface height time series at 1 Hz relative to ITRF2000 and expressed on the GRS80 ellipsoid (semi major axis of 6378137 m and an inverse flattening of 298.257222101). The altimeter sea surface height at the comparison point represents a spatial average within the footprint of the radar signal. The mooring time series also represents an integration over a specific time period, as dictated by the sampling and processing strategy adopted (§4.4.1). The buoy time series therefore required filtering to eliminate swell, surface waves and high frequency noise which are effectively averaged by both the altimeter and mooring array. Both simple temporal mean and exponential filters were implemented, with negligible differences when using filter lengths between 20

and 30 minutes. The exponential filter adopted is passed each way down the GPS buoy sea surface height time series to avoid phase distortion.

The T/P and Jason-1 altimeter data are provided on a different ellipsoid with a semi major axis of 6378136.3m and an inverse flattening of 298.257. Each GPS buoy SSH time series was therefore transformed from the GRS80 ellipsoid to the T/P ellipsoid using standard techniques (Soler, 1998).

An example of the 1 Hz GPS buoy SSH and corresponding filtered time series is shown in Figure 4-6(a). This example is taken from the first buoy deployment where the significant wave height (SWH) throughout the deployment was approximately 0.8 m. Throughout the deployment there was a consistent swell from the northwest, which is verified in the spectral analysis as having a dominant period of approximately 14 seconds (Figure 4-6b).

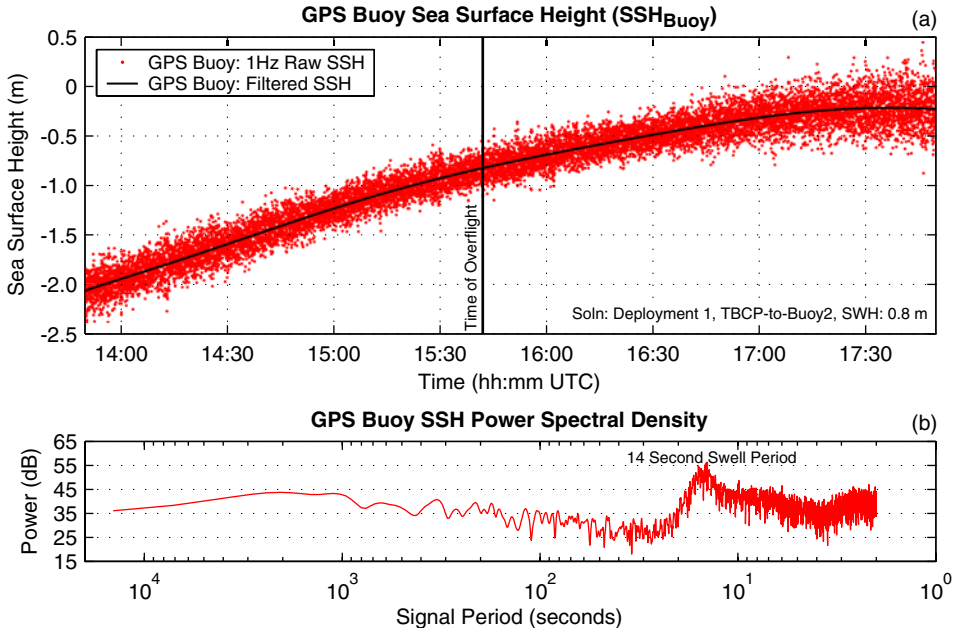

Figure 4-6 An example taken from the kinematic analysis of Buoy2 from the TBCP reference station. (a) 1 Hz SSH time series over the ~4 hour deployment. Note the filtered time series and time of overflight. (b) Power spectrum density of the SSH time series. Note the power within the signal at a frequency corresponding to the prevailing swell.

4.4.2.3 Mooring SSH Datum Solution and Error Analysis

The mooring datum solution (Eqn 4-4) was undertaken using the filtered 1 Hz SSH_{Buoy} data. When computing the mooring datum (i.e., the height of the mooring pressure-gauge zero on a conventional tide free datum, relative to the ellipsoid) the mean SSH_{Buoy} time series for each deployment was utilised (i.e., mean of TBCP-Buoy1, TBCP-Buoy2, RKCP-Buoy1 and RKCP-Buoy2). Five 'deployment mean' SSH_{Buoy} time series (Table 4-1) were then combined to compute the 'campaign mean' ($SSH_{Buoy} - d_{Mooring}$) used to define the mooring datum (Figure 4-7).

The difference between the SSH_{Buoy} and $d_{Mooring}$ time series (Figure 4-7) yields valuable information on the quality of both the SSH_{Buoy} and $d_{Mooring}$ time series. As the two sets of instruments were located in approximately the same location, the comparison is purely geometric, and no significant differential oceanographic signal is to be expected.

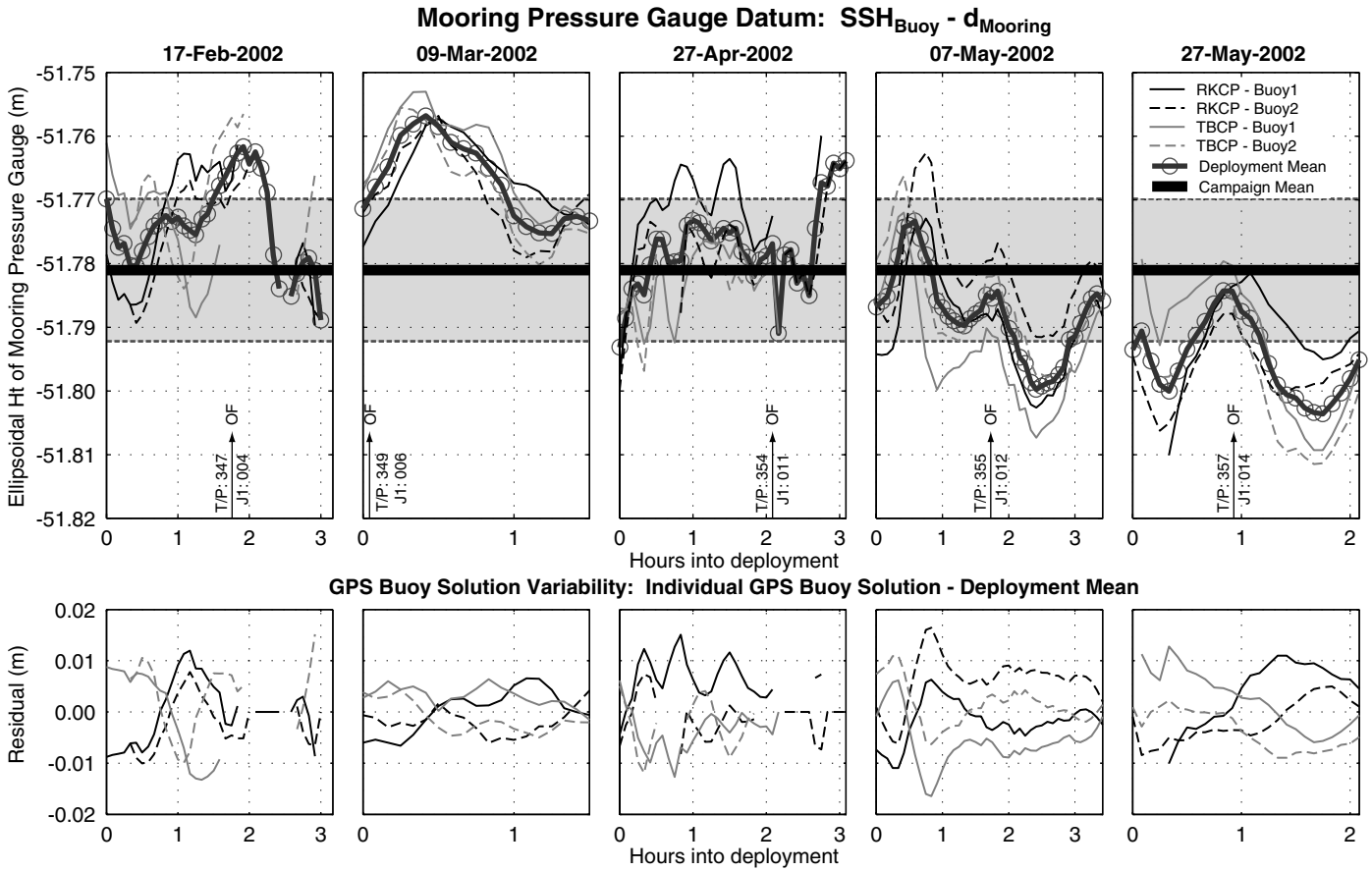

Figure 4-7 Mooring datum determination. The upper panel shows the difference between the GPS Buoy solution and the 'water depth' determined from the mooring data for the five available buoy deployments. The thick horizontal bar indicates the mooring datum estimated from the times series. The lower panels show the SSH_{Buoy} departure from the mean SSH_{Buoy} for each deployment. The observed variability of the final mooring datum estimate (± 1 standard deviation of SSH_{Buoy} - $d_{Mooring}$) is indicated by the shaded region in the upper panels. The arrows marked with 'OF' indicate the time of satellite overflight with the T/P and J-1 cycle number labelled on either side of the arrow.

It is anticipated the high frequency signal in the upper panels of Figure 4-7 largely reflects site specific and satellite constellation effects within the kinematic GPS solution. A much smaller contribution to this signal may also be related to the temporal smoothing (and hence inability to resolve high frequency events) on the mooring time series. Note solutions compared between buoys (Buoy1 and Buoy2 from the same reference station) show improved internal agreement when compared to individual buoy solutions computed from both reference stations (Buoy1 from TBCP and RKCP for example). This systematic pattern (Figure 4-7, lower panels) underscores the influence of local site-specific effects at each reference site (different sky obstructions, different multipath environment and different atmosphere).

When assessing the error budget for the mooring datum solution, it is important to consider the a posteriori variance-covariance (VCV) information from the TRACK analysis. The scale of the TRACK VCV matrix is dependent on the a priori estimates of code and carrier phase measurement precision. Using standard measurement precisions of 1 m for C1 and P2 code observations and 10 mm for L1 and L2 phase observations, formal one standard deviation error estimates for each 1 Hz sea level measurement are typically in the range of 60-100 mm. The assessment of the final error estimate of the filtered sea surface heights is complicated by the temporal correlation of the error sources in the kinematic solution. For example, residual tropospheric delay (Dodson et al., 2001) and multipath (Park et al., 2004) will both be serially correlated and hence lead to an underestimation of the final uncertainty. To gain a better understanding of the final error estimate, variability of buoy solutions (from different reference stations to both buoys, as per the lower panel in Figure 4-7), in addition to the time series of RKCP processed as a kinematic site (using TBCP as the reference station) was investigated. The RKCP-TBCP baseline length is comparable to the buoy baseline processing and hence serves as a useful guide to assessing the lower limit of processing variability. A final uncertainty of 15 mm (1σ) was adopted for each estimate forming the 'deployment mean' SSH_{Buoy} time series. In the final error budget, each of these estimates are considered independent every 30 minutes (see §4.5)

The longer term signal apparent over the five deployments shown in the upper panel of Figure 4-7 is also of interest. Given the uncertainty of both the $d_{Mooring}$ and SSH_{Buoy} time series, the signal is not considered significant. The presence of a seasonal signal in the ($SSH_{Buoy} - d_{Mooring}$) series is unlikely as both instruments were

collocated. Settlement of the mooring array is considered possible and is further investigated in §4.4.3.

The final campaign mean (i.e., *mean*($SSH_{Buoy} - d_{Mooring}$)) is used to define the mooring datum, and is applied to the mooring time series to derive $SSH_{Mooring}$. The absolute datum of the mooring time series is therefore completely dependent on the value of *mean*($SSH_{Buoy} - d_{Mooring}$). Now that an absolute datum for the $d_{Mooring}$ time series is defined, the resultant $SSH_{Mooring}$ time series is directly comparable to the two altimeters over the duration of its deployment.

4.4.3 Tide Gauge Data Processing

The tide gauge data are utilised to extend cycle-by-cycle comparisons with both the T/P and Jason-1 altimeters. As mentioned previously, to extrapolate (or transform) the tide gauge time series (r_{TG}), out to the comparison point (SSH_{TG}), corrections are required taking into account tidal differences (both in amplitude and phase), geophysical differences (tidal and non-tidal loading) and geometric differences (geoid slope and datum differences). Most studies (such as Woodworth et al., 2004 for example), rely largely on model data to achieve this transformation. The technique adopted in this Thesis takes advantage of the $SSH_{Mooring}$ time series to derive precise tidal and geometrical corrections for the tide gauge time series.

A difference time series (SSH_{Diff}) was computed using concurrent or overlapping data from the tide gauge and mooring array (Eqn 4-6), where:

$$SSH_{Diff} = SSH_{Mooring} - r_{TG} \qquad \text{Eqn 4-6}$$

The SSH_{Diff} time series has a standard deviation of 0.069 m, with the time series dominated by tidal frequencies in the diurnal band and higher. A small component of these harmonics will be differential tidal loading (predominantly differential ocean loading). A standard harmonic tidal analysis (Cartwright, 1999) was undertaken on the SSH_{Diff} time series using the "TDA" tidal analysis software (Hunter, 2002). The analysis was undertaken solving for tidal frequencies of diurnal frequency and higher. The time series is dominated by a ~4 degree phase lag in the M2 constituent, which has an amplitude of 0.089 m. Amplitude and phase data for all significant constituents (amplitude > 2 mm) are shown in Table 4-2.

Table 4-2 *Tidal amplitudes and phase lags (mooring – tide gauge) for significant constituents in the SSH_{Diff} tidal analysis.*

Constituent	Amp (m)	Phase Lag (°)	Constituent	Amp (m)	Phase Lag (°)
O1	0.004	-0.1	L2	0.005	3.7
K1	0.007	-0.4	S2	0.004	-0.9
2N2	0.004	3.4	MN4	0.004	16.5
MU2	0.005	3.6	M4	0.010	13.5
N2	0.021	3.8	2MN6	0.004	22.1
NU2	0.003	3.3	M6	0.008	22.9
M2	0.089	3.9	2MS6	0.003	22.6

Using the results from the tidal analysis, both hindcast and forecast predictions enable the generation of a predicted difference ($SSH_{PredictedDiff}$) in sea-surface height between the Burnie tide gauge and the comparison point. A typical observation sample taken over a 3 day period in March, 2002 is shown in Figure 4-8.

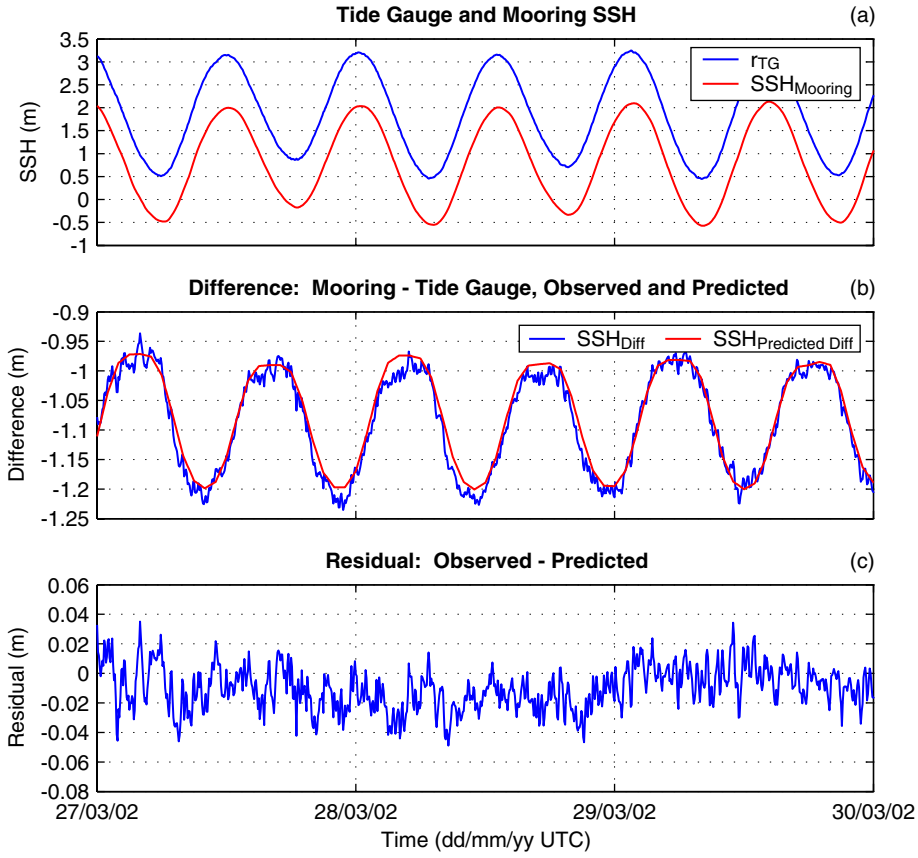

Figure 4-8 *Example r_{TG}, $SSH_{Mooring}$, SSH_{Diff} and $SSH_{Predicted\ Diff}$ data taken over three typical days in March 2002. (a) r_{TG} and $SSH_{Mooring}$, (b) SSH_{Diff} and $SSH_{Predicted\ Diff}$ and (c) residual difference SSH_{Diff} - $SSH_{Predicted\ Diff}$.*

These data are used to compute a corrected tide gauge SSH time series (Eqn 4-7) which is valid at the comparison point, where:

$$SSH_{TG} = r_{TG} + SSH_{Predicted\ Diff} \quad \text{Eqn 4-7}$$

Note that the datum for SSH_{TG} is actually defined by the mooring time series (as a result of Eqn 4-6) which is in turn defined by the SSH_{Buoy} time series (Eqn 4-4). This methodology therefore precludes the necessity to estimate a marine geoid and reduces the solution to a geometrical framework, defined by the GPS buoys.

To estimate the non-tidal contribution to the differences observed between the comparison point and Burnie tide gauge locations, along-shore, low-frequency currents and cross-shore winds were investigated. To first order, the along shore current will be balanced by an on/offshore geostrophic pressure gradient (Eqn 4-8), given by Pond and Pickard (1983) as:

$$fu = -g\frac{\delta h}{\delta y} \quad \text{Eqn 4-8}$$

where f is the coriolis parameter, u is the along-shore current (low passed), g is the acceleration due to gravity, δh is the change in SSH and δy is the offshore distance (~18 km). The low-passed currents (using a cut-off period of 2 days) from the shallow current meters from the inshore and offshore moorings were combined to derive a mean current time series. The time series of currents from the centre mooring (the ADCP) had a number of gaps and also finished earlier than the data from the other moorings, so was not used. A time series of the sea-surface setup was computed using the mean-current data and the relation provided in Eqn 4-8. Over the duration of the deployment, this correction had a magnitude of a few centimetres (standard deviation 8 mm), with a small annual signal.

An additional non-tidal difference investigated between the two locations is wind-induced sea-surface setup. An on/offshore wind stress could be balanced by an on/offshore pressure gradient as indicated in Eqn 4-9 (Pond and Pickard, 1983), as:

$$\frac{\tau_y^W}{\rho h} = g\frac{\delta h}{\delta y} \quad \text{Eqn 4-9}$$

where τ_y^W is the on-shore wind stress, ρ is the water density, h is the water depth, δh is the change in SSH and δy is the offshore distance (~18 km). Wind data from the meteorological instruments associated with the Burnie tide gauge were used for

this analysis. The effect is an order of magnitude smaller than the setup from the alongshore current, but has been included in the final setup time series (Eqn 4-10):

$$SSH_{Setup} = \delta h_{Along-shore} + \delta h_{Wind-induced} \qquad \text{Eqn 4-10}$$

For the period of current meter deployment, the corrected tide gauge SSH time series was then defined as (Eqn 4-11)

$$SSH_{TG} = r_{TG} + SSH_{PredictedDiff} + SSH_{Setup} \qquad \text{Eqn 4-11}$$

Analysis of the difference between the low passed SSH_{TG} and $SSH_{Mooring}$ time series shows the precision obtainable using this methodology (Figure 4-9).

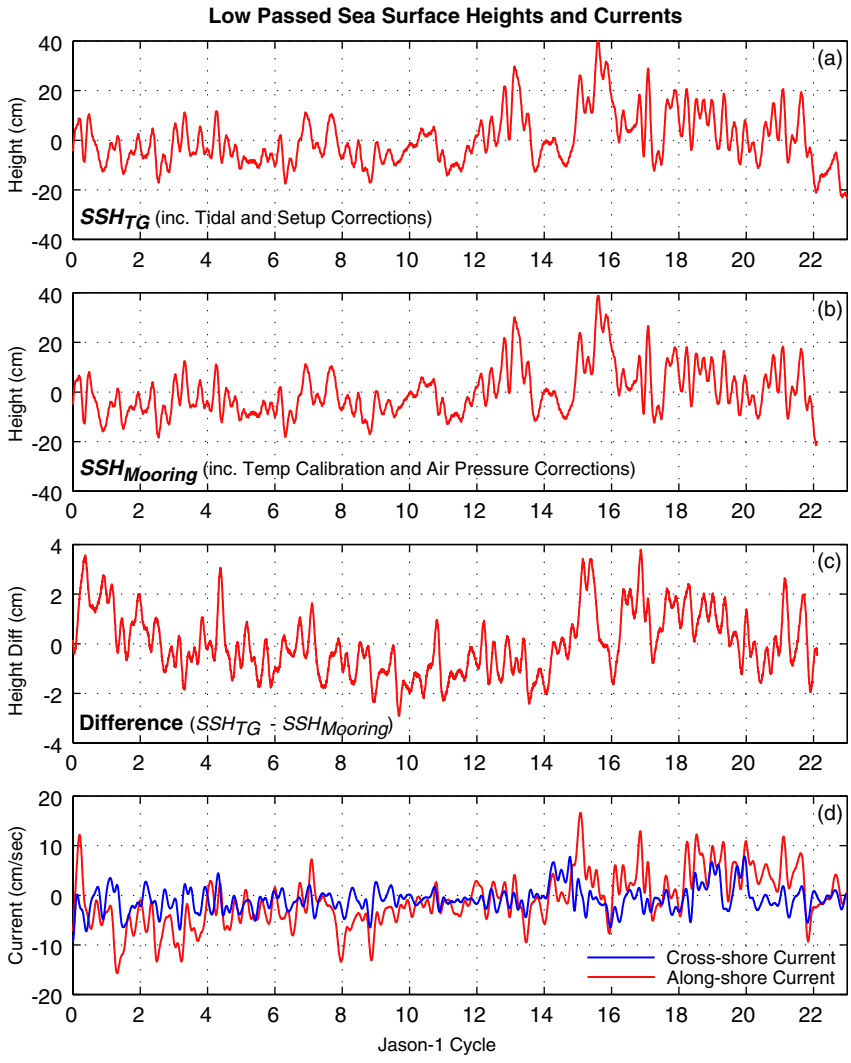

Figure 4-9 Low passed sea surface heights and currents at the Burnie and offshore comparison point locations. (a) Burnie tide gauge series with tidal and set-up corrections applied, (b) offshore mooring series, (c) difference (tide gauge – mooring) – note the different scale and (d) along- and cross-shore currents.

The difference time series (Figure 4-9c) has a range of 6.7 cm, and standard deviation of 1.3 cm. A range of signals with various frequencies and magnitudes at the 1-2 cm level are apparent in the difference time series shown in Figure 4-9(c). Contributions to these signals could include a range of error sources both at the tide gauge and mooring sites. Components are likely to include errors in the atmospheric pressure time series (at both locations), insufficient modelling of sea surface set-up induced by both wind and current variability, residual differential tidal and non-tidal deformation of the crust, errors in the computation of the dynamic height at the mooring location, consolidation of the mooring anchor into the sediment, and errors in the temperature calibration of the tide gauge.

Settlement of the mooring anchor (~700 kg) was given further consideration following the apparent linear trend observed between cycles 0-12 in Figure 4-9c. The trend, however, clearly reverses during the remaining cycles. While still considered a possible contributing factor, there is insufficient evidence to imply the mooring anchor has subsided over the deployment duration.

The influence of the current induced sea-surface setup (Eqn 4-8) on this difference time series (Figure 4-9c) is only marginal. If the setup term is not considered, the difference time series shows slightly greater low frequency variability, with limited change to the high frequency components. The effect of not being able to model the sea-surface setup outside of the mooring deployment period is considered in the formulation of the error budget (§4.5).

4.4.4 Altimeter Data Processing

4.4.4.1 TOPEX/Poseidon

The T/P analysis is based on the 1 Hz TOPEX data from the most recent MGDR-B data files (see Benada, 1997). The NASA POE orbits on the MGDR-Bs were used, and the following corrections from the MGDR-B were applied to generate the primary analysis data set:

- centre-of-gravity
- dry troposphere
- TMR wet troposphere correction (see notes below)
- sea-state bias (Gaspar 4 parameter)
- ionosphere (mean of all reasonable values between 39° 48' S and 40° 48' S. Using other smoothing strategies, such as those recommended in the GDR manuals, makes negligible difference to the final corrected SSHs).

For comparative purposes, a second T/P data set was computed using the sea-state bias (SSB) model described in Chambers et al. (2003). The Chambers et al. SSB model takes into consideration differences observed between the two onboard electronic systems used over the T/P mission ('Side A': cycles 001-235 and 'Side B': cycles 236 onwards).

Two problems with data from the TOPEX Microwave Radiometer (TMR) are well documented in the literature. The first of these is a drift in the 18 GHz brightness temperature channel (Keihm et al., 2000), which translates into a drift in the measured atmospheric water vapour and hence leads to an error in the wet troposphere correction to the altimeter range. A correction for this effect is available in the 'GCP' product provided by JPL PO.DAAC (http://podaac.jpl.nasa.gov/products/product170.html). For reasons of computational efficiency, instead of using the GCP correction, the methodology adopted in this Thesis has been to recalculate the 18 GHz brightness temperatures, (as per Ruf, 2000 and Ruf, 2002) and then compute the wet troposphere correction from the updated brightness temperatures (Keihm et al., 1995). These two methodologies are equivalent, however, the methodology presented simplifies the computational process for the T/P dataset required for this study. The final correction increases the magnitude of the MGDR-B wet troposphere correction by approximately 6-7 mm for the formation flight period (equivalent to raising the measured altimeter

SSH by approximately 6-7 mm). This is clearly essential for absolute calibration and validation activities.

The second correction required for the TMR data is the effect of the satellite yaw-steering mode, which is related to component heating (Brown et al., 2002), amounting to 2.4 mm in sinusoidal yaw and -1.4 mm for fixed yaw. The 15 hour thermal settling time has not been taken into consideration as it does not affect pass 088 for the cycles used in this study (all yaw state transitions are more than 15 hours away).

A final issue relating to the TMR data is the observed land contamination when the nadir point is ~40 km from the nearest land (Stanley and Rocky Cape, Figure 4-2). As this issue affects both T/P and Jason-1 altimeters, the methodology developed to correct for the contamination is presented in §4.4.4.3.

Adopting the extrapolated value of the corrected TMR data (§4.4.4.3), SSH_{Alt} data are computed at GDR locations either side of the comparison point. Interpolation, the tidal/loading corrections (TL_{Corr} in Eqn 4-2) and the cross-track geoid gradient correction ($ATGG_{Corr}$ in Eqn 4-2) are discussed in §4.4.4.4 and §4.4.4.5 respectively.

4.4.4.2 Jason-1

The Jason-1 processing is based on the 1 Hz data from the GDR data files (see Picot et al., 2001). The POE orbits on the GDRs were used for the primary analysis, and the following corrections from the GDR were applied:

- dry troposphere
- JMR wet troposphere correction (see notes below)
- sea-state bias
- ionosphere (using the same smoothing process as applied for T/P).

To investigate possible geographically correlated differences in orbit solutions, a secondary Jason-1 data set was generated, utilising the JPL reduced dynamic GPS orbits (as per Haines et al., 2004a). Data were supplied courtesy of Dr Bruce Haines of the Jet Propulsion Laboratory (JPL).

As expected, the Jason-1 Microwave Radiometer (JMR) wet troposphere correction showed similar land contamination effects when compared to the TMR correction

(see §4.4.4.3). Once again, a linear extrapolation of the JMR data was adopted, and applied to compute 1 Hz SSH data either side of the comparison point (SSH_{Alt}). The JMR instrument is further discussed in Brown et al. (2004b).

Final corrections, including interpolation, tidal/loading corrections and the cross-track geoid gradient correction, are discussed in §4.4.4.4 and §4.4.4.5 respectively.

4.4.4.3 TMR and JMR Land Contamination

Both TMR and JMR data showed clear signs of land contamination when the time series of brightness temperatures (and hence wet troposphere corrections) were inspected as the satellite travels on its descending pass over Bass Strait (and indeed when inspecting any transition from ocean to land). Land contamination becomes evident when the nadir point is ~40 km from the nearest land, corresponding to the approximate size of the footprint of the 18.7 GHz JMR brightness temperature channel (Brown et al., 2004a). The footprint is only marginally different for the 18.0 GHz channel used for the TMR. The exact latitude which defines the last uncontaminated estimate of troposphere wet delay is difficult to determine. This is partly due to the protrusion of the peninsula at Stanley, in addition to the shallow angle of approach of pass 088 with respect to the coastline (Figure 4-10).

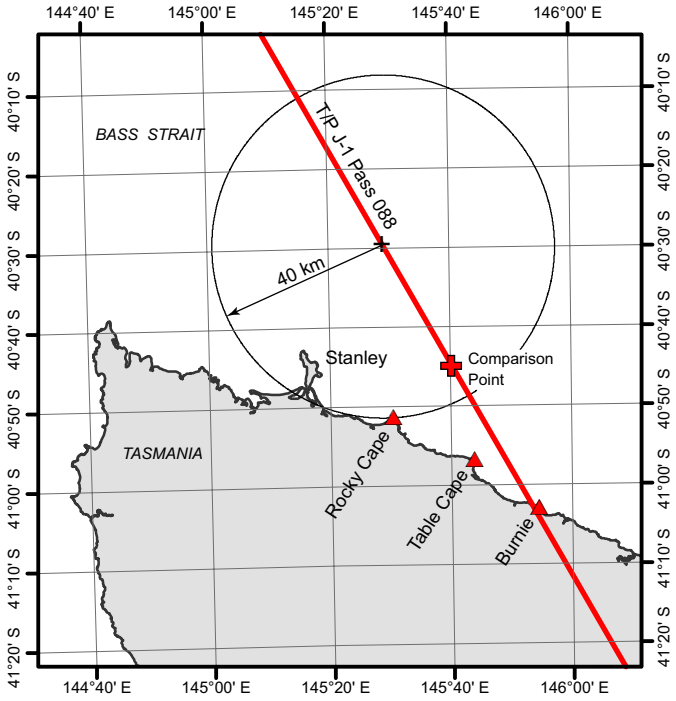

Figure 4-10 18.0 GHz TMR and 18.7 GHz JMR footprint (~40 km) at the Bass Strait Calibration site. Note the protrusion of the peninsula at Stanley and the relatively shallow angle of approach of pass 088.

Three typical examples from T/P (Figure 4-11) show the contamination as the satellite reaches a latitude of approximately 40.45° S (40° 27' S), approximately 40 km from land (Figure 4-10).

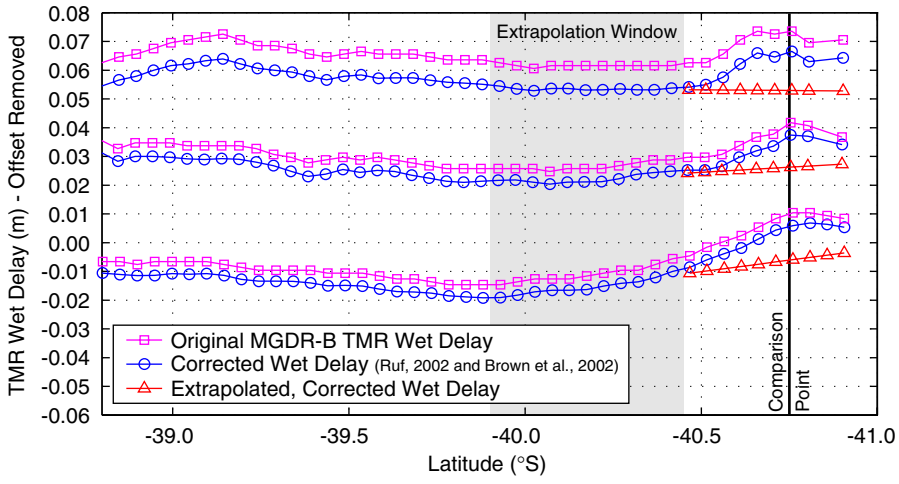

Figure 4-11 Typical TMR wet delay profiles across Bass Strait (north to south from left to right) showing the original MGDR-B TMR wet delay correction, the Ruf (2002) and Brown et al. (2002) corrected TMR correction (§4.4.4.1), and the extrapolated TMR correction. Note the extrapolation window used.

As indicated in Figure 4-11, the comparison point for this study is clearly inshore from where land contamination becomes evident. To overcome the land contamination, an extrapolation of the TMR and JMR data was required. Given the subtle yet systematic trend in the wet troposphere correction for most passes across Bass Strait, a linear extrapolation methodology appeared most appropriate. Other studies, such as Desai and Haines (2004), independently derived similar correction methodologies. Given the high spatial correlation evident in the TMR and JMR profiles, the linear extrapolation methodology utilised a latitude band between 39.9° S and 40.45° S to compute the regression coefficients. The selection of 40.45° S as the southern cut off for the extrapolation interval is considered conservative due to the unknown effect of the small peninsula extending into the radiometer footprint (Figure 4-10). TMR, JMR and the extrapolated corrections for all overflights studied at the Bass Strait site are provided in Appendix C.

Final corrected estimates, using the extrapolated methodology for the altimeter derived tropospheric wet delay (i.e., the absolute value of the adjusted GDR correction), have been compared against the wet troposphere time series computed at the Burnie GPS station. The wet troposphere delay at the Burnie GPS was computed using the GPS total zenith delays from the GAMIT analysis (see Chapter 3) and local temperature and atmospheric pressure observations taken from the Burnie site, using the methodology presented in Bevis et al. (1992). GPS data were available for comparison against 81 cycles of TMR data (between T/P cycles 232 and 365 (04/01/1999 and 14/08/2002)) and 74 cycles of JMR data (between Jason-1 cycles 001 and 101 (18/01/2002 and 06/10/2004). Results for both analyses are presented in §4.6.2.

4.4.4.4 Comparison Point Geometry and Interpolation

Following the T/P and Jason-1 GDR data processing, it is necessary to interpolate and apply final geometric corrections to derive an estimate of SSH_{Alt} at the comparison point (CP). The geometry and terminology adopted in this stage of processing is shown in Figure 4-12.

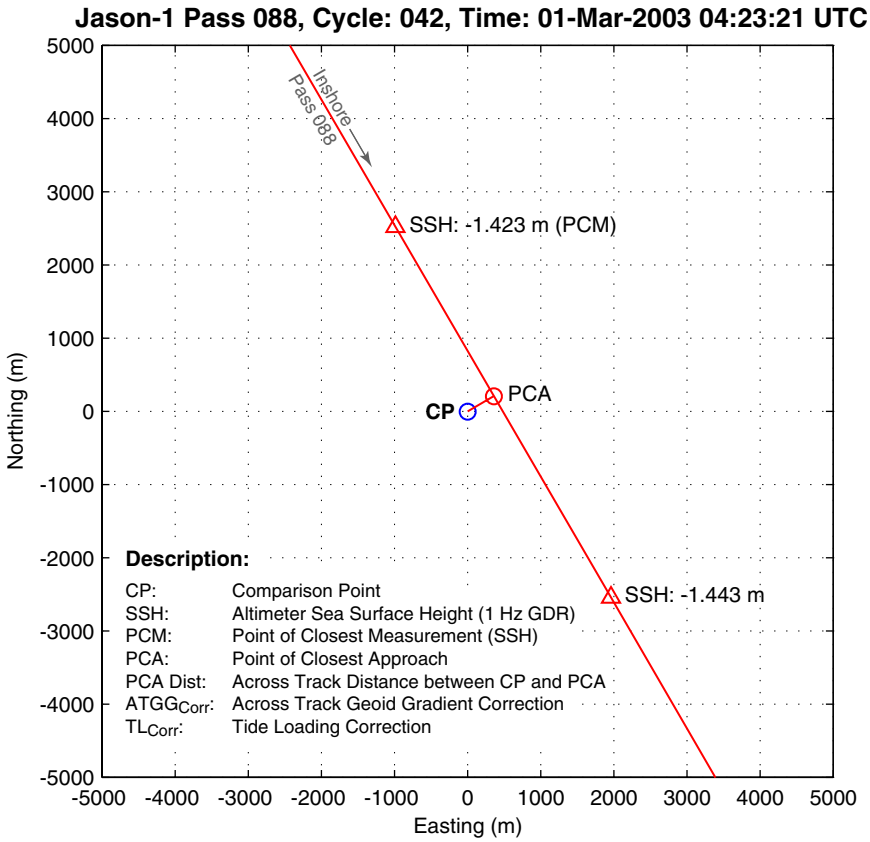

Figure 4-12 Example geometry at the comparison point (CP) taken from Jason-1 cycle 042 on the 01/03/2003. The scale represents a UTM projection centred on the comparison point.

As shown in Figure 4-12, individual 1 Hz SSH measurements from the altimeter are separated by approximately 6 km. The point of closest measurement (PCM) will vary for each overflight. Corrections for the solid earth tide, pole tide and ocean loading from the respective GDR data files (TL_{Corr}) are applied to the 1 Hz SSH measurements. The corrected SSH measurements were then linearly interpolated to the point of closest approach (PCA) to the comparison point (Figure 4-12). Negligible difference was found between using linear and cubic spline interpolation strategies. Once the location of the altimeter PCA had been determined, the cross-track separation between the PCA and the CP could be calculated (typically within $\pm$ 500 m), and utilised in the application of an cross-track geoid gradient correction ($ATGG_{Corr}$). Plots similar to Figure 4-12 for every overflight have been included in Appendix C.

4.4.4.5 Cross-track Geoid Gradient

The comparison point at the Bass Strait calibration site is situated on the nominal position of the pass 088 altimeter ground track. As the actual ground track for each altimeter repeats to within ± 500 m of this nominal position, a correction for the cross-track geoid gradient ($ATGG_{Corr}$) is required for each overflight. This correction effectively transforms the linearly interpolated SSH at the PCA to the comparison point. A range of mean sea surface (MSS) models and the Australian geoid model have been used to estimate the sea surface gradient at the comparison point. These models include GSFC00.1 (Wang, 2001), KMS01 (O. Anderson, personal communication, 2003), CLS01 (Rio and Hernandez, 2004), and AUSGeoid98 (Featherstone et al., 2001). The AUSgeoid98 model was incorporated for comparative purposes, despite not including the mean dynamic topography of the sea surface. The four models are shown in Figure 4-13 and Figure 4-14 respectively. The models show quite different features which are difficult to explain. However, in this study we are only interested in gradients, hence we may neglect absolute differences between the models. The direction and magnitude of the gradient computed at the comparison point shows a high level of agreement between models. The cross-track gradient (orthogonal to the ground track, as indicated on Figure 4-13 and Figure 4-14) adopted from the mean of all models is 10 ± 3 mm/km. This is the final correction applied to the interpolated altimeter SSH (Eqn 4-2). A conservative error value of 3 mm per overflight is adopted for this correction.

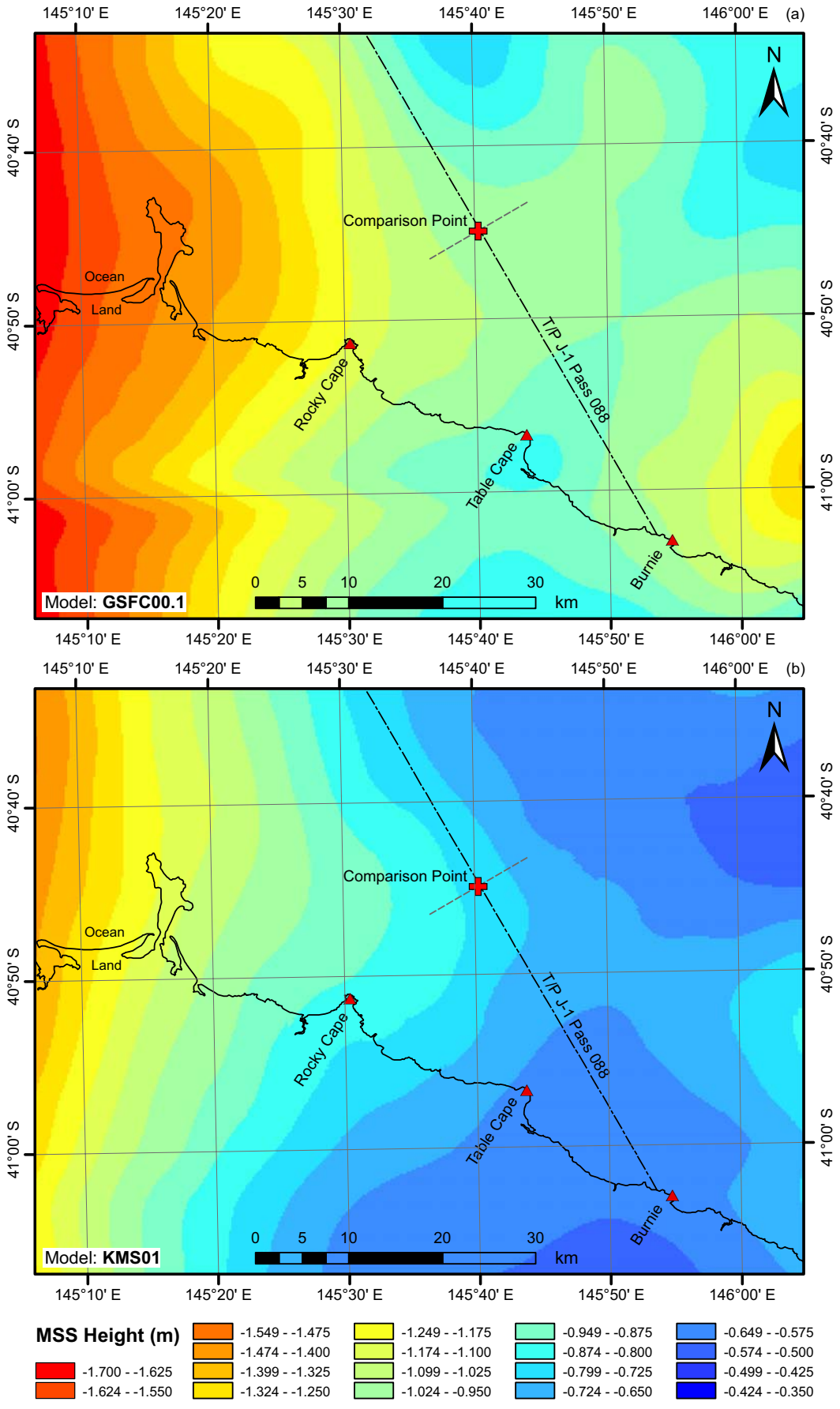

Figure 4-13 GSFC00.1 and KMS01 MSS models at the Bass Strait Site.

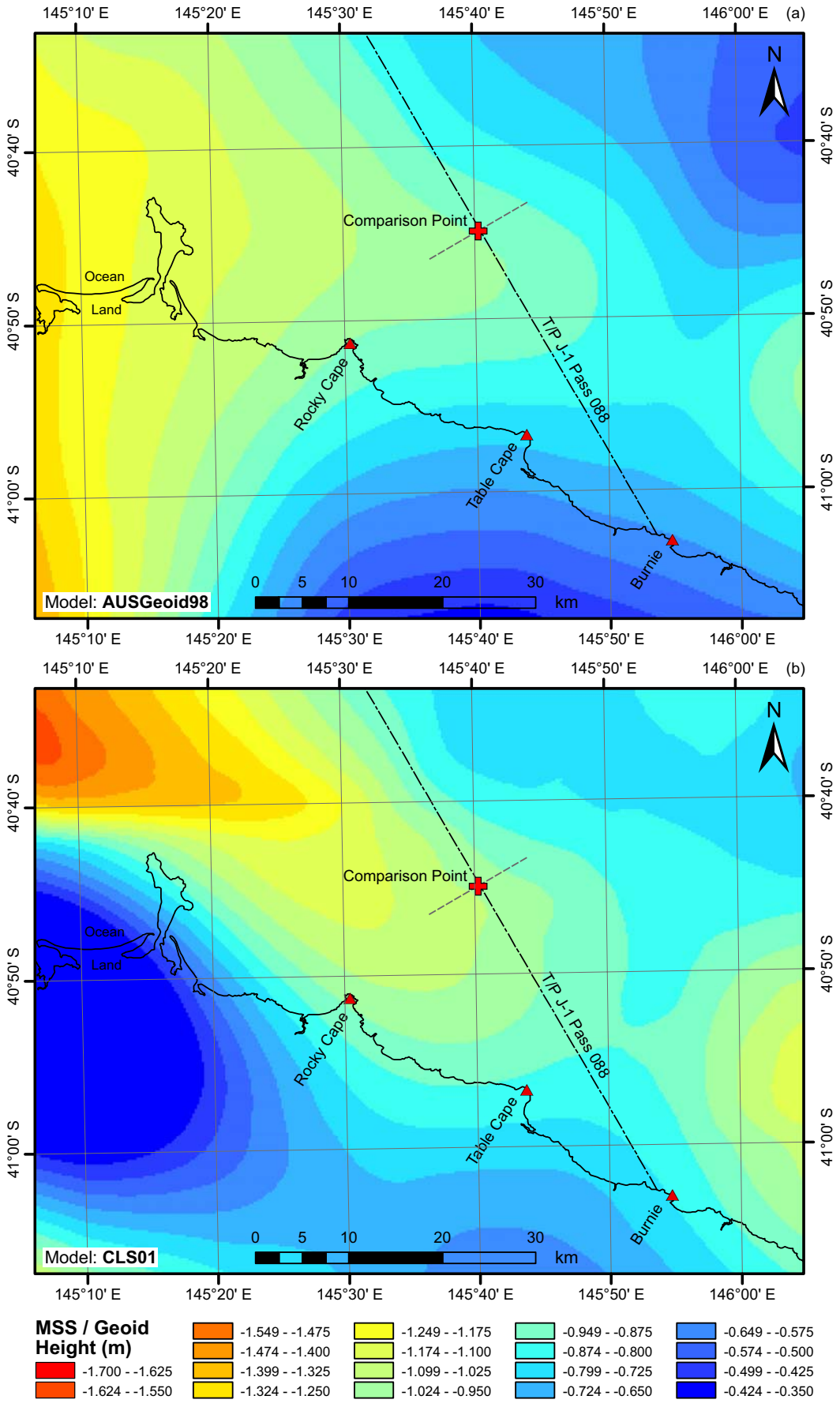

Figure 4-14 AUSGeoid98 and CLS01 models at the Bass Strait Site.

4.5 Error Budget

An error budget has been compiled for the Bass Strait calibration site in order to assess the formal uncertainty of the final absolute bias estimates for T/P and Jason-1. The error estimates have been divided into fixed (systematic) and variable (quasi-random) terms (Table 4-3). Estimates for the GPS reference station analysis, GPS kinematic analysis, and the cross-track geoid gradient have already been discussed. The error budget is complicated by the addition of the systematic terms, especially in relation to the GPS analysis (as discussed throughout Chapter 3).

Table 4-3 *Error budget for the Bass Strait calibration site during the formation flight period of the mission.*

Error Budget: Formation Flight Period		**Fixed**	**Variable**
GPS Buoy SSH (SSH_{Buoy})	- Reference station solutions	10	10
	- Kinematic solution	-	15
	- Antenna height and PCV	3	-
	- Cross-track geoid gradient	-	3
	(a) SSH_{Buoy} Total:	***10 mm***	***18 mm***
Mooring Depth ($d_{Mooring}$)	- Pressure Gauge	-	4
	- Dynamic Height	-	5
	- Atmospheric Pressure	-	10
	(b) $d_{Mooring}$ Total:	***0 mm***	***12 mm***
Mooring Datum ($SSH_{Mooring}$)	- SSH_{Buoy} [from (a) above]	10	18
	- $d_{Mooring}$ [from (b) above]	-	12
	Datum $SSH_{Mooring}$ Total: (*)	***10 mm***	***4 mm***
Altimeter SSH (SSH_{Alt})	- ***J-1 SSH_{Alt} Total:*** (**)	-	***30 mm***
	- ***T/P SSH_{Alt} Total:*** (**)	-	***35 mm***
GRAND TOTALS (Absolute Bias Uncertainty) = sqrt(Datum $SSH_{Mooring}^2$ (fixed) + Datum $SSH_{Mooring}^2$ (variable) + (sqrt(SSH_{Alt}^2 + $d_{Mooring}^2$) / sqrt (n))^2)	***J-1 Bias:*** (***)		***13 mm***
	T/P Bias: (***)		***14 mm***
e.g. J-1 = sqrt(10^2 + 4^2 + (sqrt(30^2 + 12^2) / sqrt (18))^2)			

Footnotes:

* The $SSH_{Mooring}$ error estimate assumes independent GPS buoy comparisons on a half hourly basis, therefore n = 26 over 5 buoy deployments.

** Uncertainties are per overflight, based on SWH < 1.5 m.

*** n = 18 over the formation flight period

In computing the error terms for the mooring datum solution, we assume the GPS buoy measurements can be considered independent every 30 minutes. The sample size used in deriving the variable error component is therefore 26. Estimates for the uncertainty associated with the mooring SSH have been derived from manufacturer's specifications (as discussed in §4.4.1). Estimates for the T/P SSH precision (35 mm) have been adopted from Chelton et al. (2001). For the Jason-1 SSH, 30 mm is adopted based on corrected 1 Hz GDR SSH with SWH less than 1.5 m (Menard et al., 2003).

Final uncertainties for absolute bias have been computed for the formation flight period where 18 overflights were used to compute bias estimates. The systematic terms have been summed in quadrature with the quasi-random terms (making the assumption of independent estimates). The minimum uncertainty obtainable using this technique (with unlimited overflights) is therefore at the 10 mm level. The final uncertainty for the absolute bias calculation computed over the formation flight period is 14 mm for T/P and 13 mm for Jason-1.

Outside the formation flight period, the error budget must consider the increased error associated with the corrected tide gauge sea surface heights (not indicated in Table 4-3). Analysis of atmospheric pressure differences and computed sea-surface setup (§4.4.3), over the formation flight period, indicate an additional 10 to 15 mm of variable error per overflight comparison. This additional error term is minimised by the significant increase in overflight comparisons possible using the longer tide-gauge time series, leading to an uncertainty at the 11 to 12 mm level for 100 cycles of data. We therefore have a methodology capable of delivering absolute bias estimates at the 10-15 mm uncertainty level, i.e., virtually the 1 cm goal.

4.6 Results

4.6.1 Absolute Bias Results

The principal absolute bias results are centred on the calibration phase or formation flight period of the T/P and Jason-1 mission, using the $SSH_{Mooring}$ time series as the in situ reference. Additional results are included for Jason-1 (cycles 1-101), T/P side 'A' (cycles 1-235) and T/P side 'B' (cycles 236-365). Comparison over these extended periods has been achieved using the SSH_{TG} time series as the in situ reference (Eqn 4-5). When discussing the variability of a specific absolute bias time series, the standard error about the sample mean is presented. The standard deviation of the sample is also shown in each relevant figure. Throughout the presentation of the results, absolute bias estimates from the Bass Strait site are compared with estimates from both Harvest and Corsica. Results from other studies are discussed in §4.6.1.4.

4.6.1.1 TOPEX/Poseidon and Jason-1: Calibration Phase

Results for the formation flight period (Figure 4-15a,b), computed using Eqn 4-1 and Eqn 4-4 respectively, show a mean T/P bias of -0.5 mm with a standard error about the sample mean of 3.5 mm. Results from Jason-1 using the POE orbit appear more variable, with a significant mean bias of +152.3 mm (standard error 7.7 mm). This bias is indicative of SSH_{Alt} being too high, i.e., the altimeter range is too short, or the orbit too high. The high variability and small number of overflights over this period precludes any analysis of altimeter drift at this stage of the analysis. Computing a relative bias between Jason-1 and T/P using only common cycles (Figure 4-15c), reveals a relative bias at Bass Strait of +150 mm (standard error 6.3 mm). This value is in close agreement with global estimates (for example, +154 mm adopted by Leuliette et al., 2004). The absolute bias variable error as computed in the error budget (8 mm for T/P and 9 mm for Jason-1) is in accordance with, although slightly larger than, the observed standard error about the mean bias estimates (3.5 mm for T/P and 7.7 mm for Jason-1).

To highlight the strength of the methodology presented in this Thesis, bias estimates have been computed over the same period utilising the secondary in situ reference time series, SSH_{TG} (i.e., Eqn 4-1 and Eqn 4-5). These estimates are +4.1 mm (standard error 4.7 mm) for T/P and +159.9 mm (standard error 7.6 mm) for

Jason-1. Given the significantly higher error estimates for the SSH_{TG} time series and the small number of comparisons over the formation flight period (n = 18), these estimates must be considered equivalent (c.f. -0.5 mm and +152.3 mm respectively). The strength of the technique is highlighted with only a marginal increase in variability when using the SSH_{TG} as the in situ reference time series.

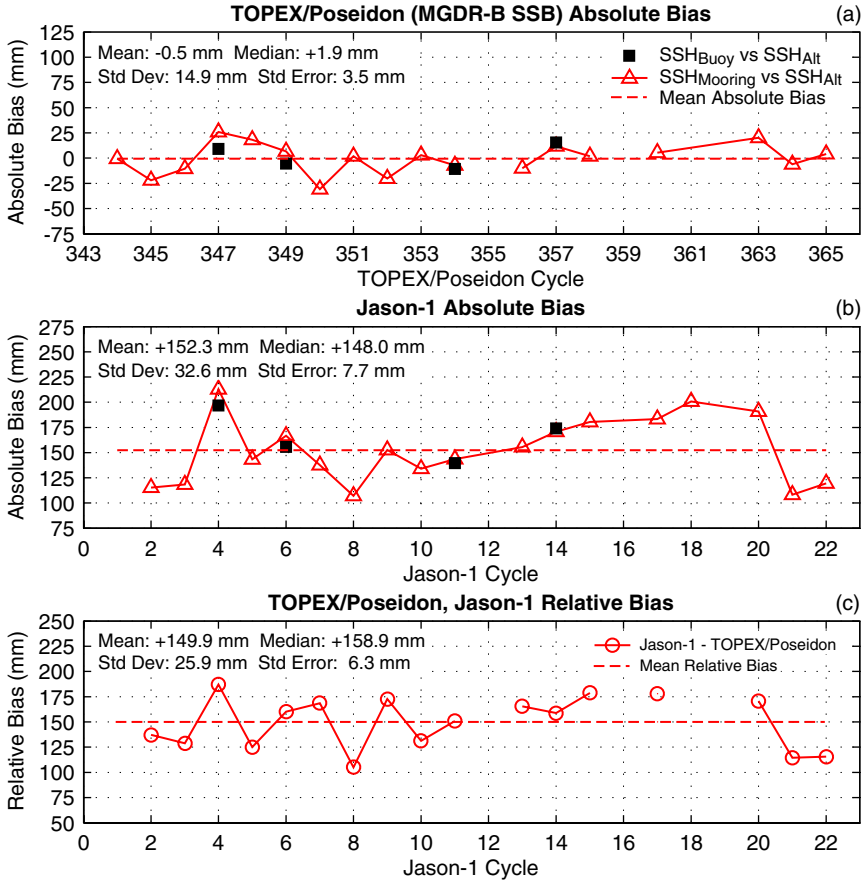

Figure 4-15 Absolute bias results for the formation flight period of the T/P and Jason-1 missions, computed against the $SSH_{Mooring}$ series. (a) T/P absolute bias (primary analysis altimeter dataset). (b) Jason-1 absolute bias (primary analysis altimeter dataset). (c) Relative bias, Jason-1 – T/P.

Over a similar period, the absolute bias at the NASA Harvest site for Jason-1 (GDR POE Orbit) was +138 ± 17 mm (Haines et al., 2003). The bias from the Corsica site is slightly lower at +120 ± 7 mm (Bonnefond et al., 2003a). Note the uncertainties placed on the Harvest bias estimate have been computed from a rigorous error budget (similar to that used here, incorporating both systematic and variable terms). The uncertainties placed on the Corsica estimate are however a measure of variability and reflect the standard error about the sample mean. The true "absolute" uncertainty of the Corsica estimate is therefore expected to be significantly larger.

Geographically correlated errors (specifically related to the orbit computation) are expected to contribute to differences between the three absolute estimates. For comparison, the altimeter processing strategy was altered to utilise the JPL GPS reduced dynamic orbit, integrated with the GRACE GGM01S gravity model (Haines et al., 2004a). In comparison, the GDR POE orbit is based on SLR and DORIS data and utilises the JMR-3 gravity model (Tapley et al., 1996). Utilising the GPS orbit at the Bass Strait site, the Jason-1 mean absolute bias reduces significantly by ~24 mm to +127.9 mm (standard error 7.1 mm), over the calibration period.

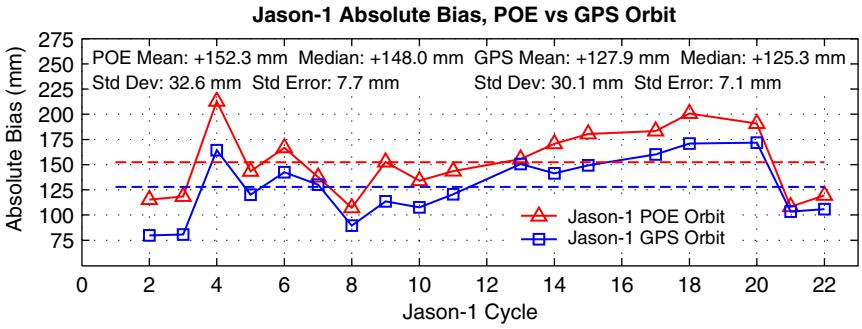

Figure 4-16 Jason-1 absolute bias over the formation flight period computed using a) POE orbits, and b) JPL GPS orbits. (Bias computed against the $SSH_{Mooring}$ time series).

The same strategy at the Harvest site results in a less significant reduction in the bias estimate of approximately 6 mm (Haines et al., 2003). Taking the orbit differences into account, bias estimates at Bass Strait and Harvest show exceptional agreement (128 and 132 mm respectively). Bias estimates from Corsica do not show any significant dependence on the orbit strategy (over the full time series), and hence remain somewhat low (120 mm) in comparison to the Harvest and Bass Strait estimates. The effect of geographically correlated errors and the influence of orbit models are discussed in further detail in the following section where the complete time series of Jason-1 data is analysed.

4.6.1.2 Jason-1: All Available Cycles

Extending the Jason-1 analysis to include all available cycles (up to and including cycle 101, 06/10/2004) and comparing against the SSH_{TG} as the in situ reference, reduces the mean absolute bias to +143.2 mm (standard error 8.9 mm) and reveals an apparent decreasing trend within the time series (Figure 4-17).

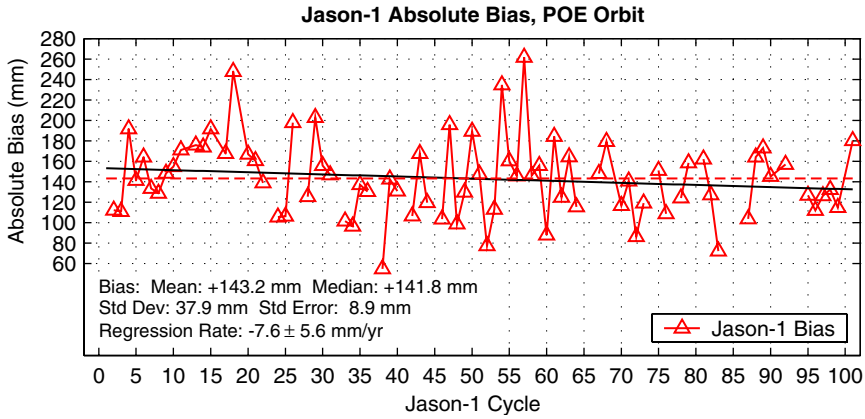

Figure 4-17 Jason-1 absolute bias using the POE orbit and standard GDR SSB model (cycles 1-101).

A weighted least squares linear regression computed using the complete Jason-1 bias time series yields a drift rate of -7.6 ± 5.6 mm/yr. The regression uses realistic estimates of uncertainty (as presented in the error budget, §4.5) in order to determine the resultant rate uncertainty (at the 1σ level). The rate uncertainty is therefore considered conservative.

The slope is used to derive an absolute bias estimate at the nominal epoch of 2002.0 (as per the convention adopted by Bonnefond et al., 2004), which equates to +153.5 mm. This compares with the Harvest results over a similar period (+140 mm @ 2002.0) and higher than Corsica estimate (+114 mm @ 2002.0), using results complied by Bonnefond et al. (2004).

The first area of further analysis for Jason-1 bias values is the effect of changing the orbit solution used, as undertaken over the calibration period. Results using the JPL reduced dynamic GPS orbit are shown in Figure 4-18. The mean bias using the GPS orbit reduces by about 16 mm to 127.3 mm, with a reduction in absolute magnitude of the linear drift to -4.4 ± 5.6 mm/yr. The absolute bias using the GPS orbit at 2002.0 is +133.2 mm. Using the GPS orbit brings the Bass Strait estimate even closer to the result from Harvest (+133 mm @ 2002.0). The

effect of the orbit at the Corsica site is negligible, with the 2002.0 absolute bias being +116 mm (both Harvest and Corsica estimates from Bonnefond et al. 2004).

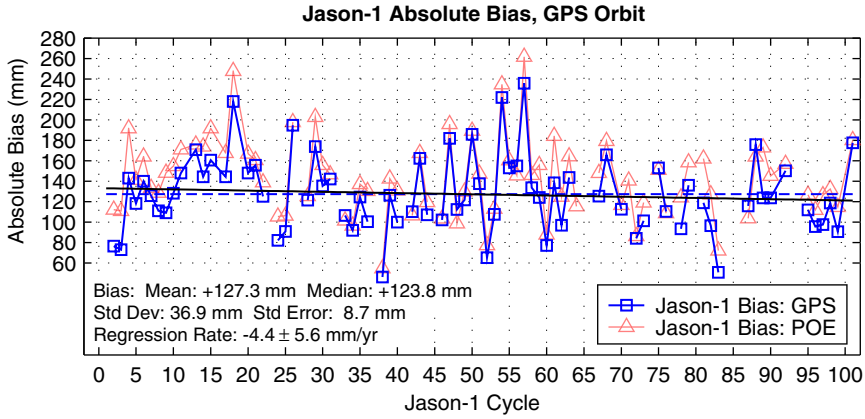

Figure 4-18 Jason-1 absolute bias using the JPL reduced dynamic GPS orbit and standard GDR SSB model (cycles 1-101). Note the bias series computed using the POE orbit is shown in the background for comparison.

These results imply geographically correlated errors exist in one or both orbit solutions. The reduction in drift is also of particular interest, implying a drift in one (or both) of the orbit solutions. To gain a further understanding of behaviour of the POE and GPS radial orbit differences at the Bass Strait site, individual differences (POE – GPS, at the comparison point) are shown in Figure 4-19.

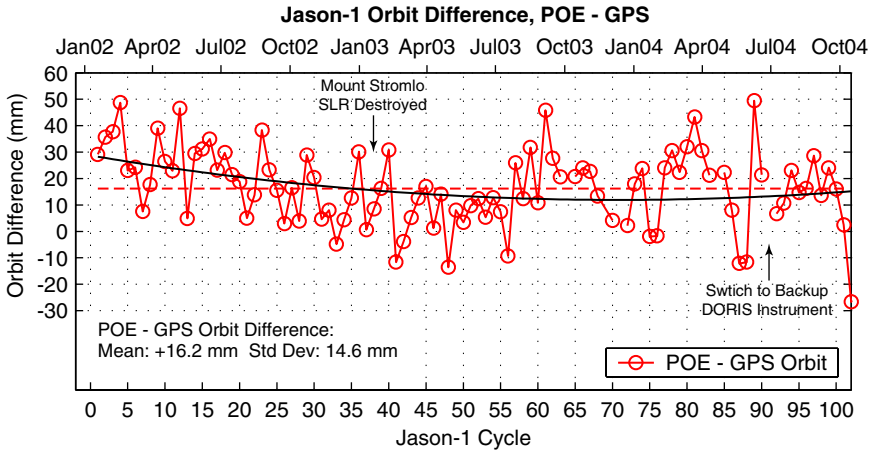

Figure 4-19 Differences in Jason-1 POE orbit and the JPL reduced dynamic GPS orbit (POE - GPS). Note the addition of the x-axis labels in both cycles and the start of every third calendar month. The solid black line represents a quadratic fit to the data.

The mean difference of 24 mm over the calibration phase of the mission (cycles 1-22) is clearly evident in Figure 4-19. The difference time series shows a clear trend between cycles 1-55 in addition to a possible periodic signal, with a 6-7 cycle

period. The linear trend appears to cease at around cycle 55, at which stage the differences show marginally higher variability. The most probable cause for the spurious drift in the differences is the degradation of the primary DORIS instrument on the Jason-1 spacecraft (hence influencing the GDR POE orbit which is based on SLR and DORIS data). The primary DORIS instrument was found to be adversely affected by radiation over the South Atlantic Anomaly (SAA), introducing spurious clock accelerations when passing over the anomaly (Willis et al., 2004). Controllers switched to the backup DORIS instrument on June 29, 2004 (cycle 91), as indicated in Figure 4-19. Preliminary results at the time of writing indicate the second instrument is also sensitive to the radiation across the SAA (Willis, 2004).

To confirm the drift is not within the GPS orbits, analysis has been undertaken comparing the POE, GPS and short arc SLR orbits (P. Bonnefond, personal communication, 2004). Results confirm that the GPS orbit is stable at the 1 cm level and the POE is suspect. Substantial SLR coverage near the Corsica calibration site explains why the drift is not observed at that site (Bonnefond, 2004), in comparison with both the Bass Strait and Harvest sites where the drift is significant. The loss of the Australian Mount Stromlo SLR station by fire in January 2003, at about Jason-1 cycle 38 (Pearlman, 2003), would have adversely affected the POE orbits in the Australian region. The reduction in SLR coverage in the Australian region would no doubt be a contributing factor to the signal observed in the orbit differences at the Bass Strait site (Figure 4-19).

Analysis of globally distributed mean differences between the GDR POE and JPL GPS orbits reveal specific geographic correlations. Analysis by Haines et al. (2004a), for example, shows distinct spatial patterns which largely reflect differences in the underlying gravity models, JGM-3 (Tapley et al., 1996) and the GRACE GGM01S (Tapley et al., 2004b) respectively. The Haines et al. (2004a) analysis for descending passes is shown in Figure 4-20. The distinct spatial pattern present within Figure 4-20 is clearly of concern with the large differences having the potential to be mis-interpreted as ocean circulation (see Haines et al., 2004a).

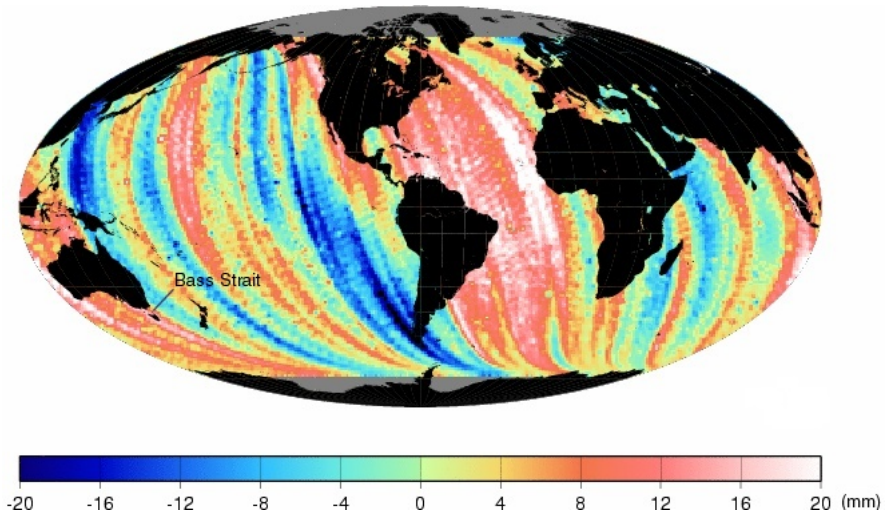

Figure 4-20 Geographically correlated orbit errors present between the GDR POE orbits and the JPL GPS orbits for all descending passes for the first 20 months of the Jason-1 mission. Figure adapted from Haines et al. (2004a) (reproduced with the permission of the author).

The area of highest and most consistent difference falls over the Atlantic Ocean and is again representative of the DORIS performance under the SAA conditions. The 'banded' appearance of the differences most likely reflects the influence of the long wavelength improvements in the GGM01S model compared with the JGM-3 model. An additional analysis of the geographical correlated errors (GCEs) associated with JGM-3 and GGM01S is presented Choi et al. (2004).

In addition to the orbit differences discussed, drift in the observed tropospheric path delay may be a contributing factor to drift present within the Jason-1 absolute bias time series (Figure 4-17). As a first investigation, the JMR correction was replaced in the GDR processing with the European Centre for Medium-Range Weather Forecast (ECMWF) modelled wet path delay estimates. Using this dataset combined with the GPS orbits, the bias drift at the Bass Strait site reduces to -2.9 $\pm$ 5.6 mm (c.f. -4.4 $\pm$ 5.6 mm as per Figure 4-18). The JMR performance has been investigated and is presented in §4.6.2 following the analysis of T/P absolute bias in the following section.

4.6.1.3 TOPEX/Poseidon: Side A and Side B

As discussed in the introductory Chapter, two different electronic systems have been in operational use onboard the T/P spacecraft (designated side 'A' and 'B'). The side 'B' altimeter was put into operation following degradation of the side 'A' unit during February 1999. The last full cycle to utilise data from the side 'A' instrument was T/P cycle 235. Utilising the corrected tide gauge sea surface heights, (SSH_{TG}) as the in situ reference dataset, absolute bias estimates for T/P side 'A' and 'B' can be computed (Figure 4-21).

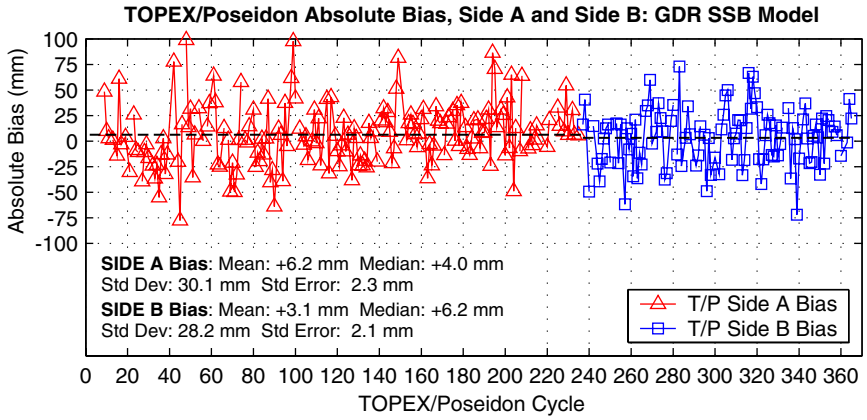

Figure 4-21 Absolute bias for T/P Side A (cycles 001-235) and T/P Side B (cycles 236-365). Note the dashed lines shows the mean bias for the respective period.

Over the side 'A' period, the mean absolute bias at the Bass Strait site is +6.2 mm (standard error 2.3 mm). The side 'B' absolute bias estimate using the MGDR-B SSB correction is +3.1 mm (standard error 2.1 mm). These values compare favourably with the estimates from the Harvest site, with bias estimates of +5 mm (side 'A') and +2 mm (side 'B'), respectively (Haines et al., 2003). Results from the site at Corsica are limited for side 'A', with the study only beginning during cycle 208. The resultant biases from Corsica are +6.6 mm and +5.6 mm for 'A' and 'B' respectively (Bonnefond et al., 2003a). The difference in side 'A' and 'B' bias estimates from Bass Strait are also in close agreement with the global tide gauge calibration solutions presented in Mitchum (2000) and Leuliette et al. (2004).

Investigations by Chambers et al. (2003), revealed a potential problem with the sea-state bias (SSB) model used in conjunction with the side 'B' data delivered as part of the MGDR-B product. The impact of the new SSB model derived by Chambers et al. (2003) was investigated as part of this study. As expected, the new SSB model makes insignificant difference for the side 'A' bias, increasing the bias by 0.5 mm to +6.7 mm (with no change to the variability). The estimate of

side 'B' bias using the Chambers SSB model is increased to +6.8 mm (standard error 2.1 mm), bringing the bias in line with the estimate for side 'A' as expected.

Despite the increased sample size, the formal uncertainty for these T/P bias estimates remains at the 10-12 mm level due to the systematic terms present in the error budget (§4.5). It can therefore be concluded that the absolute bias present in the T/P data at the Bass Strait site is not significantly different from zero.

The estimation of bias drift at an individual calibration site remains a difficult challenge. Weighted regression analysis using uncertainties from the error budget yields estimates of bias drift of +3.4 ± 1.8 mm/yr for side 'A' and +2.2 ± 3.9 mm/yr for side 'B', using the standard SSB model (1σ uncertainties). There is no significant change in the rate using the Chambers et al. (2003) SSB model. All estimates of drift in the bias series are not significant at the 95% confidence level due to the noise in the absolute bias estimates and the comparatively small sample size. The rate (side 'A', using the standard SSB model) does however compare favourably with the Harvest estimate (+2.6 ± 1.4 mm/yr, Haines et al., 2003) over the same period. A marginal positive trend for side 'A' could be attributed to the degradation of the point target response (PTR) of the side 'A' system which is not taken into consideration in the MGDR-B data processing (Hayne, 2004). There is little chance the drift is a result of drift within the TMR due to the corrections applied during processing the GDR dataset (§4.4.4.1). The positive drift rate may also be partly indicative of land *uplift* at the Burnie tide gauge site. The GPS analyses presented in the previous Chapter shows a vertical velocity at the +1.8 mm/yr level (with significant error bars of ± 1.2 mm/yr, as discussed in the Chapter 3). No conclusive statement can however be made at this level. These results confirm the difficulties associated in measuring bias drift from a single in situ calibration site.

4.6.1.4 Comparison with other Calibration Sites

As emphasised throughout this Thesis, absolute calibration of satellite altimeters using various calibration sites is only possible when homogeneous processing standards and techniques are adopted. Differences in computational standards or more simply the number of available overflights used in the computations affects the interpretation of differences of absolute bias (especially in the presence of bias drift). The following section briefly presents results from other studies which aids the interpretation of altimeter performance, yet must be treated with caution given the stated differences.

Pavlis and Mertikas (2004) present results from the Greek GAVDOS project. An absolute bias of +145 mm is derived from 21 cycles of Jason-1 data. This estimate is consistent with the three primary calibration and validation sites, despite the small sample size. Martinez-Benjamin et al. (2004) provide results from the Ibiza Island experiment in Spain (using approximately 34 cycles). Results from one tide gauge site yield comparable estimates of absolute bias (+120 mm) yet another appears in gross error by approximately 50 mm due to a levelling error. The Shum et al. (2003) study in Lake Erie (USA) yields dramatically different estimates of Jason-1 absolute bias (+58 mm). This may be suggestive of performance changes over inland lake areas, or perhaps indicative of land contamination in the estimates of wet path delay from the JMR instrument. Clearly, it is difficult to use this estimate in any form of comparison with other global sites without significant further investigation.

Results from the Woodworth et al. (2004) study (initially presented by Dong et al., 2002) in the United Kingdom provide valuable comparison for Jason-1 cycles 1-61. The study presents an absolute bias of +129 mm, computed from five tide gauges around the United Kingdom. This is in close agreement with the nearby site at Corsica. Clearly, future updates from each of these sites will further assist in the interpretation of altimeter performance, not just at the Harvest, Corsica and Bass Strait locations.

4.6.2 Radiometer Calibration Results

As discussed in the introductory Chapter, the measurement and correction for the path delay caused by the water vapour content of the troposphere is a fundamental component of the altimeter measurement system. Drift observed in the microwave radiometer on board T/P (TMR) highlights the need for concern (see Haines and Bar-Sever, 1998 and Keihm et al., 2000 for example).

Estimates of the wet delay observed from both T/P and Jason-1 (TMR and JMR respectively) were compared during the formation flight period to derive an estimate of the residual altimeter wet delay (Figure 4-22). Readers are reminded the wet delay is the absolute value of the correction supplied on the GDR, in this case, extrapolated to the comparison point.

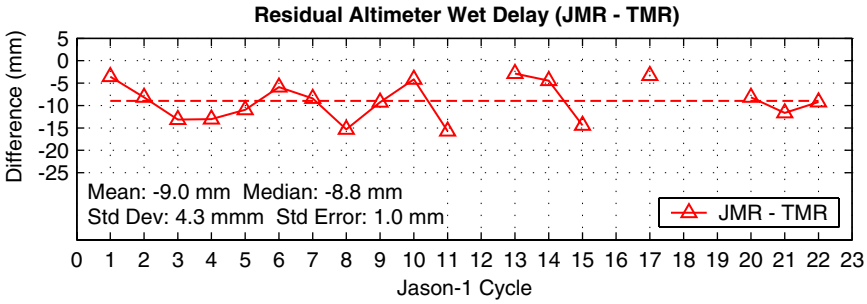

Figure 4-22 Difference in the JMR and TMR extrapolated wet delays (JMR – TMR).

Figure 4-22 shows a clear bias is present between the TMR and JMR data during the formation flight period of the mission. The mean bias (JMR wet delay – TMR wet delay) at the Bass Strait comparison point is -9 mm indicating that the JMR instrument is measuring drier when compared with the TMR. The standard deviation of the differences is 4.3 mm. The formal error estimate of the mean difference computed using 18 cycles is 4 mm (assuming each TMR and JMR measurement is independent and has a 1σ uncertainty of 12 mm (Keihm et al., 2000 and Brown et al., 2004b). The difference observed at the Bass Strait site over the calibration phase is consistent with global studies such as Brown et al. (2004b). Brown et al. (2004a) reports the JMR instrument was biased low between 8-12 mm and included a significant scale term. The scale error translated to a ~15 mm bias for dry atmospheric conditions (wet delay << 100 mm) and between 5-7 mm for wetter conditions (wet delay >> 100 mm). Over the duration of the calibration phase, the average TMR path delay at the Bass Strait site was 100.2 mm (standard deviation 26 mm, based on corrected estimates at the comparison point).

To assess the absolute accuracy and potential drift of both the TMR and JMR time series, data were compared with the BUR1 GPS derived estimates of wet delay. To assess the linear extrapolation technique used to overcome the land contamination problem, both the land contaminated values in addition to the linearly extrapolated estimates were compared (Figure 4-23). In both cases, the TMR data were corrected for known problems using Ruf (2002) and Brown et al. (2002).

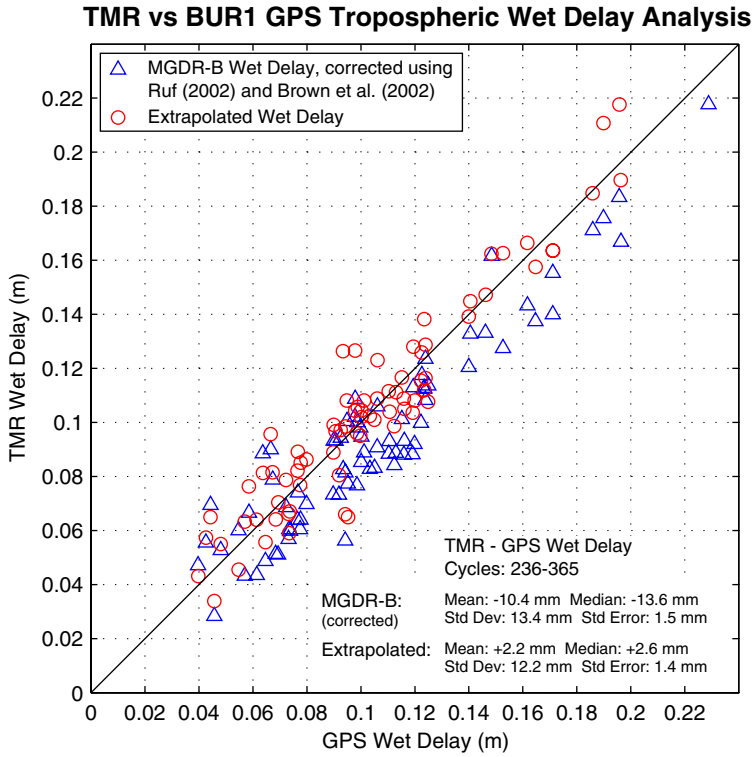

Figure 4-23 TMR vs BUR1 GPS wet delay. Both the MGDR-B TMR wet delay (corrected using the Ruf (2002) and Brown et al. (2002) corrections) and the extrapolated TMR wet delays are shown compared with the wet delay extracted from the BUR1 GPS data.

The TMR vs GPS analyses, shown in Figure 4-23, give a mean offset (TMR – GPS) for the extrapolated data of +2.2 mm (with a standard error about the sample mean of 1.4 mm). The effect of the land contamination is evident in the corrected MGDR-B TMR data (i.e., no linear extrapolation undertaken), with a mean offset of -10.4 mm (standard error 1.5 mm). The extrapolated estimate versus the GPS wet delay is not significantly different from zero which is in agreement with numerous studies of the TMR performance over this period (Brown et al., 2004b, Desai and Haines, 2004, Zlotnicki and Desai, 2004 and Edwards et al., 2004 for example).

The time series of the extrapolated TMR vs BUR1 GPS wet delay differences is shown in Figure 4-24. Weighted regression analysis using error estimates from the error budget show the drift of the time series is indistinguishable from zero (+1.0 ± 1.5 mm/yr), and in agreement with Ruf (2002).

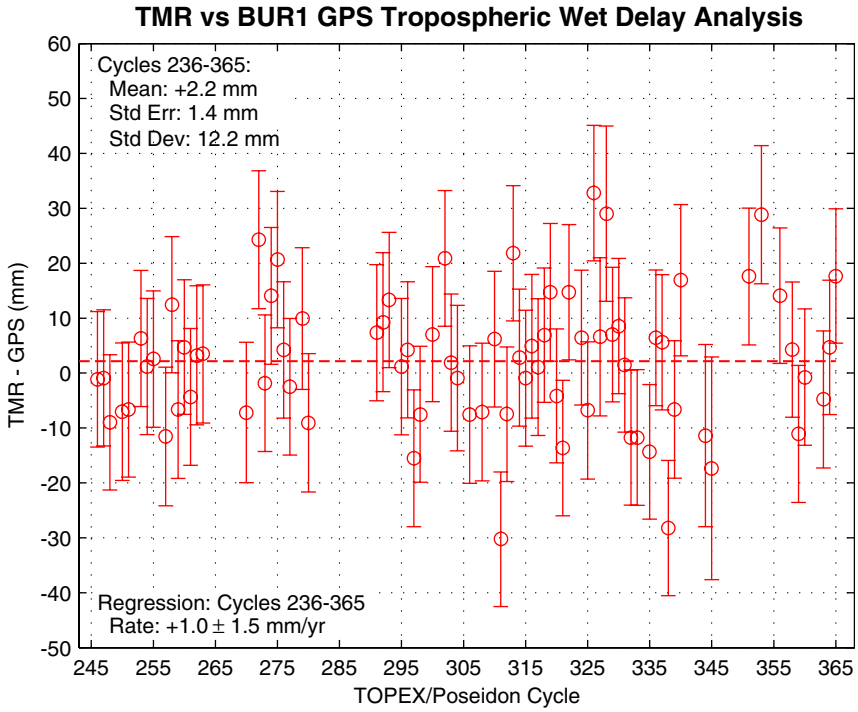

Figure 4-24 TMR – BUR1 GPS wet delay difference time series.

The extrapolation technique used in §4.4.4.3 extrapolates the TMR and JMR wet delay correction to the offshore comparison point and not to the point of closest approach to the BUR1 GPS site. Extending the extrapolation to the BUR1 GPS site has the effect of increasing the variability of the (TMR – GPS wet delay) differences (Figure 4-24). When extrapolating the complete distance to the GPS site, the mean difference changes insignificantly by 0.9 mm to +1.3 mm, with the standard deviation changing to 14.3 mm (compared with 12.2 mm previously).

From these analyses, it is possible to conclude that linear extrapolation to the comparison point yields the best comparison *at the comparison point*, yet the variability associated with the troposphere makes it difficult to further extrapolate using a simple linear model to the BUR1 GPS site. For this reason, the adopted results used the MGDR-B altimeter values extrapolated to the comparison point, and not to the GPS site.

Analysis of the Jason-1 JMR instrument is particularly interesting at the Bass Strait site. The time series of JMR – GPS wet delay differences (Figure 4-25) shows a very different picture, with both an absolute offset and drift over the duration of the available data.

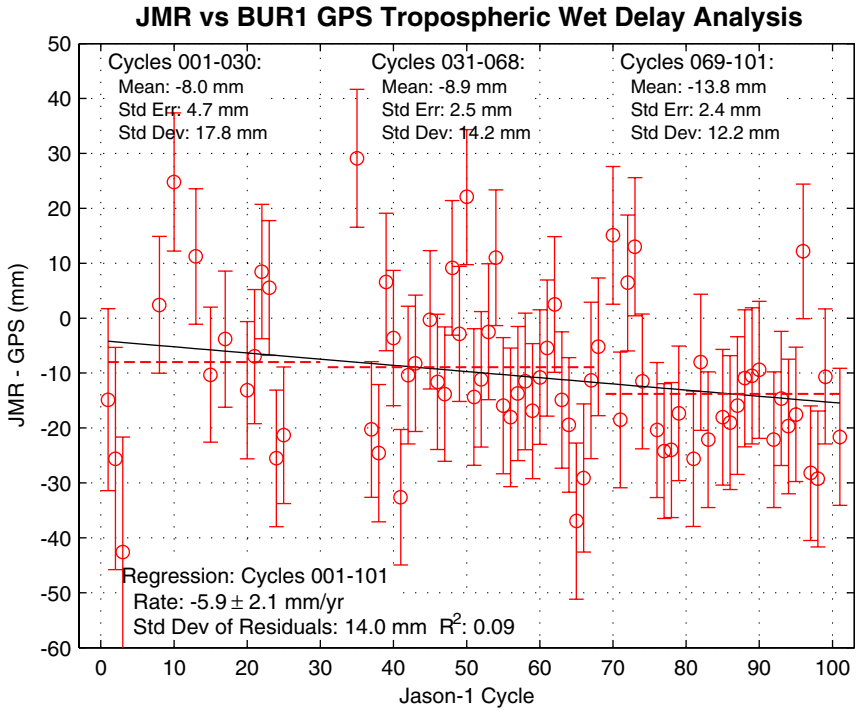

Figure 4-25 JMR – BUR1 GPS wet delay difference time series.

Comparison is limited between cycles 1 to 35 due to a number of unexpected and unavoidable outages at the GPS site (as discussed in Chapter 3). The absolute offset present (-8 mm between cycles 1-30 and up to -13.8 mm between cycles 69 and 101) suggests the JMR instrument is predominantly responsible for the relative bias observed between the JMR and TMR instruments (Figure 4-22). The strong agreement between the BUR1 GPS and the TMR data (Figure 4-24) lends additional weight to this hypothesis. An absolute bias in the JMR estimates of wet delay is therefore a contributing factor to the observed Jason-1 SSH bias.

Global analyses of JMR data by Desai and Haines (2004) and Zlotnicki and Desai (2004) indicate the 23.8 GHz channel experienced an anomaly between cycles 28-32 inducing an additional offset of +4.1 ± 2.1 mm (drier). Limited GPS comparisons before cycle 32 make this hard to verify at the Bass Strait site. Recent presentations at the Ocean Surface Topography Science Team (OSTST) meeting in November, 2004 indicate an additional jump after cycle 69 related to an instrument safe-hold event (Brown et al., 2004a). With this in mind, mean offsets were

computed before and after each observed jump. The mean offset between cycles 30 to 68 was -8.9 mm (standard error 2.5 mm) and -13.8 mm (standard error 2.4 mm) between cycles 69 to 101.

Adopting an alternative hypothesis of a linear drift over the duration of the available Jason-1 data yields a drift rate estimate of -5.9 $\pm$ 2.1 mm/yr (using a weighted linear regression). This is indicative of the JMR instrument measuring drier over time. The JMR drift estimate at the Corsica site is also at the -6 mm/yr level (Bonnefond, 2004). This appears to account for the majority of the drift present in the Jason-1 absolute bias time series (-4.4 $\pm$ 5.6 mm/yr, Figure 4-18), computed using the GPS orbits.

4.7 Summary

The use of GPS buoys combined with an oceanographic mooring array at the Bass Strait calibration site provides a unique calibration methodology for the determination of absolute altimeter bias. The methodology significantly improves the standard 'indirect' absolute calibration methodology, which typically utilises a coastal tide gauge and a regional geoid model to extrapolate the SSH estimate offshore to the comparison point. The technique used at the Bass Strait site has also allowed a rigorous 'direct' calibration over the duration of the calibration phase of the T/P and Jason-1 missions, and provided datum control for ongoing continuous calibration using measurements from a nearby tide gauge.

Over the formation flight period, the mean absolute bias is 0 $\pm$ 14 mm for T/P and +152 $\pm$ 13 mm for Jason-1. Using only common cycles, the relative bias at Bass Strait is +150 $\pm$ 11 mm (note the systematic error terms from the in situ instrumentation cancel for the determination of relative bias uncertainty). The uncertainty tolerances placed on these estimates are considered realistic given the error terms involved. The limiting error sources for the absolute bias estimates are the systematic error term associated with the GPS reference station analysis, followed by the uncertainty associated with the altimeter SSH estimates. The variable component of the error budget shows close agreement with the observed variability within the absolute bias estimates, providing further confidence in the error budget adopted.

Over the extended calibration period, the T/P side 'A' and 'B' biases are +6.2 ± 11 mm and +3.1 ± 11 mm respectively (+6.7 mm and +6.8 mm using the Chambers et al., 2003 SSB model). Each of these estimates are not statistically different from zero. Results for Jason-1 show a mean absolute bias of +143.2 ± 12 mm over cycles 1-101 (using the GDR POE orbit), with a drift of -7.6 ± 5.6 mm/yr using a formal error budget (absolute bias at 2002.0 is +153.5 mm). Using the JPL GPS orbit, the mean absolute bias decreases to +127.3 ± 12 mm, with a drift of -4.4 ± 5.6 mm/yr (absolute bias at 2002.0 is +133.2 mm). Analysis of the JMR instrument shows a drift of -5.9 ± 2.1 mm/yr, accounting for the remaining drift presenting in the absolute bias series (using the JPL GPS orbits).

The significant bias (order 130 mm) present in the Jason-1 data remains unexplained. Differences observed between the JMR, TMR and GPS wet delay estimates indicate the JMR instrument may be a small contributor to the bias, measuring drier than TMR and the GPS estimates at the 10 mm level. Variations in the orbit solutions also account for a small component of the bias. Differences observed between the two orbit solutions for the Bass Strait region can be attributed to the following:

a) degradation of the DORIS instrument, used in the POE orbit analysis, over the South Atlantic Anomaly;
b) the loss of the Australian Mt Stromlo SLR station (January 2003), also used in the POE orbit analysis; and
c) differences in the underlying gravity fields associated with each orbit computation strategy (JGM-3 for the GDR POE and GGM01S for the JPL GPS)

The distinct geographically correlated orbit differences over the Australian region (amongst others) emphasises the need for continued analysis, especially considering the evolution in obtainable precision over recent years. The geographically correlated orbit errors also highlight the benefit of a well-distributed set of calibration sites to quantify observed differences in an absolute sense.

After considering geographical differences associated with orbit computation, bias estimates from the Bass Strait site agree favourably with those from other calibration studies. Results from Harvest and Bass Strait agree to well within estimated uncertainty tolerances. Bias estimates from the Corsica site remain lower (by approximately 17 mm), yet still within the formal uncertainties. Similarly, results from the United Kingdom and Greece show close agreement,

although comparison is only possible with a reduced number of cycles from these sites at the time of writing.

Variations in computational standards may contribute to small differences in absolute bias values between different calibration sites. For example, the difference observed when standardising the pole tide algorithm for this study (Chapter 3) demonstrates the importance of correctly standardising measurement models, especially given that absolute heights are required.

The determination of an optimum SSB model remains a challenge within the altimetry community (as demonstrated by Chambers et al., 2003, see also Gaspar et al., 2002 and Labroue et al., 2004). Differences in altimeter SSH at the few centimetre level are therefore observed when adopting different SSB models. Due to shifts in the magnitude of the median correction applied with a specific SSB model, estimates of the overall absolute bias will be dependent on the SSB model adopted. The magnitude of the difference observed will also depend on the wave climate at the calibration site. Over the duration of the Jason-1 mission, the Bass Strait site is characterised by a relatively low average significant wave height (SWH) of 1.1 m (standard deviation 0.6 m). Comparatively small changes as a result of altering the SSB model are therefore seen at the Bass Strait site.

To conclude, the results presented throughout this Chapter underscore the need for careful ongoing calibration of altimeter missions, enabling the scientific community to continually monitor global sea level. A complete picture of altimeter performance can only be obtained with a geographically diverse collection of in situ calibration sites, together with complementary global tide gauge calibration studies.

Chapter 5

Tide Gauge Verification

Tasmania, the Sub-Antarctic and the Antarctic

5.1 Introduction

The tide gauge is the fundamental instrument used to determine the physical distance between the water surface and some fixed reference point on the instrument itself. Despite the emergence of technologies such as satellite altimetry, tide gauges remain imperative to the oceanographic and geodetic communities. Historically, the long history of tide gauge measurements have been exploited in studies estimating rates of secular sea level change, for example Emery and Aubrey (1991), Cartwright (1999), and more recently summarised in Church et al. (2001). As discussed in a previous Chapter, tide gauges have become increasingly important to the calibration of satellite altimeter missions (for example Mitchum, 2000). Somewhat paradoxically, tide gauges and altimeter data have also been combined to estimate rates of vertical crustal motion at the tide gauge sites (for example Nerem and Mitchum, 2002). For each of these applications the stability and accuracy of the tide gauge is of fundamental importance.

The tide gauge at Burnie forms a vital component of the instrumentation used for the Bass Strait calibration of T/P and Jason-1. The reliance on the Burnie tide gauge for the ongoing calibration of Jason-1 provides the initial impetus for an investigation into the performance and accuracy of tide gauges as presented in this Chapter.

The remaining impetus for this Chapter is derived from the significant Australian contribution to sea level measurement in the Southern Ocean and Antarctic regions. The irregular distribution of tide gauges, particularly in the Southern Ocean and around Antarctica, makes many sea level studies problematic. The irregular distribution of tide gauge sites is clearly observed in maps published by

the Permanent Service for Mean Sea Level (PSMSL, 2004). Polar regions are mostly under sampled due to the logistical and practical challenges of operating a tide gauge in a frequently hostile environment (IOC, 1990; IOC, 1992). The relevant literature is yet to yield reliable or trustworthy estimates of secular sea level change utilising data from Australian gauges in the southern polar region. Given the location and distribution of these gauges, the potential value of the data set as the time series matures is significant. Issues of datum control and system stability are therefore critical and have been investigated in this Chapter.

This Chapter focuses firstly on a brief review of modern tide gauge measurement, with an emphasis on the gauge types used at the Bass Strait calibration site and the Australian Antarctic and Sub-Antarctic installations. The work does not attempt to cover tidal theory or the analysis of long-term tide gauge data. For this readers are referred to the relevant literature such as Doodson and Warburg (1941) and Pugh (1987). A comprehensive history of tidal research is provided in Cartwright (1999). The Chapter progresses to describe an innovative methodology that utilises GPS buoy technology to estimate the absolute datum and measurement accuracy of various tide gauge installations. In the process, several interesting oceanographic phenomena are revealed and quantified. Case studies involving the application of the verification methodology are presented and include the tide gauge sites at Burnie (Bass Strait), Macquarie Island (Sub-Antarctic) and Davis Station (Antarctica).

5.2 Tide Gauge Technologies

Tide gauge technologies have evolved considerably over a long history beginning with simple graduated marks placed on rocks, boards, masonry etc. Early tide gauges were simply observed visually, and often only times of high and low water were recorded (Pugh, 1987). Mechanical gauges with clocks and recording devices appeared around the 1830's and relied typically on a float arrangement in a stilling well (IOC, 2002). Whilst float based gauges remain popular, many modern gauges are now based on the measurement of water pressure or the return travel time of an acoustic, radar or other electromagnetic propagation to the water surface. Development of digital technology has enabled the autonomous operation of most tide gauges, recording and telemetering data digitally to assimilation centres, such as the Permanent Service for Mean Sea Level (PSMSL).

Sea level measurement techniques have been well summarised in a series of Intergovernmental Oceanographic Commission (IOC) manuals and guides (IOC, 1985; IOC, 1994; IOC, 2002). Figure 5-1 shows the schematic view of a typical installation of three modern instruments; a bottom mounted pressure gauge, an acoustic gauge and a radar gauge. The following sections provide a brief review of these technologies, in the context of the case studies presented in this Chapter.

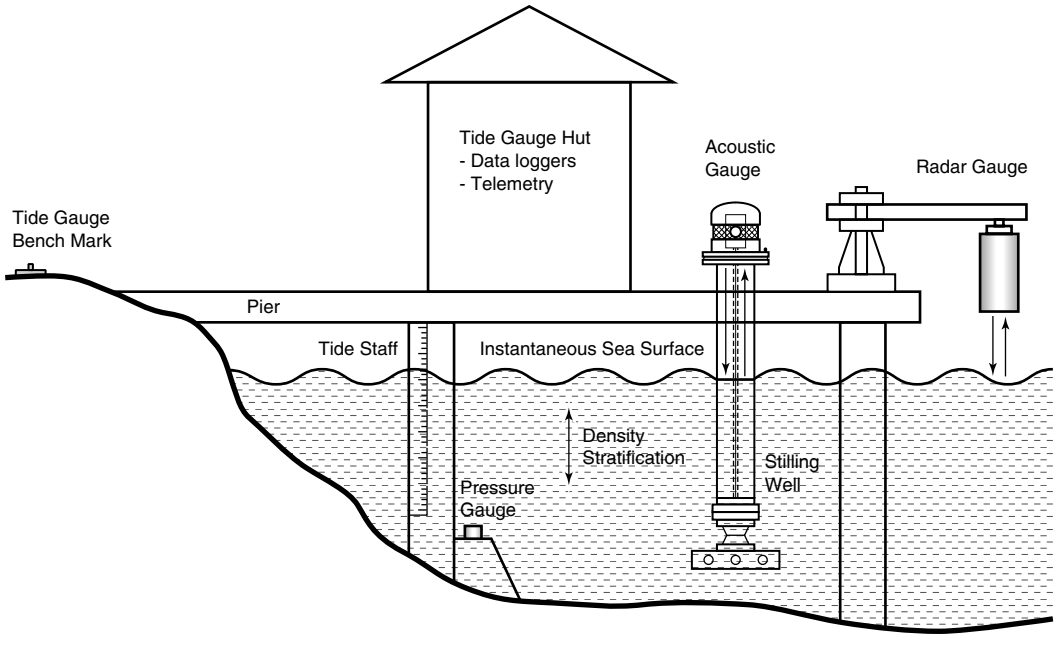

Figure 5-1 Schematic view of three modern tide gauge technologies including the bottom mounted pressure gauge, acoustic gauge and radar gauge. All gauges are shown in the standard installation configuration, orientated normal to the water surface.

5.2.1 Acoustic Tide Gauges

Acoustic tide gauges fall into the category of reflection-time gauges, as described in Pugh (1987). The principle relies on the measurement of travel time of a pulse of sound to travel from a source to the sea surface and return. The travel time of the pulse (t_p) is given by the elementary relationship:

$$t_p = \frac{2l_{SSH}}{C_a} \qquad \text{Eqn 5-1}$$

where l_{SSH} is the distance to be measured, and C_a is the velocity of sound in air (337.5 ms^{-1} at 10 °C and 1013.25 HPa atmosphere pressure). The most common high accuracy acoustic tide gauges constrain the acoustic pulses using a narrow sounding tube (IOC, 2002), traditionally mounted vertically within a stilling well (see Figure 5-1). The use of a sounding tube also allows a first order automatic calibration of the measured distance to account for variations in the speed of sound as a function of temperature, pressure and humidity. This first order calibration is achieved using an acoustic reflector (often termed the 'calibration hole'), positioned at a known distance along the sounding tube. Comparison of this known length to the observed length allows compensation of the distance measured to the sea surface using a ratio technique. Various studies, including Porter and Shih (1996) and Hunter (2003), highlight the importance of applying second order corrections based on measured temperature gradients along the sounding tube, for the highest accuracy applications. The effect of changes in relative humidity are small in comparison with changes in temperature, hence compensation for changes in humidity are most commonly neglected. A complete treatment with relevant examples of operating acoustic gauges is provided in IOC (2002).

Within Australia, the National Tidal Centre (NTC) provides management and operational support to the Australian Baseline Sea Level Monitoring Project (ABSLMP). This project maintains an array of acoustic tide gauges around the Australian coastline (Lennon et al., 1992). The tide gauge at Burnie used for the Bass Strait calibration of T/P and Jason-1 forms part of the ABSLMP array. The instrument of choice used by the NTC is the Aquatrak® acoustic sensor (Aquatrak, 2004). Aquatrak acoustic gauges are also installed at the Sub-Antarctic Australian territory of Macquarie Island (54° 30' S, 158° 57' E) and only recently in Antarctica at Mawson station (67° 36' S, 62° 52' E). Both the Macquarie Island and Mawson station installations are of particular interest as the gauge operates in an inclined position, observing through an aperture drilled through an outcrop of coastal rock.

The Burnie and Macquarie Island gauges are revisited as case studies later in this Chapter. Particular attention is given to the effects of temperature variability as discussed in Hunter (2003).

5.2.2 Pressure Gauges

The measurement of water pressure is an alternative technique to derive estimates of sea surface height relative to some fixed reference point. The sea level (h) is derived using the basic hydrostatic relationship:

$$h = \frac{(p - p_a)}{\rho g} \qquad \text{Eqn 5-2}$$

where p is the measured pressure at the submerged pressure point, p_a is the atmospheric pressure acting on the water surface, ρ is the mean density of the water column and g is the local gravitational acceleration. Whilst many pressure transducers used in tide gauges require calibration to compensate for systematic effects as a function of temperature, the largest error source is related to changes in the density of the water column.

The range of pressure based tide gauges are discussed in detail in IOC (1994) and IOC (2002). The range can be categorised depending on the location with respect to the water of the pressure transducer and the number of transducers used. The most accurate pressure system is known as the 'B gauge' as developed by the Proudman Oceanographic Laboratory (POL). The gauge uses three transducers to provide precision datum control of the overall gauge system. As discussed in Woodworth et al. (1996), the technique accommodates for effects such as instrumental drifts and stratifications in the density profile throughout the water column. A secondary category of pressure gauges include single transducer, bottom pressure recorders (BPRs). These gauges vary in relation to deployment depth, with some models developed for continuous deployments at ocean depths over periods of five years or more (for example Spencer and Vassie, 1997).

Pressure gauges are particularly common in environmentally hostile areas due to the passive sampling technique. For this reason pressure based gauges are often used in areas where the accumulation of sea ice is a problem (IOC, 1990; Summerson, 1995). The third case study in this Chapter deals with the single transducer, bottom mounted pressure gauges in use at Australian Antarctic

stations, with a focus on datum control and system accuracy at the installation at Davis Station (68° 35' S, 77° 58' E).

5.2.3 Emerging Technologies

Although not yet in widespread use on an operational basis, several emerging technologies are beginning to be applied to water level measurement applications. Many of the more recent technologies attempt to overcome the temperature dependent shortcomings of acoustic systems by using a pulse of electromagnetic radiation (radio, microwave, laser for example) as opposed to sound. An example of the radar based technology is presented in Woodworth and Smith (2003). In this case, one year of radar based data are compared against a pressure based bubbler gauge. The study highlights that the system has comparable accuracy to the pressure system and hence meets the specifications required by global networks. Logistical issues, such as the ease of installation, maintenance and the ability to operate without a stilling well, are significant advantages of the radar system. Gronlie (2002) presents a description and analysis of a similar gauge that uses microwave radiation as the transmitted signal. Once again, benefits include open-air operation and ease of installation and maintenance. The effect of sea state on the reflected pulse may be significant and requires further analysis. Each of the emerging water level measurement technologies impose specific challenges for calibration and datum control, as shown for the acoustic and pressure gauges in the case studies concluding this Chapter.

5.3 Tide Gauge Calibration Methodologies

Tide gauge calibration requirements and methodologies vary depending on the type of gauge and the installation configuration. For most modern tide gauge instruments, the fundamental parameter of interest is the physical offset of the electrical centre of the sensor (tide gauge zero) to an observable feature on the external surface of the gauge. In the case of the Aquatrak acoustic sensors, this measurement is referenced to a stainless steel collar at the head of the sounding tube.

Additional calibration parameters include analogue-to-digital conversion factors and any well-understood systematic instrumental effects, such as temperature dependence. These instrumental calibration coefficients are determined in a laboratory environment and supplied as factory based settings, often pre-programmed into micro controllers within the gauge controller or recording system. The calibration parameters can then be applied during the conversion of sensor output to linear estimates of SSH.

A separate calibration issue is the accuracy and stability of the tide gauge clock. Clock drift is a significant problem with older tide gauges requiring regular calibration against a known time standard. Modern GPS satellite-based clocks and oven-controlled oscillators have overcome many of these problems in the modern gauges.

The NTC acoustic gauges are calibrated as a complete system in a specially constructed tank at the NTC laboratories (Lennon et al., 1992). The tank is fan ventilated and equipped with precise thermistors allowing accurate and precise control over the temperature gradients along the sounding path (up to 9 m in length). Lennon et al. (1992) comments on the effect of varying the temperature profile, highlighting a 15 °C temperature gradient over a 4.5 m sounding path results in approximately 86 mm error in derived length. The NTC gauges incorporate an array of three temperature thermistors, located at the sensor head, mid-way down the sounding tube and at the water level. Current routine processing procedures by NTC do not however include corrections derived from the thermistor array, based on the arguable assumption of negligible thermal profiles occurring in practise (personal communication, J. Hunter, 2004). Both Porter and Shih (1996) and Hunter (2003) present results of trials between thermally corrected and uncorrected tide gauge data. The NTC calibration derives the physical offset of the sensor zero in addition to the precise separation distance between the sensor

zero and the calibration hole in the sounding tube. These estimates are computed at a standard uniform temperature of 20 °C.

Examples of in situ calibration of tide gauges within the literature have typically only included relative comparisons between different gauge types (for example Woodworth and Smith, 2003 and Gronlie, 2002). The European Sea Level Service is currently undertaking a project that adopts a similar strategy (ESEAS, 2004). The ESEAS project focuses on the in situ comparison of a range of eight gauges (radar, acoustic and pressure variants) installed on the same pier structure.

The work presented in this Chapter develops an in situ tide gauge verification technique based on the utilisation of the GPS buoy technology developed and presented in Chapter 2.

5.3.1 GPS Buoy Based Verification Methodology

The in situ tide gauge verification methodology is centred on the direct comparison of tide gauge data with filtered, high rate GPS buoy estimates of SSH (as shown in schematic form in Figure 5-2). Whilst the technique requires careful processing and error analysis, the GPS derived estimates of sea surface height are independent of many of the systematic errors which affect the tide gauge. The method provides a truly independent estimate of tide gauge performance in its operational in situ configuration.

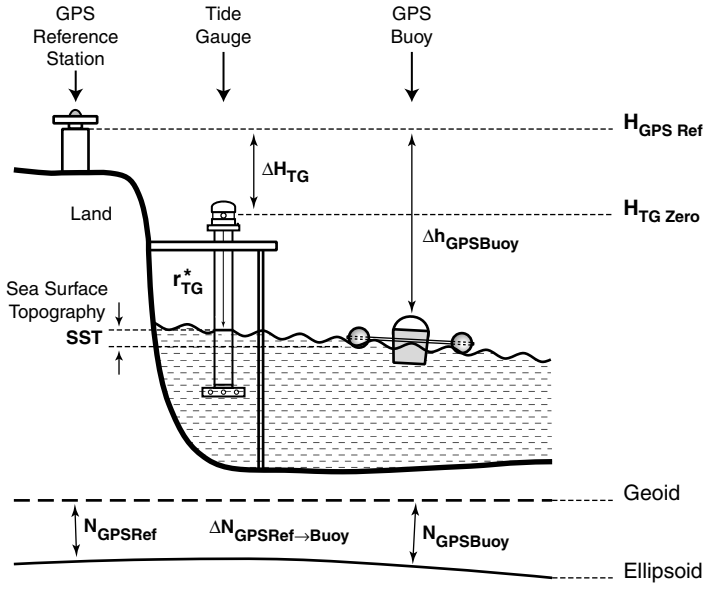

Figure 5-2 Schematic view of the GPS buoy tide gauge verification methodology.

With reference to Figure 5-2, the methodology relies on the estimation of sea surface height (SSH) at the GPS buoy, determined relative to a fixed GPS reference station (i.e., $\Delta h_{GPSBuoy}$). This connection is made using short baseline, differential GPS processing techniques (§5.3.1.2). Neglecting a range of error sources, the height measured by the tide gauge can be defined approximately with respect to the GPS buoy data as:

$$r^*_{TG} \approx \Delta H_{TG} - \Delta h_{GPSBuoy} \qquad \text{Eqn 5-3}$$

where r^*_{TG} is the estimated tide gauge observable (relative to the gauge zero), ΔH_{TG} is the orthometric height difference between the GPS reference station and the tide gauge zero and $\Delta h_{GPSBuoy}$ is the ellipsoidal height difference between the GPS reference station and the GPS buoy.

A number of complicating factors arise due to the fact the buoy is not sampling at the exact same location as the tide gauge. Firstly, $\Delta h_{GPSBuoy}$ is a time series of ellipsoidal height differences relative to the reference station. To convert these height differences to orthometric height differences, the slope of the geoid with respect to the ellipsoid must be considered (i.e., $\Delta N_{GPSRef \rightarrow Buoy}$ in Figure 5-2). Accurately estimating the geoid slope between two points is problematic due to the inaccuracy and limited spatial resolution of available geoid models. Secondly, the mean water surface between the buoy and the tide gauge may not conform to an equipotential surface, hence the effects of temperature and salinity differences, and wind and current set-up must be considered. Estimating the magnitude of these effects is also problematic considering the range of potential influences which may contribute. Within close proximity to a tide gauge location, the main effect driving sea surface topography (SST) is assumed to be wind induced sea surface set-up (see for example Pugh, 1987). Other affects such as local currents and density differences, are only expected to significantly contribute over distances greater than ~500 m. To minimise the influence of geoid slope and SST for this application, the GPS buoy is deployed as close as practically possible to the tide gauge and GPS reference station (typically within 100 m). As the baseline length decreases, $\Delta N_{GPSRef \rightarrow Buoy}$ and SST approach zero and can be neglected in Eqn 5-3. Selecting calm deployment conditions and orientating the GPS baseline vector orthogonally to the estimated long wavelength geoid slope in the region further reduces any influences of these error sources.

These error sources represent the main limitation to the absolute accuracy of this technique and must be considered in the final error analysis. Acknowledging these

previous assumptions, analysis of the GPS-derived and actual tide gauge range estimates are made by first assuming a linear relationship of the form:

$$r^{*}_{TG} = \alpha \cdot r_{TG} + \beta \qquad \text{Eqn 5-4}$$

where r^{*}_{TG} is the GPS buoy derived tide gauge value, r_{TG} is the 'raw' tide gauge measurement (using for example an acoustic gauge), α is a scale parameter and β is an offset parameter. The aim of the methodology is therefore to solve for any linear range dependent error (α) and datum or offset error (β) of the tide gauge. There is presently no indication to support any higher order range dependent error terms. For optimum results, the regression analysis requires data observed over the full dynamic range of the tide gauge (i.e., the minimum requirement is the continuous observation between one tidal minimum and maximum)

5.3.1.1 Instrumentation

The GPS buoys described in Chapter 2 have been used for the tide gauge verification experiments. The methodology dictates deploying the buoy as close as possible to the tide gauge using a moored tether. The tether must constrain the horizontal motion of the buoy, yet allow uninterrupted motion in the vertical direction. Tethering the buoy horizontally to a moored surface float has been successful and does not bias estimates of sea surface height over the duration of an experiment (see §2.4.4). Important considerations designed to minimise the GPS component of the overall error budget include the accurate estimation of the height of the GPS buoy antenna above mean water level (see §2.4.1). It is also vital to have an accurate knowledge of the phase centre offset and variation of both the reference and buoy GPS antennas (see §2.4.2). Given the accuracy tolerances required, choke ring antennas must be used and if possible, identical antenna domes on both reference and rover antennas. Battery power within the buoy design reduces the maximum potential verification period (approximately 18-20 hours using Leica CRS1000 instruments). This configuration allows ample observation time to capture the required full dynamic range of the tide gauge and successfully resolve the regression parameters. The power of the technique is obviously increased if several tidal cycles can be observed or repeated campaigns made.

Additional instrumentation includes the GPS reference station positioned as close as possible to the tide gauge to facilitate an accurate terrestrial level connection. Data are acquired from both reference and buoy stations at 10 to 1 Hz (with the higher rate reserved for studies requiring maximum information on wave shape and spectra). Secondary reference stations may be utilised for redundancy, however for maximum accuracy the baseline separation to the GPS buoy must be minimised and as stated previously, aligned orthogonally to the underlying geoid slope in the region.

Level connections between the reference station and tide gauge can be achieved using terrestrial precise levelling techniques. Typical accuracies using these techniques over short distances are at the 0.1 to 0.5 mm level.

5.3.1.2 GPS Data Processing

The kinematic GPS processing of the buoy data is simplified due to the very short baseline distance. Many of the complicating factors as encountered in the processing for the Bass Strait altimeter verification (Chapter 4), are eliminated when processing over very short baselines. In particular, both the ionospheric and tropospheric delay are highly correlated between the two stations. Residual tropospheric delay is therefore considered negligible, and ambiguity fixed, L1 and L2 solutions are of high quality without the need to form the ionosphere free, LC combination. TRACK software (Herring, 2002) is used for the GPS processing. As mentioned previously, correct modelling of antenna phase centre offsets is vital to this application. Offsets reported by Mader (2004) and available for download at NGS (2004) have been utilised for each case study presented in this Chapter.

Limitations arise in processing during periods of poor satellite geometry. Depending on the location, the surrounding environment (blocking sky coverage) and time of day, the number of satellites may fall below a minimum of five preventing a reliable, robust kinematic solution. Direct analysis of the time series of geometric dilution of precision (GDOP) estimates over the duration of an experiment provides a first approximation to areas where problems may be expected. Using a range of performance criteria, data from these periods may be excluded from the tide gauge verification.

Results from the high rate processing require filtering and transformation from GPS time to UTC before comparison with the tide gauge data. For this process it is important to match the sampling strategy used at the specific tide gauge installation. The filtering strategy is therefore discussed on an individual basis in each case study.

5.3.1.3 Tide Gauge Data Processing

In practise, tide gauge data are often supplied relative to a defined chart datum which in many cases is an estimate of the lowest astronomical tide (LAT) over a specific time period. The tide gauge data must therefore be reduced to reflect measurements of sea height relative to the tide gauge zero. This transformation requires knowledge of the datum and instrumental offsets as archived by the tide gauge data custodians.

Tide gauge data are typically provided at 6-minute intervals. The NTC acoustic gauges are configured to average readings taken in a burst sample at 1 Hz over 180 seconds. These 3-minute averages are logged every 6 minutes, with the average period centred on the time stamp. Sampling and logging configuration may vary between gauges for a variety of reasons, hence precise knowledge of the sampling strategy is vital for the GPS buoy verification methodology.

5.4 Gauge Verification at the Bass Strait Calibration Site

5.4.1 The Burnie Tide Gauge

The tide gauge at Burnie was installed in September 1992 following Burnie's selection as the first in situ calibration site in the Southern Hemisphere for the T/P satellite altimeter mission (White et al., 1994). As mentioned previously, the gauge is one of fourteen forming the Australian Baseline Sea Level Monitoring Project array, with data available through the National Tidal Centre (NTC, 2003). The tide gauge consists of an Aquatrak sensor with a Sutron terminal and data logging unit. The acoustic sensor is mounted vertically on a steel pile attached to a reclaimed rock and concrete pier on the northern extremity of the Burnie wharf complex (Figure 5-3). The pier extends into Emu Bay which forms an elongated bight in the Tasmanian coastline. The gauge is therefore sufficiently exposed to Bass Strait without significant influence from local harbour effects.

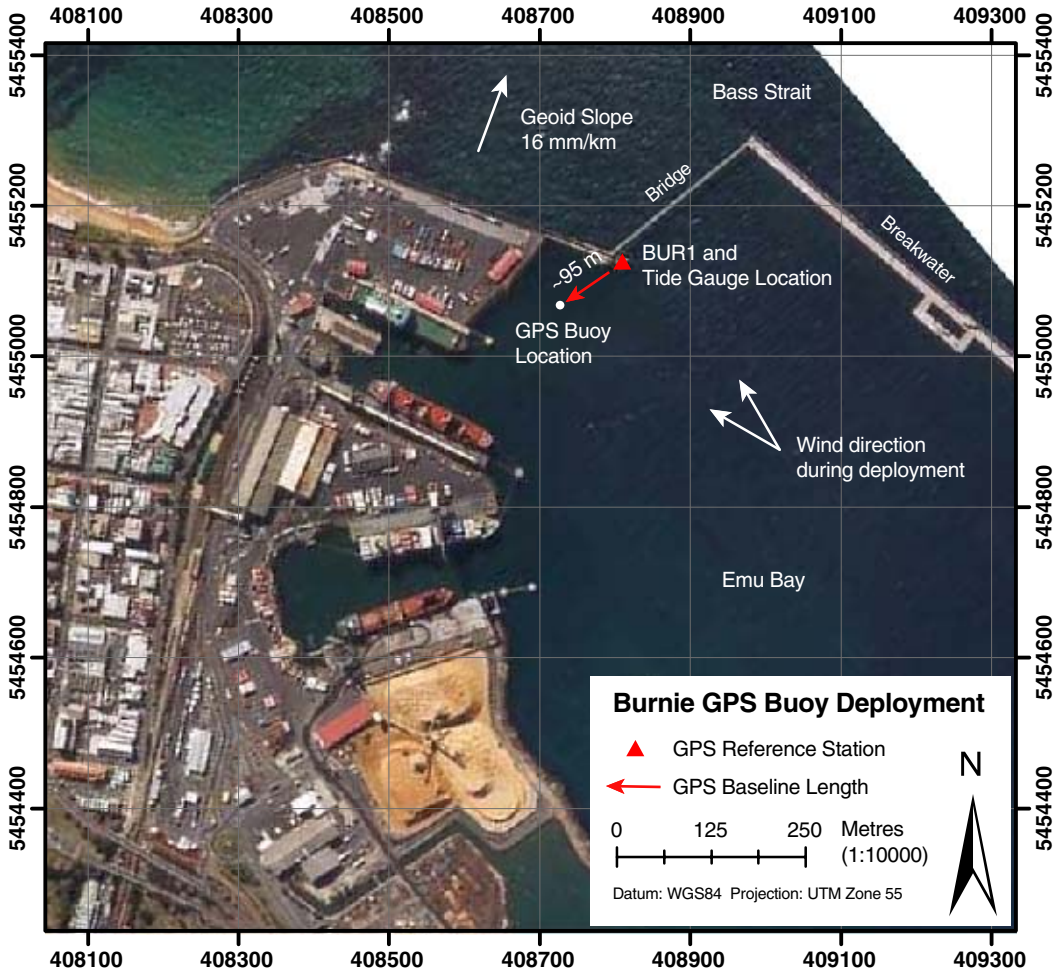

Figure 5-3 *Burnie port complex, tide gauge and GPS station locations.*

Wharf areas are often problematic for tide gauge installations due to potential settlement of reclaimed land (i.e., changes in relative sea levels). For this reason a permanently operating GPS station (BUR1) was installed at the Burnie site, co-located directly on the tide gauge support. Data from the GPS are accessed remotely and archived by Geoscience Australia (Geoscience Australia, 2003c). Periodic levelling of the tide gauge benchmark array is carried out by the Department of Primary Industry, Water and Environment (DPIWE), with results available on-line (Geoscience Australia, 2003a). The gauge and GPS installation is shown in Figure 5-4.

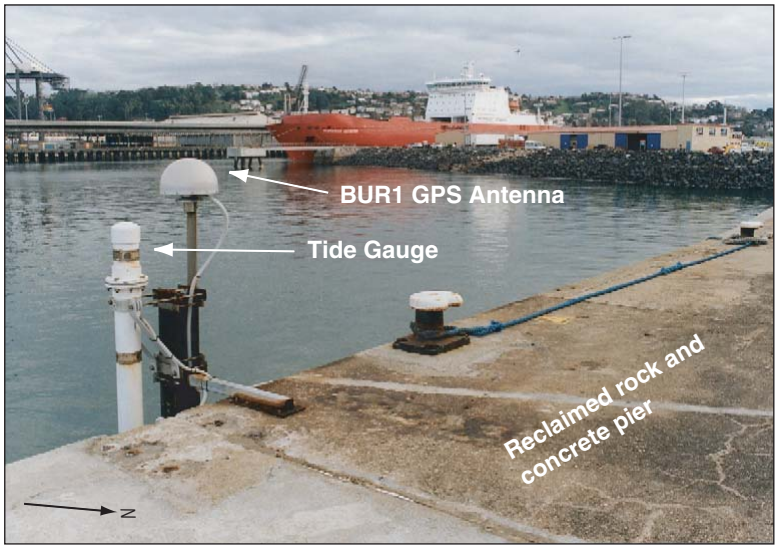

Figure 5-4 *The Burnie tide gauge and co-located GPS installation. Photograph looking west.*

The Burnie gauge is set up using the standard NTC configuration, logging one sea level estimate (an average of 3 minutes of 1 Hz samples) every 6 minutes (NTC, 2003).

5.4.2 Datum Connections at the Burnie Gauge

The datum connections at the Burnie gauge are derived from terrestrial surveys and adopted constants determined by the NTC (for example, the offset from the tide gauge zero to the electrical centre, and fixed offsets between the gauge zero and the local chart datum and the Australian Height Datum (AHD)). The first epoch of level connections between the GPS receiver and tide gauge reference mark were reported in Watson (1999). The second epoch survey was carried out as part

of this study. The datum connections adopted for the in situ verification are shown in Figure 5-5.

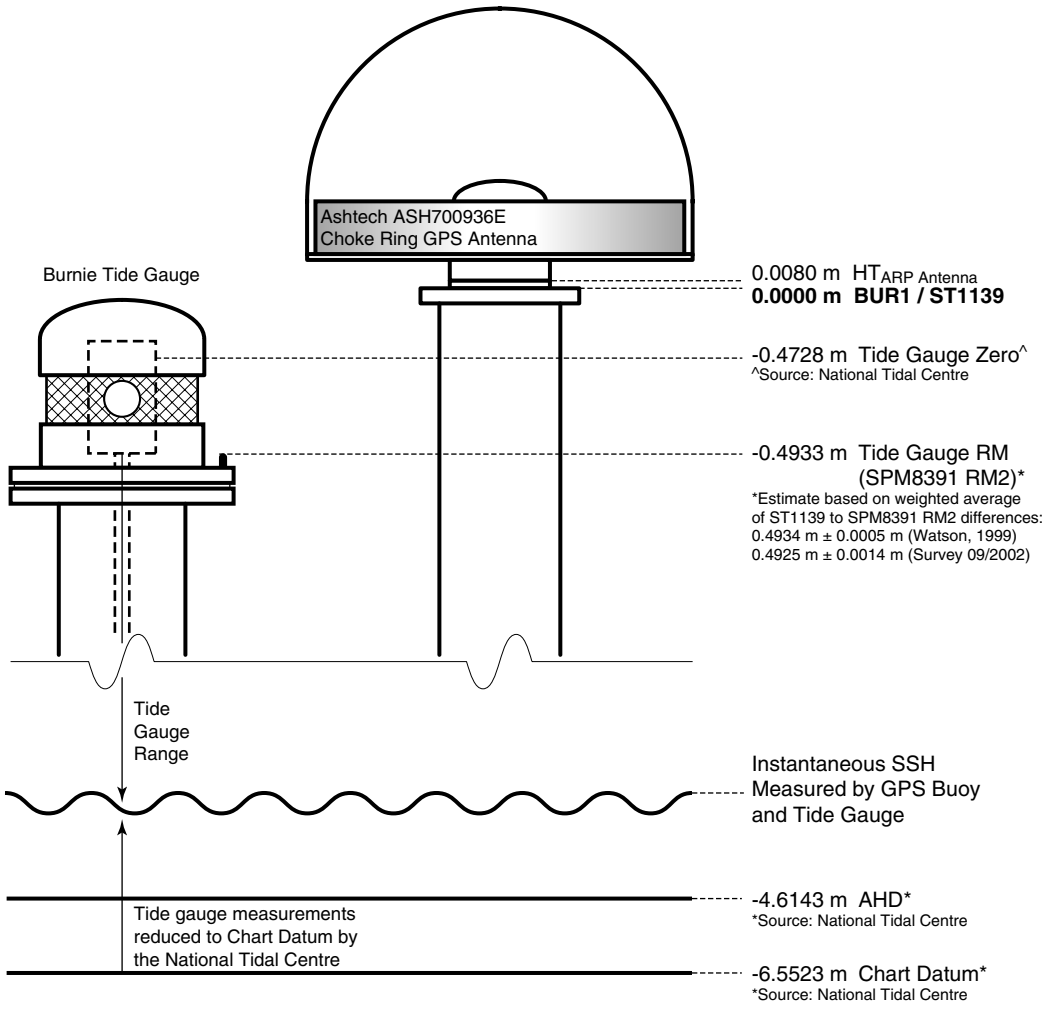

Figure 5-5 Datum differences between the collocated Burnie tide gauge and continuously operating GPS reference station.

5.4.3 In Situ Verification of the Burnie Gauge

The GPS buoy verification of the Burnie gauge was carried out on the 13th May, 2003 during moderate weather conditions (wind speeds averaging approximately 8 ms^{-1} from 117-150 °T over the duration of the experiment, see Figure 5-3). The GPS buoy was tethered (see §5.3.1.1) approximately 95 m from the tide gauge and GPS reference station (Figure 5-3). Approximately 18 hours of GPS data were obtained at 1 Hz from the buoy and reference station (01:48:30 to 20:05:39 UT). Processing was conducted as described in §5.3.1.

Both the tide gauge and GPS buoy data were reduced relative to the tide gauge zero for the regression analysis. To reflect an identical sampling strategy to the tide gauge, a filter was required for the 1 Hz GPS buoy data. A simple weighted box-car averaging filter was implemented with weights derived from the 1-sigma uncertainties placed on the 1 Hz height estimates from the TRACK GPS processing software. As the GPS buoy samples the sea surface without the protection of a stilling well, the effect of changing the length of the averaging filter was investigated. Figure 5-6 shows the variability of the filtered buoy - tide gauge time series against the length of the averaging filter used. Minimum variability between the two time series is achieved using a filter length of approximately 3 minutes duration, although within the uncertainties of the tide gauge measurement the filter length varies between ~2-6 minutes.

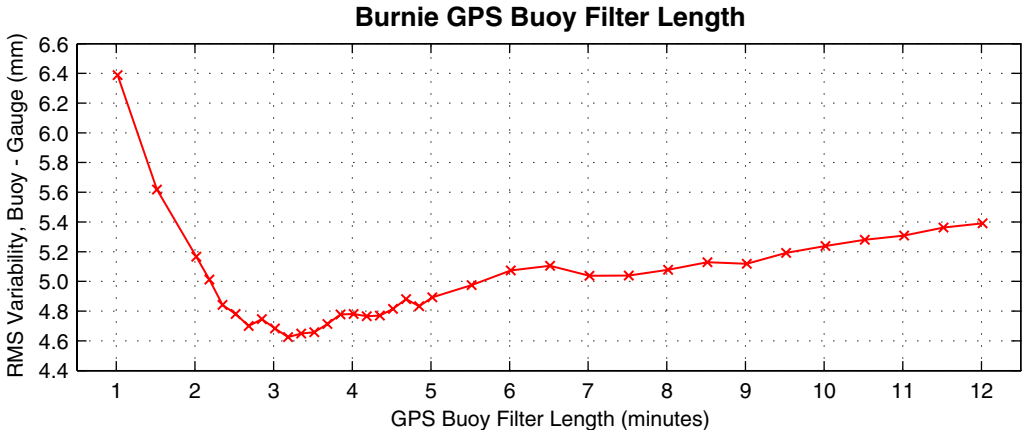

Figure 5-6 Variability (1 standard deviation) of the residual time series (filtered buoy – tide gauge), for various averaging durations of the GPS buoy data.

The tide gauge, raw and filtered and GPS buoy data are shown in Figure 5-7(a). First inspection of the 1 Hz GPS buoy results show a dynamic range in sea level at the 0.5 m level during the time of survey. The ~18 hour observation period successfully spans a complete semi-diurnal tidal cycle with a range of approximately 2.5 m. During the deployment the minimum and maximum ranges observed to the sea surface from the tide gauge zero were 0.83 m and 3.30 m respectively.

The uncertainties placed on the final filtered GPS buoy estimates (Figure 5-7b) are computed from the 1 Hz height uncertainties, assuming independent estimates every 30 seconds. The assumption of independent estimates every 30 seconds is somewhat subjective and is discussed in detail when reviewing the error budget (§5.4.3.2).

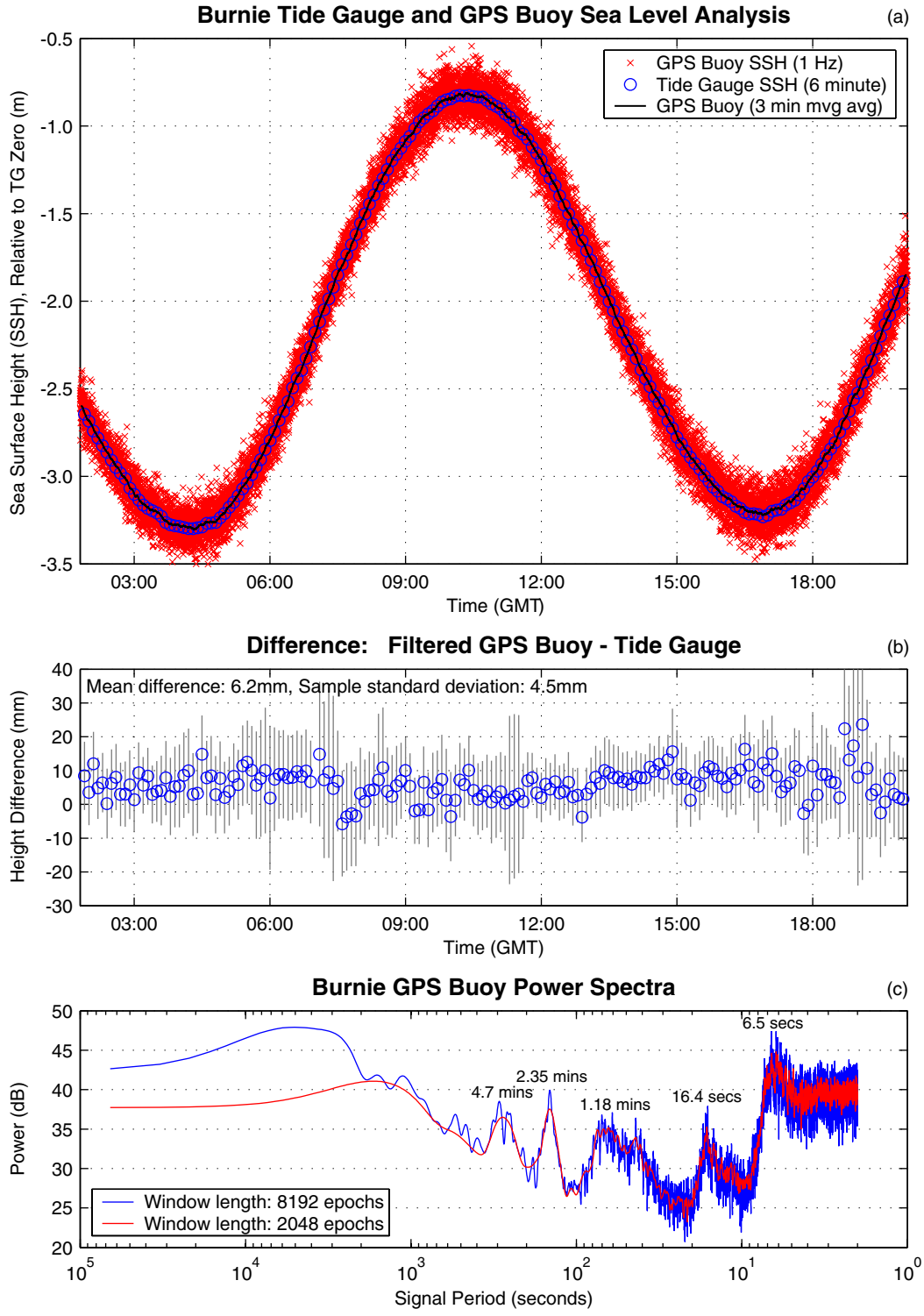

Figure 5-7 Burnie verification results using temperature corrected tide gauge data (as per Hunter, 2003). (a) Sea surface height estimates from both the tide gauge and unfiltered and filtered GPS buoy data. Note heights are relative to the tide gauge zero. (b) Residual difference between the filtered GPS buoy data and the tide gauge. (c) GPS buoy power spectra, note the high frequency swell (6.5 seconds period) and power bands at 2.35 and 4.7 minute periods respectively.

An important investigation at the Burnie site was the analysis of the temperature dependence of the gauge. As the gauge is mounted against a south-west facing concrete pier wall, temperature gradients may be expected if subjected to direct sun in the afternoon hours. Hunter (2003) provides an example from a similar gauge installed at Port Arthur in Tasmania. The Port Arthur gauge (see Pugh et al., 2002, for further details) was subjected to radiant heating from the sun at specific times of the day, especially over the summer months. Over a two year period, the temperature difference along the sounding path was typically ~1 °C, however at times it reached ~9 °C. Corrections to the range during these extreme periods approached 30 mm. During typical conditions, corrections due to the thermal gradient were at the 4 mm level, whilst corrections for expansion and contraction of the calibration tube (hence variation of the ratio method of self calibration described in Lennon et al., 1992) were at the 2 mm level.

Tide gauge data over the duration of the verification experiment (Figure 5-7a) have been corrected for temperature dependent effects as per Hunter (2003). Over this period, the correction corresponding to temperature variability down the sounding tube was quite small, exhibiting the expected diurnal heating and cooling cycle. The mean correction was 0.8 mm with the variability over the length of the record of 1.6 mm (1 standard deviation). The correction corresponding to the contraction of the calibration tube length had a mean value of 2.0 mm, with variability over the duration of the experiment at 1.6 mm (1 standard deviation). This is representative of cooler conditions over the duration of the deployment when compared to the standard 20 °C calibration temperature. The combined temperature dependent correction had the effect of reducing the residual difference between the tide gauge and filtered GPS buoy, as shown in Figure 5-7(b).

The residual signal shown in Figure 5-7(b) shows a number of outlier data points at approximately 08:00 and 19:00 GMT. These data points coincide with periods of poor satellite geometry, and hence degraded accuracy in the kinematic GPS solution. This degradation is reflected in the sigmas placed on the filter SSH estimates. A number of conclusions may be drawn after first inspection of residuals shown in Figure 5-7(b):

- The overall mean offset between the filtered GPS buoy and tide gauge data is +6.2 mm, indicating the gauge is measuring long in comparison to the GPS buoy. Note this offset includes error contributions from the entire system including the tide gauge, GPS buoy and datum connections. The

error budget and significance of this estimate is discussed in the following section.

- The standard deviation of the residual time series is at the 4 to 5 mm level which is an exceptional result. This low variability confirms the precision of both measurement systems in addition to highlighting that the GPS buoy is capable of precise sea level measurement in the presence of swell and wind driven waves approaching 0.5 m in dynamic range.

- The residual time series appears marginally non-linear over the duration of the deployment with smaller residuals on average during the period of high tide (shortest tide gauge range). This non-linearity is investigated during the regression analysis in the following section.

The power spectra computed from the 1 Hz buoy data (Figure 5-7c) reveals a range of interesting phenomena operating within the harbour. The spectra are computed by firstly removing the underlying tidal signal then estimating the power spectral density using Welch's averaged, modified periodogram method (Welch, 1967). The tidal signal is removed by solving for a linear offset, rate and amplitude and phase of the dominant K1, M2, M4 and M6 tidal constituents, using the astronomical frequencies given by Pugh (1987). Removing these four successively higher tidal frequency constituents (diurnal, semi-diurnal, four times per day and six times per day) is adequate to yield the underlying low frequency signal over the ~18 hour period. The spectra are then computed using two different windowing lengths in order to vary the frequency resolution of the estimator at different parts of the spectrum. The results (Figure 5-7c) show a dominant power band corresponding to the regular swell with a period of ~6.5 seconds. This frequency is consistent with theory given the approximate depth, fetch and wind speed at the time (Pond and Pickard, 1983). Progressing to lower frequencies, power at lower (yet significant) levels exists at periods around ~16 and ~70 seconds (1.18 minutes). Interestingly, the ~70 second frequency beats clearly at a period of ~2.35 minutes, and again (with less power) at ~4.7 minutes. These lower frequency signals are likely to reflect local harbour bathymetry, exacerbated by the unusual south easterly winds during deployment.

5.4.3.1 Regression Analysis

The regression analysis at the Burnie site reveals several interesting results (Figure 5-8). The weighted least-squares regression (as per Eqn 5-4) was completed using the filtered GPS buoy data and uncertainties as calculated in §5.4.3. Figure 5-8(a) shows the scale parameter estimate (α) of 0.99821 $\pm$ 0.00095 and offset parameter estimate (β) of 0.0020 $\pm$ 0.0023 m (error estimates from least-squares regression using conservative error budget estimates of GPS buoy SSH precision). The scale parameter appears significant while the offset parameter is indistinguishable from zero. These estimates translate to the tide gauge measuring longer than the GPS by +7.9 $\pm$ 3.9 mm at the lowest tidal level during the survey. At the highest tide level (shortest range), the gauge measures long by +3.4 $\pm$ 2.4 mm. Recall the mean difference between two datasets (neglecting the regression analysis) was +6.2 mm as shown in Figure 5-7(b).

Residuals from the regression are shown in Figure 5-8(b). As expected, the data are clearly clustered with increased samples at the tidal extremes (slowest rate of change). There are also a greater number of points clustered around low tidal levels as two tidal minima were observed and only one maxima (see Figure 5-7a). The residuals appear to be normally distributed (Figure 5-8c,d) and there is no structure within the residuals to suggest any higher order non-linear behaviour between the two time series.

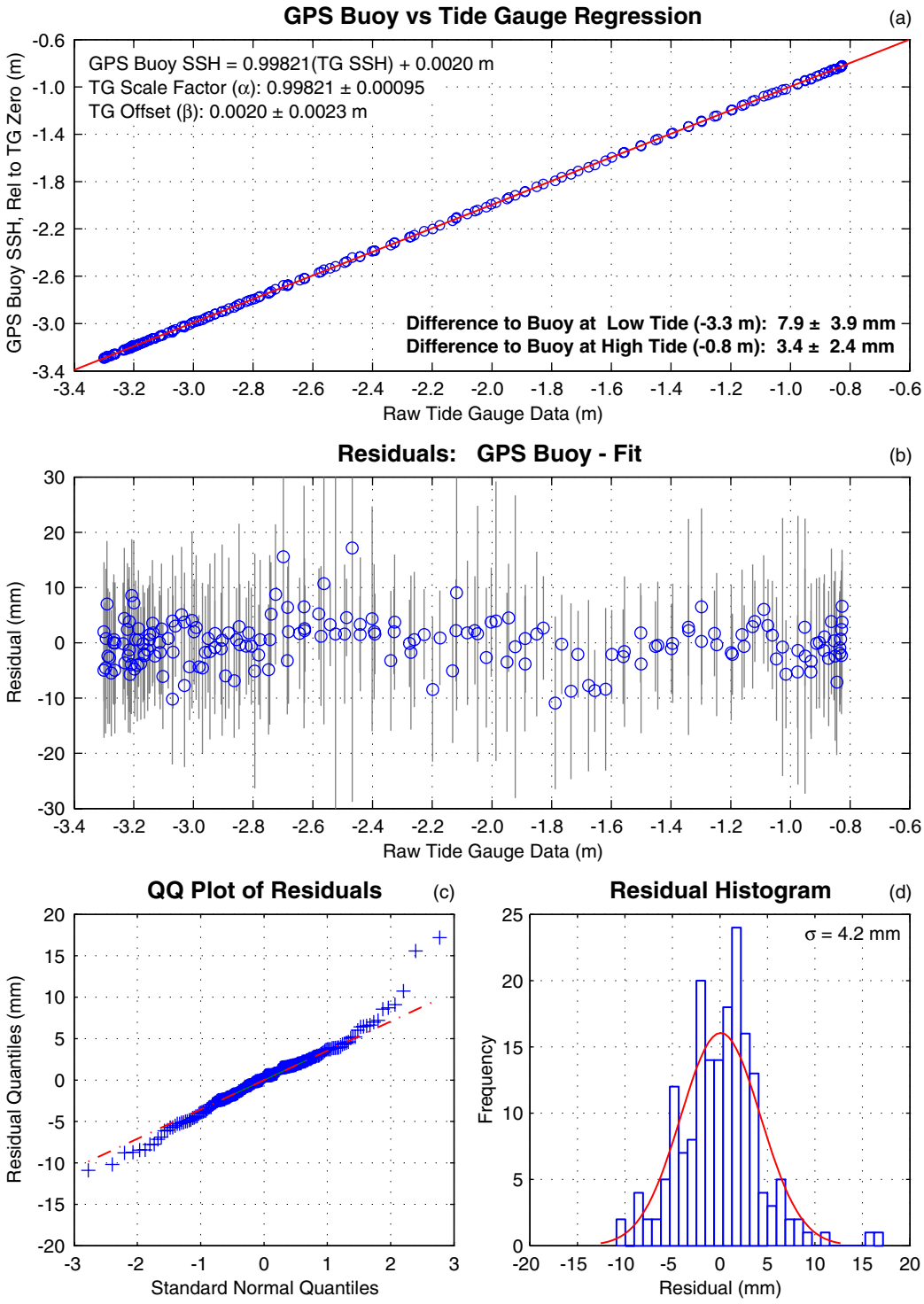

Figure 5-8 Burnie GPS buoy and tide gauge regression. Note filtered GPS buoy and temperature corrected tide gauge data have been used in this analysis. (a) GPS buoy versus tide gauge SSH, relative to the tide gauge zero. (b) Regression residuals. (c) Empirical quantile-quantile plot of the residuals. (d) Histogram of residuals and normal distribution probability density function.

5.4.3.2 Error Budget

To assess the statistical significance of the regression parameters it is important to review an error budget. The error budget is divided into two parts, with the first including terms that are invariant to the averaging process and hence represent the overall limit in absolute accuracy. These include terrestrial level connections between the tide gauge and GPS reference station (~1 mm), the connection between the tide gauge levelling fixture to the tide gauge zero (~0.5 mm), the height of the GPS buoy antenna above the mean water level (~1 mm) and the mean effect of the antenna domes (~1 to 2 mm). Additional terms include the error associated with neglecting the geoid slope ($<$ 2 mm over 100 m baseline, see Figure 5-3) and the potential effects of sea surface topography (assume $<$ 2 mm given conditions at the time). The root sum square estimate for these components (~3.6 mm) indicates the absolute error floor for this technique.

The second component of the error budget includes terms which reduce with the averaging process and are hence minimised by increasing the verification deployment period. These terms must be included in the regression analysis to derive error estimates on the regression parameters. The terms include random errors associated with the tide gauge range measurement. Assuming independent 1 Hz estimates, the final uncertainty associated with the tide gauge measurement is minimised by taking the average over the 180 samples used to compute each tide gauge SSH estimate. The "random" error contribution from the tide gauge is therefore expected to be at (or less than) the 1 mm level. Systematic effects associated with the tide gauge are ignored as they are the quantity of interest in the verification methodology. The error associated with the filtered GPS buoy SSH estimates is complicated by the systematic nature of the GPS processing. Error estimates computed by TRACK for each individual 1 Hz SSH estimate are dependent on the a priori estimates of carrier phase measurement precision. Using a standard phase measurement precision of 10 mm produces 1 Hz SSH sigmas at the 20-30 mm level. To account for systematic effects, the precision of the filtered GPS buoy SSH estimate is computed assuming independent estimates every 30 seconds. The GPS error term for each filtered GPS SSH estimate is therefore at the 8 to 12 mm level, clearly dominating the error budget. These estimates are incorporated into the weighted least-square regression yielding conservative error estimates of the regression parameters of interest.

5.4.4 Summary

The tide gauge verification experiment at the Burnie site has demonstrated the strength of the GPS buoy technique to achieve an independent, in situ verification of an acoustic tide gauge. Regression analysis between the GPS buoy and tide gauge data has shown that the technique can (importantly) determine range dependent (scale) errors with accuracies at the 1-1.5 mm per 1 m of path length with ~18 hours of data. The Burnie gauge appears to have a marginal residual scale error (following temperature correction), measuring longer than the GPS buoy by +7.9 ± 3.9 mm at the lowest tidal level, and +3.4 ± 2.4 mm at the high tide level. The difference between these estimates is considered significant considering the conservative error budget adopted. More data are required to categorically determine if the scale error is significant as expected.

The altimeter calibration methodology presented in Chapter 4 is reliant on the GPS buoy solutions to define the coordinate datum for the mooring array at the offshore comparison point. When utilising the tide gauge data (outside of the period when the mooring was deployed), the height datum of the tide gauge is effectively still defined by the GPS buoys (see §4.4.3). All geometrical differences between the mooring SSH and tide gauge SSH are removed when computing the offset and tidal differences between the two sites. When using this technique, any constant offset error in the tide gauge is therefore eliminated in the differencing process. Scale error is partially minimised when the tidal analysis is computed between the two sites (with the scale being absorbed into the tidal amplitude differences). Other absolute altimeter calibration methodologies are however much more sensitive to errors at the tide gauge (Harvest platform for example, Haines et al., 2003). Any methodology which is reliant on transferring the height datum from a GPS reference point (or other space geodetic technique) to the tide gauge and subsequently to the water surface will be adversely affected by both scale and offset errors at the tide gauge.

Potential contributing factors to the small range dependent error at the Burnie gauge include inaccuracies in the installation of the gauge (a deviation of the sounding path of ~2° from the vertical would introduce the scale error observed), inaccuracies in the calibration tube length, insufficient modelling of the expansion and contraction of the sounding tube (and calibration hole) due to temperature change or other un-modelled temperature effects, such as temperature variation in the sensor controller itself.

The effects of correcting the tide gauge observations for thermal effects (as per Hunter, 2003) were also shown to be significant. Whilst the correction was only at the 2-3 mm level, the correction was systematically positive due to the cooler conditions (when compared to the standard laboratory temperature of 20 °C). There is no doubt the overcast conditions at the time of the comparison minimised the thermal effect, preventing any significant thermal variability within the sounding tube. Given these results and those from a similar gauge at Port Arthur, seasonal heating and cooling of the calibration tube over a year has the potential to cause a systematic error in the annual and semi annual solar tidal constituents at the 2-5 mm level.

5.5 Sea level measurement in the Sub-Antarctic

5.5.1 The Macquarie Island Tide Gauge

Macquarie Island (54° 30' S, 158° 57' E) lies in the Southern Ocean approximately 1500 km to the southeast of Australia and 1300 km north of the Antarctic continent. For over 50 years the Australian Antarctic Division (AAD) has operated a scientific research station at the northern end of the Island. The island represents one of the few locations in the Southern Ocean where in situ sea level observations are possible, highlighting its importance to the geodetic and oceanographic communities (Tait et al., 1996). Many attempts have been made to observe sea level at Macquarie Island, with the first recorded attempt in 1912 by members of the Australasian Antarctic Expedition (AAE). Later in 1948 a second attempt was made and subsequently several attempts at acquiring long term sea level measurements were undertaken (Summerson and Handsworth, 1994). The extreme environmental conditions at Macquarie Island are simply not conducive to tide gauge measurement, with shore mounted systems destroyed by heavy seas and several bottom mounted units lost. In addition to extreme wave energy, excessive kelp and other marine growth and an exceptionally corrosive environment add to the difficulties faced at the Island.

The Australian Antarctic Division have persevered and installed two unique gauges at the Island, operating more or less continuously since December 1993. Both gauges are installed in inclined shafts drilled through the coastal rock extending into the water below. The gauges consist of an Aquatrak acoustic gauge and a vented pressure gauge. The installation configurations are the first of their type, as described in Summerson and Handsworth (1994). The use of an acoustic gauge in an inclined position raises several technical problems, primarily the necessity to accurately determine the inclination of the hole to enable the reduction of the observed 'inclined' sea level to an estimate relative to a vertical datum. The absolute position of this vertical datum and the effect of the relative inclination of the acoustic signal and water surface are other problematic issues. The acoustic gauge forms the focus of this case study.

The location of the Macquarie Island tide gauge with respect to the AAD research station and GPS reference stations is shown in Figure 5-9 and Figure 5-10.

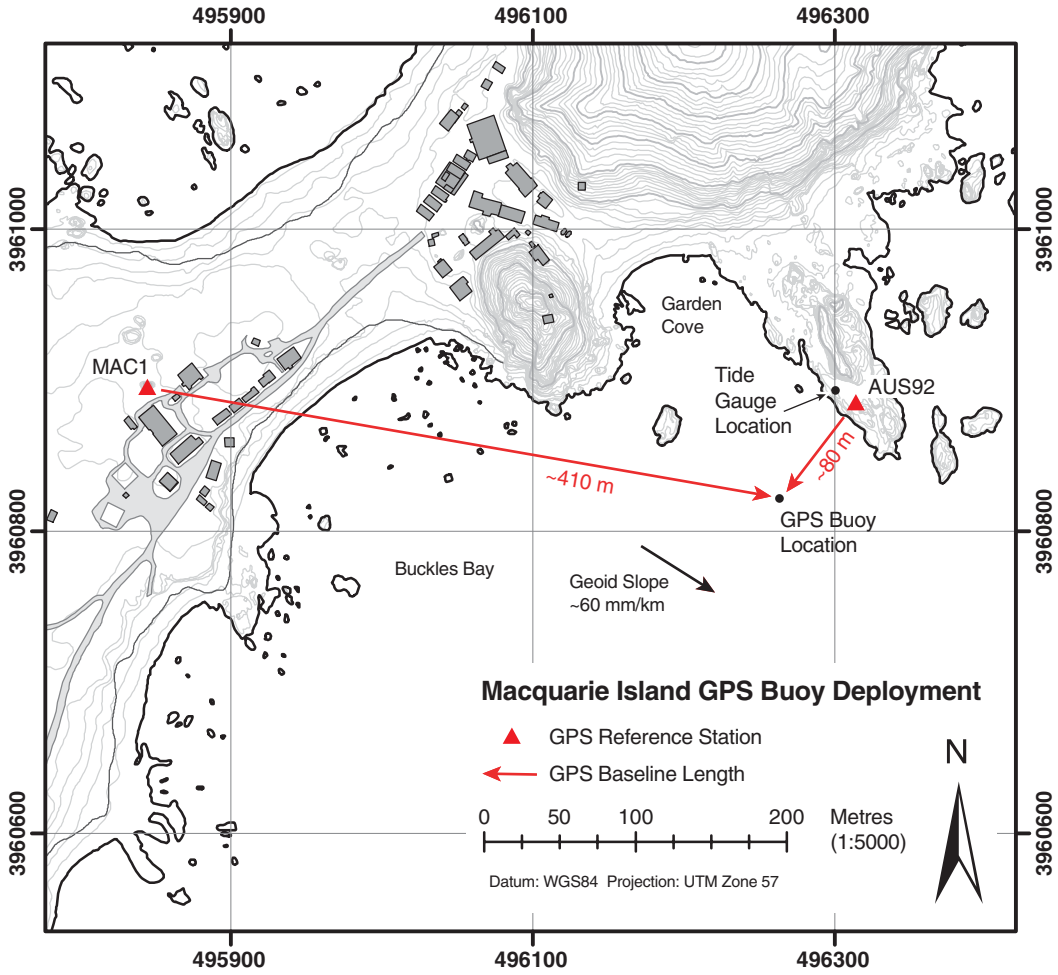

Figure 5-9 *Macquarie Island tide gauge and GPS station locations.*

Figure 5-10 *Photograph of the tide gauge and GPS station locations looking to the northeast. The prevailing weather is left to right across the image.*

The sampling strategy at the acoustic gauge is also different to the standard NTC configuration. Early tidal observations at Macquarie Island in the late 1940s revealed a pronounced oscillation with a period of approximately 6 minutes, lasting over 2 days (Longuet-Higgins, 1967). This oscillation is revisited in §5.5.4. Assuming the continued existence of this oscillation, it was considered that the standard NTC logging configuration would under sample the ~6-minute period signal. The sampling strategy was therefore modified to log SSH estimates every 3 minutes. Each 3 minute sample consists of an average of 175, 1 Hz samples. Consecutive SSH estimates from 180 samples cannot be made due to a limitation in the Aquatrak controller (hence the reduction to 175). A time stamp adjustment is required to ensure the time stamp refers to the centre of the 175 records, rather than 180.

5.5.2 Datum Connections at the Macquarie Island Acoustic Gauge

The external levelling fixture at the Macquarie Island acoustic gauge is marked on the brass rim of the tide gauge housing assembly. This point is periodically connected using terrestrial levelling techniques to various tide gauge benchmarks (TGBMs) and the permanent ARGN GPS site on the island (Geoscience Australia, 2003b). The determination of the vertical datum of the acoustic sensor is dependent on an offset measurement within the housing assembly and the measurement of the inclination of the gauge itself.

The inclination of the hole was measured by R. Handsworth (AAD) in September 1994 (Figure 5-11). The inclination was measured at 0.5 m increments down the shaft using a T2 theodolite and observing to the centre of a light lowered down the shaft. The mean observed angle was 0.5729 Radians (~ 32° 49' 29"). Over the length of the shaft, the inclination varied through a range of 0.001 Radians (~ 0° 3' 30"). The measurement of the shaft inclination was complicated by the inability to observe on both faces due to instrument malfunction (personal communication, R. Handsworth, 2004). It is therefore very difficult to assess the accuracy of the inclination estimate. As part of this study the T2 instrument has since been located and the vertical collimation error determined to be approximately 50". It is unlikely the instrument has been used since the Macquarie Island survey. Whilst the collimation error is small, there is no redundancy on the observed estimate of shaft inclination, hence its reliability is uncertain.

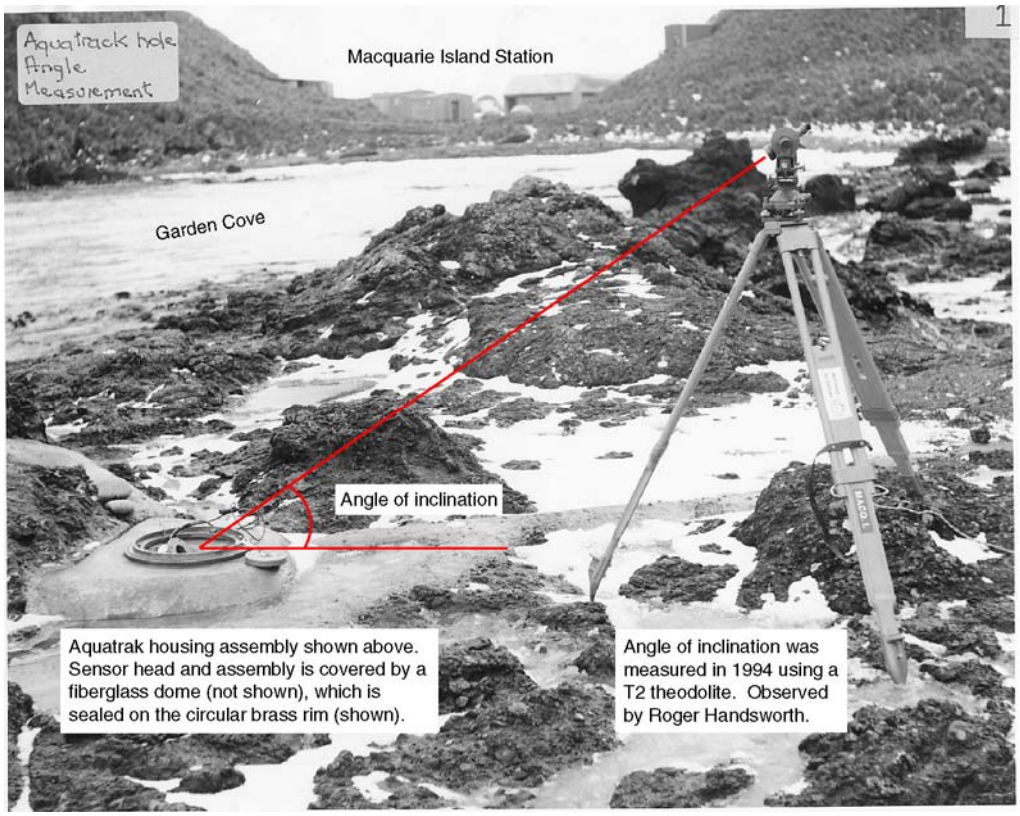

Figure 5-11 The Macquarie Island acoustic tide gauge site. Note the T2 theodolite being used to determine the inclination of the shaft. Photo looking northwest towards the station area. (Image courtesy R. Handsworth).

Various offsets within the acoustic gauge assembly have been determined by NTC during the sensor calibration. Other estimates, such as the vertical distance between the levelling fixture on the brass rim to the Aquatrak collar, were determined using in situ measurements by R. Handsworth during installation. A schematic view (in section) showing the various instrumental offsets and datum connections is shown in Figure 5-12.

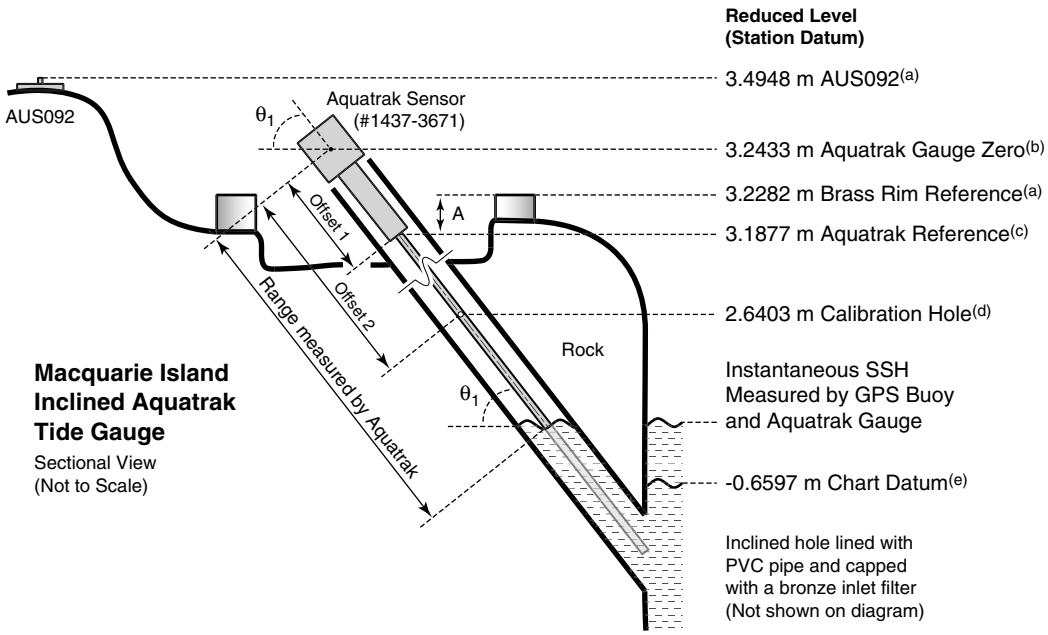

Notes:
(a)Adopted mean height from http://www.ga.gov.au/nmd/geodesy/antarc/macquari.pdf
(b)Computed from Aquatrack Reference RL + Offset 1 * Sin (θ_1).
(c)Computed from Brass Rim RL - Offset A.
(d)Computed from Aquatrack Gauge Zero RL - Offset 2 * Sin (θ_1).
(e)The Chart Datum is defined by NTC as 3.3 m below the RL of the calibration hole.
Note the RL of the calibration hole is dependent on the choice of θ_1.

θ_1 = 0.5729 Radians (32.8247˚). Observed by R. Handsworth 1999.
A = 0.0405 m. Observed by R. Handsworth 1996.
Offset 1 = 0.1025 m. Observed by the National Tidal Centre during calibration.
Offset 2 = 1.1124 m. Observed by the National Tidal Centre during calibration.
Note a rounded estimate of θ_1 (33˚, 0.576 Radians) was adopted by NTC for processing.

Figure 5-12 Schematic diagram of the inclined acoustic tide gauge at Macquarie Island. Reduced levels of the various datum surfaces are shown relative to the station datum (Geoscience Australia, 2003b).

5.5.3 In Situ Verification of the Macquarie Island Gauge

An in situ verification of the Macquarie Island gauge is required due to the unique nature of the installation configuration. The GPS buoy methodology was ideally suited to this application, enabling verification of the absolute datum and inclination of the shaft without disturbing the gauge during the deployment.

The GPS buoy was deployed during a resupply trip to Macquarie Island on the 24th March, 2003 during particularly calm weather conditions. Wind conditions were light with the sea state limited to moderate regular swell, with an observable period around 12-16 seconds. The buoy was tethered in Garden Cove approximately 80 m from the tide gauge location (Figure 5-9). The primary GPS reference station was AUS092, located within 5 m of the tide gauge. The baseline

AUS092 to the buoy was aligned approximately orthogonally to the estimated geoid slope in the region (Figure 5-9). The geoid slope was computed using two available models. At the GPS buoy location, the estimated geoid slope using the EGM96 model (Lemoine et al., 1998) is approximately 60 mm per km, orientated with a grid bearing of ~132°. The more recent and accurate GGM01S gravity model from the GRACE mission (Tapley et al., 2004) yields a slope of approximately 40 mm per km, with an orientation of ~124°. The ARGN receiver was used as a backup reference station, located approximately 410 m from the buoy location (Figure 5-10). Approximately 16.25 hours of GPS data was obtained at 1 Hz from the buoy and reference station (23:02:57 to 15:15:41 UTC). Processing was conducted as described in §5.3.1.

Once again, the tide gauge and GPS buoy data were reduced relative to the tide gauge zero for the regression analysis. A weighted box-car averaging filter was implemented to filter the GPS buoy 1 Hz SSH estimates. As for the Burnie experiment, the effect of changing the length of the averaging filter was investigated (Figure 5-13). As expected, the minimum residual variability occurs using a filter length of about 3 minutes. The response oscillates between the 2 and 3-minute levels, most probably due to aliasing effects of the underlying 6-minute sea level oscillation. Interestingly the variability approaches a second minimum at 12 minutes which again is a function of the underlying power of the 6 minute oscillation (see §5.5.4).

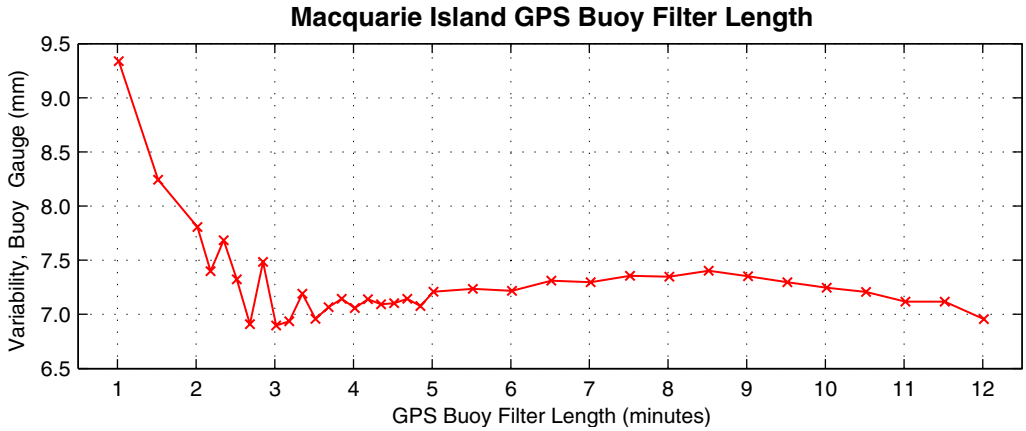

Figure 5-13 *Variability (1 standard deviation) of the residual time series (filtered buoy – tide gauge), for various averaging durations.*

As the gauge is in an inclined position, the verification and regression analysis can be undertaken two separate ways. Firstly, the observed inclination of the hole can be assumed to be error free and used to reduce the raw tide gauge estimates

relative to both the vertical direction and tide gauge zero. The regression analysis therefore solves for any residual scale and offset error between the corrected tide gauge and GPS buoy SSH estimates. This case is defined as scenario 1.

Secondly, scenario 2 assumes the inclination angle is an unknown parameter. The regression analysis therefore solves for scale and offset parameter, with the scale parameter reflecting the inclination of the hole (and any residual non linearity of the gauge).

The inclined shaft through the rock not only protects the tide gauge assembly from the harsh environmental conditions, it provides very good thermal insulation along the sounding path. Analysis of the temperature along the sounding tube provides little indication of any thermal profile affecting the propagation of the acoustic pulse. Temperature corrections were therefore not applied to the tide gauge time series.

Beginning with the scenario 1 analysis, the various SSH estimates are shown in Figure 5-14(a). The 1 Hz GPS buoy SSH data show a much larger dynamic wave range than the Burnie case study reaching the 1 m level during the time of survey. The data gap beginning at approximately 03:30 UT corresponds to a period of degraded satellite coverage which has hence been removed from the solution. The ~16 hour deployment successfully captured a complete tidal cycle (two minima and one maxima), with a range of 0.8 m. Relative to the tide gauge zero (in the vertical plane), the minimum and maximum range observed to the sea surface was approximately 2.8 m and 3.6 m respectively (in the inclined plane these ranges translate to approximately 5.2 m and 6.6 m respectively). The uncertainties placed on the final filtered GPS buoy estimates (Figure 5-14b) were computed using the same technique as described for the Burnie case study.

The residual signal shown in Figure 5-14(b) shows a slightly larger variability than the Burnie verification experiment, with a standard deviation of the difference time series of 7.2 mm. Given the dynamic swell conditions approaching the 1 m level this is considered an excellent result. The overall mean offset between the filtered GPS buoy and tide gauge data is +38 mm, indicating that on average the tide gauge is measuring long in comparison to the GPS buoy. Once again, the residual time series appears marginally non-linear with smaller residuals corresponding to the period of high tide. This non-linearity is investigated in the scenario 1 regression analysis (§5.5.3.1).

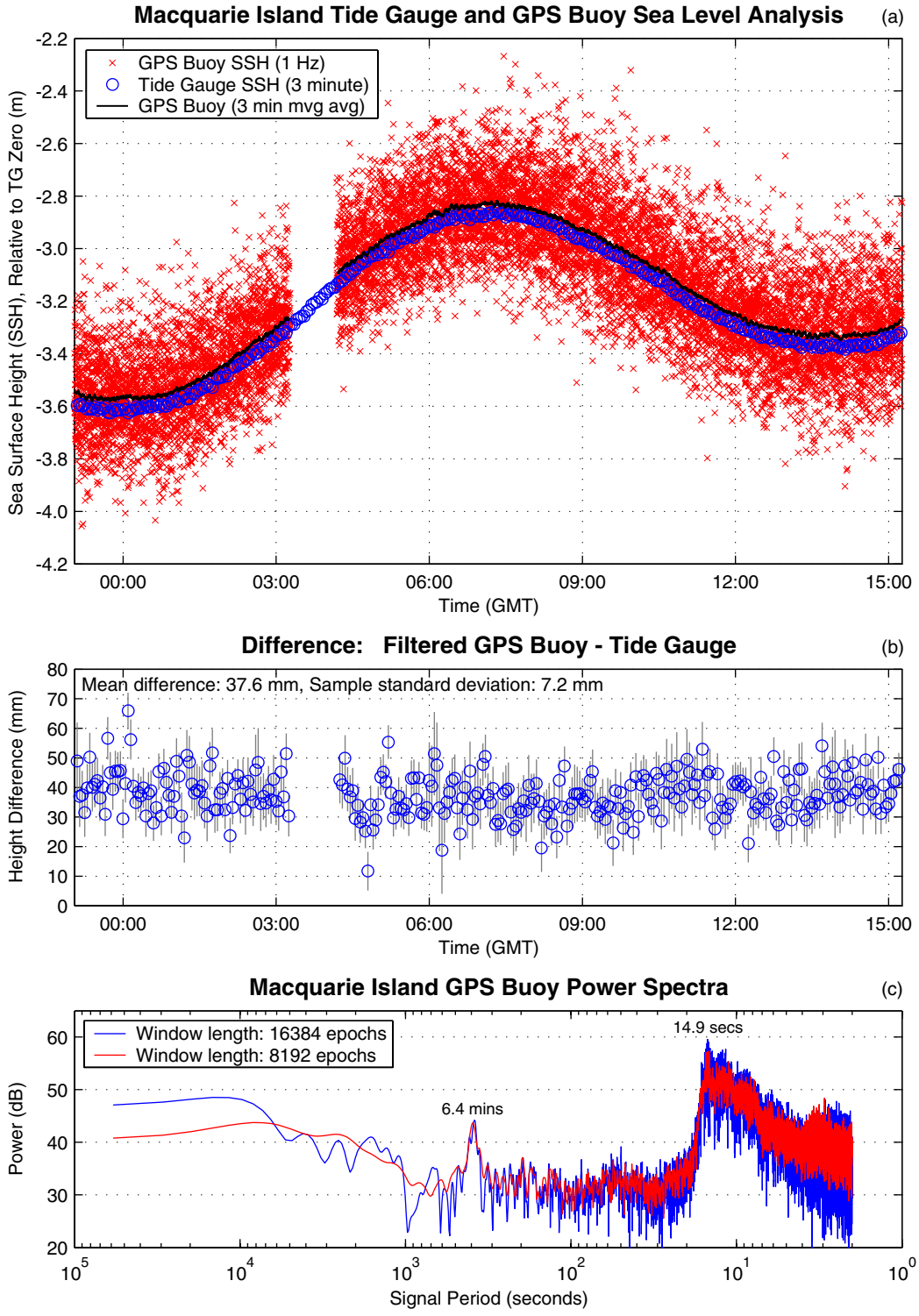

Figure 5-14 Macquarie Island verification results. (a) Sea surface height estimates from both the tide gauge and unfiltered and filtered GPS buoy data. Note heights are relative to the tide gauge zero in the vertical plane. (b) Residual difference between the filtered GPS buoy data and the tide gauge. (c) GPS buoy power spectra, note the high frequency swell (14.9 seconds period) and the dominant power bands at 6.4 minute period.

The power spectra computed from the 1 Hz buoy data (Figure 5-14c) shows the clear dominance of the swell with a period centred at 14.9 seconds. The remainder of the spectra is clear of any features with the exception of a significant peak centred at a period of 6.4 minutes. The spectra for the Macquarie Island data was computed by first removing a computed low frequency tidal signal comprising of terms including a linear offset, rate and amplitude and phase of the dominant K1 and M2 tidal constituents. The 6.4 minute signal is consistent with the oscillation alluded to by Longuet-Higgins (1967). Its confirmation by the high rate GPS data reinforces the strength of the technique in the presence of moderate swell at the 1 m level. Both the swell and periodic oscillation are re-visited in §5.5.4.

5.5.3.1 Regression Analysis – Scenario 1

The scenario 1 regression analysis (assuming a known angle of inclination) yields a scale parameter estimate (α) of 0.9925 ± 0.0017 and offset parameter estimate (β) of 0.0131 ± 0.0056 m (error estimates from weighted least-squares regression using conservative error budget estimates of GPS buoy SSH precision). Both the offset and scale parameter are clearly significant translating to the tide gauge measuring longer than the GPS by +40.2 ± 8.3 mm at the low tide mark and +34.2 ± 7.4 mm at the high tide (shortest range) level. The mean difference between two datasets (neglecting the regression analysis) was +37.5 mm (Figure 5-14b). The regression residuals (Figure 5-15b) are again clustered around the tidal stationary points (approximately -3.6 m, -3.35 m and –2.9 m respectively). The residuals appear normally distributed (Figure 5-15c,d) confirming there is no additional higher order relationship between the GSP buoy and tide gauge data.

The significance of the scale term is somewhat masked when computing differences at high and low tide given the very small range of 0.8 m. The scale parameter accounts for differences to the GPS buoy of the order of 7.5 mm (± 1 mm) per 1 m of path length in the vertical plane. Several hypotheses are proposed as the possible source of this significant non-linearity. Firstly, the thermal contraction of the sounding tube between the tide gauge zero and the calibration hole may be sufficiently great to generate such significant scale error. This is rejected as the mean temperatures remain between 5-10 °C dictating this effect would be an order of magnitude smaller than observed. Secondly, the sounding tube (and calibration hole) may have been disturbed during installation; hence the ratio self-calibration method of Lennon et al. (1992) would be generating inaccurate corrections for the

variation of the speed of sound. Finally, the assumed angle of inclination may in fact be incorrect. At this stage it is impossible to reject either of the final two hypotheses without inspection of the gauge.

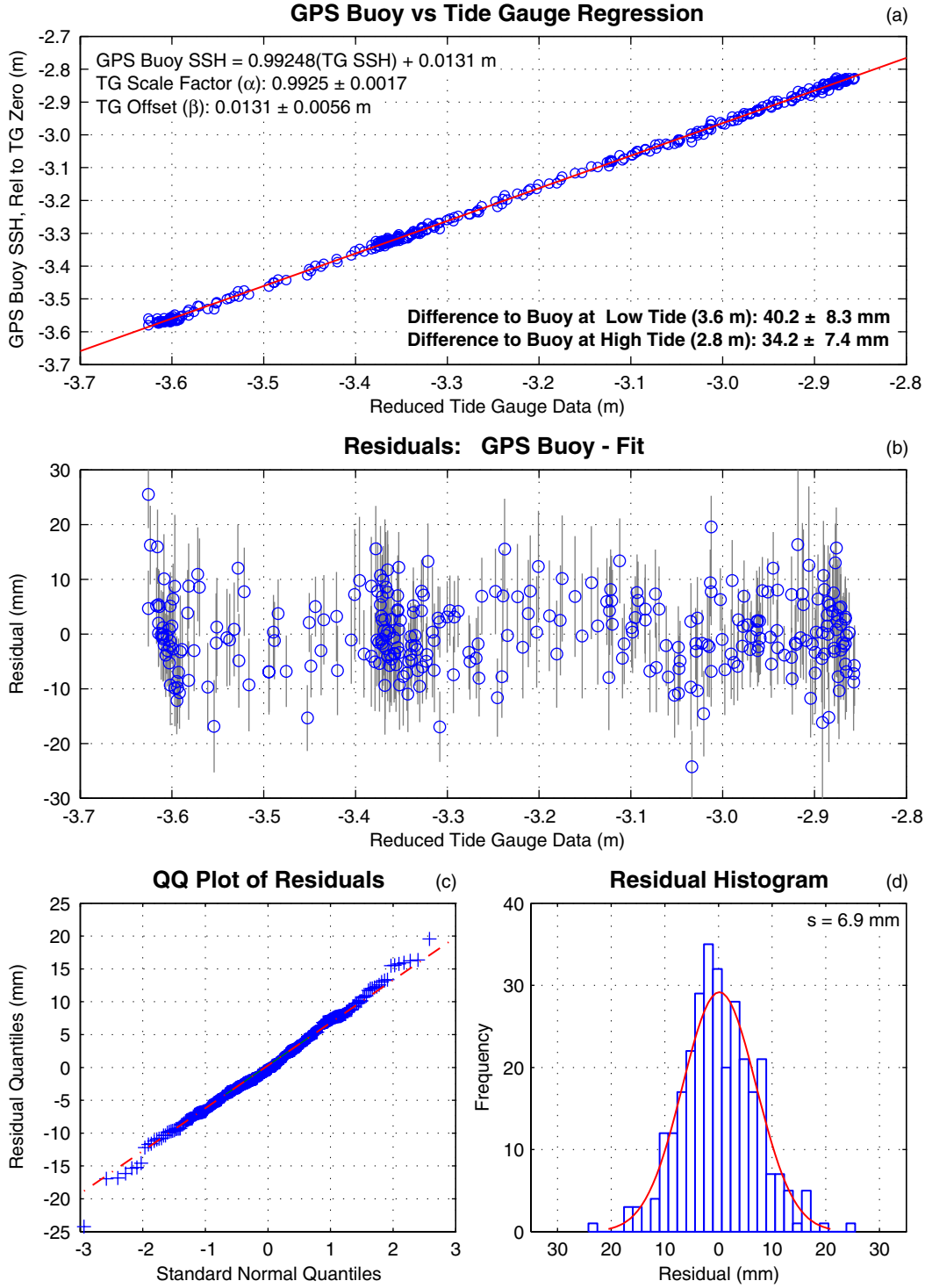

Figure 5-15 Scenario 1 regression analysis assuming a correct observed inclination angle. (a) Filtered GPS buoy versus tide gauge SSH, relative to the tide gauge zero. (b) Regression residuals. (c) Empirical quantile-quantile plot of the residuals. (d) Histogram of residuals and normal distribution probability density function.

5.5.3.2 Regression Analysis – Scenario 2

The second regression analysis (scenario 2, assuming an unknown angle of inclination) yields a scale parameter estimate (α) of –0.53799 ± 0.00093 and offset parameter estimate (β) of 0.0131 ± 0.0056 m. In this case, the scale parameter reflects the inclination of the hole and any additional residual non-linearity of the tide gauge system (caused by thermal effects for example). The scale parameter translates to a derived inclination of 32° 32' 50" ± 0° 03' 13". The derived angle is approximately 0° 16' 40" shallower than the observed angle as used for the scenario 1 regression. A component of this scale factor is residual non-linearity within the gauge system. Note that as the gauge is inclined, the effect of any small non-linearities are minimised (by a factor of approximately sin(32° 32')) when mapping the measurement to the vertical component.

The vertical offset of 13 mm is significant indicating a potential error in one of the many datum connections and NTC constants (see Figure 5-12). Despite a baseline separation of approximately 80 m, the influence of geoid slope and oceanographic effects may however be higher than expected. The various error contributions are discussed in the following section.

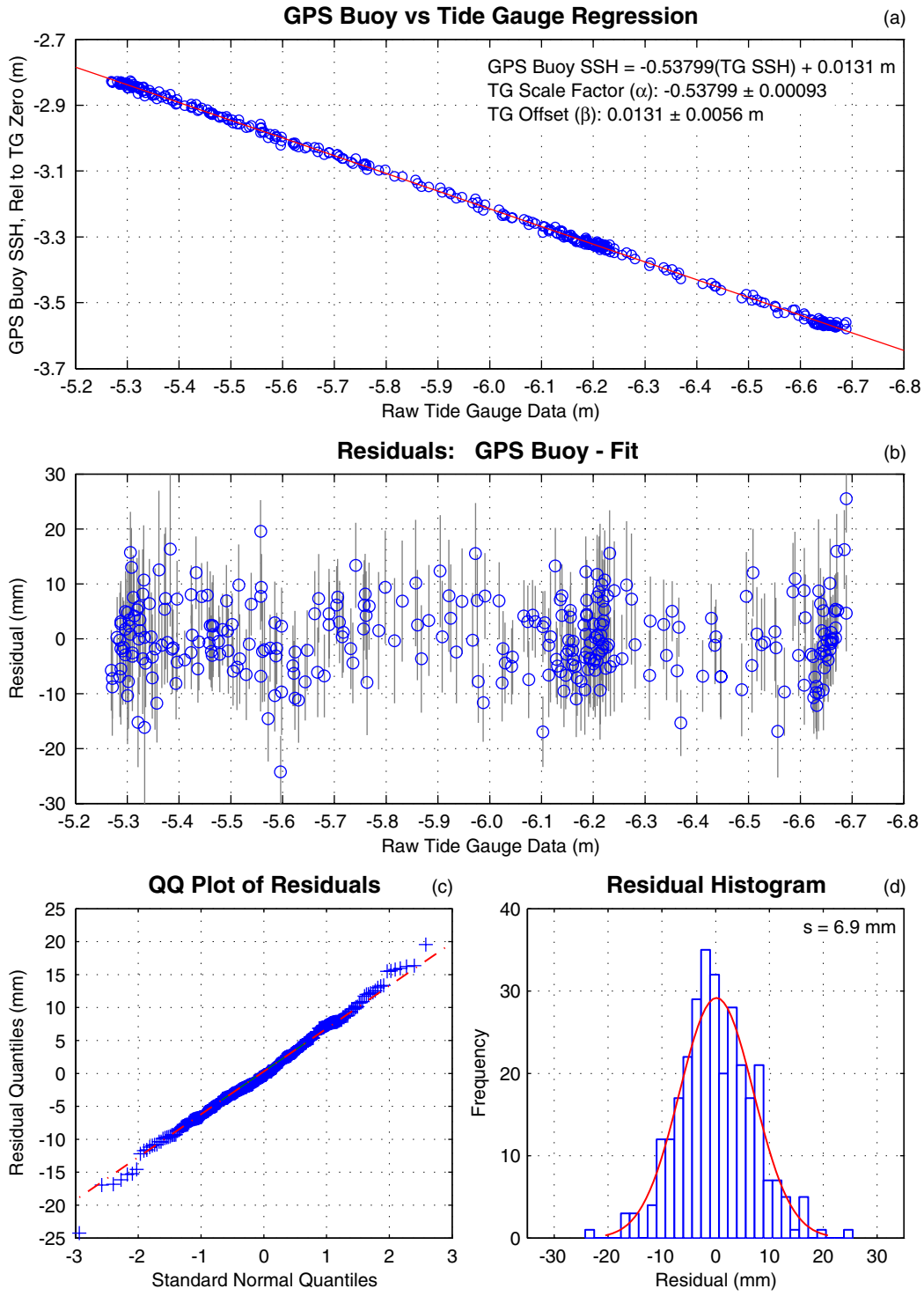

Figure 5-16 Scenario 2 regression analysis assuming an unknown inclination angle. (a) Filtered GPS buoy (vertical plane) versus tide gauge SSH (inclined plane), relative to the tide gauge zero. (b) Regression residuals. (c) Empirical quantile-quantile plot of the residuals. (d) Histogram of residuals and normal distribution probability density function.

By assuming the inclination angle of the gauge is unknown, the second scenario regression analysis derives a scale parameter which takes into consideration the inclination of the hole and any additional range dependent errors within the gauge. This holistic approach achieves an in situ calibration of the system as a whole, without differentiating between errors in the observed angle of inclination and range dependent errors within the gauge. Using this derived angle of inclination, the GPS buoy – tide gauge difference time series may be computed (Figure 5-17). The standard deviation of this sample is 6.9 mm. The same difference time series for the scenario 1 "known angle" case can be seen in Figure 5-14(b).

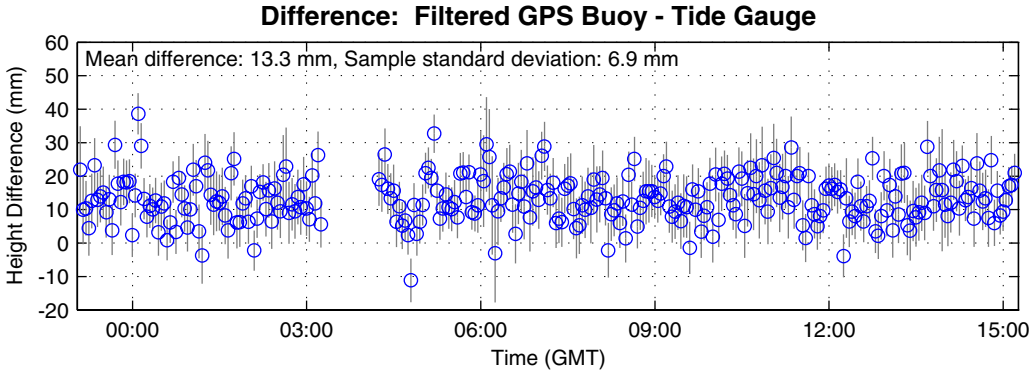

Figure 5-17 Residual difference between the filtered GPS buoy data and the tide gauge data reduced using the derived angle of inclination of 32° 32′ 50″. Note the slight reduction in variability (6.9 mm) when compared to Figure 5-14(b).

5.5.3.3 Error Budget

The error budget for the Macquarie Island case study is very similar to the Burnie verification, with most terms identical (see §5.4.3.2). Due to various redundant measurements there is no reason to suggest any of the external levelling connections (between AUS092 and the tide gauge for example) are inaccurate beyond the 1 mm level (Geoscience Australia, 2003b). An additional component is the accuracy of the antenna height of the base station (AUS092). This was measured independently three times with variability less than 1 mm.

The geoid slope is much greater at Macquarie Island compared with Burnie. The slope determined from the EGM96 model at the tide gauge site is approximately 60 mm per km. The GRACE GGM01S model provides a valuable comparison to EGM96, with a slope at the Macquarie Island site of approximately 40 mm per km. When comparing ellipsoidal versus orthometric height differences between the MAC1 and AUS092 stations, the respective geoid slopes account for only 25 mm and 13 mm (for the EGM96 and GGM01S models respectively) of the 68 mm observed difference. There is however continuing uncertainty surrounding a missing connection between the MAC1 ARP and AUS211 RM1 in the levelling results published by Geoscience Australia (2003b). This requires repeated re-observation before final conclusions can be drawn. Despite this uncertainty, the underlying direction of the geoid/ellipsoid slope is expected to be relatively accurate. Any bias introduced between the GPS buoy and tide gauge location by the geoid slope has been minimised by aligning the GPS baseline orthogonally to the direction of maximum slope.

Over an 80 m baseline it is therefore unlikely that the geoid slope has a significant effect, hence the error estimate is assumed to be less than 4 mm. Given the location and dominant swell, oceanographic effects (set-up for example) may be a significant component of the error budget and hence a contributing factor towards the observed offset. Figure 5-19 confirms the swell direction was orthogonal to the tide gauge / buoy baseline. It is only possible to speculate that the oceanographic effects are minimised due to relatively constant depth and lack of wave energy directly incident on the rocky area adjacent to the tide gauge. Future tide gauge verification experiments at the Macquarie Island site during different climatic and tidal conditions may help confirm or otherwise this hypothesis. Assuming an oceanographic contribution of less than 4 mm, the root sum square estimate for these components is at the 6 mm level. Without improved knowledge of the geoid

and potential ocean topography effects, this estimate forms the error floor for this technique at Macquarie Island.

The random component of the error budget is identical to the Burnie case study (see §5.4.3.2). These estimates have once again been incorporated into the weighted least-square regression yielding conservative error estimates of the regression parameters of interest.

5.5.4 Swell and Edge Wave Oscillations

The significant spectral peaks in the 1 Hz GPS buoy SSH time series (Figure 5-14c) warrant further analysis to determine the full potential of the GPS buoy technique. The most significant peak corresponds to a swell signal with a mean period around 15 seconds. During the deployment the swell was clearly observed from the shore and was estimated to have a period between 12 and 16 seconds. A section of 1 Hz data have been extracted to emphasise the ability of the technique to characterise the local swell regime (Figure 5-18).

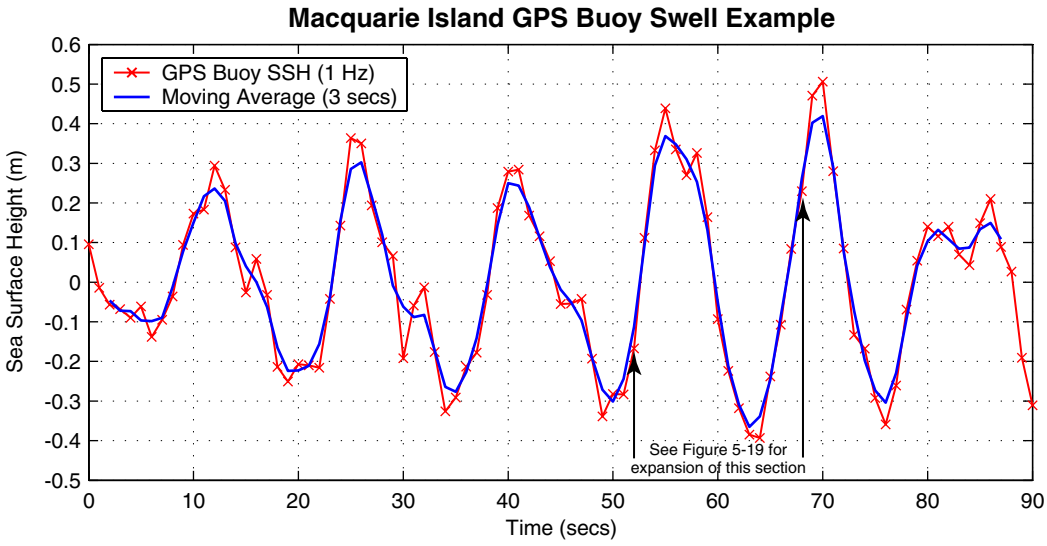

Figure 5-18 90 seconds of GPS buoy 1 Hz SSH data revealing swell with a range of 0.9 m and a period of approximately 15 seconds.

Note the variation in wave shape at approximately 15, 32, 46, 58, 73 and 84 seconds respectively. These modulations are most probably related to the reflection of the incident waves from the beach shore. Closer examination of one complete swell period (as indicated in Figure 5-18) is shown in three dimensions in Figure 5-19(a,b). Figure 5-19(b) reveals the horizontal motion of the buoy during

the swell event. During the passage of the wavefront, the buoy is displaced parallel to the wave direction. The exact direction of the shore in superimposed on Figure 5-19(b), confirming the direction of the swell and buoy displacement is orthogonal to the beach shore.

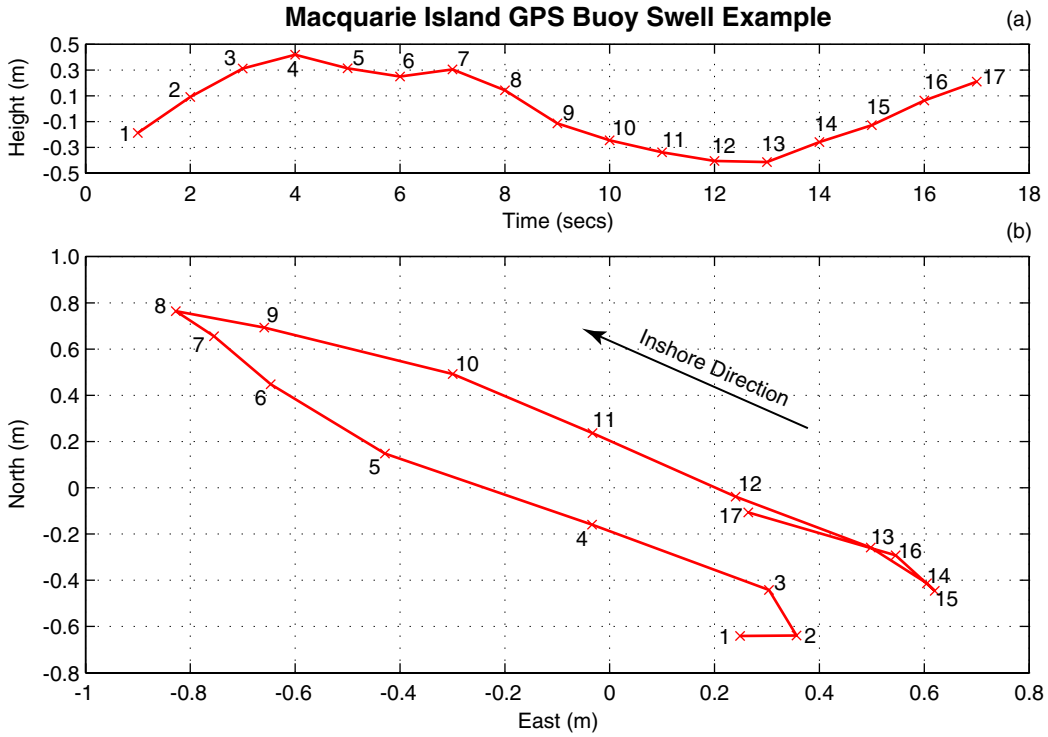

Figure 5-19 Swell signal in the 1 Hz GPS buoy results. (a) In the vertical component. (b) In the horizontal components. Note the direction of the horizontal motion and shore direction. The numbers indicate corresponding epoch count (seconds). X and Y axes show an arbitrary origin for display purposes.

The second significant spectral power band was observed with a period of approximately 6.4 minutes. The Longuet-Higgins (1967) study concluded the oscillation was most likely due to the coastal trapping of wave energy around the island. Such trapped oscillations are generally termed edge waves, as discussed in Pugh (1987). Other studies at Macquarie Island, such as the finite element tidal modelling by Henry (1996), did not progress to look at higher frequency phenomena. The most recent study by Galton-Fenzi et al. (2005) investigated a period of high rate data acquired from the Macquarie Island gauge in 2004. The Galton-Fenzi et al. (2005) study concluded the oscillation is most probably related to the fundamental natural shelf period of Buckles Bay (see Figure 5-9). The edge wave hypothesis was rejected as the oscillation was not observed on the other side of the Island as predicted in the edge wave theory. Galton-Fenzi et al. (2005)

relates the observed spread in the observed resonant frequency (between 5 to 8 minutes period) to interaction with the highly varied coastal morphology.

By utilising a simple band bass filtering technique, the shelf oscillation has been extracted from the 1 Hz GPS buoy SSH estimates. The filtering technique firstly removes the low frequency tidal components as described in §5.5.3. The resultant time series is then low pass filtered using a 91 point moving average. The 91 point sample was selected to successfully smooth the influence of the high frequency swell (period ~16 seconds) without smoothing any of the signal within the shelf oscillation frequency band. A 40 minute period between 13:00 and 13:40 UT when the oscillation was particularly active is shown in Figure 5-20. A sinusoid with period 6.35 minute has been superimposed on Figure 5-20 to illustrate the regularity of the oscillation which is in agreement with the theory presented by Galton-Fenzi et al. (2005). During this data period, the shelf oscillation has a range of 22 mm.

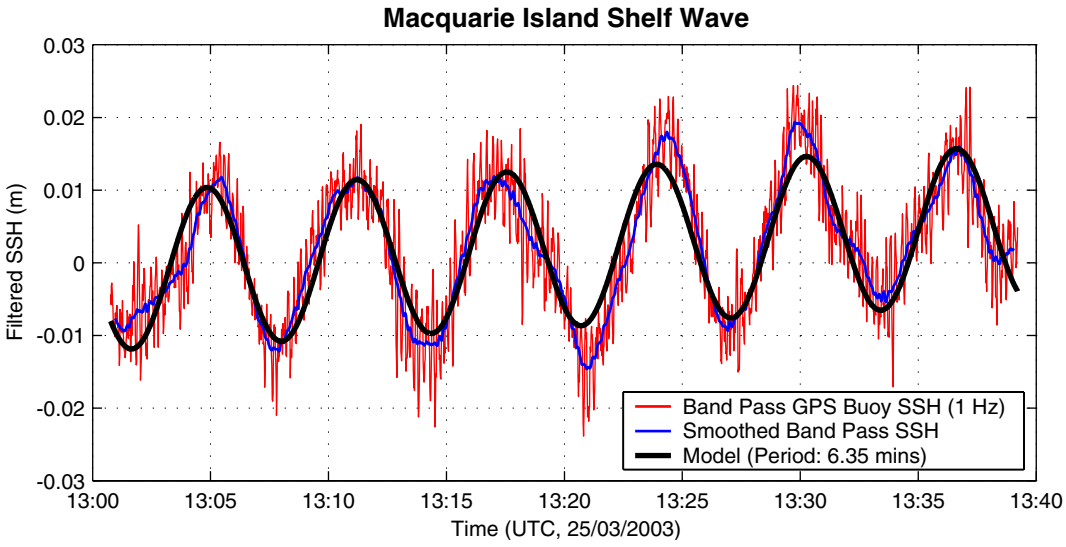

Figure 5-20 Band pass filtered GPS buoy SSH data between 13:00 and 13:40 revealing a dominant oscillation with a period of approximately 6.35 minutes. The oscillation has a range of approximately 22 mm. Note the coherence with the sinusoid model with period 6.35 minutes and amplitude 11 mm.

Further investigation into the Macquarie Island edge wave is planned for a future study. As the sampling frequency of the tide gauge is very close to the nyquist frequency of the edge wave, the effects of aliasing are to be investigated. An analysis over an extended period is proposed with measurement sites at various locations around the island to allow the observation of the relative phase of the oscillation.

5.5.5 Summary

The continuous operation of a tide gauge in the hostile environment experienced at Macquarie Island is an outstanding achievement. Local conditions have dictated an innovative approach to the gauge installation and operation. The unique installation of the Aquatrak gauge creates difficulties in defining the datum and ensuring accurate operation of the gauge. The GPS buoy verification technique is ideally suited to the Macquarie Island. Very few other practical ways of achieving an accurate in-situ calibration have been determined.

The verification experiment has firstly revealed that the inclination angle of the tide gauge hole used by the NTC is incorrect. For an unknown reason, the NTC have been utilising a truncated estimate of the angle (exactly 33°). This translates to an approximate scale error in the NTC sea level time series at the 12 parts per 1000 level. This error would therefore map into amplitudes of the tidal constituents determined by NTC.

Difficulties associated with a backup T2 theodolite, in addition to a lack of redundant measurements made in the 1994 survey of tide gauge borehole, introduces significant uncertainty in the angle measurement. The GPS buoy verification experiment can therefore provide two possible conclusions:

1. Assuming the observed angle is correct, the tide gauge system has a range dependent error in the vertical plane of approximately 7.5 parts per 1000 (7.5 mm per 1 m of tide gauge range in the vertical component). There is an additional vertical datum offset of $+0.0131 \pm 0.0056$ m.

2. Assuming the observed angle is incorrect, the GPS buoy verification technique can be modified to derive an estimate of the inclination angle. The derived angle is 32° 32' 50" ± 0° 03' 13" which is approximately 0° 16' 40" shallower than the observed angle. Note the derived angle includes any additional range dependent errors within the gauge, which cannot be decoupled from the inclination estimate during the regression analysis. The vertical datum offset remains the same for this scenario.

The first conclusion implies a significant range dependent error within the gauge, in excess of the manufacturer's specifications (Aquatrak, 2004). Considering raw range measurements between 5.2 m and 6.6 m, the implied error ranges between 39 mm and 50 mm respectively. Such an error is only possible if the distance from the

tide gauge zero to the calibration hole has been disturbed. Given the moderate and stable temperatures at Macquarie Island, it is unlikely that the error could derive from thermal contraction of the sounding tube. The alternative hypothesis is to question the accuracy of the inclination angle measurement, which leads to the second conclusion presented above.

The second conclusion provides the most accurate calibration of the complete gauge system in the absence of further information. Future routine maintenance trips to Macquarie Island shall enable the re-observation of the inclination angle and the measurement calibration hole offset in the sounding tube.

The GPS buoy verification technique has also been extremely successful in observing sea level disturbed by shelf oscillations and characterising the swell signal within Buckles Bay.

5.6 Sea level measurement in the Antarctic

5.6.1 The Davis Station Tide Gauge

Davis Station (68° 35' S, 77° 58' E) is situated on the Ingrid Christensen Coast of Princess Elizabeth Land on the Antarctic continent. Davis is the Australian Antarctic Division's most southerly permanently occupied station. Seasonal sea ice conditions around the Antarctic coastline impose the first obvious difficultly for operating a tide gauge in Antarctic conditions. Typical gauge installations, such as the acoustic gauge at the Burnie site (§5.4.1), simply would not survive the force of the seasonal ice (-2m typical thickness) if installed in the Antarctic environment. Even if a robust gauge could be manufactured, issues of freezing within the sounding tube and stilling well would still need to be overcome. Submerged pressure gauges overcome many of the environmental challenges presented in Antarctic conditions. Issues of data retrieval and datum stability must however be addressed when using a submerged pressure gauge.

The tide gauge at Davis Station began operation in March 1993 and has produced a continuous record with the exception of one main outage towards the end of 2001 (Australian Antarctic Division, 2000). The submerged pressure gauges at Australian Antarctic stations at Davis, Casey and Mawson are custom made, incorporating a Paroscientific Digiquartz™ pressure sensor (Summerson, 1995; Summerson and Handsworth, 1994). The gauge is mounted in a 700 kg mooring (Figure 5-21) which is placed on the sea floor in approximately 7 m of water.

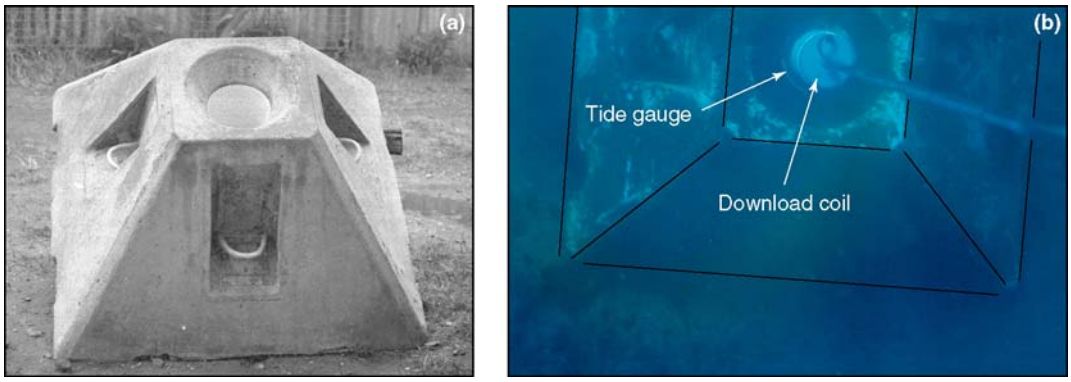

Figure 5-21 Pressure gauge mooring used at the Antarctic sites. (a) Shown out of the water. Note the central cylindrical hole for the tide gauge. (b) Shown submerged. The black lines have been added to improve definition of the mooring block. Note the location of the tide gauge and the download coil (Images courtesy R. Handsworth).

Clearly the use of a submerged gauge complicates data retrieval and the ability to physically observe and survey the datum reference point (top of the gauge). The AAD's pressure gauges are downloaded using an inductive coil which is lowered over the top section of the gauge (Figure 5-21b). As an inductive link, no physical conductive connection is required. This technique is only complicated by periods of poor visibility (algal blooms for example) when the gauge can not be seen from the surface, and hence it is impossible to guide the coil into place.

The sampling strategy involves averaging 10 minutes of 1 Hz samples, resulting in 144 records each day (the time tag is centred on the ten minute period). The location of the gauge at Davis Station is shown in Figure 5-22.

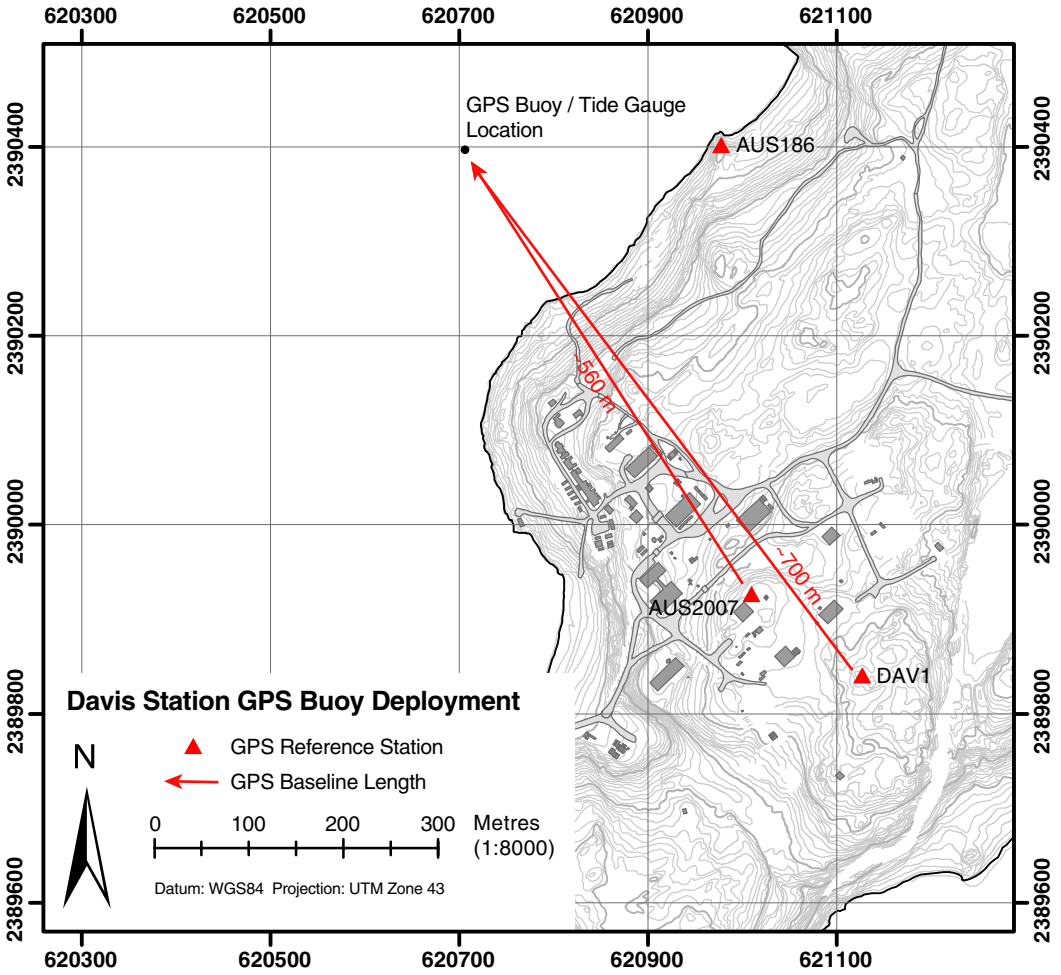

Figure 5-22 Davis Station tide gauge and GPS reference station locations.

5.6.2 Datum Connections at the Davis Station Gauge

The use of a submerged pressure gauge complicates the datum definition with respect to local tide gauge benchmarks. The tide gauge zero is known precisely with respect to the top surface of the gauge, as indicated in Figure 5-23 (not to scale).

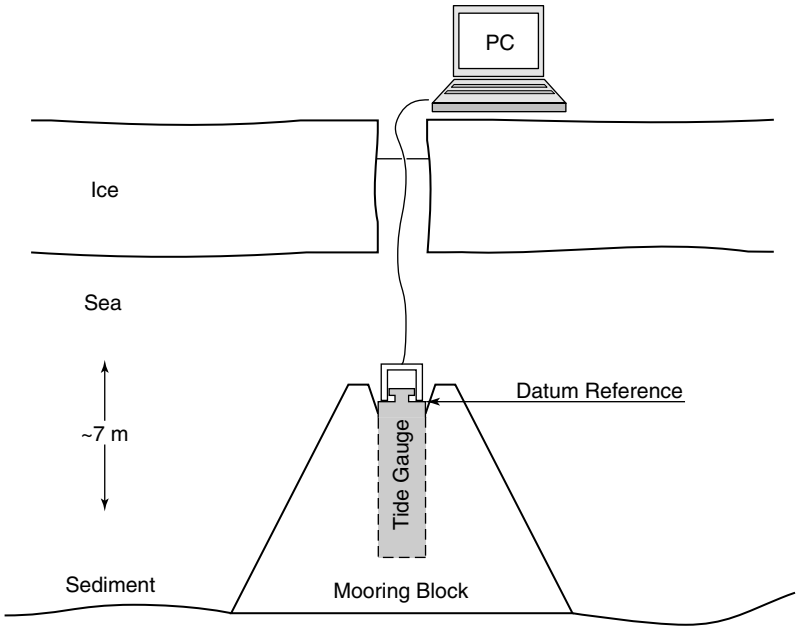

Figure 5-23 Schematic illustration of the Davis time gauge installation. The download coil is shown in place (not to scale). Note the position of the datum reference on the top of the gauge.

Two main techniques have been used at the AAD Antarctic gauges in an attempt to determine the physical height difference between the gauge reference point and local tide gauge benchmarks. Firstly, direct measurement is possible (Figure 5-24a), using a staff placed on the gauge reference point. This is complicated by the 'blind' placement of the staff on the top surface of the gauge. A custom levelling staff is also required given the ~7 m height difference. Correcting for thermal effects (contraction at low temperatures) is a further difficulty. The second technique involves timed water level measurements which are made with reference to local benchmarks. The technique requires extremely calm conditions to enable the direct observation of water level on a staff that is temporally fixed in the water, close to the gauge location (Figure 5-24b). The timed water level measurements can then be compared against the pressure gauge observations.

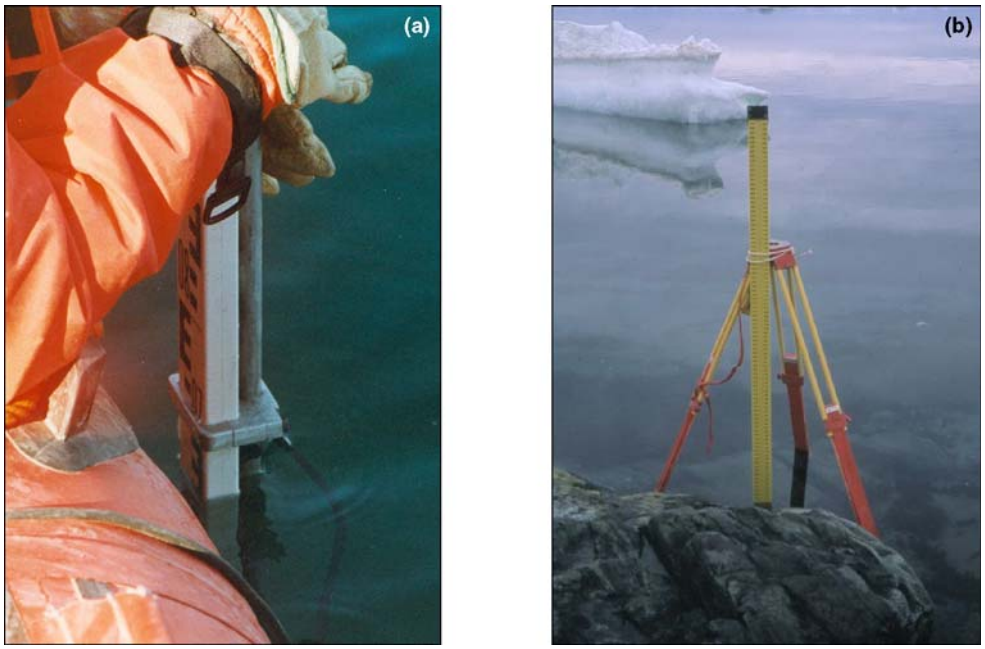

Figure 5-24 Datum connections to the submerged pressure gauges. (a) Direct measurement. (b) Timed water level measurements (Images courtesy of R. Handsworth).

The timed water level measurement technique is limited by two factors. Firstly, it is rarely sufficiently calm to consistently observe water levels at accuracies at the 1 mm level, especially without the aid of any form of stilling well. Secondly, the tide gauge pressure measurements are converted to sea level with an assumed water density (UNESCO, 1983). Any variations in the density of the seawater from the nominal value used in the data reductions will affect the tide gauge observations and hence bias the datum connection. Studies, such as Allison et al. (1985), show significant annual variation in salinity (and hence density) at Antarctic locations due to the interaction of the freeze/thaw cycle, in addition to high amounts of freshwater melt draining from continental Antarctica in the summer period. It is anticipated the variation in density may introduce systematic errors up to the 5 mm level at Antarctic locations. The issue of density is clearly of fundamental importance for all pressure gauges, as discussed by Woodworth et al. (1996). Pressure gauges in non hostile environments are able to overcome this issue by observing with three pressure sensors, with one located at depth, one at approximately MSL and one clear of the water surface. This enables both correction for atmospheric pressure and the in situ determination of water density (based on a known distance between the sensors at depth and at MSL). Clearly the seasonal sea ice precludes the use of this technique at Antarctic installations.

The task of timed water level measurements can be automated with the use of time lapse video. Hyslop and Watson (1998) used several hours of video footage taken

from the sea ice to a levelling staff resting on the top of the Mawson tide gauge. GPS was also used on the ice surface in an early attempt at investigating the use of GPS to define the tide gauge datum. Other studies, such as Aoki et al. (2000) and Aoki et al. (2002), investigated the use of GPS in measuring tidal displacement on fast ice near Syowa station in Antarctica. The study involved comparing a 9 month period of GPS data with data from a bottom mounted pressure gauge. GPS data were available episodically for 54% of the 9 month period, primarily due to equipment difficulties. The study involved a relative comparison of the two datasets, without any attempt to solve for the absolute datum of the pressure gauge. Aoki et al. (2002) concluded the GPS system was a valuable aid in calibrating and validating long term sea level signals. King and Aoki (2003) revisited the Syowa data using a Precise Point Positioning (PPP) algorithm (Zumberge et al., 1997), demonstrating the suitability of the PPP technique for the generation of data suitable for assimilation into numerical tide models.

The task of using timed water level measurements to define the datum (and stability) of the tide gauge is clearly limited by the unknown density of the sea water. The aim of the verification experiment presented in the following section is therefore twofold:

1) To assess the scale error of the Davis pressure gauge, as undertaken in the previous two verification studies. Note the influence of density differences on the tidal range (~ 1 m) will be significantly less (and considered insignificant) than over the entire range (~7 m) of the tide gauge.

2) Determine the suitability of short baseline GPS to define the ellipsoidal height of the pressure gauge zero (assuming high accuracy density observations are available for future gauge calibrations).

5.6.3 In Situ Verification of the Davis Station Gauge

The verification of the bottom mounted gauge at Davis Station was undertaken using the UTAS Mk II GPS buoy in December 2002. Data were acquired by R. Coleman (11/12/2002) by placing the buoy directly over the pressure gauge location, after cutting through the sea ice (Figure 5-25).

Figure 5-25 GPS buoy over the Davis bottom mounted pressure gauge.

The primary GPS reference station used was AUS2007, with the ARGN site AUS099 (DAV1) used as a backup (Figure 5-22). Unlike the previous gauge verification experiments, logistical constraints dictated a dissimilar receiver and antenna had to be utilised at the primary reference station (Trimble geodetic receiver with a Zephyr antenna). Due to the damping of the high frequency sea surface variability (swell and wind waves) by the sea ice, data were obtained at 10 second intervals from the GPS buoy and AUS2007 (in comparison to 1 Hz used for the Burnie and Macquarie Island verification experiments). Data at the ARGN site was fixed at the standard operational 30 second rate.

Approximately 16 hours and 15 minutes of GPS data are obtained at the GPS buoy and reference stations (5:46:30 to 22:02:30 UT). Processing was conducted as described in §5.3.1. The tide gauge data were reduced relative to the tide gauge zero (i.e., the 5.866 m difference to LAT routinely removed by the NTC was added back to the tide gauge data). The comparison between the pressure gauge and GPS buoy data is presented in Figure 5-26(a), with the residual difference shown in Figure 5-26(b). The interpretation of the residual difference differs from the two previous case studies. In this case, there is no "known" survey tie between the benchmark and the tide gauge zero. Therefore, the residual difference has been reduced to define the ellipsoidal height difference between the reference site and the tide gauge zero. The mean value (Δh = -30.2998 m) is therefore dependent on the seawater density at the time of the experiment.

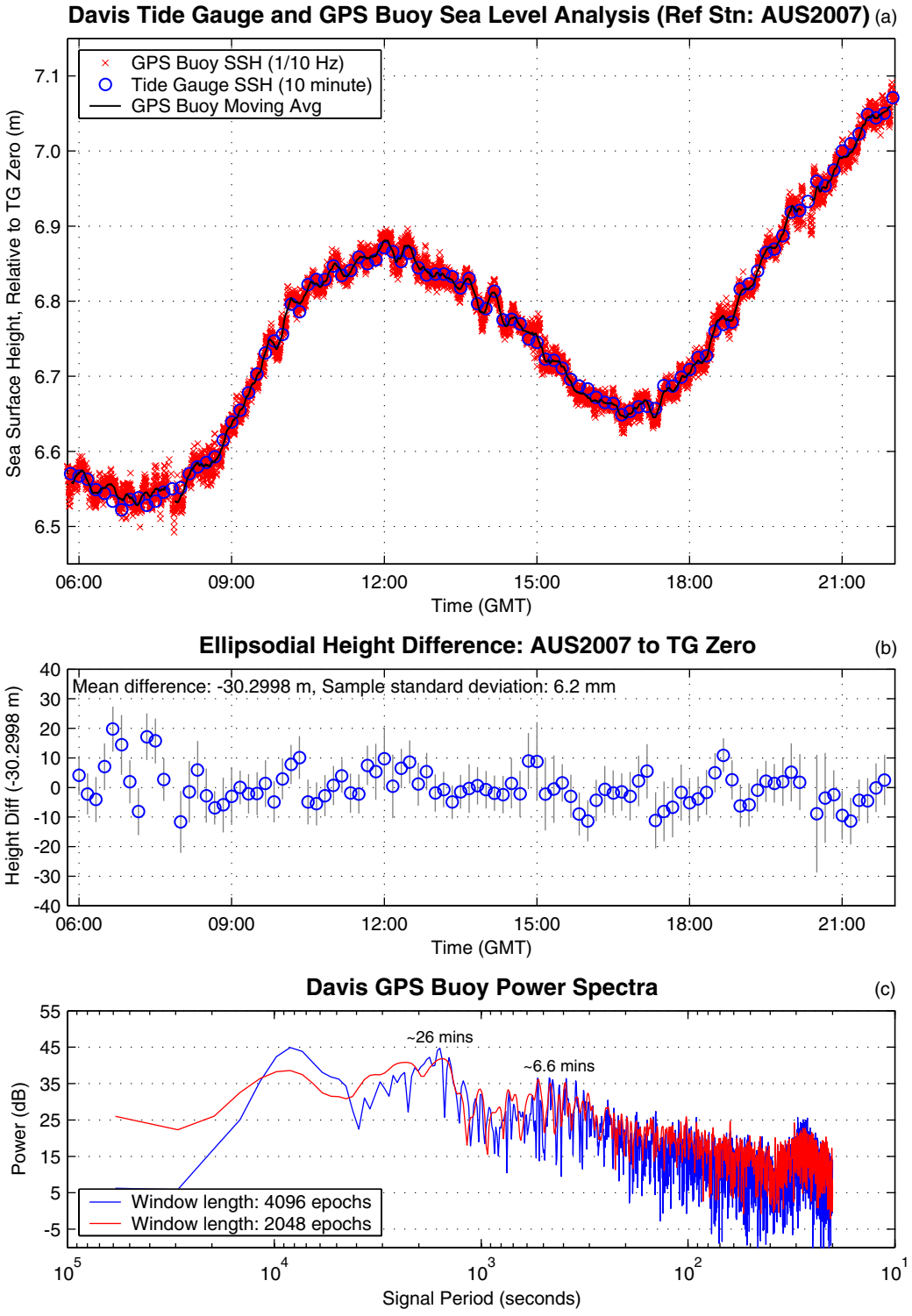

Figure 5-26 Davis Station verification results. (a) Sea surface height estimates from both the tide gauge and unfiltered and filtered GPS buoy data. Note heights are relative to the tide gauge zero. (b) Ellipsoidal height difference between AUS2007 and the TG Zero computed using filtered GPS buoy data and the tide gauge. (c) GPS buoy power spectra, note the power bands at ~26 minutes and ~6.6 minutes (period).

The GPS buoy time series shown in Figure 5-26(a) reflects the dampened ocean conditions under the influence of the sea ice. A mixture of diurnal and semi-diurnal tides are clearly evident. High frequency periodic variability is also evident (see for example at around 14:00 where the oscillation is particularly energetic). The power spectra (Figure 5-26c) shows a dominant peak at ~26 minutes period, in addition to an even higher frequency oscillation (with lower energy) at ~6.6 minutes period. This again highlights the ability of the GPS buoy methodology to characterise the local oceanographic signature in the coastal environment.

The residual time series has a standard deviation of 6.2 mm. The first 2-3 hours shows higher variability, corresponding to a period of poor satellite coverage. Neglecting errors within the tide gauge (including the density correction), the limiting factor in terms of the achievable accuracy will be systematic differences associated with mixing antenna types, in addition to the effect of the antenna dome on the GPS buoy. The estimated error floor for this experiment is therefore likely to be at the 5 mm level. It is anticipated that results at the 2-3 mm level would be possible over very short baselines, using the same receiver, antenna and radome configurations at either end of the baseline.

The mean ellipsoidal height difference between the DAV1 reference station and the tide gauge zero is -34.5048 m (standard deviation of the time series 5.7 mm). The power spectra using the GPS buoy solution relative to DAV1 also shows peaks at ~26 and ~6.6 minutes period. The longer baseline from DAV1 and the use of a different antenna radome places greater uncertainty on the results from the DAV1 site. See Appendix D for plots from the DAV1 analysis.

5.6.3.1 Regression Analysis

Using GPS buoy data processed relative to AUS2007, the scale error of the tide gauge was investigated (Figure 5-27). The regression analysis yields a scale parameter estimate (α) of 0.9938 $\pm$ 0.0061 (error estimates from weighted least-squares regression using conservative error budget estimates of GPS buoy SSH precision). The scale parameter is clearly not significant at a 95% confidence level. This is confirmed with results when using the GPS data processed relative to DAV1. In this case, the scale error is determined to be 1.0021 $\pm$ 0.0094 (note the higher uncertainty due to less data, now 30 second epochs, and larger uncertainties placed on each GPS buoy estimate of sea level).

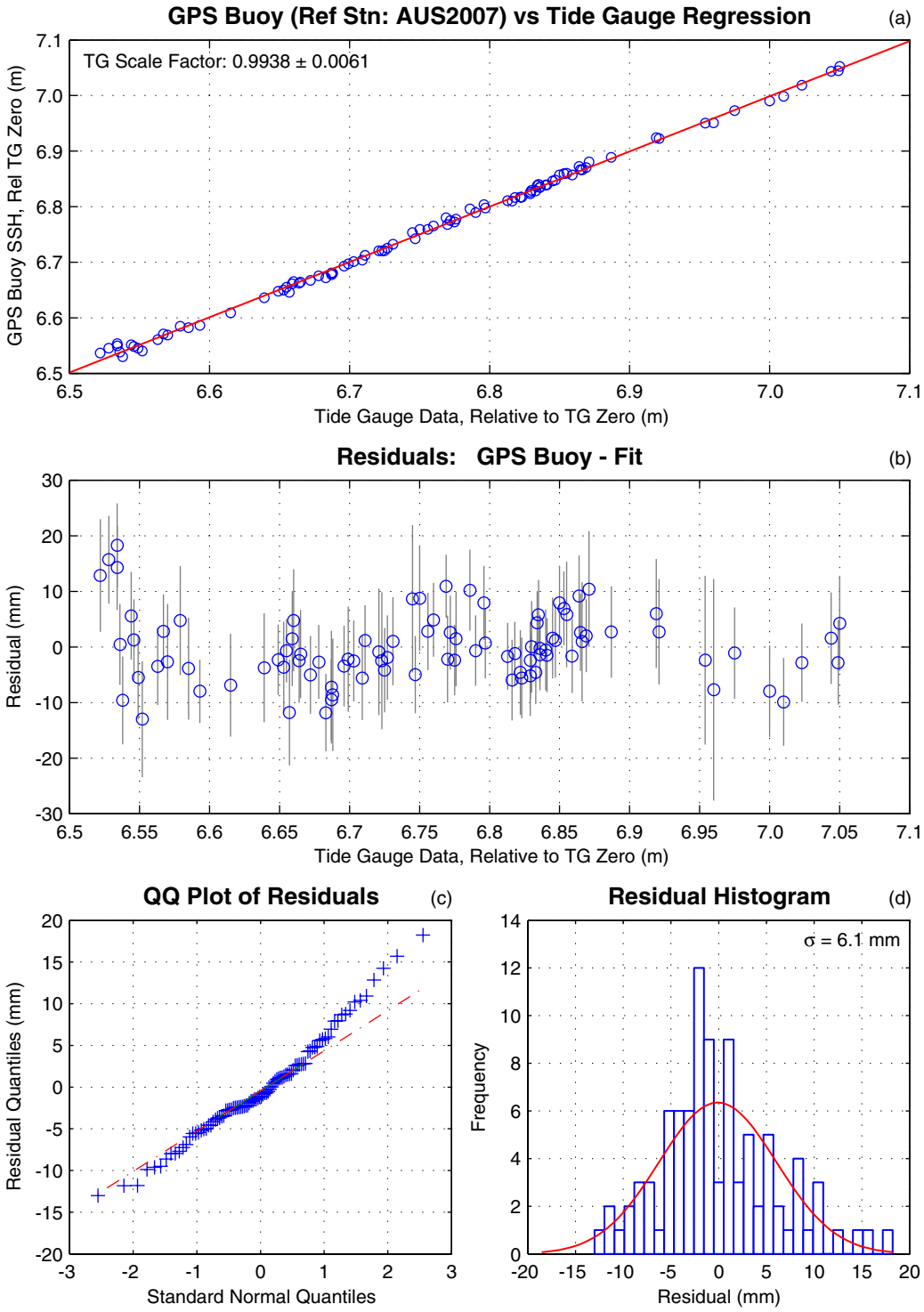

Figure 5-27 Davis GPS buoy and tide gauge regression. (a) GPS buoy versus tide gauge SSH, relative to the tide gauge zero. (b) Regression residuals. (c) Empirical quantile-quantile plot of the residuals. (d) Histogram of residuals and normal distribution probability density function.

The distribution of data over the period (Figure 5-27a,b) shows the impact of observing only over a 16 hour period when tide gauge observations were available

at a 10 minute time base. This is also reflected in the quantile-quantile plot (Figure 5-27c). The 16 hour limit was as a result of reduced battery performance under colder conditions. The collection of data over at least one additional tidal cycle would significantly strengthen the regression, aiding in the resolution of the scale parameter.

5.6.4 Summary

The GPS buoy deployment at Davis station represents proof of concept methodology. Defining the datum of a bottom mounted tide gauge in the Antarctic environment remains a challenging problem. The GPS buoy methodology offers one solution to the datum definition at Antarctic sites. The in situ observation of sea water density is however the limiting factor. The accuracy of the GPS height connection must also be maximised by ensuring:

1) Identical GPS receivers and antennas are used at the reference and buoy sites;

2) Assuming the GPS buoy radome is used, an equivalent radome should be used on the reference station; and

3) The baseline lengths are kept to absolute minimum. At Davis station, this implies the use of the primary tide gauge benchmark (AUS186, Figure 5-22) which is within ~270 m of the tide gauge location.

The experiment at the Davis site has shown there is no significant scale error in the current installation. The GPS buoy technique has been successful in identifying localised, high frequency oscillations at the tide gauge site. At the time of writing, GPS buoy data have been recently acquired over a seven day period at the tide gauge site, allowing a further investigation of the gauge scale error. A strategy for sampling the sea water and accurately estimating water density during future calibration experiments is also under development.

5.7 Summary and Recommendations

The GPS buoy technology developed in this Thesis has been successfully applied to a coastal application involving the calibration and verification of tide gauge installations. As discussed throughout this Thesis, the global tide gauge network remains as important and significant to the scientific and broader community as it was before the prevalence of satellite-based measurements. In the context of this Thesis, tide gauges still represent the preferred technique for the estimation of altimeter bias drift. Tide gauges are also fundamental to most, if not all, absolute calibration studies, as demonstrated at the Bass Strait calibration site. The tide gauge verification methodology presented in this Chapter provides one technique to ensure the gauges are operating according to specifications.

The continuous operation of gauges in the environment presented in the sub-Antarctic and Antarctic remains a credit to the Australian Antarctic Division. The environment dictates that unique installations are required. Assessment of offset and scale error at these gauges therefore requires an innovative approach. The GPS buoy approach is ideally suited to both environments, with exceptional results obtained from each of the three experiments undertaken.

The following recommendations may be made in relation to future use of the GPS buoys for tide gauge verification experiments:

1) The floatation position of the buoy (i.e., the height of the antenna ARP with respect to the water surface) must be precisely determined in water of comparable density to where the verification experiment will take place. Ideally, this also implies the same battery and associated equipment is used for each experiment.
2) Identical receivers and antennas (preferably geodetic choke ring antennas) must be utilised at both the reference station and within the GPS buoy.
3) If utilising a radome on the GPS buoy, an identical radome and attachment mechanism must be used on the GPS reference station.
4) The recommended data acquisition rate is 1 Hz. Ideally, several tidal cycles of data should be acquired to maximise the strength of the regression analysis.
5) GPS baseline lengths must be kept to an absolute minimum, preferably within 100-200 m.
6) The GPS buoy should be deployed as close as practically possible to the tide gauge to minimise systematic oceanographic and geometric effects.

7) Finally, at Antarctic installations, in situ water density must be observed if the absolute height of the tide gauge zero is required.

Chapter 6

Conclusions

6.1 The Bass Strait Calibration Site

The research presented in this Thesis represents a significant contribution to the international satellite altimeter calibration and validation effort. The Bass Strait site is now recognised as the third dedicated T/P ~ Jason-1 absolute calibration site, joining the NASA and CNES supported sites at Harvest and Corsica respectively (Haines et al., 2004b). Achieving results of comparable accuracy to the NASA and CNES sites is considered a significant achievement, particularly as the research requires a multidisciplinary approach. Results from this research have been particularly valuable given the Bass Strait site is the sole in situ calibration site in the Southern Hemisphere and the only one of its kind on a descending T/P and Jason-1 altimeter pass.

The source of the significant Jason-1 absolute bias (approximately +154 mm at 2002.0 using the POE orbit, or +133 mm at 2002.0 using the GPS orbit) remains unexplained, except to say it is globally consistent. Investigations have shown that irregularities in the JMR instrument account for a small component of the difference. Small geographically correlated differences in the different orbit solutions have also been shown to contribute. At the time of writing, many hours of checking and rechecking by mission partners NASA and CNES have failed to find a cause for the puzzling bias. The reluctance of this problem to be solved serves to illustrate to the scientific and broader community that high accuracy altimetry is far from a routine science and still offers scope for significant improvements in understanding. The bias also underscores the need for continuous calibration and cross calibration of altimeter missions into the future.

The quality of the results at the Bass Strait site have improved by an order of magnitude since the initial study in 1992 (White et al., 1994). The unique methodology developed, incorporating the offshore mooring array, GPS buoy

deployments and coastal tide gauge, has enabled the computation of absolute bias estimates with exceptionally low variability when compared with other calibration studies in the literature. Outside the main calibration phase of the Jason-1 mission, the variability of bias estimates at the Bass Strait site is still comparable to that at Harvest, which has the benefit of using a purely direct methodology for every overflight. The computation of both tidal and geometrical differences between the offshore comparison point and the coastal tide gauge using actual observed data gives the Bass Strait site its strength in comparison to other studies in the literature. The use of episodic GPS buoy deployments to solve for the datum of the offshore pressure gauge, which is then used to compute the geometrical and tidal differences to the coastal tide gauge provides an elegant geometrical solution to the calibration problem. This approach has removed the need to estimate a precise relative geoid, the source of greatest uncertainty in many calibration studies (including the original study at the Bass Strait site).

The geographically correlated orbit errors investigated in this Thesis underscore the benefit of a well-distributed set of calibration sites to quantify observed differences in an absolute sense. This is considered one of the primary advantages of in situ calibration sites. There is no doubt, however, that the "calibration task" requires a multifaceted approach, including both in situ calibration sites and global studies using the tide gauge network. The two techniques are therefore considered complementary and fundamental to altimeter missions.

Both the Bass Strait site and other in situ calibration sites are limited by the close proximity of the comparison point to land. The close proximity dictates additional measures are required to overcome land contamination of the radiometer instrument to avoid bias in the SSH_{Alt} observations. In most cases, the proximity to land also translates to a particular wave regime being sampled which is not necessarily representative of true oceanic conditions. In situ calibration sites are also limited by comparatively few degrees of freedom which limit the potential to derive statistically significant estimates of altimeter bias drift. Despite the expected high uncertainty, drift estimates from the Bass Strait site show remarkable agreement with global estimates, further testament to the success of the methodology adopted at the site.

6.2 GPS Buoy Development

The development of the wave rider GPS buoys used at the Bass Strait site has been fundamental to the success of this calibration study. The buoy design and investigations into tethering and dome configuration have advanced GPS based water level measurement, underscoring the power of the technique to both offshore and coastal applications.

The GPS buoy tide gauge verification methodology has proved extremely successful. The technique has aided in the identification of a small scale error at the Burnie tide gauge, in addition to highlighting significant errors in inclination of the Macquarie Island gauge. Further errors in the reduction of data from the Macquarie Island gauge were also revealed. The application of the GPS buoys to the calibration of gauges in the sub-Antarctic and Antarctic has provided an extremely viable technique to investigate the performance of gauges which operate in such difficult environments. Following from the recommendations provided in the previous Chapter, a regular series of GPS buoy deployments have been incorporated into the Australian Antarctic Division's tide gauge program. This effort will maximise the significant contribution these gauges make to the global sea level network, and the study of absolute sea level change.

6.3 Future Implications and Research Directions

The Earth is already experiencing climate change which for the first time in the history of the planet is occurring as a result of anthropogenic influences (Church et al., 2001). The implications of climate change on the global community and its environment remain one of the most pressing issues facing society in the 21st century.

Regional and global mean sea level change is one of the more certain consequences of climate change (Church et al., 2004). There is no doubt accurate scientific monitoring is required to facilitate the management of that change. The currently accepted estimate for global mean sea level change from the T/P and Jason-1 altimeter missions is at the +3.0 mm/yr level (Figure 6-1). The uncertainty bounds placed on this estimate are notably still significant, primarily due to the uncertainty in many of the underlying models as discussed throughout this thesis.

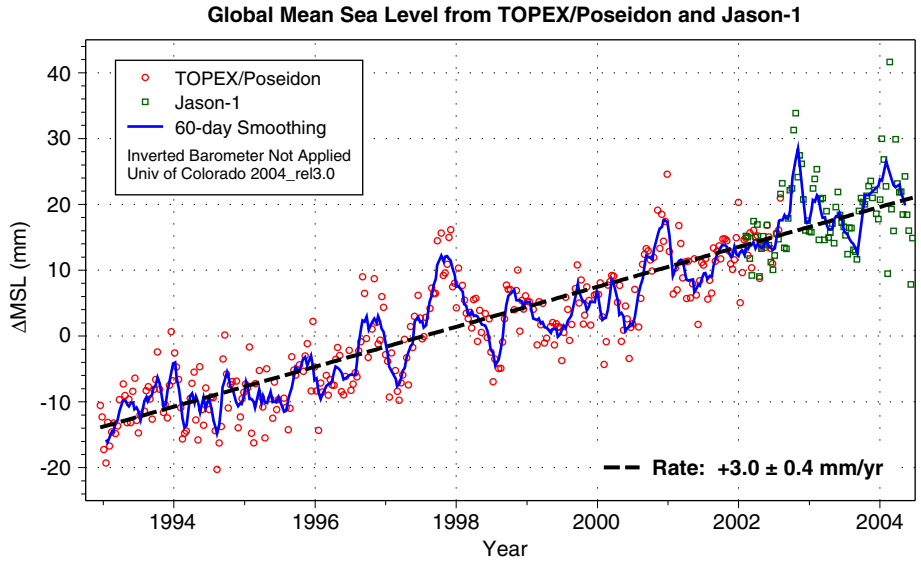

Figure 6-1 *Global mean sea level from T/P and Jason-1. Computed by Nerem et al. (2004), reproduced with permission.*

These estimates of sea level change are only possible with careful and ongoing calibration of altimeter missions, as discussed in this Thesis. Cross calibration of future altimeter missions will remain essential for continued sea-level studies. Calibration of Jason-1 with respect to T/P has been partially simplified by the simultaneous operation of both spacecraft in a formation flight configuration. The complexities associated with operating satellite equipment dictates this may not, and most probably will not, be the case for future follow-on missions such as Jason-2. In this eventuality, cross calibration will rely heavily on absolute calibration sites, including the Bass Strait site. In situ calibration sites will also remain imperative for the verification of geographically correlated errors, as discussed in this Thesis. Estimates of altimeter drift will require continued operation of global tide gauge networks and complementary calibration techniques, underscoring the need to maintain tide gauge networks into the future, and to monitor the vertical position of each tide gauge site.

This Thesis has clearly demonstrated the importance of maintaining high computational standards, especially when considering inter-comparison between different geodetic platforms. Updating the solid Earth tide within the GAMIT suite represents an important progression, given the reliance on this software in much of the geodetic literature. The full effect of the updated models is currently being investigated, with preliminary results indicating small, yet significant effects on vertical velocity estimates. Clearly, however, this is just one of many

improvements which are required to increase our understanding of the signal composition of geodetic time series.

Research and development into GPS and other Global Navigation Satellite Systems (GNSS), including the proposed European Galileo system, has the potential to improve positioning accuracy in the vertical component, enabling improved estimation of the velocity in the vertical direction. Improved estimates of vertical position and velocity will benefit both the in situ and global tide gauge altimeter calibration techniques, further reducing the calibration uncertainty. The modernisation of GPS and possible integration of the Galileo system is also set to influence kinematic GNSS applications (Eissfeller et al., 2002). Improved ambiguity resolution techniques, available with the introduction of the third GPS frequency, L5, may reduce the baseline distance constraint on kinematic solutions. This may in turn significantly improve the potential applications for GPS equipped buoys, particularly for altimeter calibration and validation activities.

Improvements in the realisation of the terrestrial reference frame will form a necessary part of the geodetic research and development for future satellite altimeter calibration studies. The next generation International Terrestrial Reference Frame, ITRF2004 (Ferland, 2004) due for release in 2005, will be the first step in creating a more robust reference frame to which the orbit of altimeters will be referenced. An improved treatment of non-linear site motions and other discontinuities in site position has the potential to significantly improve the realisation of the reference frame. Further understanding of phenomena, such as glacial isostatic adjustment, seasonal hydrological loading, atmospheric pressure loading and ocean tide loading, are also required to achieve even greater accuracy and reduction in positional uncertainty. Advances in the understanding and application of Earth deformation theory are also required. For example, the existing conflict between computing deformation in the CE frame, yet correcting for the deformation in the CF frame must be resolved. The interaction of many of these geophysical signals with software and site specific issues (for example, aliasing of errors introduced from multipath) represents another area requiring further research. The continuing improvement in the understanding of the Earth's gravity field through missions such as GRACE will also benefit altimetry, geodesy and other Earth sciences. Improvements in geopotential models and their associated time variability will not only assist orbit determination, but allow improvement to models describing mass variability, and hence periodic surface deformation.

6.4 Final Conclusions

Each of the aims set out in the introductory Chapter of this Thesis have been achieved. An improved, unique, absolute calibration methodology has been developed and implemented at the Bass Strait calibration site, supporting the calibration and cross calibration of the TOPEX/Poseidon and Jason-1 altimeter missions.

This particular calibration study has relied heavily on the further development of GPS based water level measurement techniques. The GPS buoy design developed has proved to be an extremely powerful research tool for calibration studies. Developed primarily for calibration and validation activities in the offshore environment, the GPS buoy design has also been successfully applied to a near-shore application involving the calibration of unique coastal tide gauges in the Sub-Antarctic and Antarctic.

Despite an intense global calibration effort, several questions remain unanswered as both the source of the Jason-1 absolute bias and drift within the JMR instrument continue to be investigated. Results presented in this Thesis reflect the state of the art in absolute satellite altimeter calibration at the time of writing. The Bass Strait calibration site will continue to monitor Jason-1 in the lead up to the launch of Jason-2 and beyond. Future improvements in design and accuracy associated with these future missions will no doubt continue to push calibration efforts to the next level. By its very nature, this will continue to make the calibration task both demanding and challenging for the scientific community.

Bibliography

Agnew, D. C. (1992). "The Time-Domain Behavior of Power-Law Noises." Geophysical Research Letters, 19(4), pp333-336.

Akrour, B., Santerre, R., and Geiger, A. (2003). "Comparison of the Methods for Calibrating the Phase Centre of GPS Antennae." Geomatica, 57(4), pp411-417.

Allinson, C. R., Clarke, P. J., Edwards, S. J., King, M. A., Baker, T. F., and Cruddace, P. R. (2004). "Stability of Direct GPS Estimates of Ocean Tide Loading." Geophysical Research Letters, 31(15).

Allison, I., Tivendale, C. M., and Copson, G. R. (1985). "Annual Salt and Energy Budget beneath an Antarctic Fast Ice Cover." Annals of Glaciology, 6, pp182-186.

Altamimi, Z., Sillard, P., and Boucher, C. (2002). "ITRF2000: A New Release of the International Terrestrial Reference Frame for Earth Science Applications." Journal of Geophysical Research B: Solid Earth, 107(10).

Anderson, O. B. (2004). "The Geodesist's Handbook 2004." Journal of Geodesy, 77(10-11), pp559-797.

Andreatta, V., Meertens, C., and Jackson, M. (2001). "UNAVCO SCIGN Dome Testing." University NAVSTAR Consortium Report, Boulder, Colorado, USA.

Aoki, S., Ozawa, T., Doi, K., and Shibuya, K. (2000). "GPS Observation of the Sea Level Variation in Lutzow-Holm Bay, Antarctica." Geophysical Research Letters, 27(15), pp2285-2288.

Aoki, S., Shibuya, K., Masuyama, A., Ozawa, T., and Doi, K. (2002). "Evaluation of Seasonal Sea Level Variation at Syowa Station, Antarctica, Using GPS Observations." Journal of Oceanography, 58(3), pp519-523.

Aquatrak 2004. "Aquatrak Acoustic Liquid Level Sensors." Aquatrak Corporation, Available at: http://www.aquatrak.com/.

Australian Antarctic Division. (2000). "Tide Gauge Records, Davis, Australian Antarctic Territory." Published by the Australian Antarctic Data Centre, Kingston, Tasmania, Australia.

Bahurel, P., De Mey, P., Le Provost, C., and Le Traon, P. Y. (2002). "A Godae Prototype System with Applications - Example of the MERCATOR System." in En route to GODAE, Biarritz, France, Published by CNES, pp137-142.

Beavan, J., Tregoning, P., Bevis, M., Kato, T., and Meertens, C. (2002). "Motion and Rigidity of the Pacific Plate and Implications for Plate Boundary Deformation." Journal of Geophysical Research-Solid Earth, 107(B10).

Benada, J. R. (1997). "PO.DAAC Merged GDR (TOPEX/Poseidon) Generation B User's Handbook, Version 2." JPL D-11007 (PO.DAAC).

Bevis, M., Businger, S., Herring, T., Rocken, C., Anthes, R., and Ware, R. (1992). "GPS Meteorology: Remote Sensing of Atmospheric Water Vapor Using the Global Positioning System." Journal of Geophysical Research, 97(D14), pp15,787-15,801.

Bisnath, S., Wells, D., Howden, S., Dodd, D., Wiesenburg, D., and Stone, G. (2004). "Development of an Operational RTK GPS-Equipped Buoy for Tidal Datum Determination." The International Hydrographic Review, 5(1), pp76-86.

Blewitt, G., Lavalee, D., Clarke, P., and Nurutdinov, K. (2001). "A New Global Mode of Earth Deformation: Seasonal Cycle Detected." Science, 294(5550), pp2342-2345.

Blewitt, G., and Lavallee, D. (2002). "Effect of Annual Signals on Geodetic Velocity." Journal of Geophysical Research B: Solid Earth, 107(7), pp9-1-9-11.

Blewitt, G. (2003). "Self-Consistency in Reference Frames, Geocenter Definition, and Surface Loading of the Solid Earth." Journal of Geophysical Research B: Solid Earth, 108(2), 10pp.

Bock, Y., Wdowinski, S., Fang, P., Zhang, J., Williams, S., Johnson, H., Behr, J., Genrich, J., Dean, J., Van Domselaar, M., Agnew, D., Wyatt, F., Stark, K., Oral, B., and et, a. (1997). "Southern California Permanent GPS Geodetic Array: Continuous Measurements of Regional Crustal Deformation between the 1992 Landers and 1994 Northridge Earthquakes." Journal of Geophysical Research, 102 B8, pp18013-18033.

Bonnefond, P., Exertier, P., Laurain, O., Menard, Y., Orsoni, A., Jan, G., and Jeansou, E. (2003a). "Absolute Calibration of Jason-1 and TOPEX/Poseidon Altimeters in Corsica." Marine Geodesy, 26(3-4), pp261-284.

Bonnefond, P., Exertier, P., Laurain, O., Menard, Y., Orsoni, A., Jeansou, E., Haines, B. J., Kubitschek, D. G., and Born, G. (2003b). "Leveling the Sea Surface Using a GPS-Catamaran." Marine Geodesy, 26(3-4), pp319-334.

Bonnefond, P. (2004). "Absolute Calibration of Jason-1 and TOPEX/Poseidon Altimeters in Corsica." in Ocean Surface Topography Science Team Meeting (OST/ST), St. Petersburg, Florida.

Bonnefond, P., Haines, B., and Nerem, R. (2004). "Local to Global CalVal Experiments: Report of the Splinter Session." in Ocean Surface Topography Science Team Meeting (OST/ST), St. Petersburg, Florida.

Born, G. H., Parke, M. E., Axelrad, P., Gold, K. L., Johnson, J., Key, K. W., Kubitschek, D. G., and Christensen, E. J. (1994). "Calibration of the TOPEX Altimeter Using a GPS Buoy." Journal of Geophysical Research-Oceans, 99(C12), pp24517-24526.

Boucher, C., Altamimi, Z., and Sillard P. (eds). (1999). "The 1997 International Terrestrial Reference Frame (Itrf97)." IERS Technical Note No 27, Observatoire de Paris, Paris.

Boucher, C. (2001). "Terrestrial Coordinate Systems and Frames." in Encyclopedia of Astronomy and Astrophysics, P. Murdin, ed., Institute of Physics Publishing, Bristol, pp3289-3292.

Boucher, C., Altamimi, Z., Sillard, P., and Feissel-Vernier M. (eds). (2004). "The ITRF2000." IERS Technical Note No 31, Verlag des Bundesamts fur Kartographie und Geodasie, Frankfurt am Main, 270pp.

Braun, J., Stephens, B., Ruud, O., and Meertens, C. (1997). "The Effect of Antenna Covers on GPS Baseline Solutions." University NAVSTAR Consortium Report, Boulder, Colorado, USA.

Brown, S., Ruf, C. S., and Keihm, S. J. (2002). "Brightness Temperature and Path Delay Correction for TOPEX Microwave Radiometer Yaw State Bias." Technical Memo, 8 August 2002.

Brown, S., Ruf, C., Keihm, S., and Hu, S. (2004a). "Recalibration of the Jason Microwave Radiometer." in Ocean Surface Topography Science Team Meeting (OST/ST), St. Petersburg, Florida.

Brown, S., Ruf, C., Keihm, S., and Kitiyakara, A. (2004b). "Jason Microwave Radiometer Performance and on-Orbit Calibration." Marine Geodesy, 27(1-2), pp199-220.

Brunner, F. K., Hartinger, H., and Troyer, L. (1999). "GPS Signal Diffraction Modelling: The Stochastic Sigma-[Delta] Model." Journal of Geodesy, 73(5), pp259-267.

Calmant, S., Cheng, K., Jan, G., Kuo, C., Shum, C., Yi, Y., and Ballu, V. (2004). "Comparison of Sea Surface Heights Derived from Satellite Altimetry and from Ocean Bottom Pressure Gauges: The SW Pacific MOTEVAS Project." Marine Geodesy, 27(3-4), pp597-613.

Cardellach, E., Behrend, D., Rius, A., and Font, J. (1999). "Oceanographic Applications of GPS Buoys." in OceanObs99 - The Ocean Observing System for Climate, Saint Raphaël, France.

Cardellach, E., Behrend, D., Ruffini, G., and Rius, A. (2000). "The Use of GPS Buoys in the Determination of Oceanic Variables." Earth Planets and Space, 52(11), pp1113-1116.

Cartwright, D. E. (1999). "Tides, a Scientific History." Cambridge University Press, Cambridge, 292pp.

Cazenave, A., Dominh, K., Ponchaut, F., Soudarin, L., Cretaux, J. F., and Le Provost, C. (1999). "Sea Level Changes from Topex-Poseidon Altimetry and Tide Gauges, and Vertical Crustal Motions from DORIS." Geophysical Research Letters, 26(14), pp2077-2080.

Chadwell, C. D., and Bock, Y. (2001). "Direct Estimation of Absolute Precipitable Water in Oceanic Regions by GPS Tracking of a Coastal Buoy." Geophysical Research Letters, 28(19), pp3701-3704.

Chambers, D. P., Ries, J. C., Shum, C. K., and Tapley, B. D. (1998). "On the Use of Tide Gauges to Determine Altimeter Drift." Journal of Geophysical Research-Oceans, 103(C6), pp12885-12890.

Chambers, D. P., Tapley, B. D., and Stewart, R. H. (1999). "Anomalous Warming in the Indian Ocean Coincident with El Nino." Journal of Geophysical Research-Oceans, 104(C2), pp3035-3047.

Chambers, D. P., Hayes, S. A., Ries, J. C., and Urban, T. J. (2003). "New TOPEX Sea State Bias Models and Their Effect on Global Mean Sea Level." Journal of Geophysical Research-Oceans, 108(C10).

Chelton, D. B., Ries, J. C., Haines, B. J., Fu, L., and Callahan, P. S. (2001). "Satellite Altimetry." in Satellite Altimetry and Earth Sciences - A Handbook of Techniques and Applications, L. L. Fu and A. Cazenave, eds., Volume 69, International Geophysics Series, Academic Press, San Diego, California, USA., pp1-131.

Chen, G. (1998). "GPS Kinematic Positioning for the Airborne Laser Altimetry at Long Valley, California." Thesis for Doctor of Philosophy in Geophysics, Massachusetts Institue of Technology, Cambridge, MA, 169pp.

Chen, J. L., Wilson, C. R., Eanes, R. J., and Nerem, R. S. (1999). "Geophysical Interpretation of Observed Geocenter Variations." Journal of Geophysical Research-Solid Earth, 104(B2), pp2683-2690.

Cheney, R., Miller, L., Agreen, R., Doyle, N., and Lillibridge, J. (1994). "TOPEX/Poseidon - the 2-Cm Solution." Journal of Geophysical Research-Oceans, 99(C12), pp24555-24563.

Cheng, K. (2004a). "GPS Buoy Campaigns for Vertical Datum Improvement and Radar Altimeter Calibration." Report No. 470, Department of Civil and Environmental Engineering and Geodetic Science, The Ohino State University, Columbus, Ohio, USA, 74pp.

Cheng, K. (2004b). "Radar Altimeter Absolute Calibration Using GPS Water Level Measurements." Report No. 469, Department of Civil and Environmental Engineering and Geodetic Science, The Ohino State University, Columbus, Ohio, USA, 68pp.

Choi, K.-R., Ries, J. C., and Tapley, B. D. (2004). "Jason-1 Precision Orbit Determination by Combining SLR and DORIS with GPS Tracking Data." Marine Geodesy, 27(1-2), pp319-331.

Christensen, E., Haines, B., Keihm, S., Morris, C., Norman, R., Purcell, G., Williams, B., Wilson, B., Born, G., Parke, M., Gill, S., Shum, C., Tapley, B., Kolenkiewicz, R., and Nerem, R. (1994). "Calibration of TOPEX/Poseidon at Platform Harvest." Journal of Geophysical Research-Oceans, 99(C12), pp24465-24485.

Church, J. A., Gregory, J. M., Huybrechts, P., Kuhn, M., Lambeck, K., Nhuan, M. T., Qin, D., and Woodworth, P. L. (2001). "Changes in Sea Level." in Climate Change 2001: The Scientific Basis, J. T. Houghton, Y. Ding, D. J. Griggs, M. Noguer, P. van der Linden, X. Dai, K. Maskell, and C. I. Johnson, eds., Cambridge University Press, United Kingdom and New York, USA., pp639-694.

Chruch, J. A., White, N. J., Coleman, R., Lambeck, K., and Mitrovica, J. X. (2004). "Estimates of the Regional Distribution of Sea Level Rise over the 1950-2000 Period." Journal of Climate, 17(13), pp2609-2625.

Colombo, O. L. (2000). "Detecting Tsunami in the High Seas: How GPS Might Contribute to an Early Warning System." in ION National Technical Meeting Proceedings, January 26-28, Anaheim, California, USA., Published by the Institute of Navigation.

Colombo, O. L., Evans, A. G., Vigo, M. I., Benjamin, J. J., and Ferrandiz, J. M. (2000). "Long-Baseline (> 1000 Km), Sub-Decimeter Kinematic Positioning of Buoys at Sea, with Potential Application to Deep-Sea Studies." in ION GPS-00, September 19-22, Salt Lake City, Utah, USA., Published by the Institute of Navigation.

Colombo, O. L., Evans, A.G., Ando, M., Tadokoro, K., Sato, K., Yamada, T. (2001). "Speeding up the estimation of floated ambiguities for sub-decimeter kinematic positioning at sea. " in ION GPS-2001, September 2001, Salt Lake City, Utah, USA., Published by the Institute of Navigation.

Comp, C. J., and Axelrad, P. (1996). "An Adaptive SNR-Based Carrier Phase Multipath Mitigation Technique." in ION GPS-96, September 17-20, Kansas City, Missouri, USA., Published by the Institute of Navigation.

Cretaux, J.-F., Soudarin, L., Davidson, F. J. M., Gennero, M.-C., Berge-Nguyen, M., and Cazenave, A. (2002). "Seasonal and Interannual Geocenter Motion from SLR and DORIS Measurements: Comparison with Surface Loading Data." Journal of Geophysical Research B: Solid Earth, 107(12).

Dach, R., and Dietrich, R. (2000). "Influence of the Ocean Loading Effect on GPS Derived Precipitable Water Vapor." Geophysical Research Letters, 27(18), pp2953-2956.

Daubechies, I. (1992). "Ten Lectures on Wavelets." Society for Industrial and Applied Mathematics (SIAM), Philadelphia, 357pp.

de Vries, J. J., Waldron, J., and Cunningham, V. (2003). "Field Tests of the New Datawell Dwr-G GPS Wave Buoy." Sea Technology, 44(12), pp50-55.

Desai, S. D. (2002). "Observing the Pole Tide with Satellite Altimetry." Journal of Geophysical Research-Oceans, 107(C11), pp3186, doi: 10.1029/2001JC001224.

Desai, S. D., and Haines, B. J. (2004). "Monitoring Measurements from the Jason-1 Microwave Radiometer and Independent Validation with GPS." Marine Geodesy, 27(1-2), pp221-240.

Dodson, A. H., Chen, W., Penna, N. T., and Baker, H. C. (2001). "GPS Estimation of Atmospheric Water Vapour from a Moving Platform." Journal of Atmospheric and Solar-Terrestrial Physics, 63(12), pp1331-1341.

Dong, D., and Bock, Y. (1989). "Global Positioning System Network Analysis with Phase Ambiguity Resolution Applied to Crustal Deformation Studies in California." Journal of Geophysical Research-Solid Earth and Planets, 94(B4), pp3949-3966.

Dong, D., Herring, T. A., and King, R. W. (1998). "Estimating Regional Deformation from a Combination of Space and Terrestrial Geodetic Data." Journal of Geodesy, 72(4), pp200-214.

Dong, D., Fang, P., Bock, Y., Cheng, M. K., and Miyazaki, S. (2002a). "Anatomy of Apparent Seasonal Variations from GPS-Derived Site Position Time Series." Journal of Geophysical Research B: Solid Earth, 107(4).

Dong, D., Yunck, T., and Heflin, M. (2003). "Origin of the International Terrestrial Reference Frame." Journal of Geophysical Research-Solid Earth, 108(B4).

Dong, X., Woodworth, P., Moore, P., and Bingley, R. (2002b). "Absolute Calibration of the TOPEX/Poseidon Altimeters Using UK Tide Gauges, GPS, and Precise, Local Geoid-Differences." Marine Geodesy, 25(3), pp189-204.

Doodson, A. T., and Warburg, H. D. (1941). "Admiralty Manual of Tides." Her Majesty's Stationery Office, London, 270pp.

Douglas, B. C., Cheney, R. E., and Agreen, R. W. (1983). "Eddy Energy of the Northwest Atlantic and Gulf of Mexico Determined from GEOS-3 Altimetry." Journal of Geophysical Research, 88(C14), pp9595-9603.

Eanes, R. J., and Bettadpur, S. (1995). "The CSR 3.0 Global Ocean Tide Model." Technical Memorandum CSR-TM-95-06, Centre for Space Research, University of Texas, Austin, TX.

Edwards, S., Moore, P., and King, M. A. (2004). "Assessment of the Jason-1 and TOPEX/Poseidon Microwave Radiometer Performance Using GPS from Offshore Sites in the North Sea." Marine Geodesy, 27(3-4), pp717-727.

Eissfeller, B., Tiberius, C., Heinrichs, G., and Pany, T. (2002). "Real-Time Kinematic in the Light of GPS Modernisation and Galileo." GPS World, Oct 1, pp1-4.

Elosegui, P., Davis, J. J., Mitrovica, J. X., Bennett, R. A., and Wernicke, B. P. (2003). "Crustal Loading near Great Salt Lake, Utah." Geophysical Research Letters, 30(3).

Emery, K. O., and Aubrey, D. G. (1991). "Sea Levels, Land Levels, and Tide Gauges." Springer Verlag, New York, 237pp.

ESEAS 2004. "European Sea Level Service, Research Infrastructure Project Work Package 4 - Objectives." Available at: http://www.eseas.org/eseas-ri/management/structure/wp4/.

Estey, L. H., and Meertens, C. M. (1999). "TEQC: The Multi-Purpose Toolkit for GPS/GLONASS Data." GPS Solutions, 3(1), pp42-49.

Exertier, P., Bonnefond, P., Laurain, O., and Barlier, F. (1998). "Calibration of Radar Altimeters in the Corsica Area: Recent Improvements in View of Jason-1 Mission." in TOPEX/Poseidon Science Working Team (SWT) Meeting, Poster Presentation, October 13-15, Keystone, Colorado, USA.

Farrell, W. E. (1972). "Deformation of the Earth by Surface Loads." Reviews of Geophysics and Space Physics, 10, pp761-797.

Featherstone, W. E., Kirby, J. F., Kearsley, A. H. W., Gilliland, J. R., Johnston, G. M., Steed, J., Forsberg, R., and Sideris, M. G. (2001). "The AUSGeoid98 Geoid Model of Australia: Data Treatment, Computations and Comparisons with GPS-Levelling Data." Journal of Geodesy, 75(5-6), pp331-336.

Feigl, K. L., Agnew, D. C., Bock, Y., Dong, D., Donnellan, A., Hager, B. H., Herring, T. A., Jackson, D. D., Jordan, T. H., King, R. W., Larsen, S., Larson, K. M., Murray, M. H., Shen, Z. K., and Webb, F. H. (1993). "Space Geodetic Measurement of Crustal Deformation in Central and Southern California, 1984-1992." Journal of Geophysical Research-Solid Earth, 98(B12), pp21677-21712.

Ferland, R. 2004. "Call for ITRF2004 and Supplementation of IERS CPP." IGS Electronic Mail, Message Number 5064, Available at: http://igscb.jpl.nasa.gov/mail/igsmail/2004/msg00288.html.

Fleming, K., Johnston, P., Zwartz, D., Yokoyama, Y., Lambeck, K., and Chappell, J. (1998). "Refining the Eustatic Sea-Level Curve since the Last Glacial Maximum Using Far- and Intermediate-Field Sites." Earth and Planetary Science Letters, 163(1-4), pp327-342.

Forberg, M., Schone, T., Galas, R., and Reigber, C. (2003). "Altimetry Calibration and Inter-Calibration Using a Ruggedized GPS-Buoy." Geophysical Research Abstracts, European Geophysical Society, 5(10102).

Fu, L., Christensen, E. J., Yamarone, C. A., Lefebvre, M., Menard, Y., Dorrer, M., and Escudier, P. (1994). "TOPEX/Poseidon Mission Overview." Journal of Geophysical Research, 99(C12), pp24,369-24,381.

Fu, L., and Cheney, R. E. (1995). "Application of Satellite Altimetry to Ocean Circulation Studies - 1987-1994." Reviews of Geophysics, 33, pp213-223.

Fu, L., and Cazenave, A. (2001). "Satellite Altimetry and Earth Sciences - a Handbook of Techniques and Applications." Academic Press, San Diego, California, USA., 463pp.

Fu, L. (2003). "Wide-Swath Altimetric Measurement of Ocean Surface Topography." JPL Publication 03-002, Jet Propulsion Laboratory, Pasadena, California, USA, 67pp.

Galton-Fenzi, B. K., Scott, W. D., and Handsworth, R. J. (2005). "Variability in the Fundamental Resonant Period of Buckles Bay, Macquarie Island." Continental Shelf Research, In Press.

Gaspar, P., Labroue, S., Ogor, F., Lafitte, G., Marchal, L., and Rafanel, M. (2002). "Improving Nonparametric Estimates of the Sea State Bias in Radar Altimeter Measurements of Sea Level." Journal of Atmospheric and Oceanic Technology, 19(10), pp1690-1707.

Geiger, A., Kahle, H.-G., Favey, E., Mertikas, S. P., and Forsberg, R. (2003). "Airborne Altimetry and GPS-Based Buoy Deployment: Contribution to Calibration of Satellite

Radar Altimetry at the Jason Calibration Site Gavdos, Greece." in IUGG 2003, June 30 - July 11, Sapporo, Japan.

Geoscience Australia. (2003a). "Geodetic Connections to the Tide Gauge at Burnie." Archived by Geoscience Australia, Canberra, Australia. Results Available at: http://www.ga.gov.au/nmd/geodesy/abslma/burnie.pdf.

Geoscience Australia. (2003b). "Geodetic Connections to the Tide Gauge at Macquarie Island." Archived by Geoscience Australia, Canberra, Australia. Results Available at: http://www.ga.gov.au/nmd/geodesy/antarc/macquari.pdf.

Geoscience Australia. (2003c). "GPS Data Records, Burnie." Archived by the Space Geodesy Analysis Centre, Geoscience Australia, Canberra, Australia. Station Log Available at: ftp://ftp.ga.gov.au/igs/station_logs/.

Giberson, W. E. (1991). "Seasat-A: A Retrospective." International Journal of Remote Sensing, 12(8), pp1613-1617.

Gronlie, O. (2002). "Electromagnetic Sensor Measures Water Level." Sea Technology, 43(9), pp10-13.

Haines, B. J., Christensen, E. J., Norman, R. A., Parke, M. E., Born, G. H., and Gill, S. K. (1996). "Altimeter Calibration and Geophysical Monitoring from Collocated Measurements at the Harvest Oil Platform." EOS Trans. Suppl., 77(22, W16).

Haines, B. J., and Bar-Sever, Y. E. (1998). "Monitoring the TOPEX Microwave Radiometer with GPS: Stability of Columnar Water Vapor Measurements." Geophysical Research Letters, 25(19), pp3563-3566.

Haines, B. J., Dong, D., Born, G. H., and Gill, S. K. (2003). "The Harvest Experiment: Monitoring Jason-1 and TOPEX/Poseidon from a California Offshore Platform." Marine Geodesy, 26(3-4), pp239-259.

Haines, B., Bar-Sever, Y., Bertiger, W., Desai, S., and Willis, P. (2004a). "One-Centimeter Orbit Determination for Jason-1: New GPS-Based Strategies." Marine Geodesy, 27(1-2), pp299-318.

Haines, B., Bonnefond, P., Watson, C., Born, G., Coleman, R., Exertier, P., Gill, S. K., Jan, G., Jeansou, E., Laurain, O., and White, N. (2004b). "Continuous Monitoring the Jason-1 and TOPEX/Poseidon Ocean Altimetry Missions from Dedicated Calibration Sites." in IEEE International Geoscience and Remote Sensing Symposium, Anchorage, Alaska, Published by the IEEE.

Hayne, G. S., Hancock, D. W., and Purdy, C. L. (1994). "TOPEX Altimeter Range Stability Estimates from Calibration Mode Data." in TOPEX/POSEIDON Research News, October 1994, JPL 410-42, Issue 3, pp18-22.

Hayne, G. S. 2004. "TOPEX Altimeter Range Stabilty Estimate Update." NASA GSFC Wallops Flight Facility, Available at: http://topex.wff.nasa.gov/docs/RangeStabUpdate.html.

Heflin, M., Bertiger, W., Blewitt, G., Freedman, A., Hurst, K., Lichten, S., Lindqwister, U., Vigue, Y., Webb, F., Yunck, T., and Zumberge, J. (1992). "Global Geodesy Using GPS without Fiducial Sites." Geophysical Research Letters, 19(2), pp131-134.

Heflin, M. 2001. "GPS Time Series Data Set." IGS Electronic Mail, Message Number 3635, Available at: http://igscb.jpl.nasa.gov/mail/igsmail/2001/msg000479.html.

Hein, G., Landau, H., and Blomenhofer, H. (1990). "Determination of Instantaneous Sea Surface, Wave Heights, and Ocean Currents Using Satellite Observations of the Global Positioning System." Marine Geodesy, 14(1), pp217-224.

Hein, G., Blomenhofer, H., Landau, H., and Traveira, E. (1992). "Measuring Sea Level Changes Using GPS in Buoys." in Sea Level Changes: Determination and Effects, P. L. Woodworth, D. T. Pugh, J. G. DeRonde, R. G. Warrick, and J. Hannah, eds., Geophysical Monograph Series, Volume 69, IUGG.

Henriksen, S. W. (ed). (1977). "National Geodetic Satellite Program." NASA Report SP-365, National Aeronautics and Space Administration, Washington DC, USA.

Henry, R. F. (1996). "Preliminary Results from a Finite Element Tidal Model of Macquarie Island." in Proceedings of the Southern Ocean Workshop, (M. E. Tait and D. Strauss, eds.), March 17-18, Adelaide, Australia.

Herring, T. A. (1999). "Geodetic Applications of GPS." Proceedings of the IEEE, 87(1), pp92-110.

Herring, T. A. (2001). "SVSNR and SPCSNR SNR Analysis Package." Version 1.00, Massachusetts Institute of Technology, Cambridge, Massachusetts, USA.

Herring, T. A. (2002). "Documentation for the Global Kalman Filter VLBI and GPS Analysis Software (GLOBK), Release 10." Department of Earth, Atmospheric, and Planetary Science, Massachusetts Institute of Technology and Scripps Institution of Oceanography, University of California at San Diego.

Herring, T. A. (2002). "TRACK GPS Kinematic Positioning Program." Version 1.07, Massachusetts Institute of Technology, Cambridge, MA.

Hudnut, K. W. (1999). "SCIGN Adaptors and Radomes." Report to the Southern Californian Integrated GPS Network, Available on-line at: http://pasadena.wr.usgs.gov/office/hudnut/99.scign/index.htm.

Hugentobler, U., Schaer, M., and Fridez, P. (2001). "Documentation for the Bernese GPS Analysis Software, Version 4.2." Astronomical Institute, University of Berne.

Hugentobler, U. 2004. "Bernese GPS Software: Error in Computation of Tides." BSW Electronic Mail, Available at: http://www.aiub.unibe.ch/download/bswmail/bswmail.0190.

Hunter, J. R. (2002). "TDA1537 Tidal Analysis Software." Version 1537, University of Tasmania, Available at http://www.antcrc.utas.edu.au/~johunter/tides.html.

Hunter, J. R. (2003). "On the Temperature Correction of the Aquatrak Acoustic Tide Gauge." Journal of Atmospheric and Oceanic Technology, 20(8), pp1230-1235.

Hyslop, J., and Watson, C. (1998). "Annual Surveying and Mapping Report from the 1997/98 Summer Season." Australian Antarctic Division, Kingston, Tasmania, Australia.

IOC. (1985). "Manual on Sea Level Measurement and Interpretation, Volume 1 - Basic Proceedures." Manuals and Guides No. 14, Intergovernmental Oceanographic Commission, 78pp.

IOC. (1990). "IOC Workshop on Sea Level Measurements in Antarctica." Workshop Report No. 69, Intergovernmental Oceanographic Commission, Leningrad, USSR, 14pp.

IOC. (1992). "IOC Workshop on Sea Level Measurements in Antarctica." Workshop Report No. 69 (Supplement), Intergovernmental Oceanographic Commission, Leningrad, USSR, 102pp.

IOC. (1994). "Manual on Sea Level Measurement and Interpretation, Volume 2 - Emerging Technologies." Manuals and Guides No. 14, Intergovernmental Oceanographic Commission, 52pp.

IOC. (2002). "Manual on Sea Level Measurement and Interpretation, Volume 3 - Reappraisals and Recommendations as of the Year 2000." Manuals and Guides No. 14, Intergovernmental Oceanographic Commission, 55pp.

Jamason, P., Bock, Y., Fang, P., Gilmore, B., Malveaux, D., Prawirodirdjo, L., and Scharber, M. (2004). "SOPAC Web Site (http://sopac.ucsd.edu)." GPS Solutions, 8(4), pp272-277.

JGR. (1994). "Special Issue on TOPEX/Poseidon Geophysical Evaluation." Journal of Geophysical Research, 99(C12), pp24,369-25,062.

JGR. (1995). "Special Issue on TOPEX/Poseidon Scientific Results." Journal of Geophysical Research, 100(C12), pp24,893-25,382.

Johansson, J. M., Davis, J. L., Scherneck, H.-G., Milne, G. A., Vermeer, M., Mitrovica, J. X., Bennett, R. A., Jonsson, B., Elgered, G., Elosegui, P., Koivula, H., Poutanen, M., Ronnang, B. O., and Shapiro, I. I. (2002). "Continuous GPS Measurements of Postglacial Adjustment in Fennoscandia 1. Geodetic Results." Journal of Geophysical Research B: Solid Earth, 107(8).

Kato, T., Terada, Y., Kinoshita, M., Kakimoto, H., Isshiki, H., Moriguchi, T., Takada, M., Tanno, T., Kanzaki, M., and Johnson, J. (2001). "A New Tsunami Monitoring System Using RTK-GPS." in U.S. National Tsunami Hazard Mitigation Program Review and International Tsunami Symposium, 7-10 August 2001, Seattle, Washington, USA.

Kedar, S., Hajj, G. A., Wilson, B. D., and Heflin, M. B. (2003). "The Effect of the Second Order GPS Ionospheric Correction on Receiver Positions." Geophysical Research Letters, 30(16).

Keihm, S. J., Janssen, M. A., and Ruf, C. S. (1995). "TOPEX/Poseidon Microwave Radiometer (TMR): III Wet Troposphere Range Correction Algorithm and Pre-Launch Error Budget." IEEE Transactions on Geoscience and Remote Sensing, 33, pp147-161.

Keihm, S. J., Zlotnicki, V., and Ruf, C. S. (2000). "TOPEX Microwave Radiometer Performance Evaluation, 1992-1998." IEEE Transactions on Geoscience and Remote Sensing, 38(3), pp1379-1386.

Kelecy, T., Born, G., and Rocken, C. (1992). "GPS Buoy and Pressure Transducer Results from the August 1990 Texaco Harvest Oil Platform Experiment." Marine Geodesy, 15(1), pp225-243.

Kelecy, T. M., Born, G. H., Parke, M. E., and Rocken, C. (1994). "Precise Mean Sea-Level Measurements Using the Global Positioning System." Journal of Geophysical Research-Oceans, 99(C4), pp7951-7959.

Kelly, K. A., Caruso, M. J., Singh, S., and Qiu, B. (1996). "Observations of Atmosphere Ocean Coupling in Midlatitude Western Boundary Currents." Journal of Geophysical Research-Oceans, 101(C3), pp6295-6312.

Key, K., Anderson, S., Axelrad, P., MacDoran, P., and Born, G. (1996). "Analysis of Fast Pegasus GPS Equipment and Algorithms." Colorado Center for Astrodynamics Research, University of Colorado Report 96-032, Boulder, Colorado, USA, 27pp.

Key, K. W., Parke, M. E., and Born, G. H. (1998). "Mapping the Sea Surface Using a GPS Buoy." Marine Geodesy, 21(1), pp67-79.

Key, K. W., Born, G. H., Leaman, K. D., and Vertes, P. (1999). "A New GPS Data Processing Algorithm for the Positioning of Oceanographic Experiments." Journal of Atmospheric and Oceanic Technology, 16(8), pp1127-1137.

King, M., and Aoki, S. (2003). "Tidal Observations on Floating Ice Using a Single GPS Receiver." Geophysical Research Letters, 30(3).

King, R., Neil, A., McClusky, S., and Herring, T. (1996). "Ashtech Radome Tests on Dorne Margolin Choke Ring Antennas." in IGS Analysis Center Workshop, (R. Neilan, P. Van Scoy, and J. Zumberge, eds.), March 19-21, Silver Spring, Maryland, USA., Published by the International GPS Service, pp309-320.

King, R., and Bock, Y. (2003). "Documentation for the GAMIT GPS Analysis Software, Release 10.1." Department of Earth, Atmospheric, and Planetary Science, Massachusetts Institute of Technology and Scripps Institution of Oceanography, University of California at San Diego.

Labroue, S., Gaspar, P., Dorandeu, J., Zanife, O., Mertz, F., Vincent, P., and Choquet, D. (2004). "Nonparametric Estimates of the Sea State Bias for the Jason-1 Radar Altimeter." Marine Geodesy, 27(3-4), pp453-481.

Lambert, A., Pagiatakis, S. D., Billyard, A. P., and Dragert, H. (1998). "Improved Ocean Tide Loading Corrections for Gravity and Displacement: Canada and Northern United States." Journal of Geophysical Research-Solid Earth, 103(B12), pp30231-30244.

Langbein, J., and Johnson, H. (1997). "Correlated Errors in Geodetic Time Series: Implications for Time-Dependent Deformation." Journal of Geophysical Research-Solid Earth, 102(B1), pp591-603.

Langley, R. B. (1998). "A Primer on GPS Antennas." GPS World, 9(7), pp73-77.

Le Provost, C., Bennett, A. F., and Cartwright, D. E. (1995). "Ocean Tides for and from TOPEX/Poseidon." Science, 267(5198), pp639-642.

Leatherman, S. P. (2001). "Social and Economic Costs of Sea Level Rise." in Sea Level Rise - History and Consequences, B. C. Douglas, M. S. Kearney, and S. P. Leatherman, eds., Volume 75, International Geophysics Series, Academic Press, San Diego, California, USA., pp181-223.

Lemoine, F. G., Kenyon, S. C., Factor, J. K., Trimmer, R. G., Pavlis, N. K., Chinn, D. S., Cox, C. M., Klosko, S. M., Luthcke, S. B., Torrence, M. H., Wang, Y. M., Williamson,

R. G., Pavlis, E. C., Rapp, R. H., and Olson, T. R. (1998). "The Development of the Joint NASA GSFC and NIMA Geopotential Model EGM96." Report NASA/TP-1998-206861, NASA Goddard Space Flight Center, Greenbelt, Maryland, USA.

Lennon, G., Woodland, M., and Suskin, A. (1992). "Acoustic Sea Level Measurements in Australia." in IOC Workshop Report No. 81, Joint IAPSO-IOC workshop on sea level measurements and quality control, Paris, Intergovernmental Oceanographic Commission, pp26-39.

Leuliette, E. W., Nerem, R. S., and Mitchum, G. T. (2004). "Calibration of TOPEX/Poseidon and Jason Altimeter Data to Construct a Continuous Record of Mean Sea Level Change." Marine Geodesy, 27(1-2), pp79-94.

Liebsch, G., Eberlein, L., and Dietrich, R. (2003). "Realisation of a Multisensoral Observation System for the Determination of Offshore Sea-Level Heights." Geophysical Research Abstracts, European Geophysical Society, 5(10122).

Longuet-Higgins, M. S. (1967). "On the Trapping of Wave Energy Round Islands." Journal of Fluid Mechanics, 29(4), pp781-821.

Luthcke, S. B., Zelensky, N. P., Rowlands, D. D., Lemoine, F. G., and Williams, T. A. (2003). "The 1-Centimeter Orbit: Jason-1 Precision Orbit Determination Using GPS, SLR, DORIS, and Altimeter Data." Marine Geodesy, 26(3-4), pp399-421.

Mader, G. L., and MacKay, J. (1996). "Calibration of GPS Antennas." in IGS Analysis Centre Workshop, (R. Neilan, P. Van Scoy, and J. Zumberge, eds.), March 19-21, 1996, Silver Spring, Maryland, USA, Published by the International GPS Service, pp81-105.

Mader, G. L. (1999). "GPS Antenna Calibration at the National Geodetic Survey." GPS Solutions, 3(1), pp50-58.

Mader, G. L. 2004. "GPS Antenna Calibration at the National Geodetic Survey." National Oceanic and Atmospheric Administration, National Geodetic Survey, Available at: http://www.ngs.noaa.gov/ANTCAL/Files/summary.html.

Mao, A., Harrison, C. G. A., and Dixon, T. H. (1999). "Noise in GPS Coordinate Time Series." Journal of Geophysical Research B: Solid Earth, 104(2), pp2797-2816.

Marine Geodesy. (2003). "Special Issue on Jason-1 Calibration/Validation." Marine Geodesy, 26(3-4).

Martinez-Benjamin, J. J., Martinez-Garcia, M., Gonzalez Lopez, S., Nunez Andres, A., Buill Pozuelo, F., Espino Infantes, M., Lopez-Marco, J., Martin Davila, J., Garate Pasquin, J., Garcia Silva, C., Bonnefond, P., Laurain, O., Baron Isanta, A. M., Ortiz Castellon, M. A., Talaya Lopez, J., Perez Gomez, B., Alvarez Fanjul, E., Rodriguez Velasco, G., Gomis, D., Marcos, M., Menard, Y., Jan, G., Jeansou, E., Lyard, F., and Roblou, L. (2004). "Ibiza Absolute Calibration Experiment: Survey and Preliminary Results." Marine Geodesy, 27(3-4), pp657-681.

Mathews, P. M., Buffett, B. A., and Shapiro, I. I. (1995). "Love Numbers for Diurnal Tides: Relation to Wobble Admittances and Resonance Expansions." Journal of Geophysical Research, 100(B6), pp9935-9948.

Mathews, P. M., Dehant, V., and Gipson, J. M. (1997). "Tidal Station Displacements." Journal of Geophysical Research, 102 B9, pp20469-20477.

Mathews, P. M. (2001). "Love Numbers and Gravimetric Factor for Diurnal Tides." Journal of the Geodetic Society of Japan, 47(1), pp231-236.

McCarthy, D. (1992). "IERS Standards (1992)." IERS Technical Note No 13, Observatoire de Paris, Paris.

McCarthy, D. (1996). "IERS Conventions (1996)." IERS Technical Note No 21, Observatoire de Paris, Paris.

McCarthy, D., and Petit, G. (2002). "Convetions and Combinations." in IERS Technical Note No 30, Proceedings of the IERS Workshop on Combination Research and Global Geophyiscal Fluids, Bavarian Academy of Sciences, Munich, Germany, Verlag des Bundesamts fur Kartographie und Geodasie, Frankfurt am Main, pp63-65.

McCarthy, D., and Petit G. (eds). (2004). "IERS Conventions (2003)." IERS Technical Note No 32, Verlag des Bundesamts fur Kartographie und Geodasie, Frankfurt am Main, 127pp.

McClusky, S., Balassanian, S., Barka, A., Demir, C., Ergintav, S., Georgiev, I., Gurkan, O., Hamburger, M., Hurst, K., Kahle, H., Kastens, K., Kekelidze, G., King, R., Kotzev, V., Lenk, O., Mahmoud, S., Mishin, A., Nadariya, M., Ouzounis, A., Paradissis, D., Peter, Y., Prilepin, M., Reilinger, R., Sanli, I., Seeger, H., Tealeb, A., Toksoz, M. N., and Veis, G. (2000). "Global Positioning System Constraints on Plate Kinematics and Dynamics in the Eastern Mediterranean and Caucasus." Journal of Geophysical Research-Solid Earth, 105(B3), pp5695-5719.

Melbourne, W. G. (1985). "The Case for Ranging in GPS-Based Geodetic Systems." in Vol 1, Proceedings of the First International Syposium in Precise Positioning with the Global Positioning System, Rockville, Maryland, pp373-386.

Menard, Y., Jeansou, E., and Vincent, P. (1994). "Calibration of the TOPEX/Poseidon Altimeters at Lampedusa: Additional Results at Harvest." Journal of Geophysical Research, 99(C12), pp24,487-24,504.

Menard, Y., and Haines, B. (2001). "Jason-1 Calval Plan." CNES-NASA/JPL doc, Ref. TP2-J0-PL-974-CN, CNES, Toulouse, France.

Menard, Y., Fu, L., Escudier, P., Parisot, F., Perbos, J., Vincent, P., Desai, S., Haines, B., and Kunstmann, G. (2003). "The Jason-1 Mission." Marine Geodesy, 26(3-4), pp131-146.

Mertikas, S. P., and the Gavdos Team (2002). "Recent Developments in the Calibration-Verification Site of Gavdos, Greece." in TOPEX/Poseidon Science Working Team (SWT) Meeting, Poster Presentation, October 21-23, New Orleans, Louisiana, USA.

Mikromak. (1998). "Winanalyze - Automatic Motion Analysis Package." Version 1.4, Berlin, Germany. Available at http://www.mikromak.com/en/products/en_winanalyze.htm.

Millet, F. W., Arnold, D. V., Gaspar, P., Warnick, K. F., and Smith, J. (2003a). "Electromagnetic Bias Estimation Using in Situ and Satellite Data: 2. A Nonparametric Approach." Journal of Geophysical Research-Oceans, 108(C2).

Millet, F. W., Arnold, D. V., Warnick, K. F., and Smith, J. (2003b). "Electromagnetic Bias Estimation Using in Situ and Satellite Data: 1. RMS Wave Slope." Journal of Geophysical Research-Oceans, 108(C2).

Mitchum, G. T. (1994). "Comparison of TOPEX Sea Surface Heights and Tide Gauge Sea Levels." Journal of Geophysical Research, 99(C12), pp24,541-24,553.

Mitchum, G. T. (1998). "Monitoring the Stability of Satellite Altimeters with Tide Gauges." Journal of Atmospheric and Oceanic Technology, 15(3), pp721-730.

Mitchum, G. T. (2000). "An Improved Calibration of Satellite Altimetric Heights Using Tide Gauge Sea Levels with Adjustment for Land Motion." Marine Geodesy, 23(3), pp145-166.

Moore, T., Close, G., and Moore, R. (2000). "RiGHt: River Level Monitoring Using GPS Heighting." in ION GPS-00, September 19-22, Salt Lake City, Utah, USA., Published by the Institute of Navigation.

Moore, T., Roberts, G., Veneboer, T., Pattinson, M., Close, G., and Moore, R. (2002). "New Developments in River Level Monitoring Using GPS Heighting." in ION GPS-02, September 24-27, Portland, Oregon, USA., Published by the Institute of Navigation.

Morgan, P., Bock, Y., Coleman, R., Feng, P., Garrard, D., Johnston, G. M., Luton, G., McDowall, B., Pearse, M., Rizos, C., and Tiesler, R. (1996). "A Zero Order GPS Network for the Australian Region." Unisurv S-46, University of New South Wales, School of Geomatic Engineering, Syndey, 187pp.

Morris, C. S., and Gill, S. K. (1994). "Evaluation of the TOPEX/Poseidon Altimeter System over the Great-Lakes." Journal of Geophysical Research-Oceans, 99(C12), pp24527-24539.

Munekane, H., and Matsuzaka, S. (2004). "Nontidal Ocean Mass Loading Detected by GPS Observations in the Tropical Pacific Region." Geophysical Research Letters, 31(8).

Munk, W. H., and MacDonald, G. J. (1975). "The Rotation of the Earth : A Geophysical Discussion." 1st ed, Cambridge University Press, Cambridge, xix, 323pp.

National Tidal Centre. (2005). "The Australian Baseline Sea Level Monitoring Project, Monthly Data Report, January 2005." W. Mitchell, ed., Published by the National Tidal Centre, Bureau of Meteorology, Australia. Available at: http://www.bom.gov.au/fwo/IDO60201/IDO60201.200501.pdf.

Nerem, R. S., Haines, B. J., Hendricks, J., Minster, J. F., Mitchum, G. T., and White, W. B. (1997). "Improved Determination of Global Mean Sea Level Variations Using TOPEX/Poseidon Altimeter Data." Geophysical Research Letters, 24(11), pp1331-1334.

Nerem, R. S., Eanes, R. J., Ries, J. C., and Mitchum, G. T. (2000). "The Use of a Precise Reference Frame for Sea Level Change Studies." in Towards and Integrated Global Geodetic Observing System (IGGOS), R. Rummel, H. Drewes, W. Bosch, and H. Hornik, eds., Springer-Verlag, Munich, Germany, pp8-12.

Nerem, R. S., and Mitchum, G. T. (2001a). "Observations of Sea Level Change from Satellite Altimetry." in Sea Level Rise - History and Consequences, B. C. Douglas, M. S. Kearney, and S. P. Leatherman, eds., Volume 75, International Geophysics Series, Academic Press, San Diego, California, USA., pp121-163.

Nerem, R. S., and Mitchum, G. T. (2001b). "Sea Level Change." in Satellite Altimetry and Earth Sciences - a Handbook of Techniques and Applications, L. L. Fu and A. Cazenave, eds., Volume 69, International Geophysics Series, Academic Press, San Diego, California, USA., pp329-349.

Nerem, R. S., and Mitchum, G. T. (2002). "Estimates of Vertical Crustal Motion Derived from Differences of TOPEX/Poseidon and Tide Gauge Sea Level Measurements." Geophysical Research Letters, 29(19), pp40-1 - 40-4.

Nerem, R. S., Leuliette, E., and Mitchum, G. T. (2004). "CU2004_Rel3.0: Mean Sea Level." University of Colorado, Available at: http://sealevel.colorado.edu/.

NGS (2004). "GPS Antenna Calibration Results." National Oceanic and Atmospheric Administration, National Geodetic Survey, Available at: http://www.ngs.noaa.gov/ANTCAL/.

Nikolaidis, R. M. (2002). "Observation of Geodetic and Seismic Deformation with the Global Positioning System." Thesis for Doctor of Philosophy in Earth Sciences, University of California, San Diego, 249pp.

NTC. (2003). "Tide Gauge Records, Burnie." Published by the National Tidal Centre (NTC), Bureau of Meteorology, Australia. Metadata Available at: http://www.asdd.sa.gov.au/asdd/ANZSA1004000185.html.

Park, K. D., Nerem, R. S., Schenewerk, M. S., and Davis, J. L. (2004). "Site-Specific Multipath Characteristics of Global IGS and CORS GPS Sites." Journal of Geodesy, 77(12), pp799-803.

Parke, M., Blaha, J., and Shum, C. (1997). "Precise Sea Surface Measurements Using DGPS Buoys." in Workshop on methods for monitoring sea level, (R. Neilan, P. Van Scoy, and P. Woodworth, eds.), March 17-18, Pasadena, California, USA, pp117-123.

Pas, K. (2004). "Testing the Equivalence of Regional and Global GPS Solutions." Engineering Masters Thesis, Technical University of Delft, Delft, The Netherlands.

Pavlis, E. C. (2003). "Monitoring the Origin of the TRF with Space Geodetic Techniques." in 13th International Workshop on Laser Ranging, October 5-10, 2002, Washington DC, USA, NASA/CP-2003-212248, pp113-120.

Pavlis, E. C., and Mertikas, S. P. (2004). "The Gavdos Mean Sea Level and Altimeter Calibration Facility: Results for Jason-1." Marine Geodesy, 27(3-4), pp631-655.

Pearlman, M. (2003). "Loss of Stromlo Ranging Station." SLR Electronic Mail, Message No. 1041, Available at: <http://www.aiub.unibe.ch/download/IGSMAIL/04238>.

Pedlosky, J. (1996). "Ocean Circulation Theory." Springer, New York, 453pp.

Peltier, W. R. (2001). "Global Glacial Isostatic Adjustment and Modern Instrumental Records of Relative Sea Level History." in Sea Level Rise - History and Consequences,

B. C. Douglas, M. S. Kearney, and S. P. Leatherman, eds., Volume 75, International Geophysics Series, Academic Press, San Diego, California, USA., pp65-95.

Penna, N. T., and Baker, T. F. (2002). "Ocean Tide Loading Considerations for GPS Processing around Australia." Geomatics Research Australasia, 77, pp1-26.

Penna, N. T., and Stewart, M. P. (2003). "Aliased Tidal Signatures in Continuous GPS Height Time Series." Geophysical Research Letters, 30(23).

Percival, D. B., and Walden, A. T. (2000). "Wavelet Methods for Time Series Analysis." Cambridge University Press, Cambridge, 594pp.

Petrov, L., and Ma, C. P. (2003). "Study of Harmonic Site Position Variations Determined by Very Long Baseline Interferometry." Journal of Geophysical Research-Solid Earth, 108(B4).

Petrov, L., and Boy, J. P. (2004). "Study of the Atmospheric Pressure Loading Signal in VLBI Observations." Journal of Geophysical Research, 109(B4), ppB03405, doi: 10.1029/2003JB002500.

Picot, N., Case, K., Desai, S., and Vincent, P. (2001). "AVISO and PO.DAAC User Handbook. IGDR and GDR Jason Products." SMM-MU-M5-OP-13184-CN (AVISO), JPL D-21352 (PO.DAAC), 106pp.

Pond, S., and Pickard, G. L. (1983). "Introductory Dynamical Oceanography." 2nd ed, Pergamon Press, Oxford, 329pp.

Porter, D. L., and Shih, H. H. (1996). "Investigations of Temperature Effects on Noaa's Next Generation Water Level Measurement System." Journal of Atmospheric and Oceanic Technology, 13(3), pp714-725.

Poutanen, M., Vermeer, M., and Makinen, J. (1996). "The Permanent Tide in GPS Positioning." Journal of Geodesy, 70(8), pp499-504.

PSMSL 2004. "Geographical Distribution of Psmsl Stations." Permanent Service for Mean Sea Level, Available at: http://www.pol.ac.uk/psmsl/images/allpsmsl.gif.

Pugh, D. (1987). "Tides, Surges and Mean Sea Level: A Handbook for Engineers and Scientists." John Wiley and Sons, Chichester, 472pp.

Pugh, D., Hunter, J. R., Coleman, R., and Watson, C. S. (2002). "A Comparison of Historical and Recent Sea Level Measurements at Port Arthur, Tasmania." The International Hydrographic Review, 3(3), pp27-46.

Puri, K., Dietachmayer, G., Mills, G., Davidson, N., Bowen, R., and Logan, L. (1998). "The New BMRC Limited Area Prediction System, LAPS." Australian Meteorological Magazine, 47, pp203-223.

Rabbel, W., and Schuh, H. (1986). "The Influence of Atmospheric Loading on VLBI Experiements." Journal of Geophysics, 59, pp164-170.

Ray, J. (ed). (1999). "IERS Analysis Campaign to Investigate Motions of the Geocentre." IERS Technical Note No 25, Observatoire de Paris, Paris.

Ray, J., Dong, D., and Altamimi, Z. (2004a). "IGS Reference Frames: Status and Future Improvements." GPS Solutions, 8(4), pp251-266.

Ray, J., Schrama, E., and Altamimi, Z. (2004b). "Reference System Session at EGU2005." IGS Electronic Mail, Message Number 5059, Available at: http://igscb.jpl.nasa.gov/mail/igsmail/2004/msg00283.html.

Rio, M. H., and Hernandez, F. (2004). "A Mean Dynamic Topography Computed over the World Ocean from Altimetry, in-Situ Measurements and a Geoid Model." Journal of Geophysical Research, (submitted).

Roca, M., Francis, R., Font, J., Rius, A., Cardellach, E., Schuler, T., Hein, G., Lefèvre, F., Durandeu, J., LeTraon, P., Bouzinac, C., Gomis, D., Ruiz, S., Marcos, M., Monserrat, S., Scharroo, R., Doornbos, E., Richter, A., Liebsch, G., Dietrich, R., and Martellucci, A. (2002). "RA-2 Absolute Range Calibration." in EnviSat Validation Workshop, December 9-13, Frascati, Italy, ESA Publication SP-531, August 2003.

Rocken, C., Kelecy, T. M., Born, G. H., Young, L. E., Purcell, G. H., and Wolf, S. K. (1990). "Measuring Precise Sea Level from a Buoy Using the Global Positioning System." Geophysical Research Letters, 17(12), pp2145-2148.

Rocken, C., Meertens, C., Stephens, B., Braun, J., VanHove, T., Perry, S., Rudd, O., McCullum, M., and Richardson, J. (1995). "UNAVCO Academic Research Infrastructure (ARI) Receiver and Antenna Test Report." University NAVSTAR Consortium Report, Boulder, Colorado, USA.

Ruf, C. S. (2000). "Detection of Calibration Drifts in Space Borne Microwave Radiometers Using a Vicarious Cold Reference." IEEE Transactions on Geoscience and Remote Sensing, 38(1), pp44-52.

Ruf, C. S. (2002). "TMR Drift - Correction to 18ghz Brightness Temperatures, Revisited." Report to TOPEX Project, 3 June, 2002.

Sanli, D. U., and Blewitt, G. (2001). "Geocentric Sea Level Trend Using GPS and > 100-Year Tide Gauge Record on a Postglacial Rebound Nodal Line." Journal of Geophysical Research B: Solid Earth, 106(1), pp713-719.

Scherneck, H. G. (1991). "A Parametrized Solid Earth Tide Model and Ocean Tide Loading Effects for Global Geodetic Base-Line Measurements." Geophysical Journal International, 106(3), pp677-694.

Scherneck, H.-G., and Haas, R. (1999). "Effect of Horizontal Displacements Due to Ocean Tide Loading on the Determination of Polar Motion and Ut1." Geophysical Research Letters, 26(4), pp501-504.

Scherneck, H. G., Johansson, J. M., Vermeer, M., Davis, J. L., Milne, G. A., and Mitrovica, J. X. (2001). "Bifrost Project: 3-D Crustal Deformation Rates Derived from GPS Confirm Postglacial Rebound in Fennoscandia." Earth Planets and Space, 53(7), pp703-708.

Scherneck, H. G., Johansson, J. M., Koivula, H., van Dam, T., and Davis, J. L. (2003). "Vertical Crustal Motion Observed in the Bifrost Project." Journal of Geodynamics, 35(4-5), pp425-441.

Schone, T. 2003. "SEAL: Moored GPS Buoy." Available at: http://op.gfz-potsdam.de/seal/buoy/main_gpsbuoy.html.

Schone, T., Reigber, C., and Braun, A. (2003). "GPS Offshore Buoys and Continuous GPS Control of Tide Gauges." The International Hydrographic Review, 4(3), pp64-70.

Schone, T., Forberg, M., and Esselborn, S. (2004a). "Bottom Mounted Tide Gauges for Radar Altimetery Monitoring." in Ocean Surface Topography Science Team Meeting (OST/ST), St. Petersburg, Florida.

Schone, T., Forberg, M., Galas, R., Reigber, C., and Esselborn, S. (2004b). "Altimeter Calibration Using a Ruggedized GPS-Buoy." in Ocean Surface Topography Science Team Meeting (OST/ST), St. Petersburg, Florida.

Schone, T. 2005. "Tiga GPS Tide Gauge Benchmark Monitoring Pilot Project." Project Home Page, Available at: http://129.247.162.38/tiga/index_TIGA.html.

Schueler, T., Zimmermann, B., and Hein, G. (2003). "Radar Altimeter Calibration of the EnviSat Satellite: An Autonomous System of High-Precision for Instantaneous Sea Surface Height Determination." in ION National Technical Meeting Proceedings, January 22-24, Anaheim, California, USA., Published by the Institute of Navigation.

Schupler, B., and Clark, T. (1991). "How Different Antennas Affect the GPS Observable." GPS World, Nov/Dec 1991, pp32-36.

Schupler, B. R. (2001). "The Response of GPS Antennas - How Design, Environment and Frequency Affect What You See." Physics and Chemistry of the Earth, Part A: Solid Earth and Geodesy, 26(6-8), pp605-611.

Schutz, B. E., Kruizinga, G., Kuang, D., Abusali, P., Shum, C. K., Gutierrez, R., Nelson, S., and Rodriguez, E. (1995). "Galveston Bay Experiment for Altimeter Calibration." in Fall AGU Meeting: Poster Presentation, San Francisco, California, USA.

Schwiderski, E. W. (1980). "Ocean Tides, Part I: Global Ocean Tidal Equations; Part II: A Hydrodynamical Interpolation Model." Marine Geodesy, 3, pp161-255.

Seeber, G., Menge, C., Volksen, S., and Schmitz, M. (1997). "Precise GPS Positioning Improvements by Antenna and Site Dependent Effects." in IAG Symposium No 118, (F. K. Brunner, ed.), September 3-9, Rio de Janeiro, Brasil, Spinger Verlag.

Shum, C., Yi, Y., Cheng, K., Kuo, C., Braun, A., Calmant, S., and Chambers, D. (2003). "Calibration of Jason-1 Altimeter over Lake Erie." Marine Geodesy, 26(3-4), pp335-354.

Sillard, P., Altamimi, Z., and Boucher, C. (1998). "The ITRF96 Realization and Its Associated Velocity Field." Geophysical Research Letters, 25(17), pp3223-3226.

Soler, T. (1998). "A Compendium of Transformation Formulas Useful in GPS Work." Journal of Geodesy, 72(7-8), pp482-490.

Spencer, R., and Vassie, J. M. (1997). "The Evolution of Deep Ocean Pressure Measurements in the UK." Progress in Oceanography, 40(1-4), pp423-435.

Stammer, D. (1997). "Steric and Wind-Induced Changes in TOPEX/Poseidon Large-Scale Sea Surface Topography Observations." Journal of Geophysical Research-Oceans, 102(C9), pp20987-21009.

Steblov, G. M., Kogan, M. G., King, R. W., Scholz, C. H., Burgmann, R., and Frolov, D. I. (2003). "Imprint of the North American Plate in Siberia Revealed by GPS." Geophysical Research Letters, 30(18).

Stewart, R. H. (1985). "Methods of Satellite Oceanography." University of California Press, Berkeley, 360pp.

Summerson, R. M. V., and Handsworth, R. J. (1994). "Instrumentation for Sea Level Measurement in Antarctica and the Southern Ocean." in PACON '94, Recent Advances in Marine Science and Technology, (O. Bellwood, H. Choat, and N. Saxena, eds.), James Cook University of North Queensland, Australia, pp375-384.

Summerson, R. M. V. (1995). "Monitoring Sea Level in the Southern Ocean - the Australian Experience." in IOC Workshop Report No. 115, IOC/GLOSS-IAPSO Workshop on Sea Level Variability and Southern Ocean Dynamics, 31 January, Bordeaux, France, Intergovernmental Oceanographic Commission, pp24-29.

Sun, H. P., Ducarme, B., and Dehant, V. (1995). "Effect of the Atmospheric Pressure on Surface Displacements." Journal of Geodesy, 70, pp131-139.

Sun, W. K., and Sjoberg, L. E. (2001). "Permanent Components of the Crust, Geoid and Ocean Depth Tides." Journal of Geodynamics, 31(3), pp323-339.

Tait, M. E., Summerson, R. M. V., Lennon, G. W., and Handsworth, R. J. (1996). "Macquarie Island - a Platform for Monitoring Sea Level and Its Role in Climate Variability." in Ocean Atmosphere Pacific Conference, 23-27 October, Adelaide, Australia, pp345-351.

Tapley, B. D., and et, a. (1994). "Precision Orbit Determination for TOPEX/Poseidon." Journal of Geophysical Research, 99(C12), pp24,383-24,404.

Tapley, B. D., Watkins, M. M., Ries, J. C., Davis, G. W., Eanes, R. J., Poole, S. R., Rim, H. J., Schutz, B. E., Shum, C. K., Nerem, R. S., Lerch, F. J., Marshall, J. A., Klosko, S. M., Pavlis, N. K., and Williamson, R. G. (1996). "The Joint Gravity Model 3." Journal of Geophysical Research-Solid Earth, 101(B12), pp28029-28049.

Tapley, B. D., and Kim, M. C. (2001). "Applications to Geodesy." in Satellite Altimetry and Earth Sciences - a Handbook of Techniques and Applications, L. L. Fu and A. Cazenave, eds., Volume 69, International Geophysics Series, Academic Press, San Diego, California, USA., pp371-406.

Tapley, B. D., Bettadpur, S., Ries, J. C., Thompson, P. F., and Watkins, M. M. (2004a). "Grace Measurements of Mass Variability in the Earth System." Science, 305(5683), pp503-505.

Tapley, B. D., Bettadpur, S., Watkins, M., and Reigber, C. (2004b). "The Gravity Recovery and Climate Experiment: Mission Overview and Early Results." Geophysical Research Letters, 31(9).

Torrobella, J., and the GRAC-II Team. (2003). "Light GPS Buys Used in the Calibration of EnviSat Altimeter." Geophysical Research Abstracts, European Geophysical Society, 5(14296).

Tregoning, P., Lambeck, K., Stolz, A., Morgan, P., McClusky, S. C., van der Beek, P., McQueen, H., Jackson, R. J., Little, R. P., Laing, A., and Murphy, B. (1998). "Estimation of Current Plate Motions in Papua New Guinea from Global Positioning System Observations." Journal of Geophysical Research-Solid Earth, 103(B6), pp12181-12203.

Tregoning, P., Morgan, P., and Coleman, R. (2004). "The Effect of Receiver Firmware Upgrades on GPS Vertical Timeseries." Cahiers du Centre Européen de Géodynamique et de Séismologie, 23, pp37-46.

Tregoning, P., and van Dam, T. (2005). "The Effects of Atmospheric Pressure Loading and 7-Parameter Transofrmations on Estimates of Geocenter Motion and Station Heights from Space-Geodetic Observations." Journal of Geophysical Research, In Press.

Twilley, R. J., and Digney, P. W. (2001). "The Australian Regional GPS Network." Physics and Chemistry of the Earth Part a-Solid Earth and Geodesy, 26(6-8), pp629-635.

UNESCO. (1983). "Algorithms for Computation of Fundamental Properties of Seawater." UNESCO Technical Papers in Marine Science, No 44., 53pp.

van Dam, T., and Wahr, J. (1987). "Displacements of the Earth's Surface Due to Atmospheric Loading: Effects on Gravity and Baseline Measurements." Journal of Geophysical Research, 92, pp1281-1286.

van Dam, T., Blewitt, G., and Heflin, M. B. (1994). "Atmospheric Pressure Loading Effects on Global Positioning System Coordinate Determinations." Journal of Geophysical Research, 99(B12), pp23,939-23,950.

van Dam, T., and Herring, T. A. (1994). "Detection of Atmospheric Pressure Loading Using Very Long Baseline Interferometry Measurements." Journal of Geophysical Research, 99, pp4505-4517.

van Dam, T. M., and Wahr, J. (1998). "Modeling Environment Loading Effects: A Review." Physics and Chemistry of the Earth, 23(9-10), pp1077-1087.

van Dam, T., Wahr, J., Milly, P. C. D., Shmakin, A. B., Blewitt, G., Lavallee, D., and Larson, K. M. (2001). "Crustal Displacements Due to Continental Water Loading." Geophysical Research Letters, 28(4), pp651-654.

van Dam, T., Plag, H. P., Francis, O., and Gegout, P. (2002). "GGFC Special Bureau for Loading: Current Status and Plans." in IERS Technical Note No 30, Proceedings of the IERS Workshop on Combination Research and Global Geophyiscal Fluids, Bavarian Academy of Sciences, Munich, Germany, Verlag des Bundesamts fur Kartographie und Geodasie, Frankfurt am Main, pp180-198.

van Dam, T., and Francis O. (eds). (2003). "Proceedings of the Workshop: The State of GPS Vertical Positioning Precision: Separation of Earth Processes by Space Geodesy." Centre Européen de Géodynamique et de Séismologie, Luxembourg, ECGS Cahiers bleus Vol 23, 176pp.

van Dam, T., and Tregoning, P. (2005). "Correcting GPS Data for Atmospheric Pressure Loading at the Observation Level." In Preparation for submission to the Journal of Geophysical Research.

Wahr, J. (1981). "The Forced Nutations of an Elliptical, Rotating, Elastic, and Oceanless Earth." Geophysical Journal of the Royal Astronomical Society, 64, pp705-727.

Wang, Y. M. (2001). "GSFC00 Mean Sea Surface, Gravity Anomaly, and Vertical Gravity Gradient from Satellite Altimeter Data." Journal of Geophysical Research C: Oceans, 106(12), pp31167-31174.

Watson, C. S. (1999). "A Contribution to Absolute Sea Level in Tasmania." Thesis for Bachelor of Surveying with Honours, University of Tasmania, Hobart, Australia, 197pp.

Weber, R., Bruyninx, C., Scherneck, H. G., Rothacher, M., Andersen, P. H., Baker, T. F., and van Dam, T. (2002). "GPS / GLONASS and Tidal Effects." in Report from the Subgroup on GPS / GLONASS of the IAG/ETC Working Group 6 (Solid Earth Tides in Space Geodetic Techniques), Marrees Terrestres Bulletin d'informations, Number 134, pp10559-10566.

Welch, P. D. (1967). "The Use of Fast Fourier Transform for the Estimation of Power Spectra: A Method Based on Time Averaging over Short, Modified Periodograms." IEEE Transactions on Audio Electroacoutstics, AU(15), pp70-73.

White, N. J., Coleman, R., Church, J. A., Morgan, P. J., and Walker, S. J. (1994). "A Southern-Hemisphere Verification for the TOPEX/Poseidon Satellite Altimeter Mission." Journal of Geophysical Research-Oceans, 99(C12), pp24505-24516.

Williams, S., Bock, Y., and Fang, P. (1998). "Integrated Satellite Interferometry: Tropospheric Noise, GPS Estimates and Implications for Interferometric Synthetic Aperture Radar Products." Journal of Geophysical Research-Solid Earth, 103(B11), pp27051-27067.

Williams, S. D. P. (2002). "The Effect of Coloured Noise on the Uncertainties of Rates Estimated from Geodetic Time Series." Journal of Geodesy, 76(9-10), pp483-494.

Williams, S. D. P., Bock, Y., Fang, P., Jamason, P., Nikolaidis, R. M., Prawirodirdjo, L., Miller, M., and Johnson, D. J. (2004). "Error Analysis of Continuous GPS Position Time Series." Journal of Geophysical Research B: Solid Earth, 109(3), ppB03412 1-19.

Willis, P. (2004). "Preliminary Results on the Sensitivity to Radiations of the Back-up DORIS/Jason Oscillator." in Ocean Surface Topography Science Team Meeting (OSTST), St. Petersburg, Florida.

Willis, P., Haines, B., Berthias, J. P., Sengenes, P., and Le Mouël, J. (2004). "Behavior of the DORIS/Jason Oscillator over the South Atlantic Anomaly." Submitted to Compte-Rendus de l'Académie des Sciences.

Winkler, M. F., and Wooley, R. T. (2002). "Current Direction and Velocity Measurements Using GPS Receivers Mounted on Floats at Tom Bevill Lock and Dam." Report: ERDC/CHL CHETN-IX-11, U.S. Army Engineer Research and Development Center, Vicksburg, Mississippi, USA., 7pp.

Woodworth, P. L., Vassie, J. M., Spencer, R., and Smith, D. E. (1996). "Precise Datum Control for Pressure Tide Gauges." Marine Geodesy, 19(1), pp1-20.

Woodworth, P. L., and Smith, D. E. (2003). "A One Year Comparison of Radar and Bubbler Tide Gauges at Liverpool." The International Hydrographic Review, 4(3), pp42-49.

Woodworth, P., Moore, P., Dong, X., and Bingley, R. (2004). "Absolute Calibration of the Jason-1 Altimeter Using Uk Tide Gauges." Marine Geodesy, 27(1-2), pp95-106.

Wubbena, G. (1985). "Software Developments for Geodetic Positioning with GPS Using TI4100 Code and Carrier Mesurements." in Vol 1, Proceedings of the First International Syposium in Precise Positioning with the Global Positioning System, Rockville, Maryland, pp403-412.

Wubbena, G., Schmitz, M., Menge, F., Seeber, G., and Volksen, C. (1997). "A New Approach for Field Calibration of Absolute GPS Antenna Phase Centre Variations." Journal of the Institute of Navigation, 44(2), pp247-255.

Wubbena, G., Schmitz, M., Menge, C., Boder, V., and Seeber, G. (2000). "Automated Absolute Field Calibration of GPS Antennas in Real-Time." in ION GPS-00, September 19-22, Salt Lake City, Utah, USA., Published by the Institute of Navigation.

Wunsch, C., and Stammer, D. (1998). "Satellite Altimetry, the Marine Geoid, and the Oceanic General Circulation." Annual Review of Earth and Planetary Sciences, 26, pp219-253.

Yokoyama, Y., Esat, T. M., and Lambeck, K. (2001). "Coupled Climate and Sea-Level Changes Deduced from Huon Peninsula Coral Terraces of the Last Ice Age." Earth and Planetary Science Letters, 193(3-4), pp579-587.

Zhang, J., Bock, Y., Johnson, H., Fang, P., Williams, S., Genrich, J., Wdowinski, S., and Behr, J. (1997). "Southern California Permanent GPS Geodetic Array: Error Analysis of Daily Position Estimates and Site Velocities." Journal of Geophysical Research-Solid Earth, 102(B8), pp18035-18055.

Zhu, S. Y., Massmann, F. H., Yu, Y., and Reigber, C. (2003). "Satellite Antenna Phase Center Offsets and Scale Errors in GPS Solutions." Journal of Geodesy, 76(11-12), pp668-672.

Zlotnicki, V., and Desai, S. D. (2004). "Assessment of the Jason Microwave Radiometer's Measurement of Wet Tropospheric Path Delay Using Comparisons to SSM/I and TMI." Marine Geodesy, 27(1-2), pp241-253.

Zumberge, J. F., Heflin, M. B., Jefferson, D. C., Watkins, M. M., and Webb, F. H. (1997). "Precise Point Positioning for the Efficient and Robust Analysis of GPS Data from Large Networks." Journal of Geophysical Research, 102(B3), pp5005-5017.

Appendix A

GPS Buoy Analysis

Appendix A is provided on the CD-ROM accompanying this Thesis (see the final page for the CD-ROM). Readers viewing a digital copy of this Thesis may obtain a copy of the CD-ROM by contacting:


```
Centre for Spatial Information Science (CenSIS)
School of Geography and Environmental Studies
University of Tasmania
Private Bag 76
Hobart, Tasmania
Australia 7001
```


The following pages provide hardcopy samples from each sub-directory for Appendix A on the CD-ROM, as outlined below:

Sub-directory	Description
Deployment Summaries	An individual plot is included for each buoy solution, for each deployment. As two reference stations were used with two buoys, this translates to four plots per deployment (TBCP to Buoy1, TBCP to Buoy2, RKCP to Buoy1 and RKCP to Buoy2). See page A-2 for an example and description.
Buoy vs Mooring	Contains a plot for each deployment showing the four buoy solutions against the mooring sea surface height. See page A-3 for an example and description.

Deployment Summaries Sub-Directory:

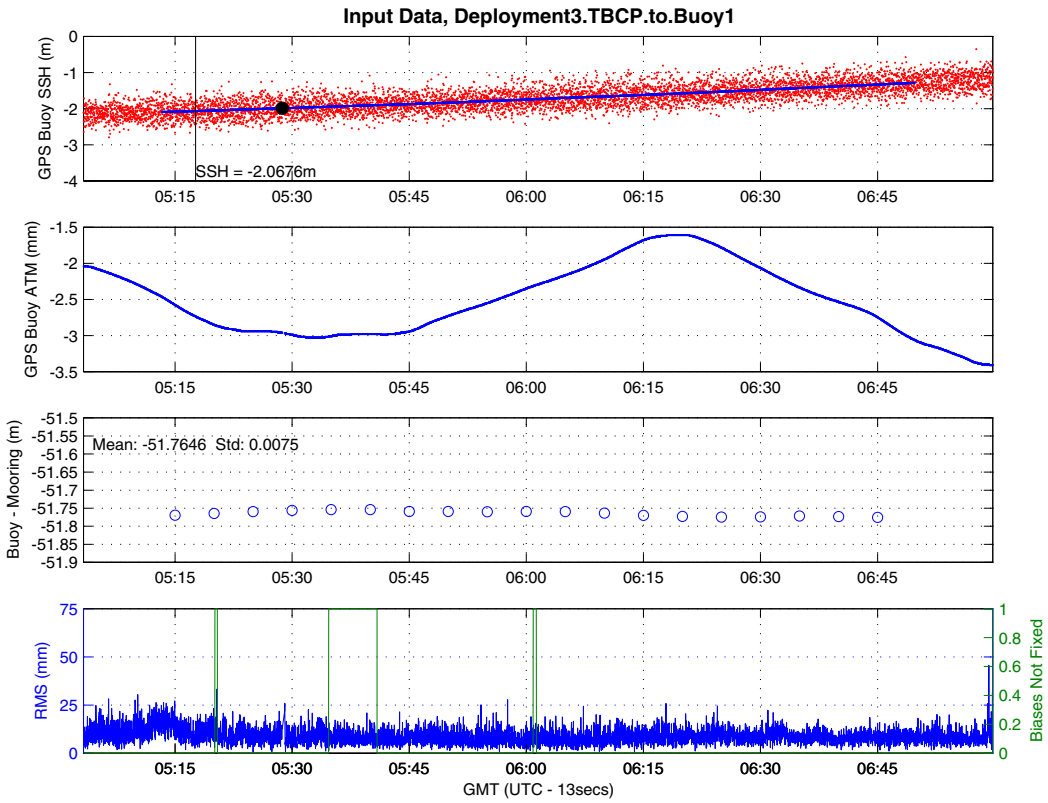

Figure A-1 *TBCP to Buoy1 solution for deployment 3. Description below.*

Top Panel: *1 Hz estimates of sea surface height (SSH) from the GPS buoy (red) with filtered GPS buoy SSH shown in blue. Vertical black line indicates time of altimeter overflight. The black dot indicates a data gap typically caused by large swell events.*

Second Panel: *1 Hz estimates of residual tropospheric delay between the reference station and the GPS buoy.*

Third Panel: *Filtered GPS buoy SSH – Mooring SSH*

Bottom Panel: *1 Hz RMS from the TRACK analysis shown in blue. Number of bias parameters not fixed shown in green.*

Buoy vs Mooring Sub-Directory:

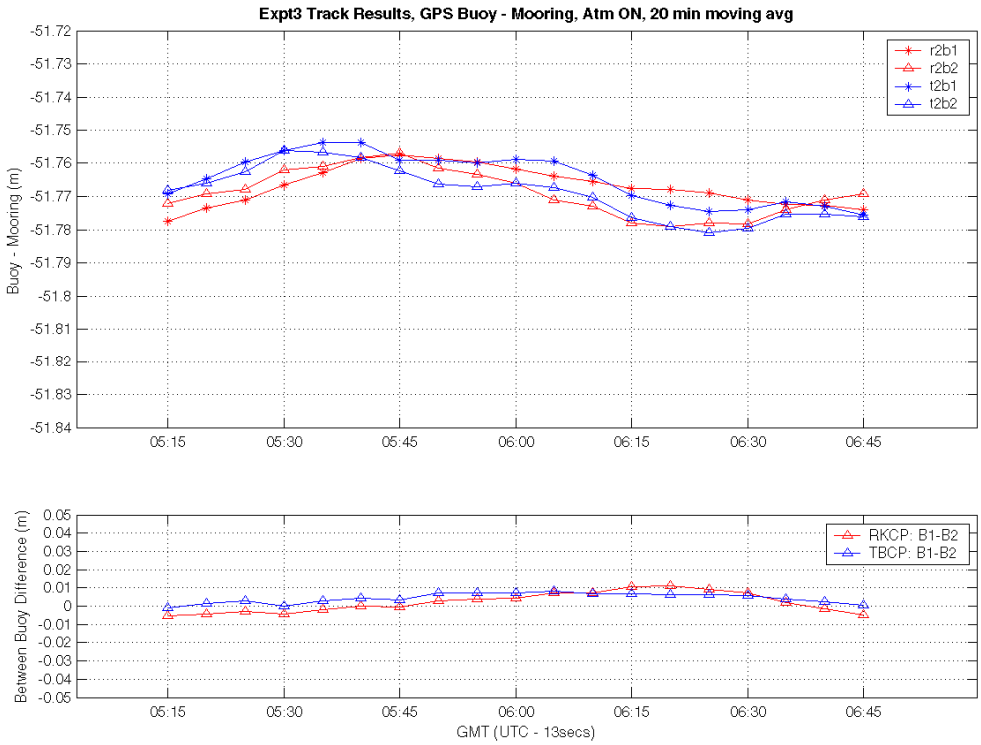

Figure A-2 GPS buoy vs mooring sea surface height (SSH) for all solutions during deployment 3. The top panel shows the filtered GPS buoy SSH – the Mooring SSH (i.e., the ellipsoidal height of the mooring zero). The lower panel shows the difference between Buoy1 and Buoy2 SSH from the RKCP and TBCP reference stations.

Appendix B

Working at the 1-cm Level

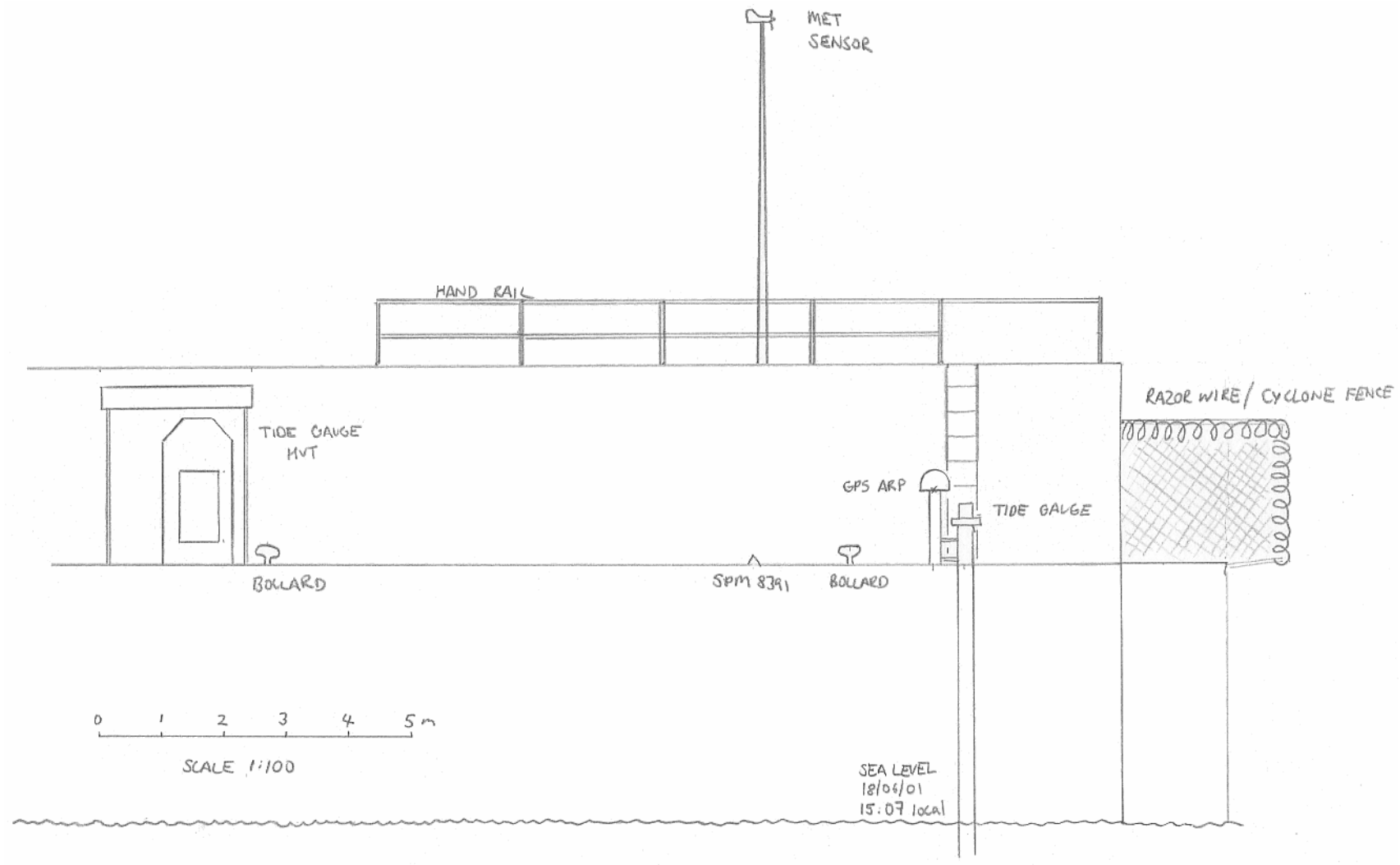

Figure B-1 Elevation view of the Burnie (BUR1) GPS site, looking directly towards the break water (looking N 20° E)

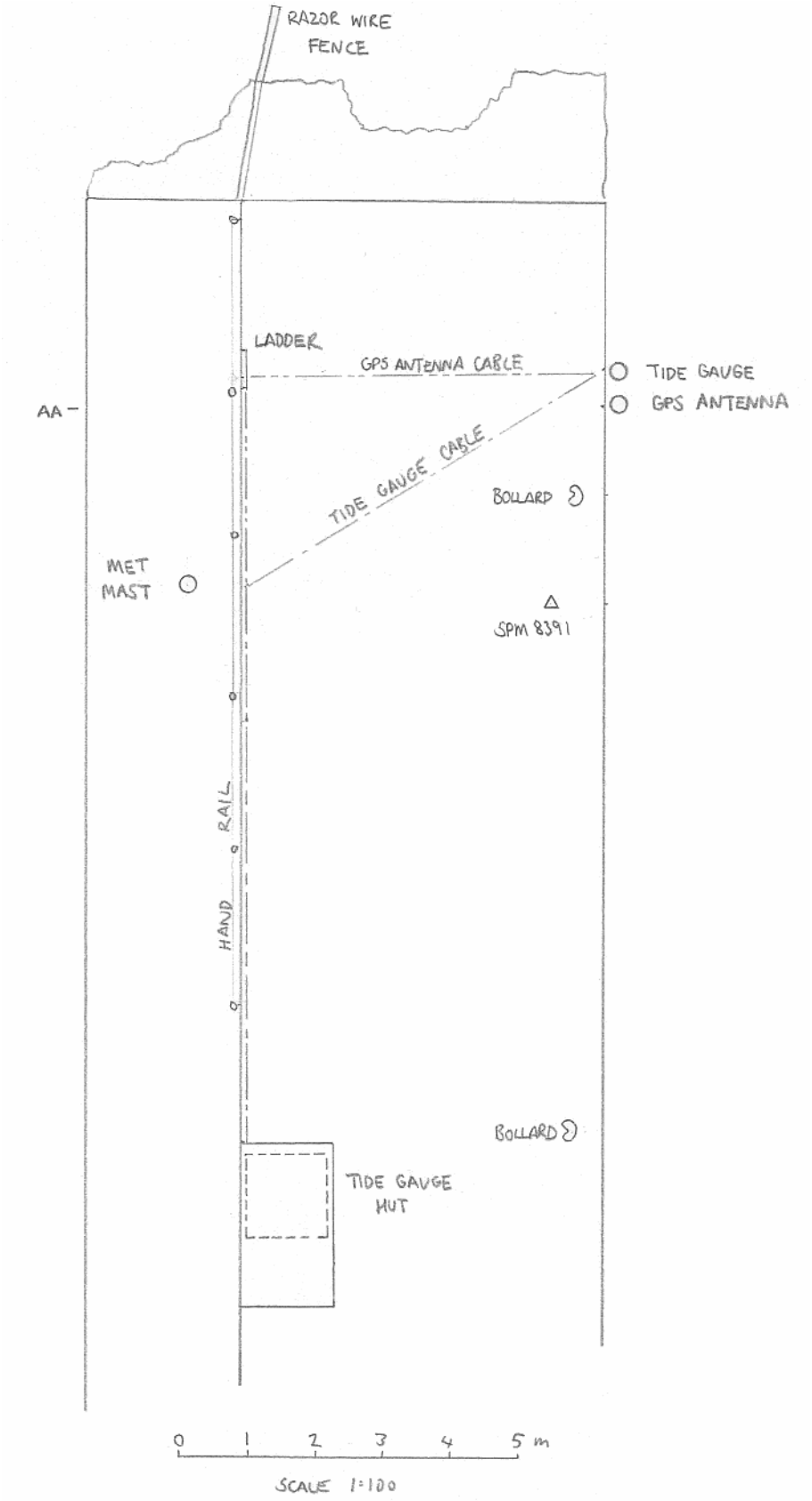

Figure B-2 Plan view of the Burnie (BUR1) GPS site. Note the position of Section AA which is shown in the next figure.

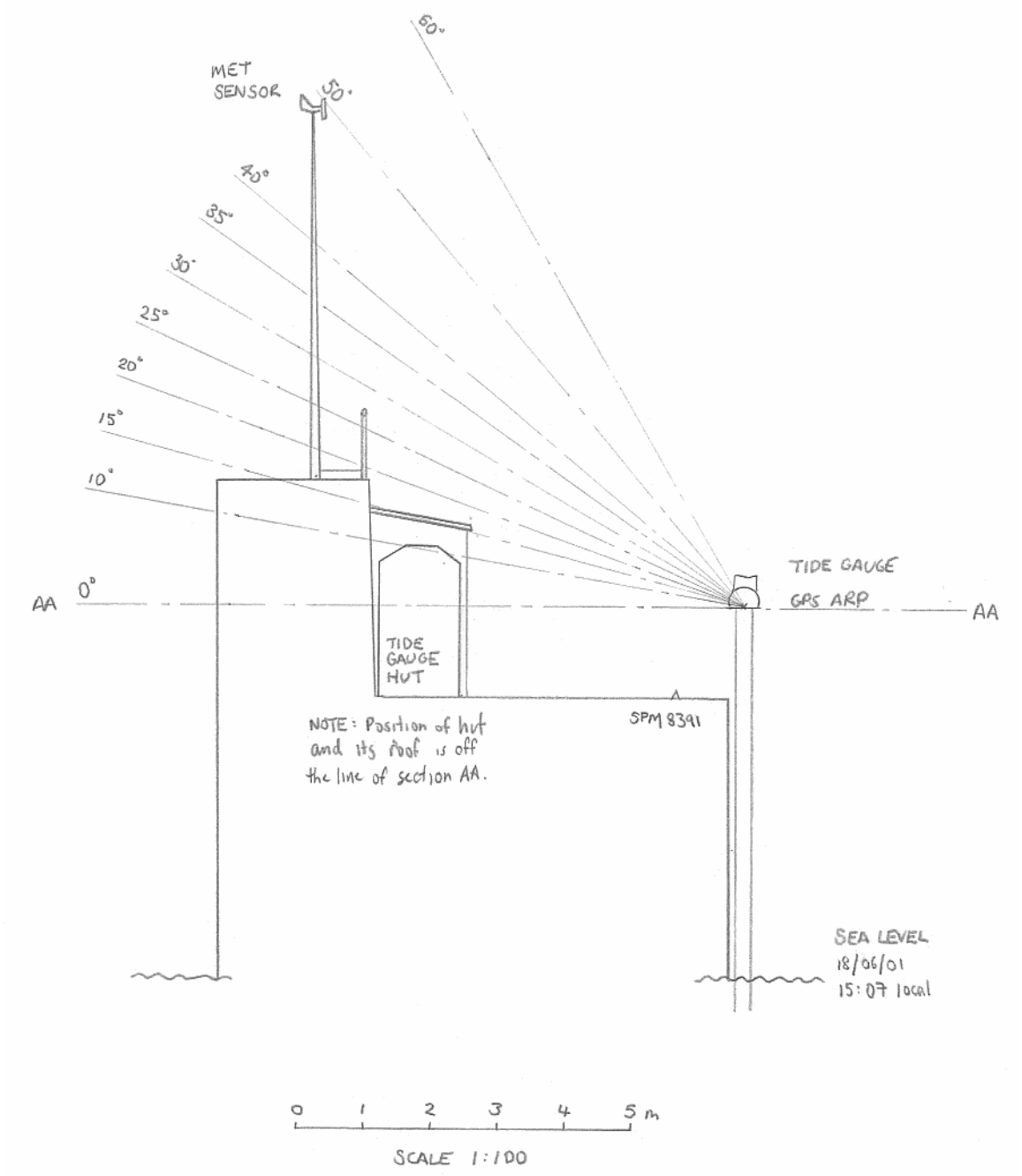

Figure B-3 Section AA at the Burnie (BUR1) GPS site

Solid Earth Tide, Site: DARW

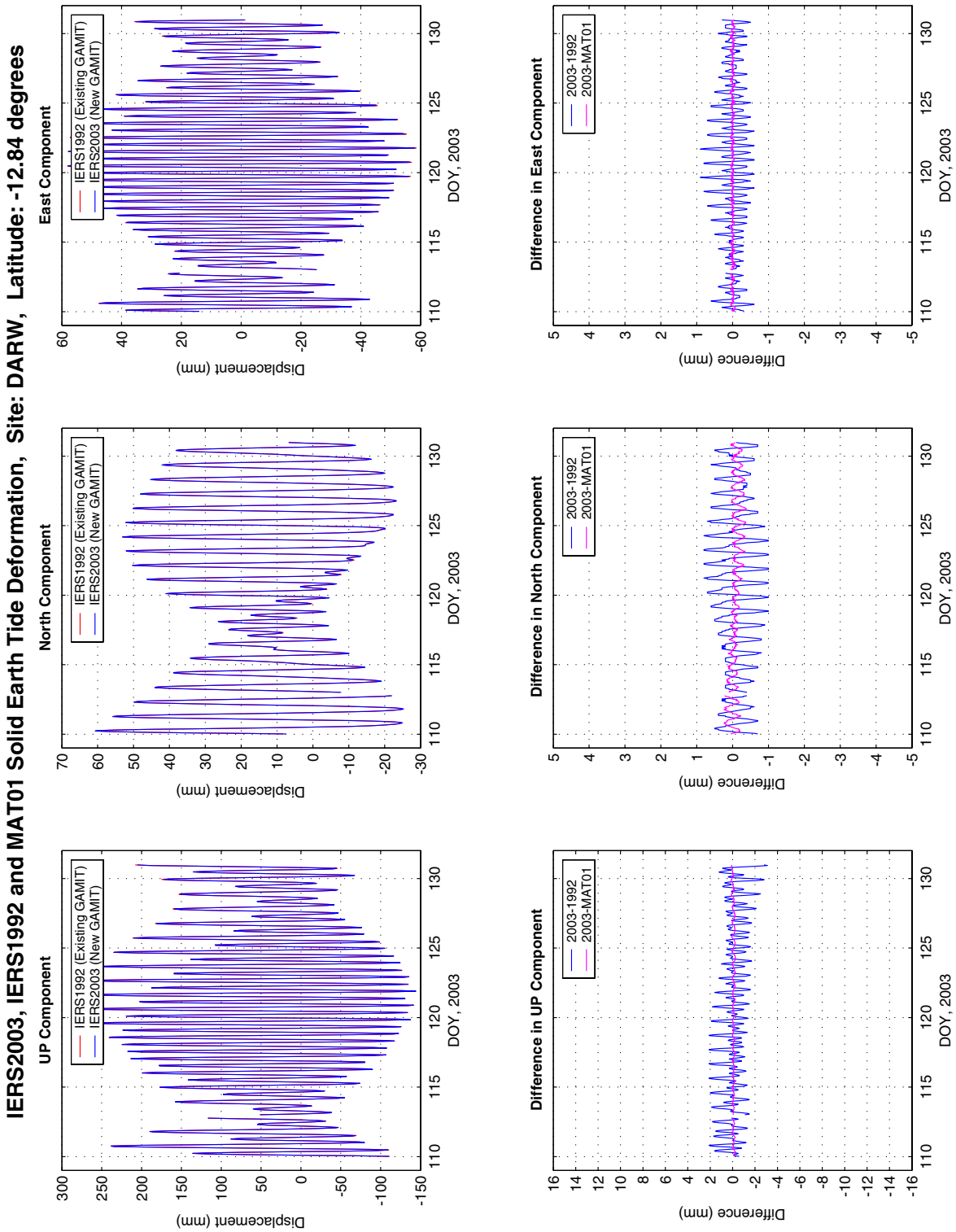

Solid Earth Tide, Site: ALIC

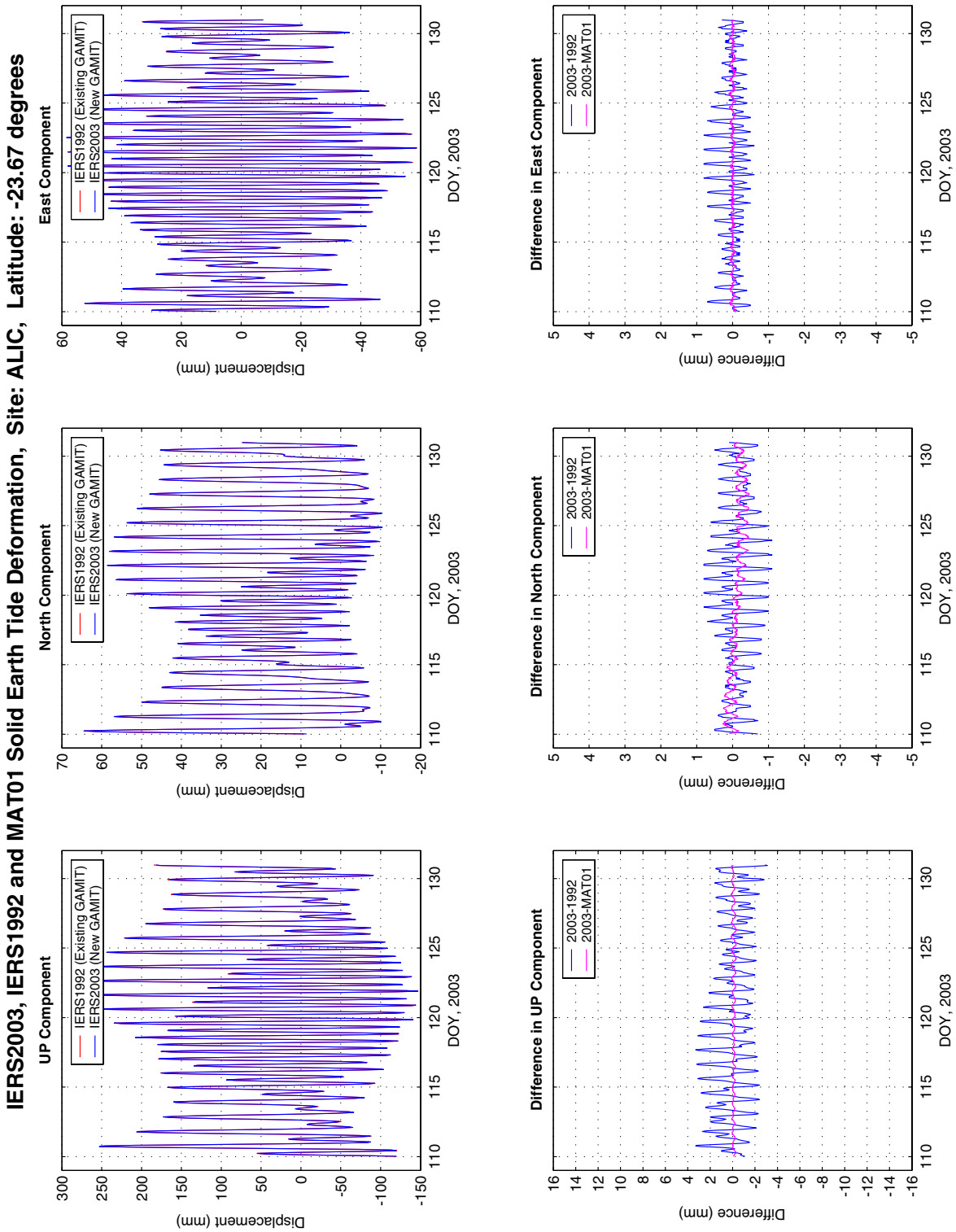

Solid Earth Tide, Site: CEDU

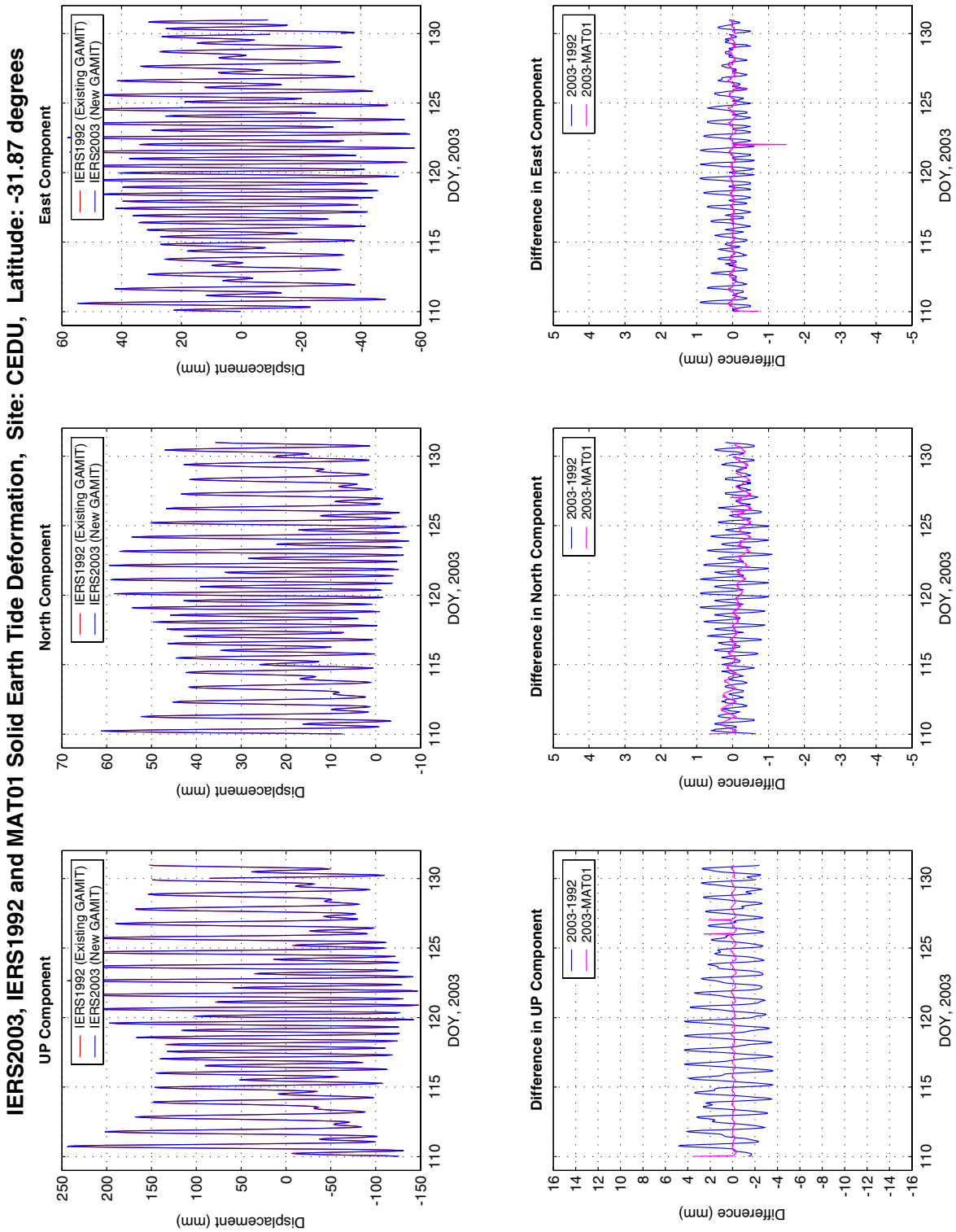

Solid Earth Tide, Site: HOB2

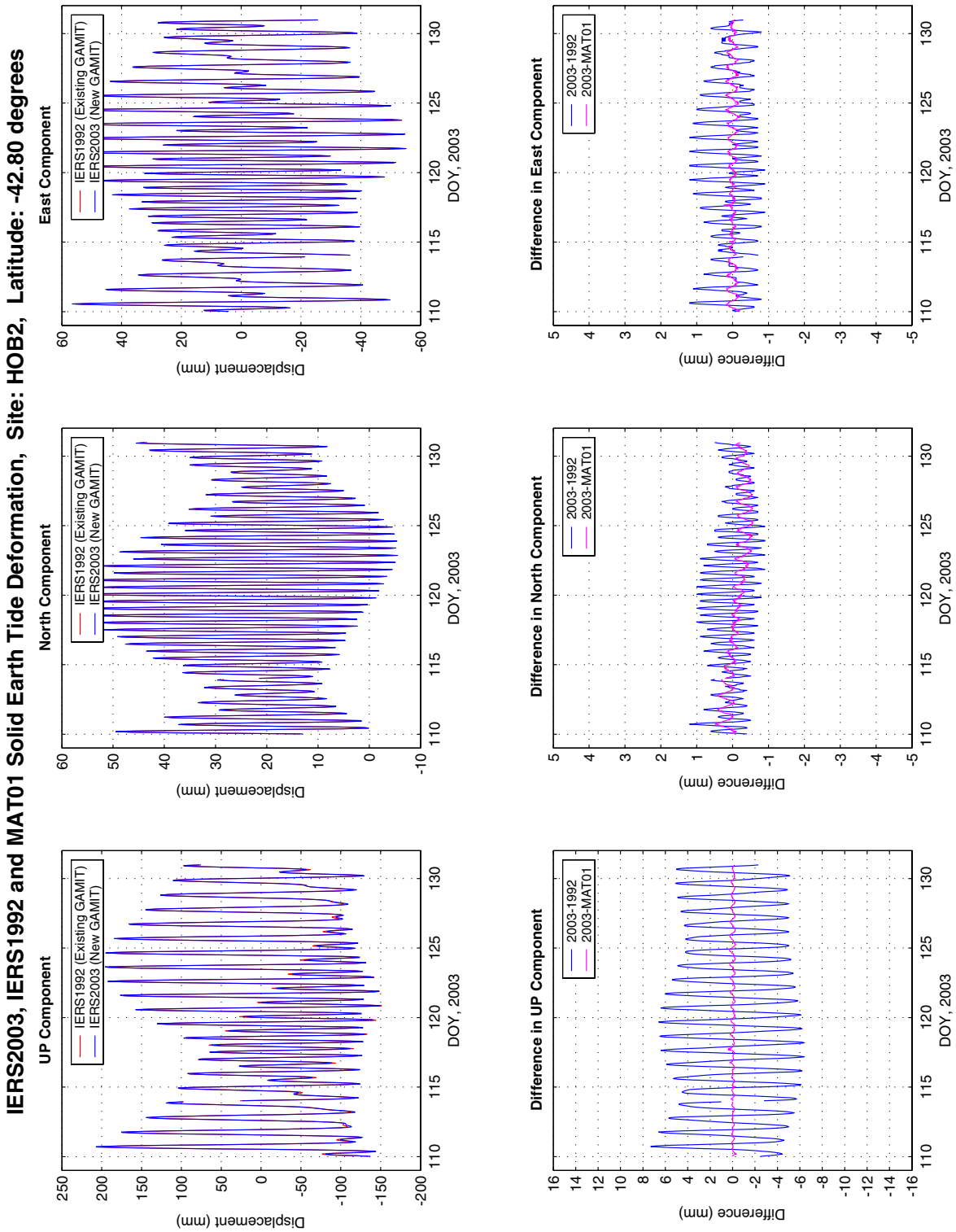

Solid Earth Tide, Site: MAC1

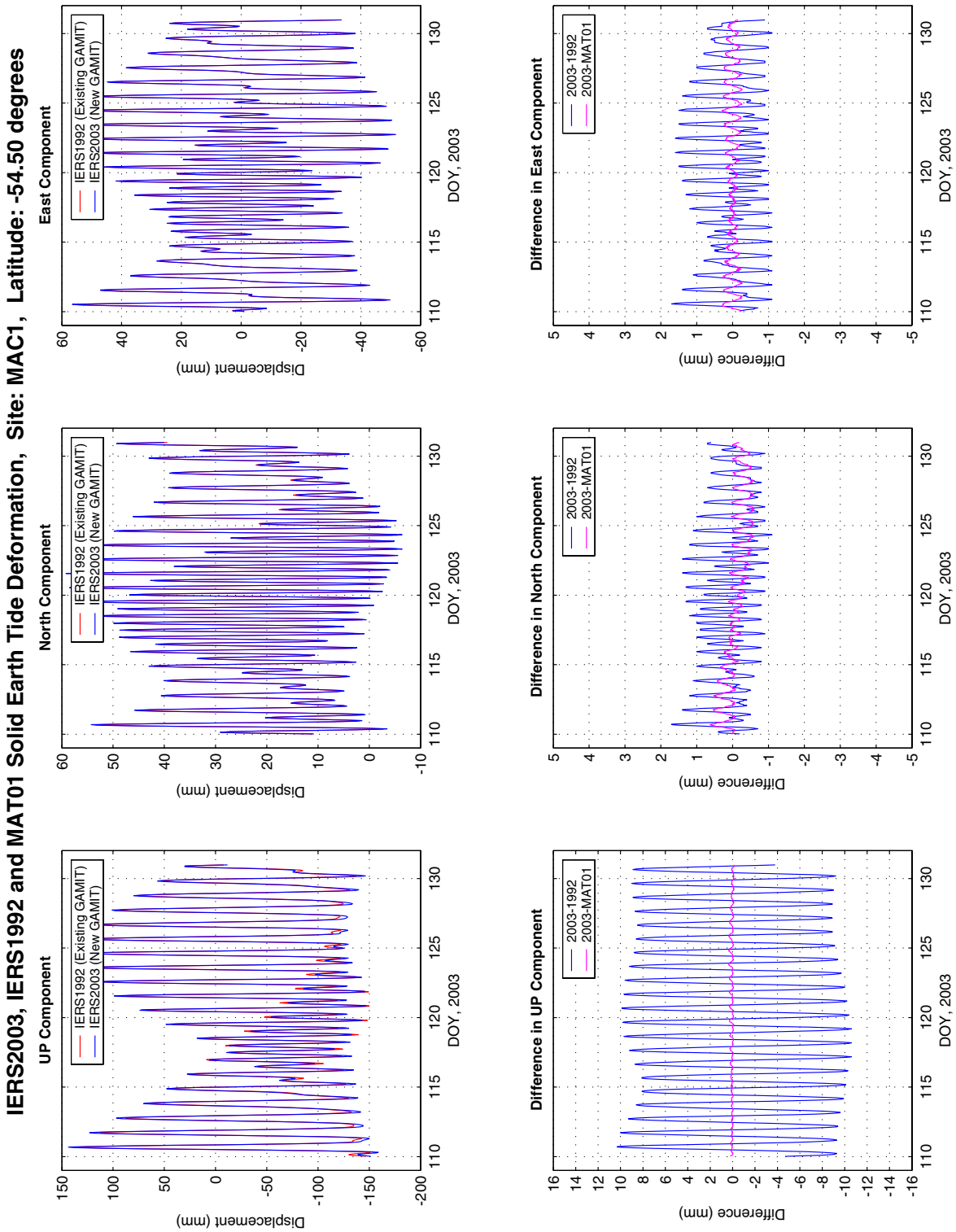

Solid Earth Tide, Site: CAS1

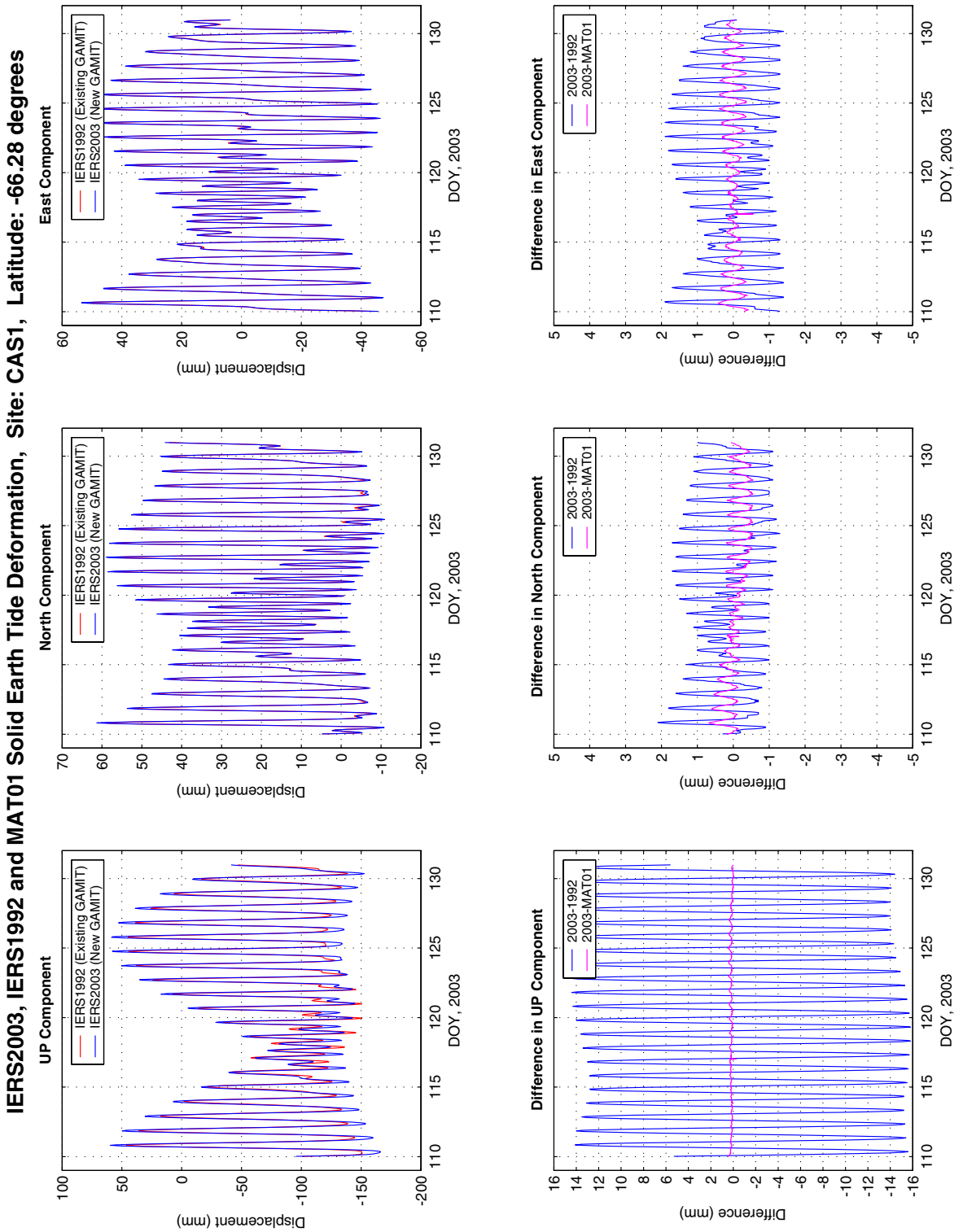

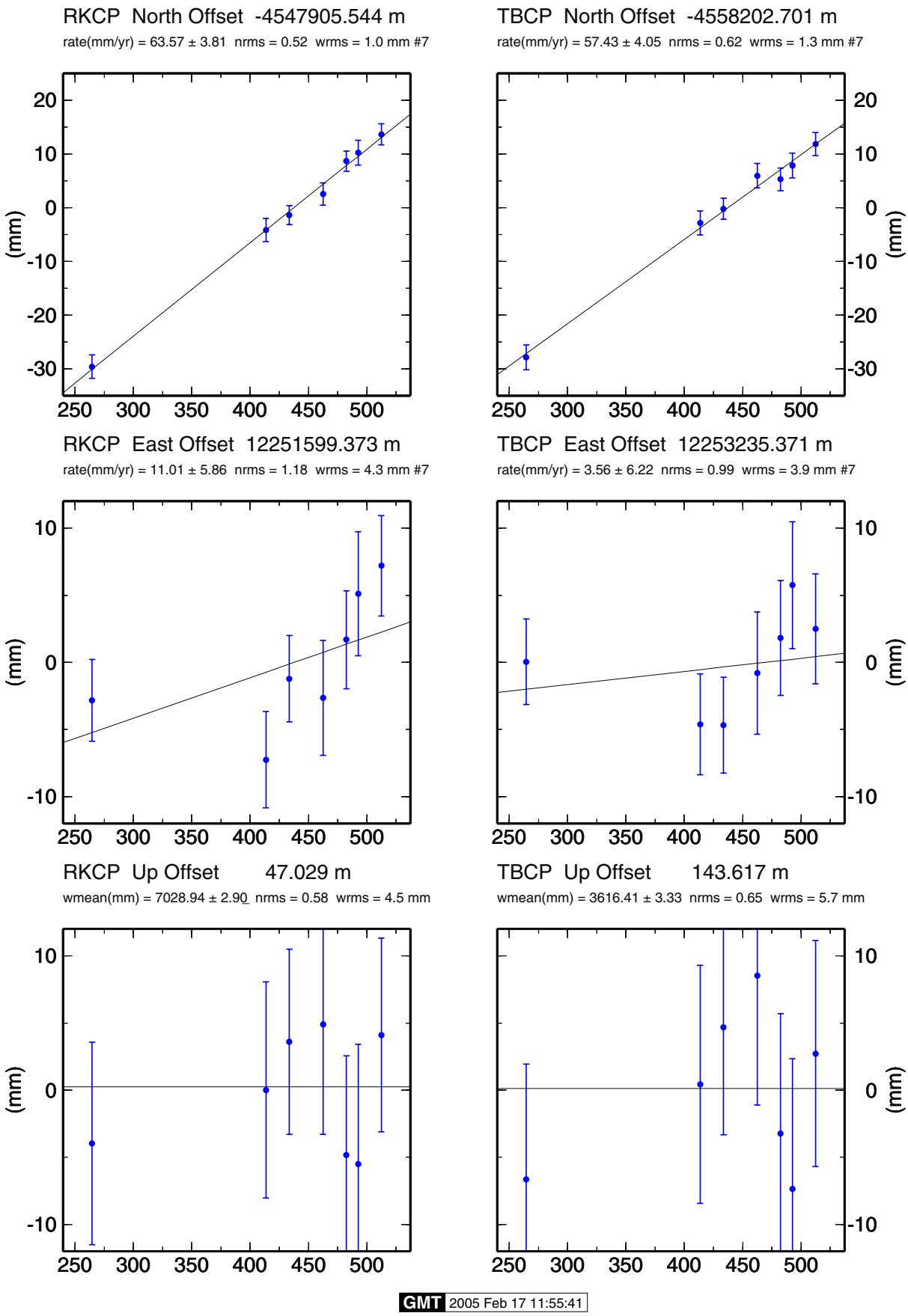

Figure B-4 GLRED Analysis for the RKCP and TBCP sites.

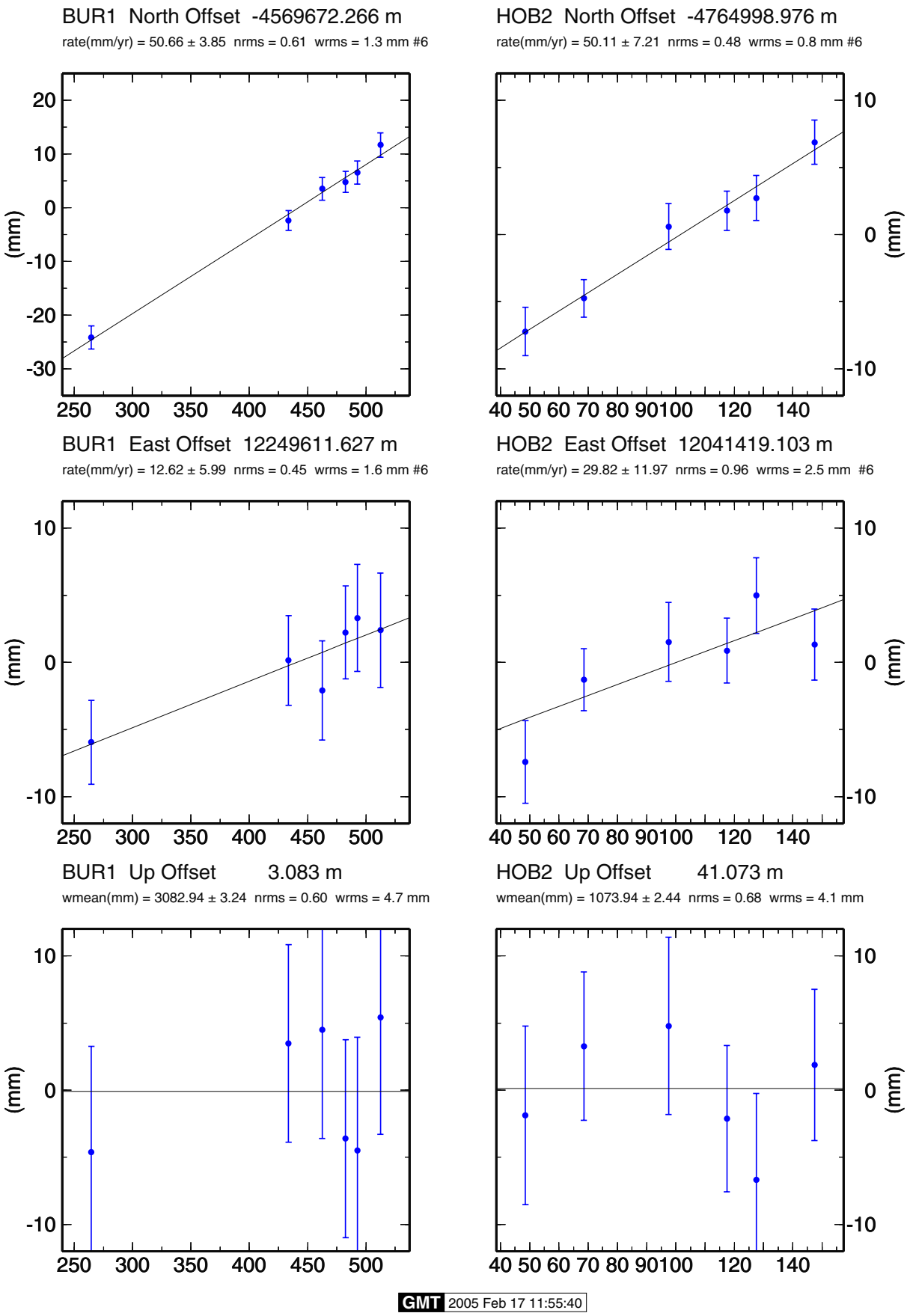

Figure B-5 GLRED Analysis for the RKCP and TBCP sites.

Time Series Information

Results from the time series analysis undertaken in Chapter 3 have been included on the CD-ROM supplement supplied with this Thesis.

Numerical and graphical results have been compiled in a viewer which operates in Microsoft® Office Excel 2003. The AutoFilter function within Excel has been utilised to simplify the navigation of the results. For example, to view results from all solutions (PJM, JPL, SOP and GA), for the HOB2 site, in the vertical component only, users can follow the steps shown in Figures B-6 to B-9.

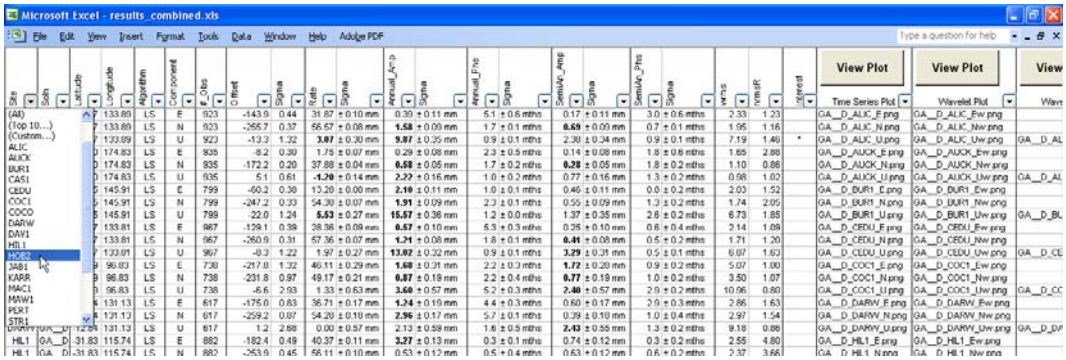

Figure B-6 Select the HOB2 site from the "site" AutoFilter drop down list.

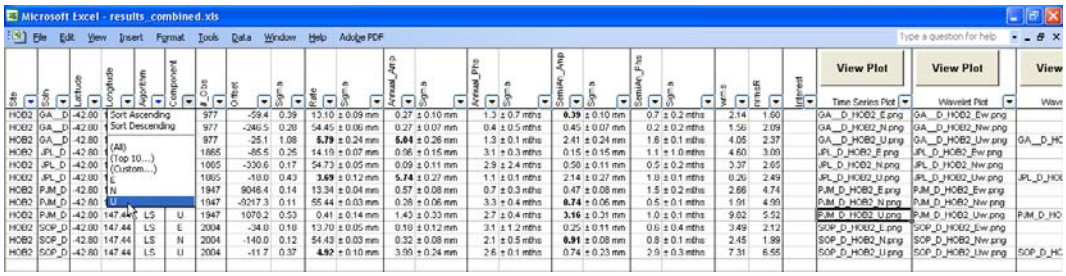

Figure B-7 Select the U component (U = UP = vertical component) from the "component" AutoFilter drop down list. Note after the previous selection only results for the HOB2 site are visible.

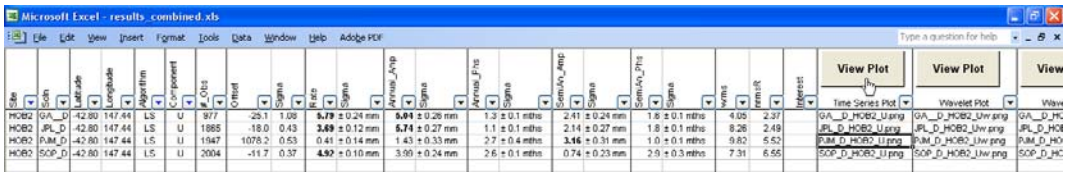

Figure B-8 Now results for all solutions, only results for HOB2, only for the vertical component, are visible. Clicking on the time series plot file name (PJM_D_HOB2_U.png) and then clicking the "View Plot" button reveals the time series plot. The same technique is used to show the discrete wavelet and continuous wavelet analysis plots respectively.

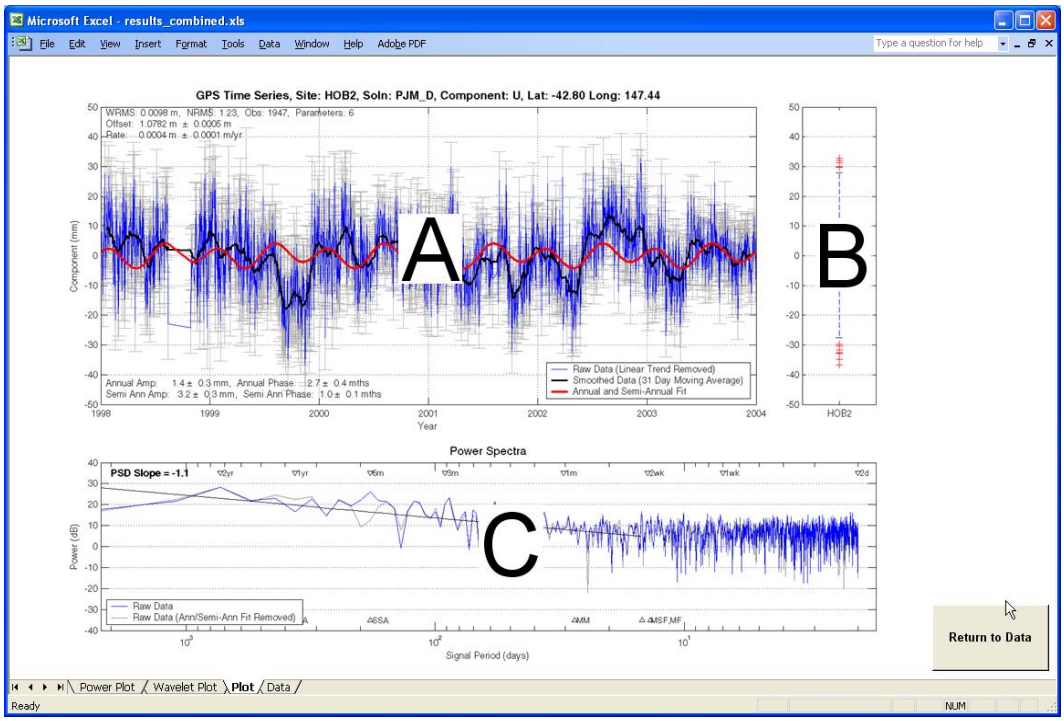

Figure B-9 Time series plot window is shown. Click the "Return to Data" button to return to the previous window. Panels A, B and C are defined below.

Information included in the time series figure includes:

A) Time series between 1998-2004 is shown in the spatial domain (offset and trend removed), with 1-sigma error bars. A smoothed version of the time series (31 day moving average) is shown, in addition to the annual and semi-annual model fit. Various statistics are shown in the upper and lower left hand corners.

B) Box plot of the raw data.

C) Power spectra of both the raw (offset and trend removed) and the postfit data (offset, trend, semi-annual and annual terms removed). Tidal frequencies have been included for reference.

Both the discrete and continuous wavelet figures are self-explanatory.

For further assistance with the AutoFilter, see the online help within Excel.

Appendix C

Absolute Calibration in Bass Strait

Appendix C is provided on the CD-ROM accompanying this Thesis. In addition to barometric charts from each buoy deployment, the following pages provide hardcopy samples from each sub-directory on the CD-ROM, as outlined below:

Sub-directory	Description
Mooring	Contains plots of the dynamic height computed at the offshore mooring. Computed by Dr Neil White.
	See page C-2 for an example.
Topex Overflight Summaries	Shows ancillary data for each T/P overflight at the comparison point. In addition to altimeter data, other information shown includes mooring and tide gauge time series, current meter time series, temperature and atmospheric pressure time series (at Burnie) and the radiometer time series.
	See page C-3 for an example.
TMR Extrapolation	Shows the T/P microwave radiometer time series crossing Bass Strait for each overflight. The "corrected" and "extrapolated" time series are shown when approaching the comparison point.
	See page C-4 for an example.
TMR vs GPS	Shows the T/P microwave radiometer data plotted against the BUR1 GPS wet delay time series for each overflight. Temperature and pressure time series are also shown.
	See page C-5 for an example.
Jason Overflight Summaries	As per T/P however using Jason-1 data.
	See page C-6 for an example.
JMR Extrapolation	As per T/P however using Jason-1 data.
	See page C-7 for an example.
JMR vs GPS	As per T/P however using Jason-1 data.
	See page C-8 for an example.

Barometric Charts:

Table C-1 GPS buoy deployment at the Bass Strait calibration site.

Deployment	Date	T/P Cycle	Jason-1 Cycle
1	21/09/2001	332	-
2	17/02/2002	347	4
3	09/03/2002	349	6
4	07/04/2002	352	9
5	27/04/2002	354	11
6	07/05/2002	355	12
7	27/05/2002	357	14

Deployment 1:

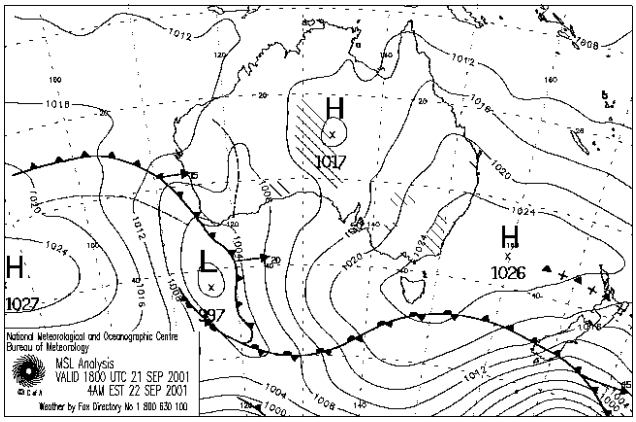

Deployment 2:

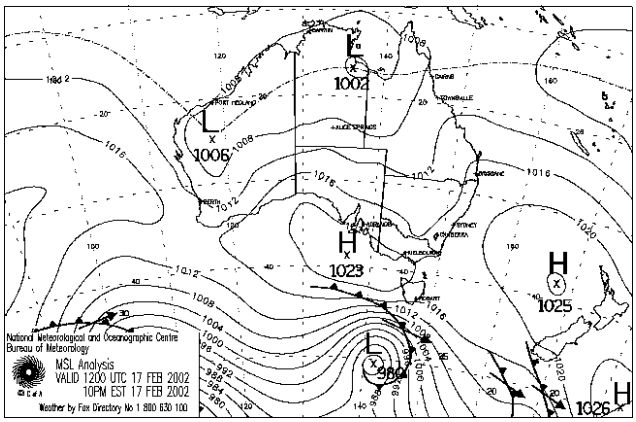

Deployment 3:

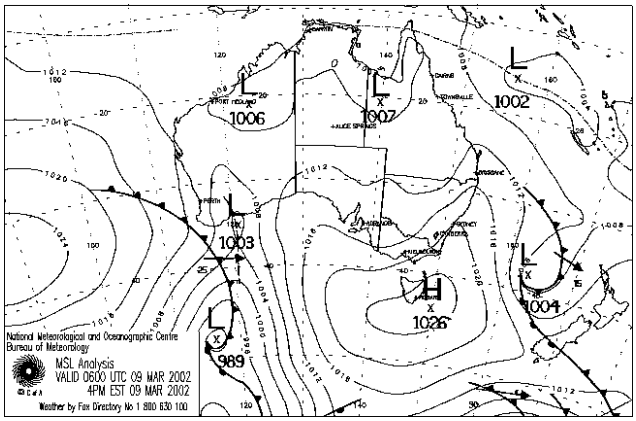

Deployment 4:

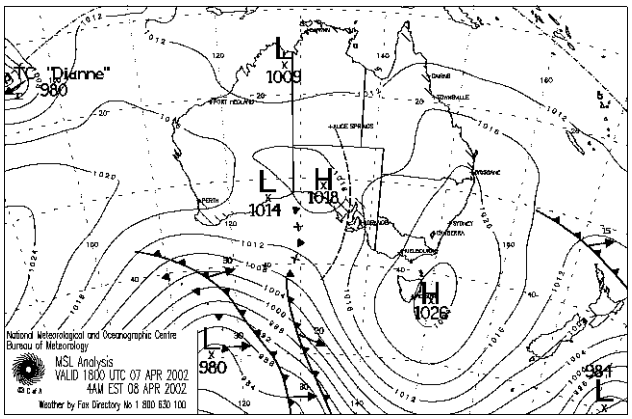

Deployment 5:

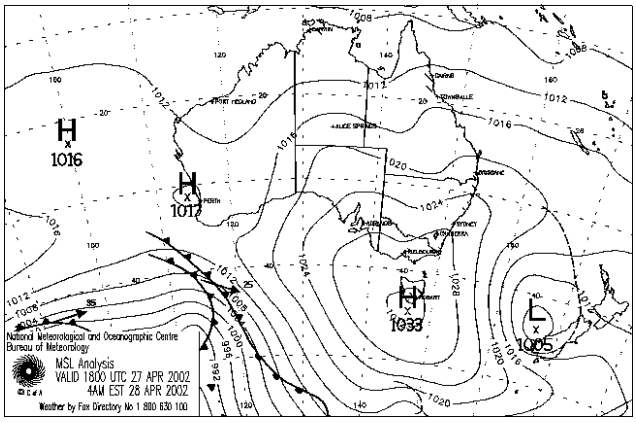

Deployment 6:

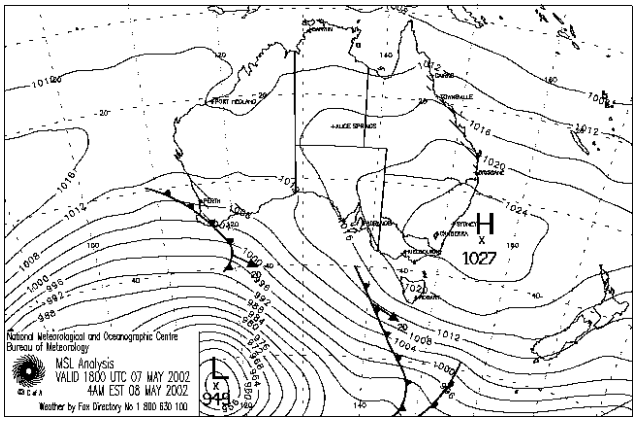

Deployment 7:

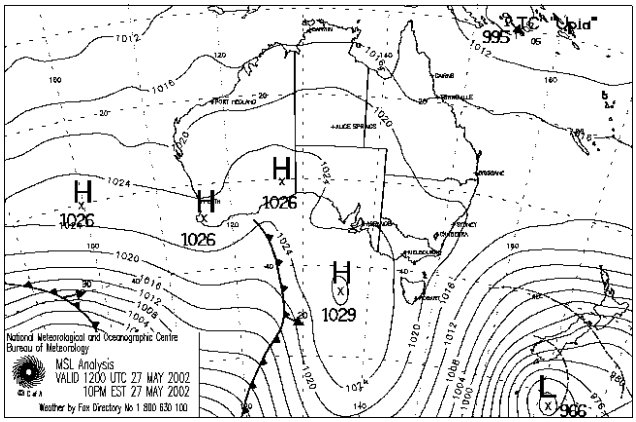

Mooring Sub-Directory:

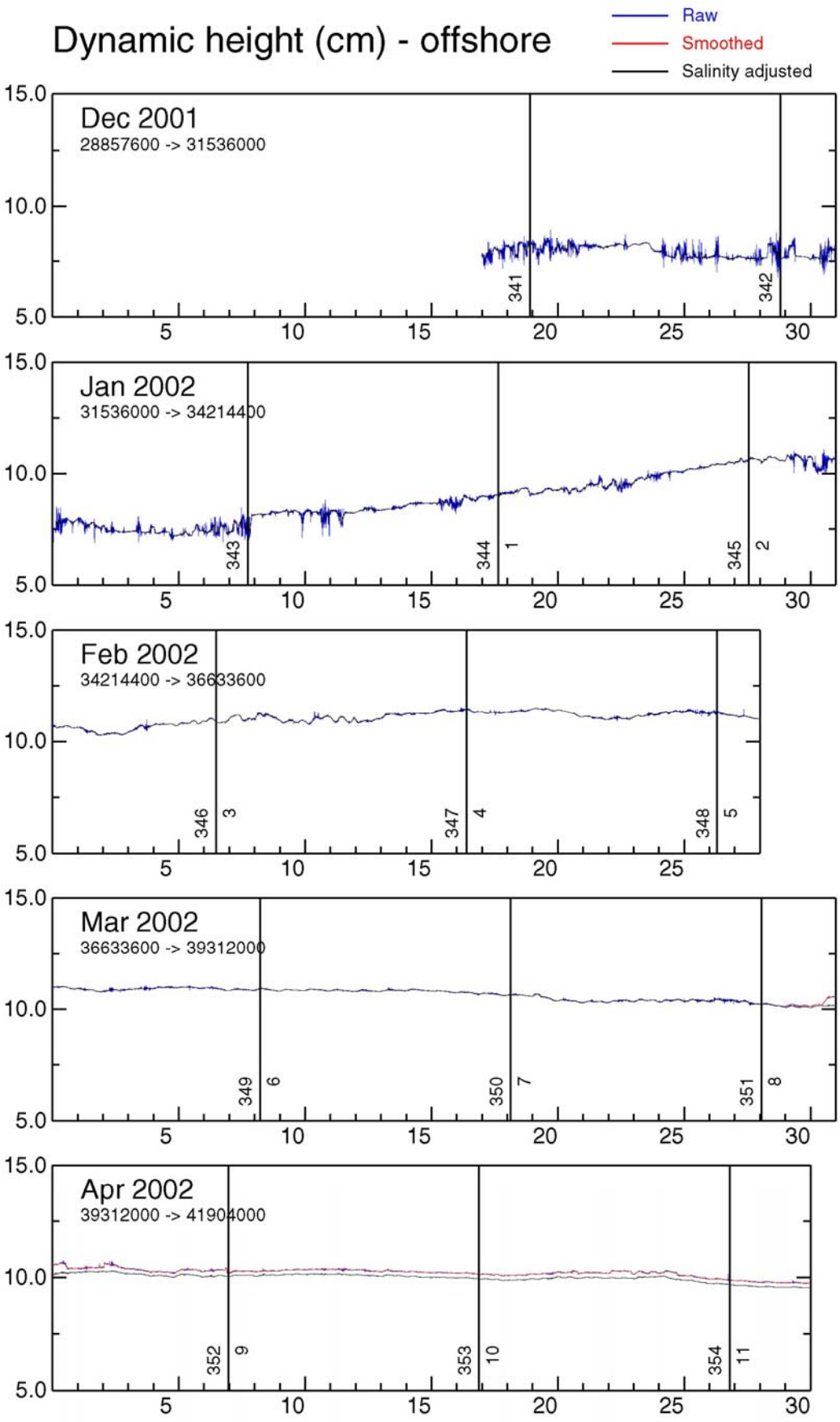

Topex Overflight Summaries Sub-Directory:

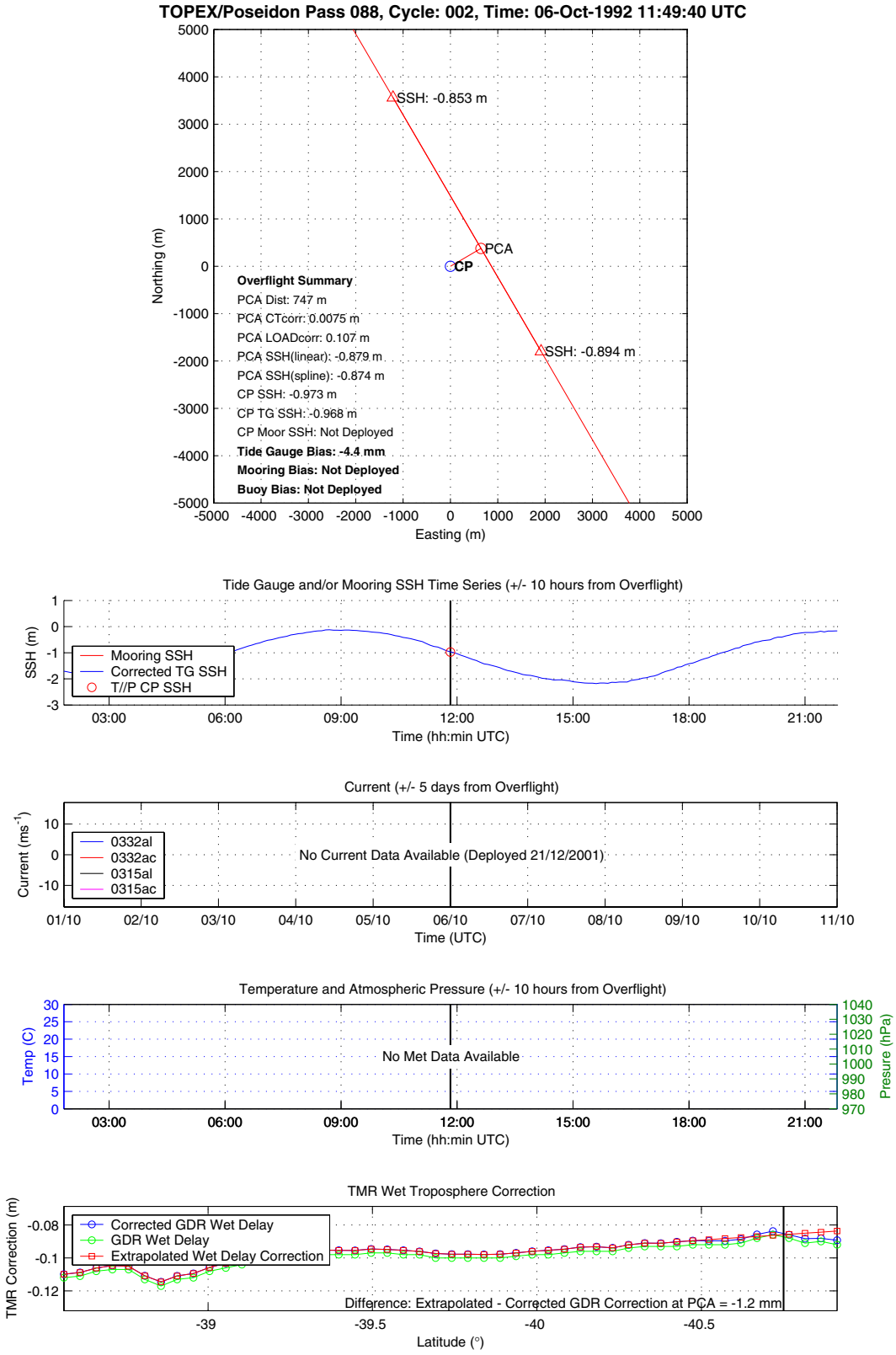

TMR Extrapolation Sub-Directory:

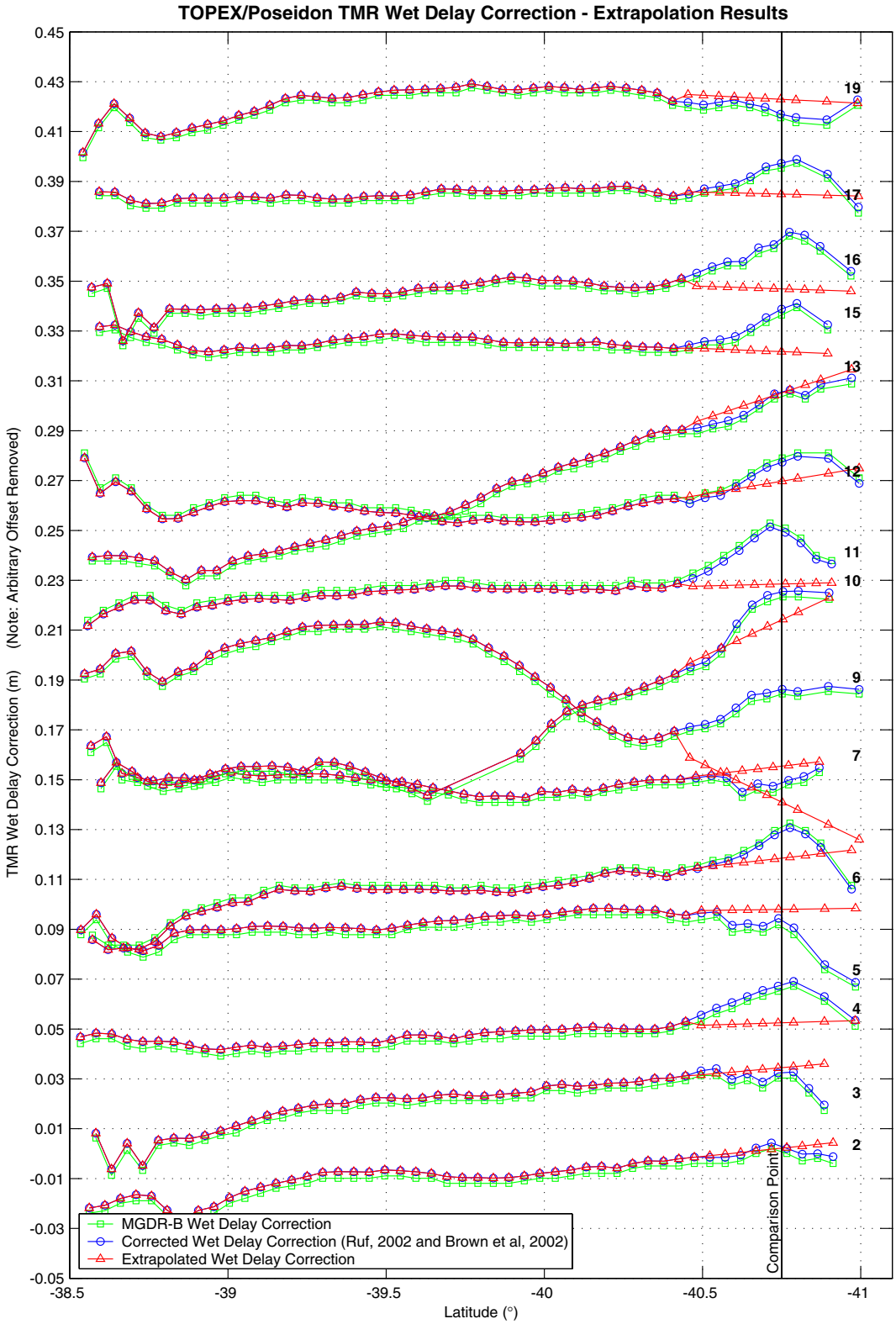

TMR vs GPS Sub-Directory:

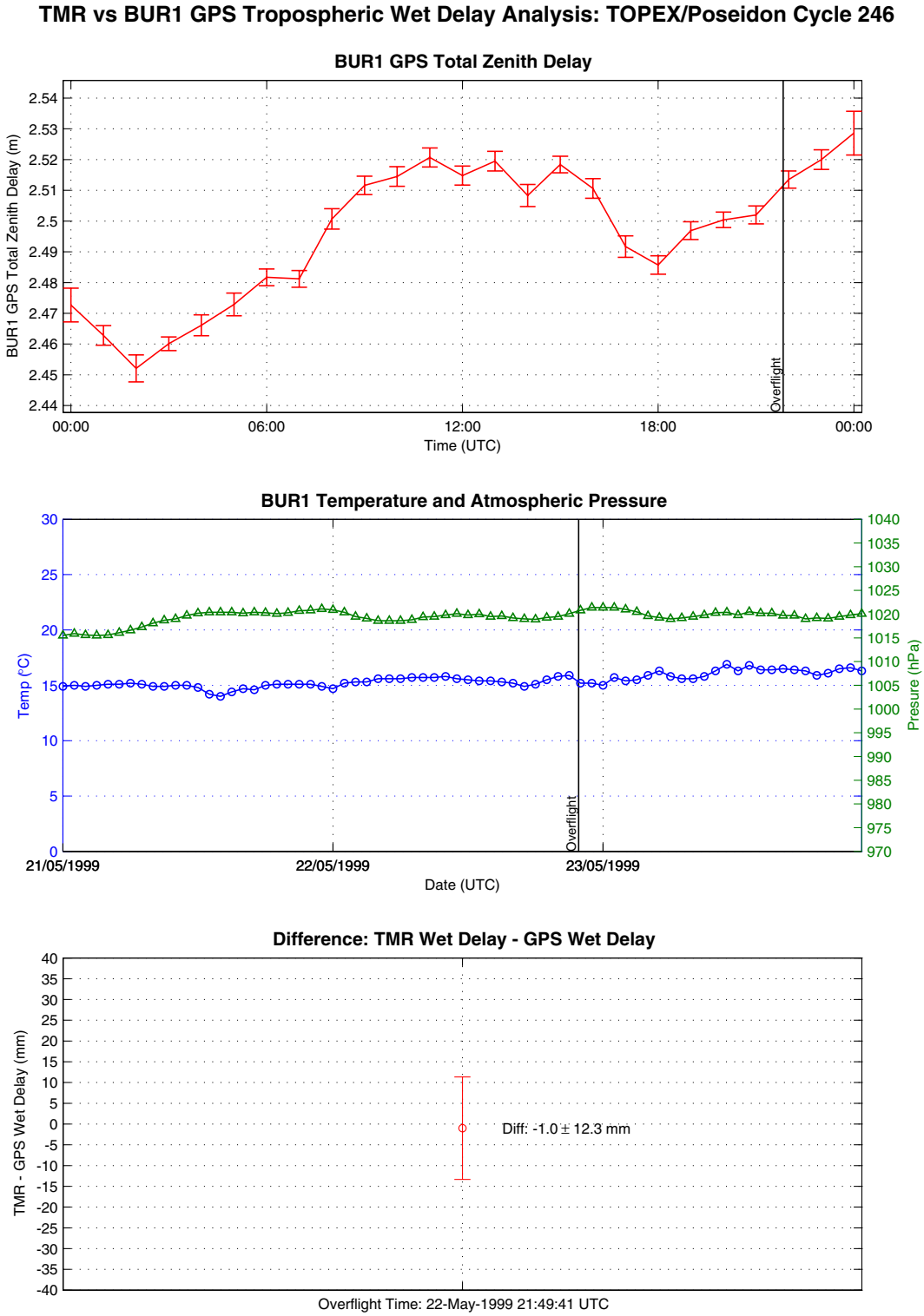

Jason Overflight Summaries Sub-Directory:

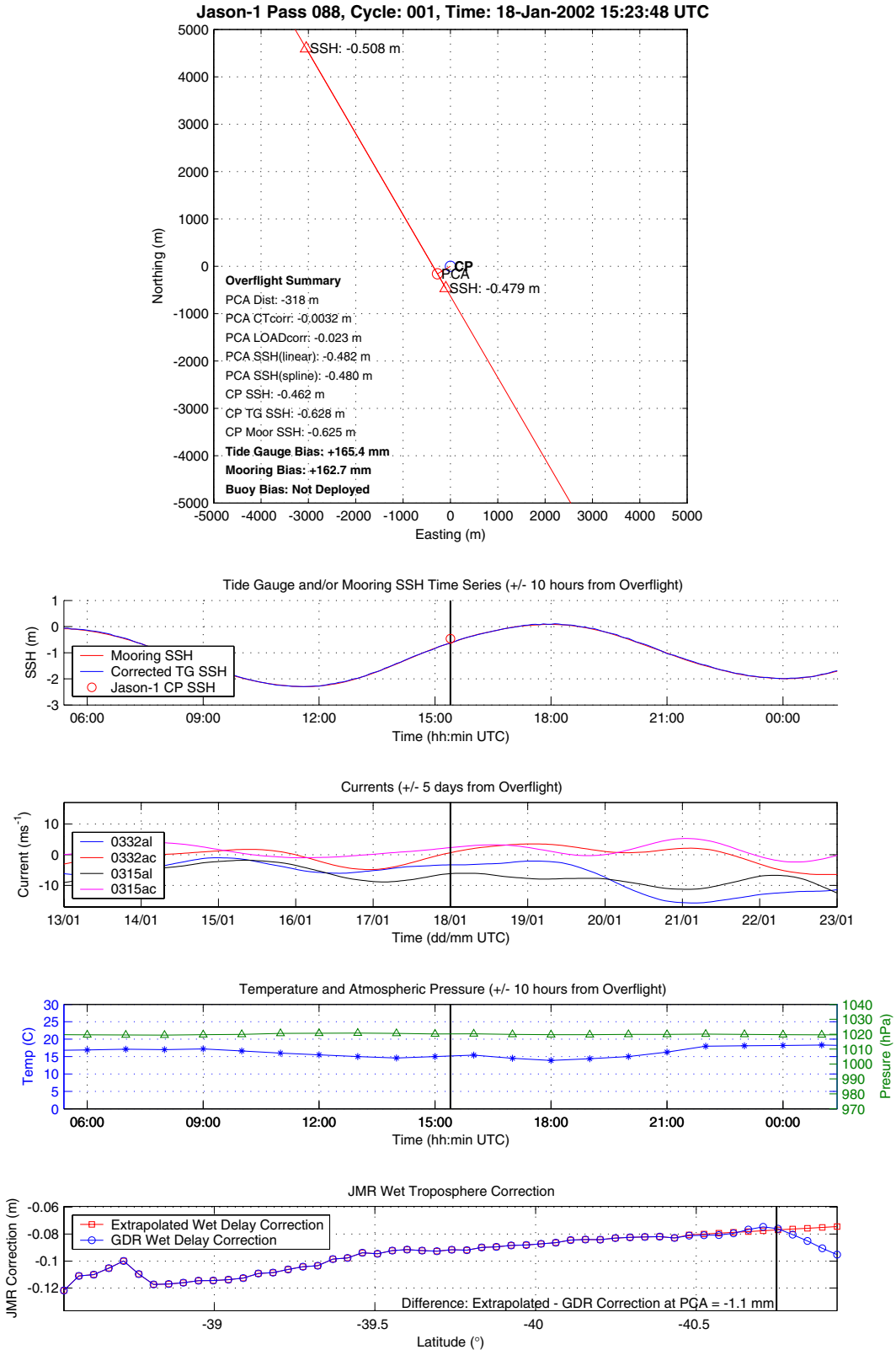

JMR Extrapolation Sub-Directory:

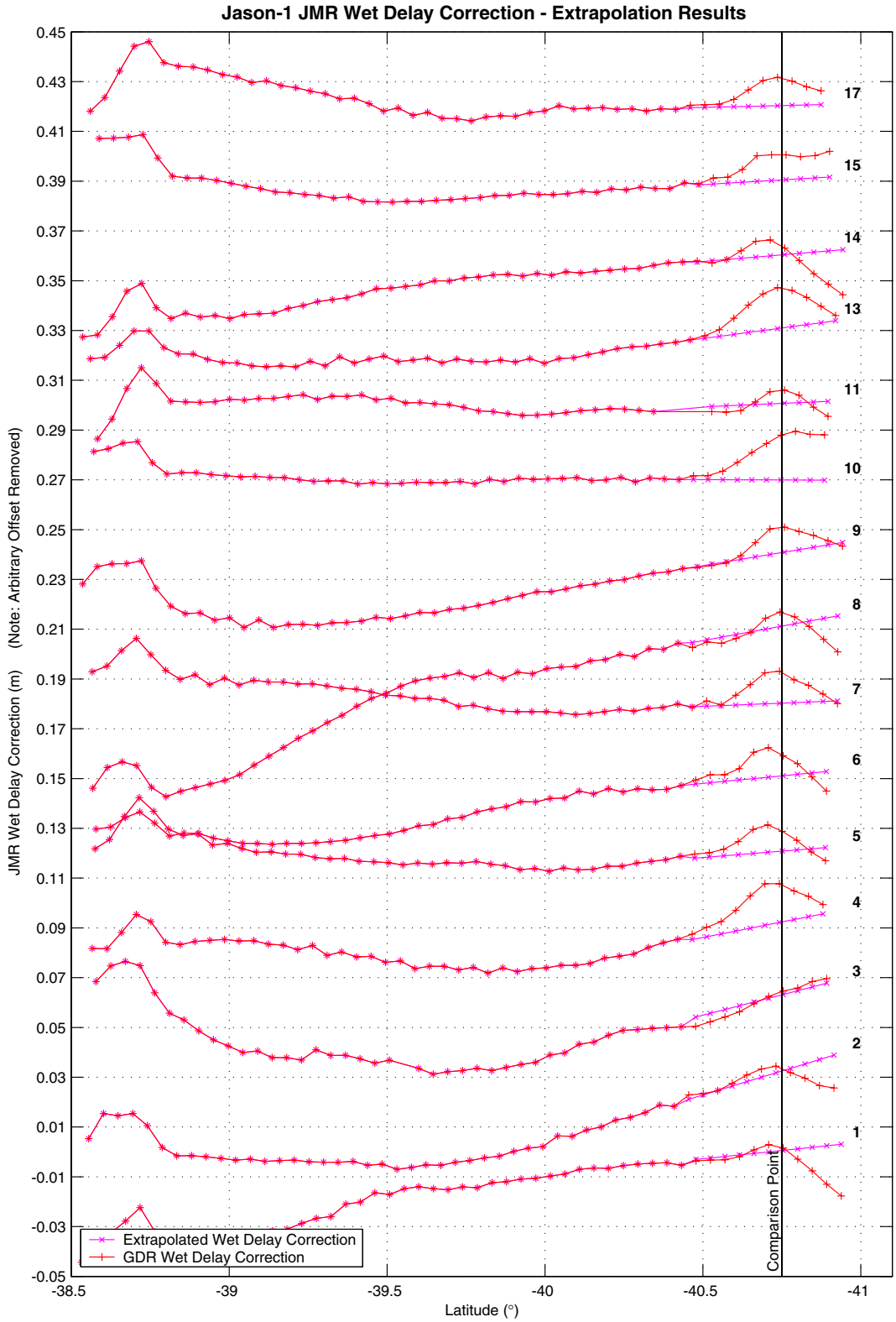

JMR vs GPS Sub-Directory:

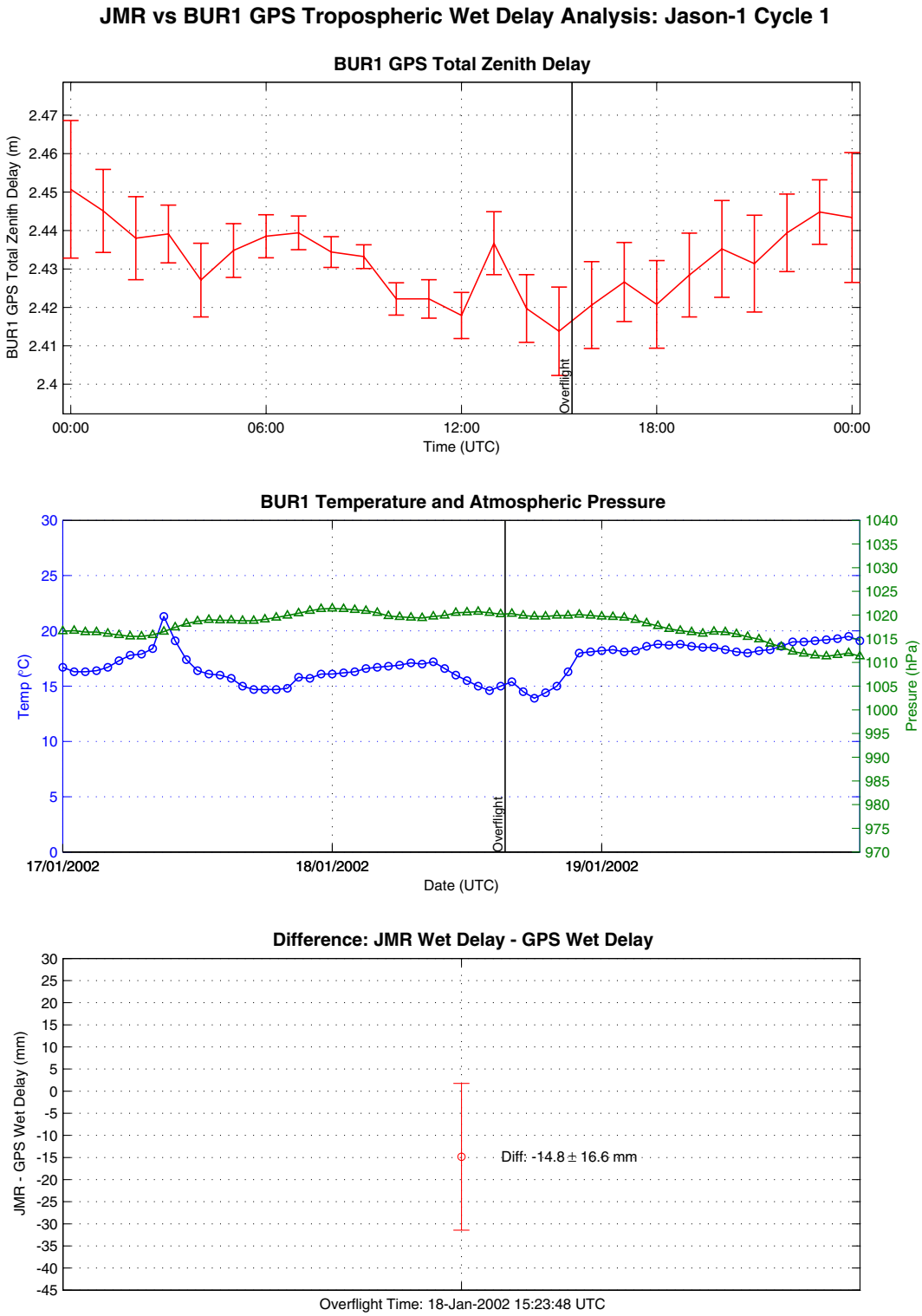

Appendix D

Tide Gauge Verification

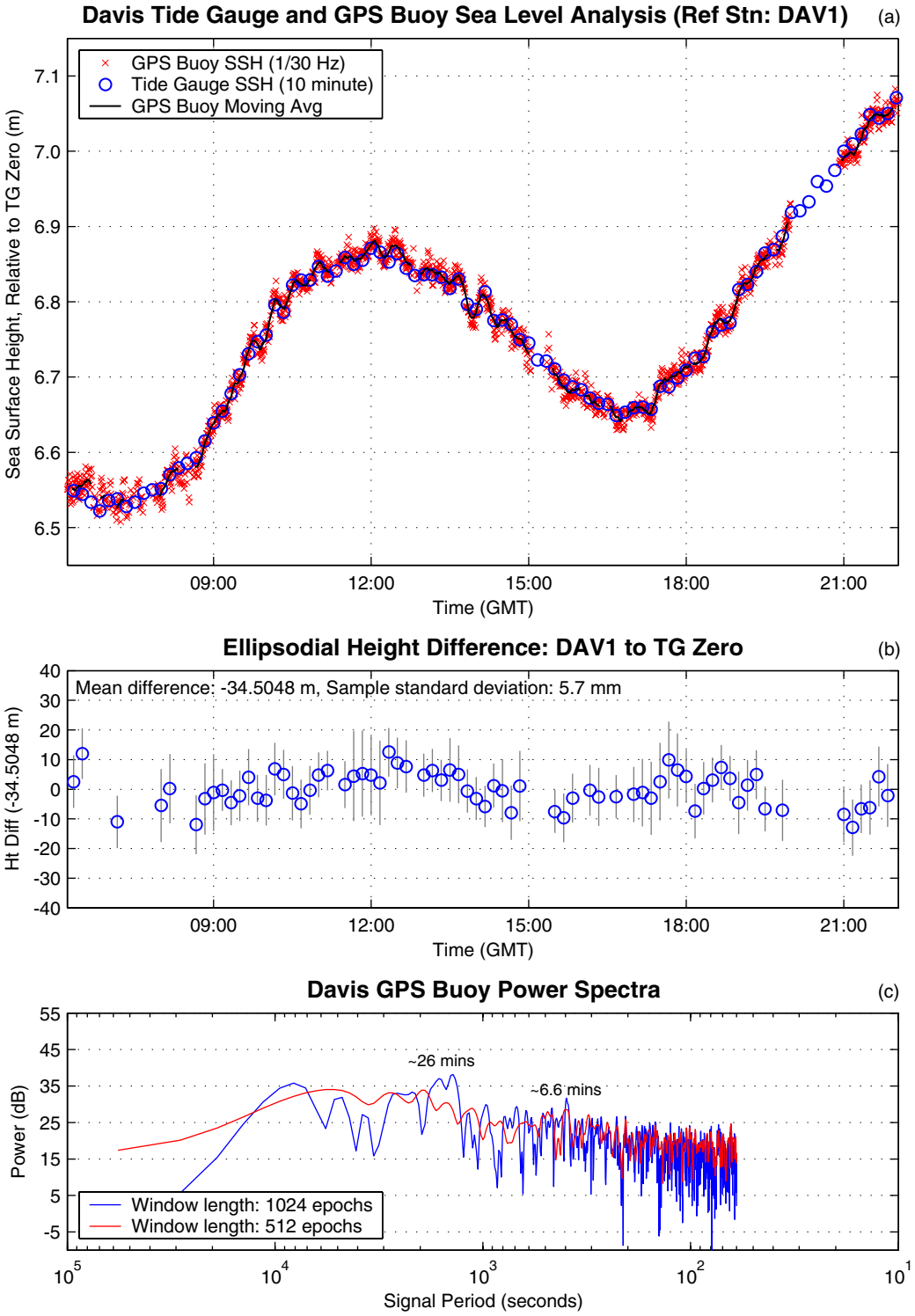

Figure D-1 Davis Station verification results. (a) Sea surface height estimates from both the tide gauge and unfiltered and filtered GPS buoy data. Note heights are relative to the tide gauge zero. (b) Ellipsoidal height difference between DAV1 and the TG Zero computed using filtered GPS buoy data and the tide gauge. (c) GPS buoy power spectra, note the power bands at ~26 minutes and ~6.6 minutes (period).

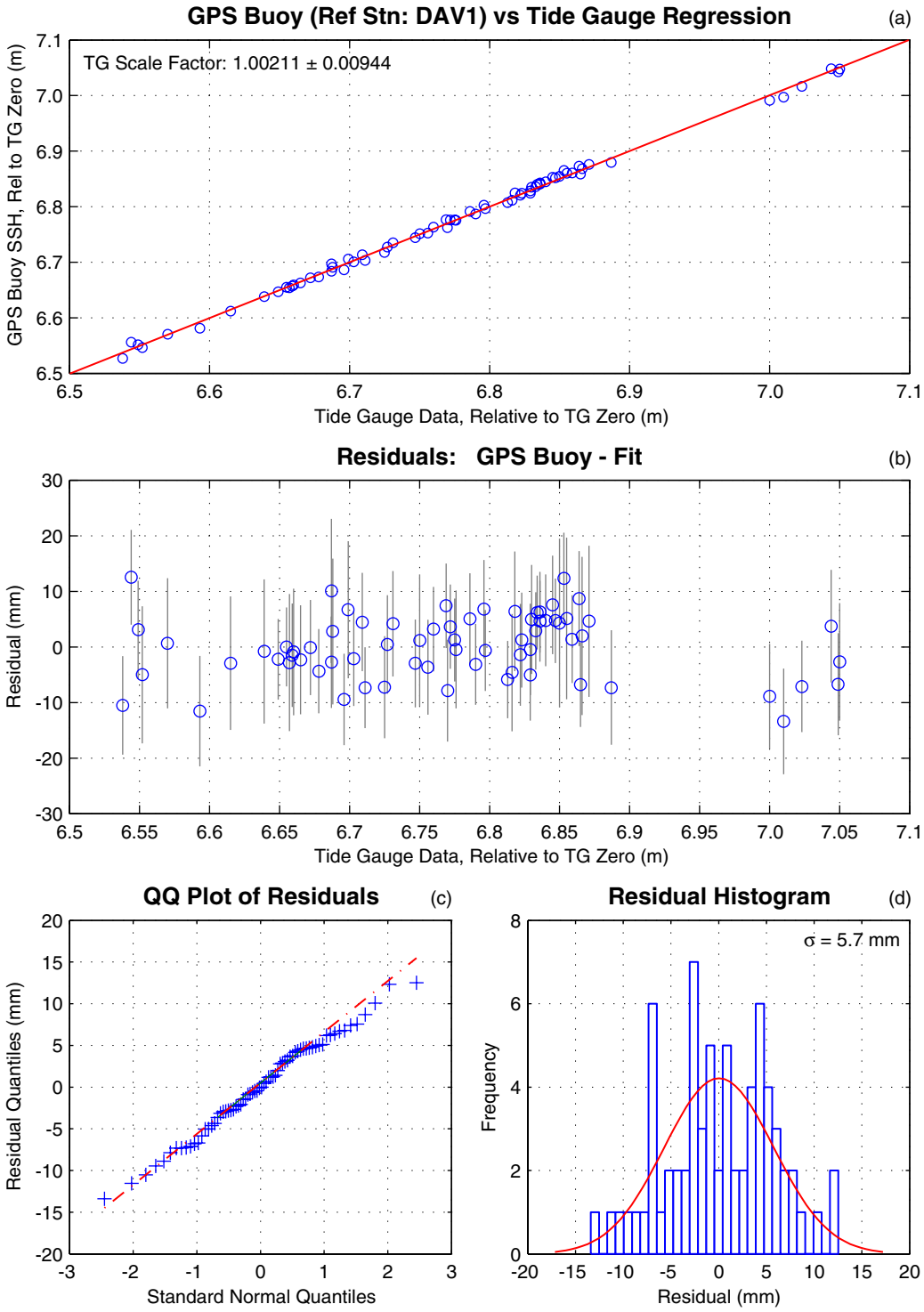

Figure D-2 Davis GPS buoy and tide gauge regression (processed relative to DAV1). (a) GPS buoy versus tide gauge SSH, relative to the tide gauge zero. (b) Regression residuals. (c) Empirical quantile-quantile plot of the residuals. (d) Histogram of residuals and normal distribution probability density function.